ABSTRACT

TASDEMIR, EMRAH. Applications of Grouted Shear Stud Connections for Steel Moment Resisting Frames. (Under the direction of Mervyn J. Kowalsky, Ph.D.)

Reinforced moment connections were employed to combat undesirable impacts of stress accumulation in the welded interface of moment connections after the 1994 Northridge earthquake. Recently, a novel reinforced connection scheme, called grouted shear stud (GSS) connection, was studied and applied to steel bridge bents to avoid adverse effects of lateral loads in the welded region between cap beams and steel pipes. The reinforcing scheme intended to eliminate the weld between the cap beam and steel pipe by providing more strength with an outer pipe, which was connected to the cap beam to accommodate the steel pipe, shear studs, and grout. The objective of producing a ductile connection without having any damage at the critical weld region was achieved by this novel scheme.

This study focuses on the possible applications of grouted shear stud (GSS) connections for steel moment resisting frames, specifically, beam to column connections. Discussion and suggestions on possible connections were made with 3D drawings to show the applicability of grouted shear stud (GSS) connections to steel moment resisting frames. A design process was proposed by considering capacity design principles for beam to column connections. The research was conducted by utilizing finite element models for different parameters. In total, 12 parametric study matrices, which include 48 beam to column connection models of two different beam section sizes, were provided. A study on shear stud behavior was also conducted. Several performance indices were adopted to evaluate behavior

of beam to column connections with varying design parameters. Design recommendations and topics for future work are also discussed.

Applications of Grouted Shear Stud Connections for Steel Moment Resisting Frames

by
Emrah Tasdemir

A thesis submitted to the Graduate Faculty of
North Carolina State University
in partial fulfillment of the
requirements for the degree of
Master of Science

Civil Engineering

Raleigh, North Carolina

2014

APPROVED BY:

_____	_____
Mervyn J. Kowalsky Committee Chair	James Nau

_____

Rudolf Seracino

DEDICATION

Devoted to my parents and my family.

BIOGRAPHY

Emrah Tasdemir was born in a small city of Turkey in November, 1985. He had his elementary, middle and high school education in the same city. After high school education, he decided to get civil engineering education in Istanbul University where he had a great interest in structural engineering. In 2008, he got his bachelor degree. Afterward, he applied to get a graduate degree in Structural and Earthquake engineering at Istanbul Technical University. During his education at Istanbul Technical University, he decided to obtain experience in the field of construction. He got an engineering position at Ministry of Environment and Urban Planning. He worked about one year as a construction management engineer. After working one year, he applied to a scholarship program, funded by Ministry of Education, to pursue graduate education abroad, which was his dream since he started his education at Istanbul University. He quit his graduate education and job to pursue his dream in USA. He took English education in Rochester/ New York to satisfy requirements for pursuing graduate education in American universities. He met Dr. Mervyn Kowalsky who helped him to deepen his knowledge in earthquake engineering at NCSU. Emrah completed his Master of Science education in July 2014.

ACKNOWLEDGMENTS

I am very grateful to God for helping me to overcome hardship during my research. I would like to thank to Dr.Mervyn J. Kowalsky for accepting me as a student to work with him on this intriguing project. His guidance, encouragement and support lead me to broaden my horizon on steel structures. I would like to also thank to Dr. James Nau for being my committee member and conveying his deep knowledge in steel structures to facilitate my understanding in this topic. I would like to thank Dr. Rudolf Seracino for being my committee member.

I would like to thank to my colleagues Diego Aguirre, Milad Hallaji, Omar Khalafalla and all Dr. Kowalsky's research group students for giving me their support during my research. I would like to thank to my Turkish friends for making me feel at home.

I am very thankful to my parents, my family and my fiancé for supporting me during this journey. I am very grateful to Turkish Ministry of Education for financial supporting me to make my dream true.

TABLE OF CONTENTS

LIST OF TABLES

LIST OF FIGURES

CHAPTER 1

1. Introduction

1.1.Overview

Earthquake excitation induces a high demand in terms of lateral loads in regions of high-seismic activity; for that reason, civil structures should be designed with the capability not only to sustain such forces, but also to prevent loss of life and reduce economic damages as well.

Over the years, detailed steel moment resisting frames have been widely used for resisting the action of lateral loads. In the United States, design and detailing of such structural systems can be performed based on capacity principles postulated in the AISC 360-10 specification for structural steel buildings (2010) and AISC 341-10 seismic provision for structural steel buildings (2010).

Structural elements such as beams, columns, panel zones, and connections are considered by design codes (e.g., AISC 341-10, 2010; AISC 358-10, 2010) as capacity protected components, such that they must not suffer any type of failure under the occurrence of a seismic event. In order to mitigate seismically-induced damage at certain regions of a structure and to prevent failure of protected components, contribution of each structural member in the behavior of the structure should be carefully evaluated and taken into account. Occasionally, failure of protected members may lead to undesirable structural performances which could result in local or global collapse of a structure.

The 1994 Northridge earthquake showed that moment connections (known as “Pre-Northridge” connections) for steel buildings were exposed to brittle cracking which did not

lead to any total collapse at that time (Mahin, 1998). In those connections, full penetration welds were employed to attach flanges of the beam to the column flange in the field, and a shear tab was used to join beam web to column flange by bolts as shown in Figure1.1 (Chen and Lin, 2013).

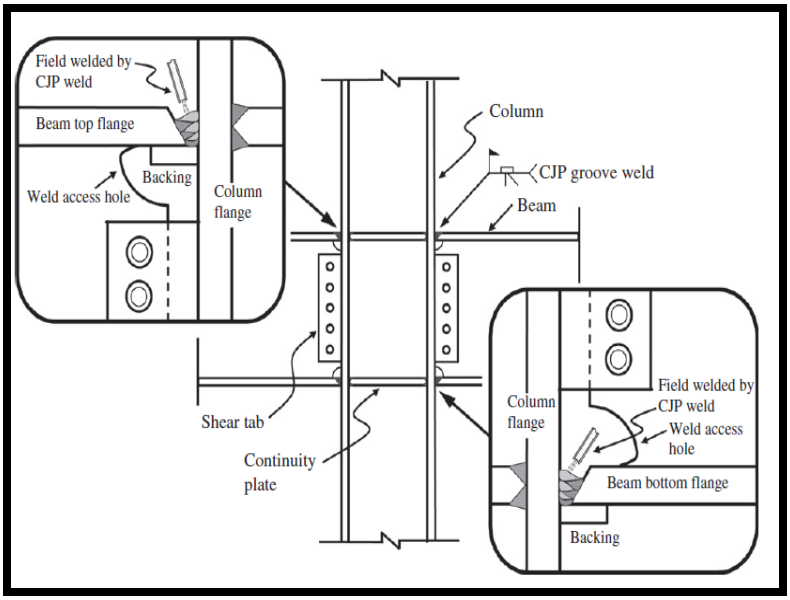

Figure 1-1: Pre-Northridge Connection (from Chen and Lin, 2013)

Due to brittle damage at the welded region of beam to column connections, many researchers have explored methods for enhancing seismic resistance of welded connections. Some examples of improved moment connections studied and tested after the 1994 Northridge earthquake, shown in Figure 1.2, include the following methods: attaching a cover plate to thicken flanges of the beam at its ends (Engelhardt and Sabol, 1998); gradually

increasing beam flanges adjacent to column flange faces (Chen and Lin, 2013); or reducing the area of flanges of the beam (Chen et al., 1996) at a specific location of the beam section.

The examples given illustrate the two kinds of techniques that have been broadly adopted to enhance welded moment connections after the 1994 Northridge earthquake: section strengthening and section weakening techniques. The section strengthening techniques aim to produce a connection, which can keep high plastic strain demand remote from the beam-column connected regions and has the capability of developing more strength than the beam section without having any failure. Alternatively, the section weakening techniques can be adopted to induce high plastic strain demand, which can give rise to brittle weld cracking, distant from the welded region of moment connections by reducing a pre-specified amount of flange or web area of the beam section. Both enhancing methods aim to protect the critical region of welded connections from undesirable effects of strain accumulation that might cause brittle cracking in the welded regions. (Bruenue, 2011)

The current study primarily focuses on the application of a novel moment connection for steel moment resisting frames. The enhanced connection, called the Grouted Shear Stud (GSS) connection, is based on the section reinforcing method that was previously studied by Fulmer et al. (2012). Subsequent chapters focus on the application of GSS for beam to column connections. In addition, finite element structural models are developed in order to investigate the behavior of the connection. Based on the outcomes of the analyses, design recommendations are provided for beam to column connections using GSS.

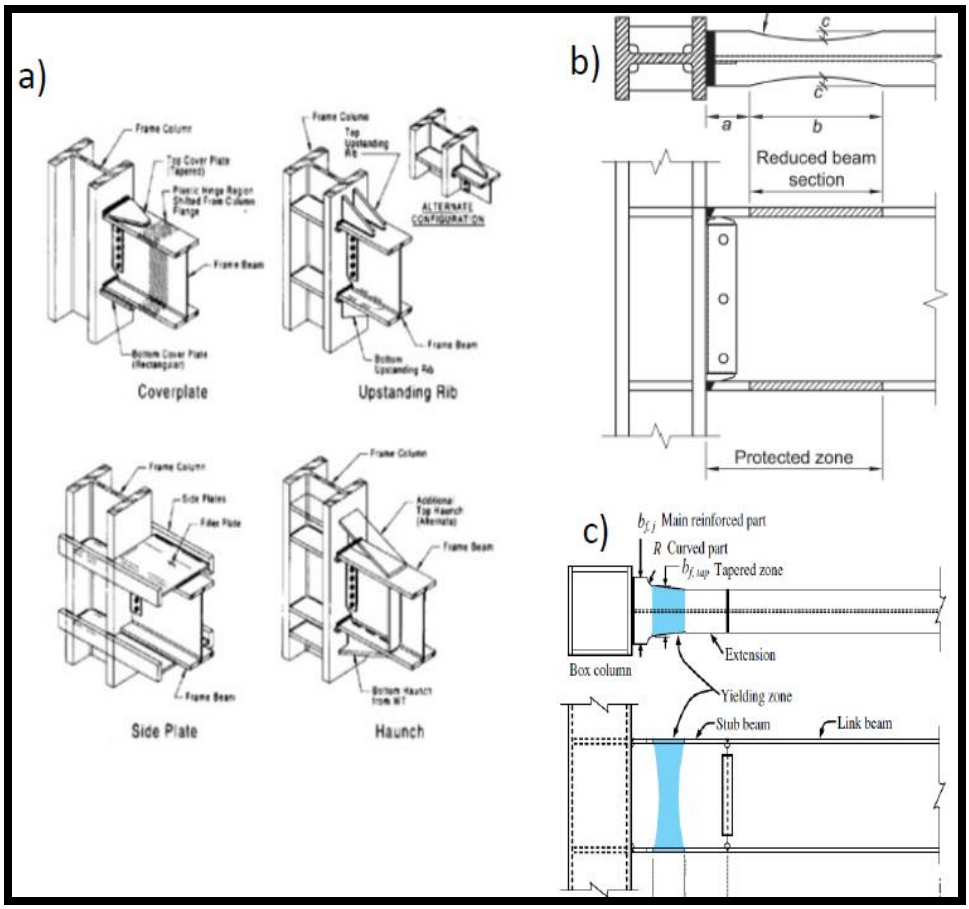

Figure 1-2: Examples of Improved Connections: a) Reinforced Connections (from Engelhardt and Sabol,1998) b) Reduced Beam section (from AISC 358-10 (2010)) c) Widened Beam Flange (from Chen and Lin, 2013)

1.2.Motivation

This study is based on the work performed by Fulmer et al. (2012). Their research presented a novel reinforced connection method in which the main purpose was to transfer the plastic action far from the bottom soffit of the cap beam to a specific region of the pipe pile. In addition, the method provides a ductile section, which can accommodate substantial

inelastic rotation by means of the composite connection named Grouted Shear Stud (GSS) connection.

1.2.1.Study by Fulmer et al. (2012)

Past research efforts (Fulmer et al., 2010), which were based on existing construction practices of bridge bents from the Alaska D.O.T shown in Figure 1.3, have revealed that applying a different arrangement of welds has not been shown to prevent brittle fracture at the toe of welds, where the cap beam was attached to the pipe pile.

Figure 1-3: Bridge and Brittle Fracture at Toe of Weld (from Fulmer et al., 2012)

In order to prevent early brittle failure in the welded region, researchers aimed to produce a reinforced connection type in accordance with the capacity design approach. The objective of the researchers was that the reinforced section would not experience any inelastic deformation while plastic action shifts into the steel pile as local buckling at the predetermined location of the steel pile.

Figure 1-4: Component of Grouted Shear Stud Connection (from Fulmer et al. 2012)

For attaining such an outcome mentioned above, a pipe pile was placed into a larger and stubby pile, which had a greater strength capacity than that of the innermost or driven pile; the outer pile was welded to the cap beam in order to accommodate the driven pile and grout as shown in Figure 1.4. Conceptually, this connection incorporated an even number of shear studs distributed on the stub pile inner surface and outside surface of the embedded part

of the driven pile. The goal was to produce a force-transfer mechanism along with the help of high strength grout, such that the welding of the cap beam to the driven pile could be avoided, while the total plastic moment capacity of the pile could be reached. Determination of shear connector strength was based on the model suggested by ANSI/AISC 360-10 (2010). Determination of the shear stud number was based on the idea that the driven pipe develops its yield strength in the entire cross section before the shear studs, which were located on the embedded part of the steel pipe pile's outside surface, reach their full shear capacity.

Figure 1-5: A View of Buckled Pipe and Lateral Loaded Steel Bent (from Fulmer et al., 2012)

Researchers conducted an experimental program using an HSS16x0.50 pipe pile and an HP14x117 cap beam with material properties ASTM A500 Gr. B and ASTM A572 Gr.50,

respectively. Experimental findings showed that the objective of moving the plastic deformation into the pipe pile as local buckling, which is shown in Figure 1.5, without having any inelastic action in the welded region, was accomplished. The strain propagation in the connected region, in which the connection remained elastic during the tests, is shown in Figure 1.6. Moreover, finite element models were developed using finite element software ABAQUS in order to provide insight into the performance of the tested connection. For these finite element models, nonlinear and elastic materials for steel and grout members were considered, respectively.

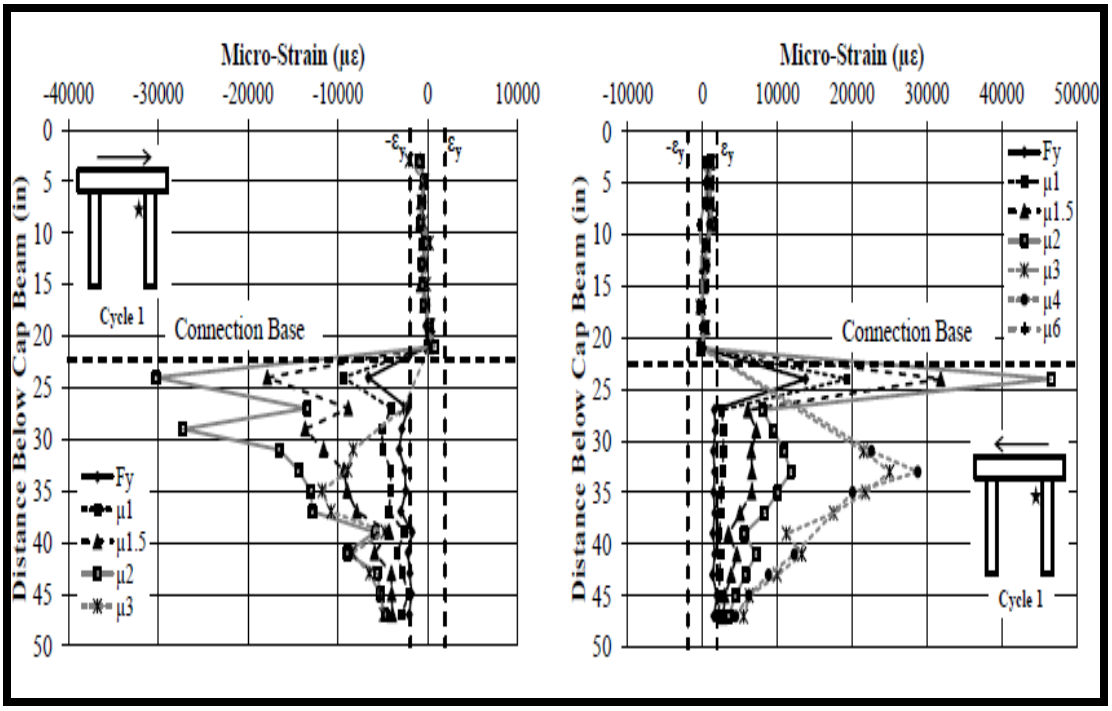

Figure 1-6: Strain Elevation for Different Ductility Levels (from Fulmer et al., 2012)

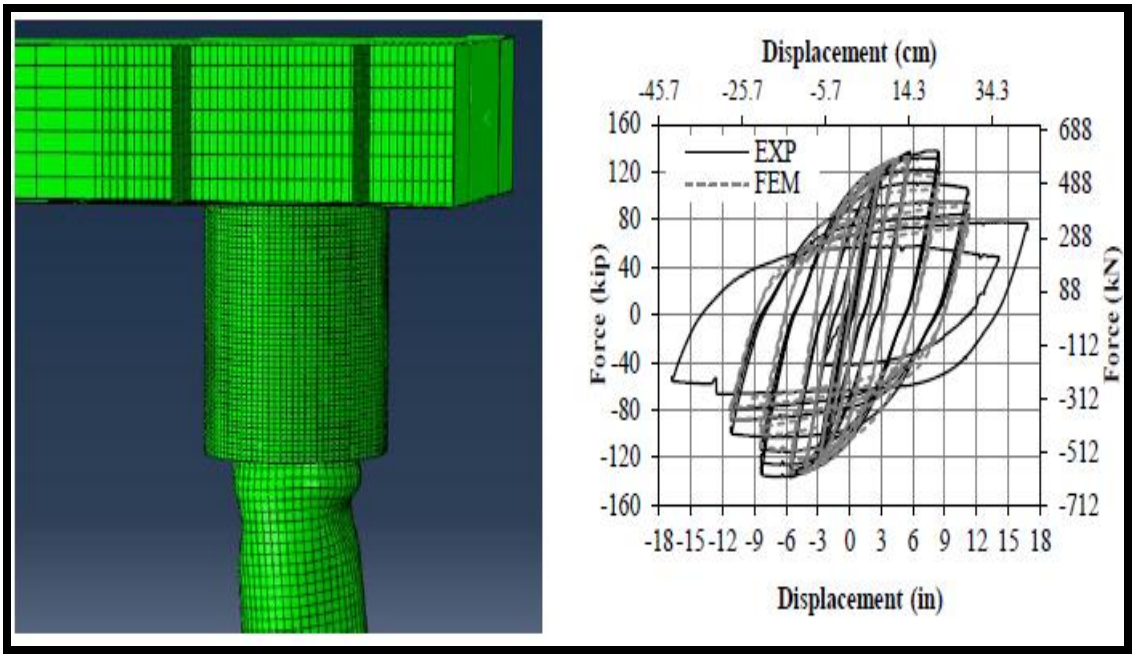

Figure 1-7: Finite Element and Test Results Comparison (from Fulmer et al., 2012)

Buckling behavior of the pipe pile was successfully predicted by the finite element models as shown in Figure 1.7. In addition, force-displacement hysteretic curves of simulated and experimental results followed a similar pattern.

1.3.Research Goals

The main goal of this study is to explore the feasibility of using Grouted Shear Stud connections in steel moment resisting frames, specifically beam to column connections. In order to gain a better understanding, the study will explore the following objectives:

- Discuss possible applications of Grouted Shear Stud connections with feasible construction methods.

- Investigate effects of different parameters such as stud number, stud configurations, and stub height, among others, by performing finite element analyses of grouted shear stud beam to column connections.
- Suggest design recommendations based on the findings obtained from the finite element model analyses.
- Suggest topics for future research.

1.4.Organization of Thesis

Chapter 2 discusses possible applications of GSS connections for steel moment resisting frame structures for different types of joints such as beam to column, column splice, and column base connections, along with design and detail considerations. Chapter 3 presents a literature review specifically focused on beam to column connections. Chapter 4 includes the developed finite element models and details such as material models, shear stud modeling, model geometry, and boundary conditions, among others. Chapter 5 presents parametric study matrices and results from the simulations for different parameters. Chapter 6 provides discussion of the results of individual parameters given in Chapter 5. Finally, Chapter 7 discusses the results based on the findings from previous chapters and design recommendations. This chapter also presents an illustrative discussion for future work topics.

CHAPTER 2

2. Possible Application of GSS for Steel Moment Resisting Frames

2.1.Overview

This chapter will address possible applications of grouted shear stud (GSS) connections to steel moment resisting frames based on existing steel moment resisting frame construction practices and engineering judgment. In short, the provided steel moment frame connection details for beam to column connections, column splice connections, and column base connections should facilitate construction. In considering cost-efficiency of the construction process, a designer should provide connection details that would not prevent construction of other structural components, and would not cause a delay. The suggestions for an efficient construction process of possible GSS connections will be made by considering this reasoning.

2.2.Application of GSS to Beam to Column Connections

Beam to column connections in steel moment resisting frames are critical connections that should be meticulously constructed. In the view of the fact that moment gradient in such connections has varying magnitude during earthquakes, welding quality may be an issue. Consequently, the welding process should be done such that there would not be any flaw that may cause crack initiation (Bruneau et al., 2011). Considering a welding process which would not cause any flaw is a key part of the construction process; three construction methods for application of Grouted Shear Stud to beam to column connections are suggested.

The first method, column tree construction, is commonly used in Japan and Taiwan. This technique was designed to eliminate any kind of field welding at beam to column moment connections in order to improve the weld quality (Chen et al., 2013).

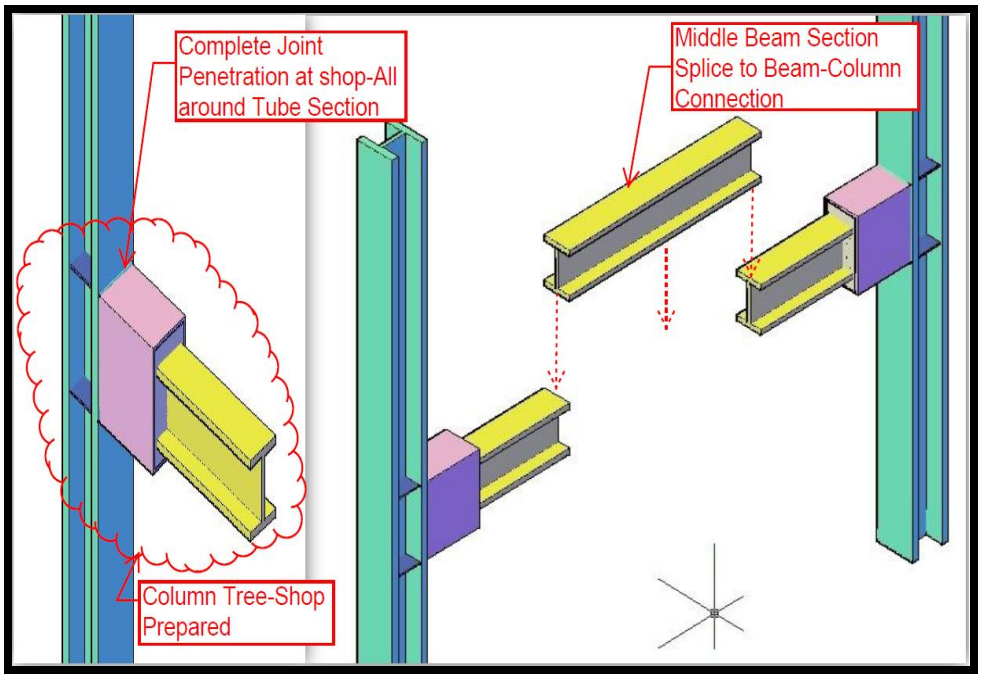

Figure 2-1: Column Tree Construction of GSS Beam to Column Connection

The construction process begins with placing the required number of shear studs on the top and bottom faces of the beam flanges. If it is necessary, in the workshop, shear studs can also be placed on the web of the beam, and both inside surfaces of the top and bottom plates of the stub section. Stub sections, which are fabricated by the welding of four plates, are welded on a column flange face with a complete joint penetration weld to construct a section as shown Figure 2.1, which can accommodate the beam and grout. Visual and

ultrasonic inspection should be conducted in order to complete the workshop welding process. Beams are inserted into the stub from its studded end, as shown in Figure 2.1, and extend over to the column flange face. As mentioned in Chapter 1, the purpose of this connection is to eliminate the need for welds between beams and columns by providing shear studs and grout (Fulmer et al., 2012). Stub sections, as shown in Figure 2.1, are grouted after the beam is placed. After the grout has cured, the entire column tree is ready for transport to a construction site where column tree connections are spliced to the mid part of a beam with either welds or bolts. The location of splices should be far from the plastic hinge region where high plastic strain demand can cause failure in the splice connections. Details about beam splices will not be discussed in this study.

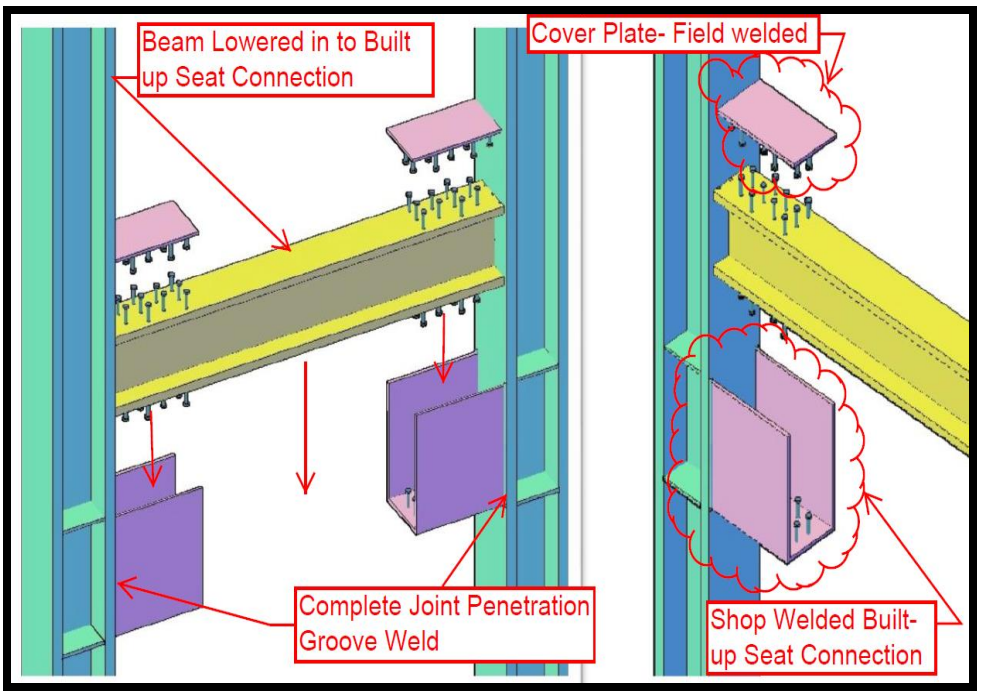

Figure 2-2: Top Cover Plate Field Welded Construction Method

Recognizing steel moment construction practices in other parts of the world, two construction methods that include field welding are discussed. The two methods can be distinguished by the last plate that is welded to construct the stub. Since three plates are welded in the workshop to constitute a seat-like connection to accommodate the beam studded ends, the last plate will be used to complete a stub section in order to allow casting of grout into the connection.

The first method involves welding three plates to a column flange face in the workshop with complete joint penetration welds. In this case, only the bottom and top stub plates may have the required number of shear studs on their inside surfaces. As can be seen in Figure 2.2, the beam flanges will not allow for locating shear studs on the inside surface of the side plates. Therefore, if the designer wants to utilize this construction process, the number of shear studs and location should be taken into account. In this type of connection construction, three edges of the top cover plate will be welded in the field, as shown in Figure 2.2. After lowering the studded beam ends into the seat-like connection as shown in Figure 2.2, the cover plate will be welded to the complete stub. Finally, grout can be poured into the stub section. As mentioned before, no weld is necessary between the column and the beam.

Based on finite element analysis, the weld between the top/bottom cover plates and the column flange face is the most critical region, as it is here that transition of bending forces takes place. Under this force transfer mechanism, welding quality has vital importance that a designer and contractor must be aware of.

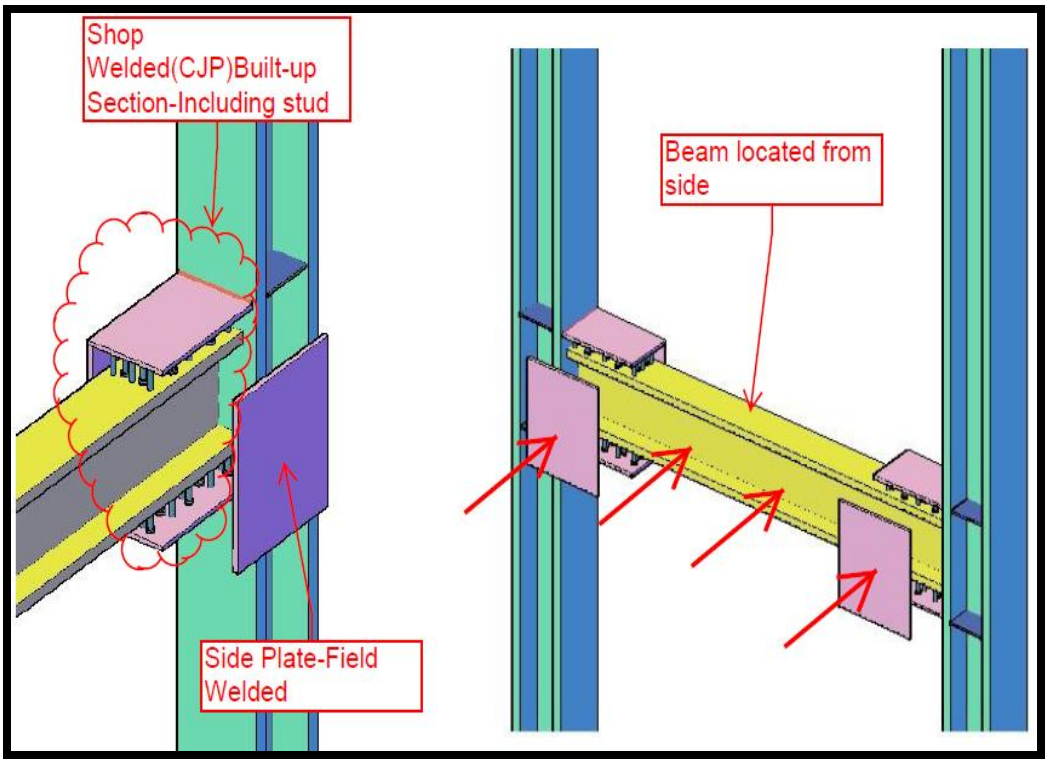

Figure 2-3: Side Plate Field Welded Construction Method

Unlike field welding of the top cover plate, the second method employs a side plate to constitute a stub section, as shown in Figure 2.3. Studded beam ends are located inside a seat-like connection from its side. Afterward, the side plates are welded in the field to complete the stub section. Welding of the side plate edge to the column flange face can be done from the top corner to the bottom corner. This construction process allows placing shear studs on the inside surface of the side plates of the stub section and the beam web. Shear studs located on the top and bottom soffits of the beam and stub plates' inside surfaces may cause difficulties when the beam is located in the seat-like connections; therefore, a designer can utilize one of many shear stud configurations presented in the following chapters. In

light of finite element analysis, the welded region between the side plates and column flanges does not experience high stress compared to the top and bottom of the welded region of the stub plates. Therefore, this construction process can be a good alternative to construction processes that require field welds, as mentioned above.

The shear stud configuration is an important parameter that affects behavior of the design, and will be considered fully in the following chapters. Configuration of shear studs also has an effect on construction processes, as certain configurations may require different construction methods. Several different configurations will be discussed with finite element analyses in successive chapters.

Considering key points of the design and the connection detailing including simplicity, smoothness and cost-effectiveness, this chapter presents three different detailing options that give designers an opportunity to select the most applicable design methods from various design details.

2.3.Application of GSS to Column Splices

Because transportation length of structural members is limited to 12m (Simao et al., 2012), column splicing becomes an unavoidable part of steel moment frames. Column splice connections are also employed when a designer needs to decrease column size in upper stories. Generally, splices are located at a certain distance (4 ft. per AISC 341-10) above beam top flange surfaces.

Economical designs use column splices to reduce column size, when moment and axial demand in columns reduce in upper stories. Column splice design has crucial

importance, since stiffness and strength of columns must be continuous in upper stories in order to generate a healthy structure in terms of seismic performance (Simao et al., 2012). Several methods have been suggested for constructing column splices in many design manuals (e.g., AISC Steel Construction Manual 14th Edition (2011)), some of which incorporate heavy field welding. As far as welds are concerned, column ends must be directly welded to each other or to a bearing plate between them. Since field welding is the only way to construct a welded splice, any quality issue may cause additional problems. For instance, any flaw or imperfection in the welded region may induce a secondary moment effect which may create a splice susceptible to buckling (Lindner, 2008).

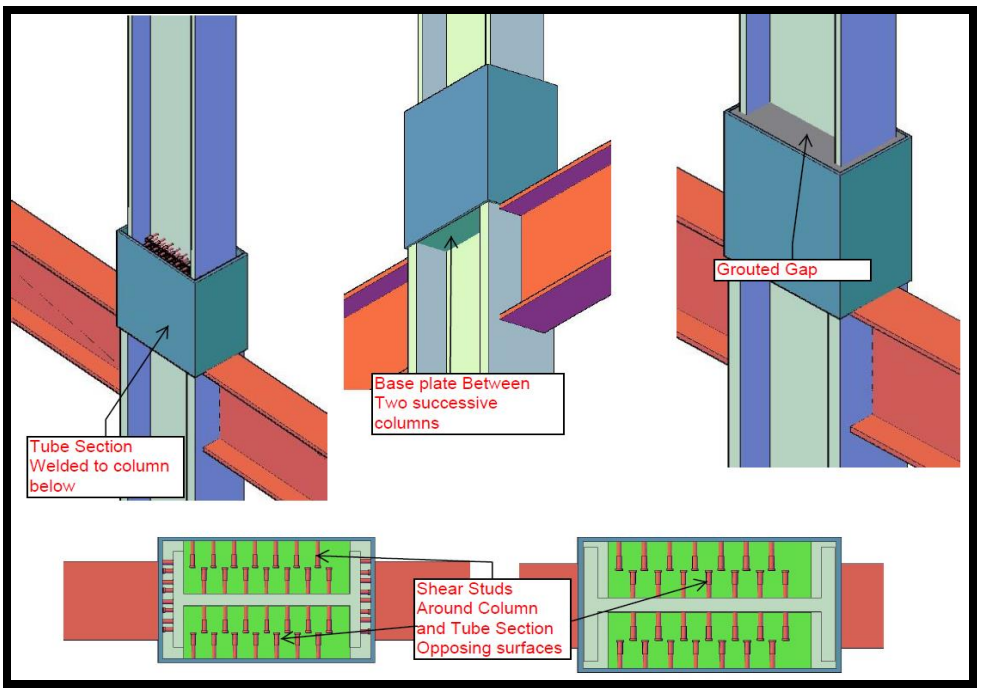

Figure 2-4: Grouted Shear Stud Connection Details for Column Splices

In order to avoid field welding and eliminate any kind of imperfection due to weld quality, grouted shear stud (GSS) connections can be used for splicing columns. In contrast to application of grouted shear stud (GSS) to beam to column connections, column splice connections include only shop welding details, as shown in Figure 2.4. As previously mentioned, column sizes can change or remain constant at upper stories. Therefore, depending on the column size requirement, the number of shear studs and their location may change in order to generate a more robust connection. To construct a splice connection, two column ends need to be sawed in the workshop. Afterward, a base plate must be welded to the lower level column in order to accommodate the upper level column and grout. Based on column sizes, the studded plates utilized to construct the stub are either welded to the base plate or welded around the top part of the lower level column. Finally, the studded and sawed upper level column end is placed into the constructed stub, which has a bottom plate, and filled with grout. As was previously stated, the grouted shear stud (GSS) connection can reduce or entirely eliminate field welding.

2.4.Application of GSS to Column Base Connection

Because large actions (moment, shear, axial load) transfer through column bases to the foundation, they are crucial components of steel moment resisting frames. Since seismic demand on column bases is so severe, careful consideration of the column base connection design is necessary in order to comply with capacity design approaches. Plastic hinge formation in steel moment frames is expected to take place at the bottom end of the first story column. In order to accomplish this without experiencing failure in the column base, column

base connections should be designed for a strength level which allows connections to remain elastic during excitation.

In the aim of reaching this full-strength capacity of the column without causing any strength loss in the connection, several column base connections have been suggested in the literature, including the embedded column base, the exposed column base and the semi-embedded column base connection (Grauvilardell et al., 2005). Utilizing Grouted Shear Stud connections to generate an embedded column base connection can be advantageous; unlike other embedded column base construction methods mentioned in the research of Pertold et al. (2000), column ends can be directly supported by stub bottom plates to reduce the time necessary for the casting process.

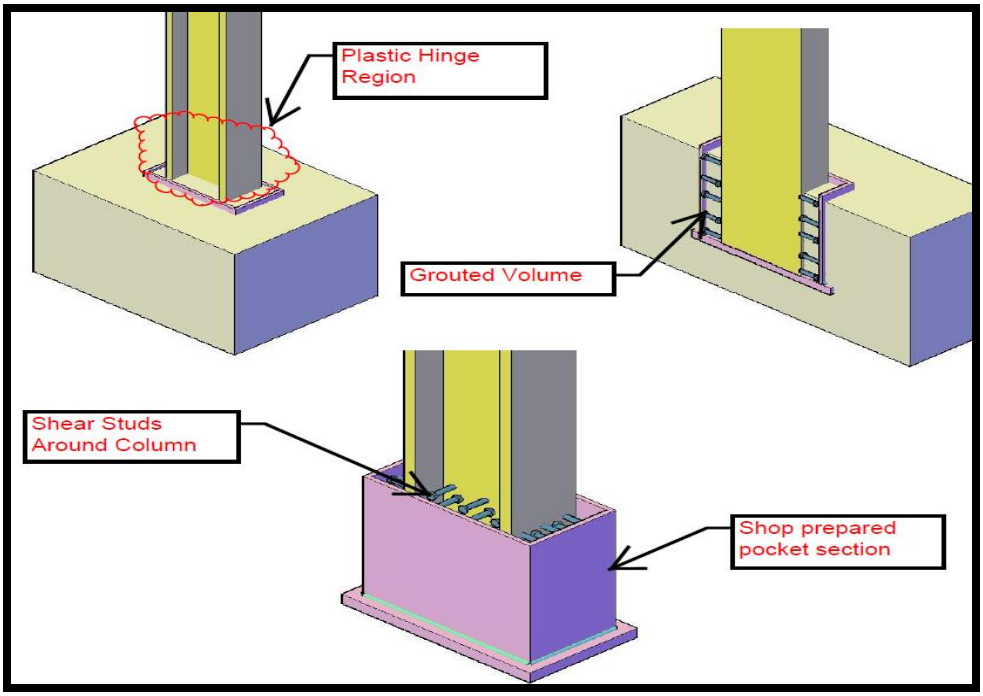

Figure 2-5: Grouted Shear Stud Application for Embedded Column Base

Having a steel tube around the grout region can provide confinement that can increase strength capacity of the grout to relocate plastic damage into the column, and also may generate a fully "fixed boundary condition" (Pertold et al., 2000) which must be taken into account when conducting global frame analysis. Furthermore, embedding column into foundation will reduce amount of concrete below the column. By inserting the column end into a stub section, which has shear studs and a large bottom plate, one can reduce likely punching failure in the foundation. Unlike other embedded column base connections mentioned in research of Pertold et al. (2000), having a larger base plate will help connections to sustain more overturning moments caused by the column. Shear stud configuration and required numbers can be found after the detailed finite element analyses. Since detailed finite element analysis was done only for beam to column connections in this study, design requirements are not discussed for column base connections.

Grouted Shear Stud connections can also be applied as exposed column base connections. Similarly, the objective behind this connection is to shift the plastic hinge into the column by providing a stronger connection than the column. Different from other exposed column based connections, grouted shear stud connections may require a wider base plate because of an increase in required moment demand at the bottom of the column. Consequently, the required number of anchors may need to be increased to prevent any failure which can cause strength degradation in the connection. Required shear stud numbers and configurations can be determined after conducting detailed finite element analyses or experiments. More shear studs may be required in this connection because of the increase in the moment and axial demand on column base connection.

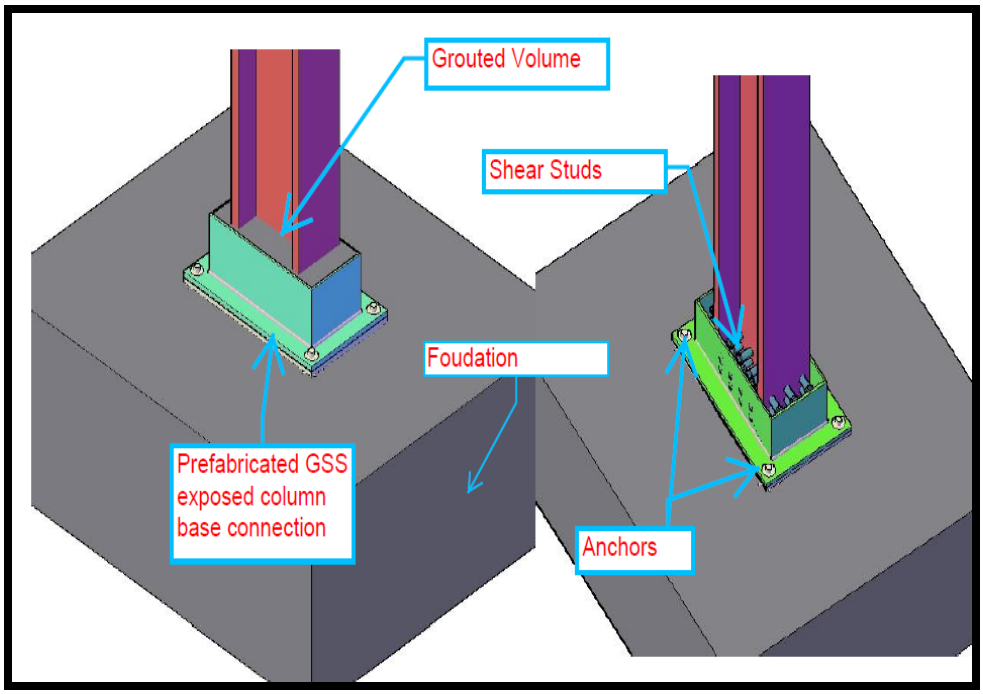

Figure 2-6: Exposed Column Base Grouted Shear Stud Connection

2.5.Proposed Design Procedure for Grouted Shear Stud Beam to Column Connections Based on Capacity Design Approach

Application of GSS beam to column connections is the focus of this study, as stated before. This subsection discusses the design procedure for beam to column grouted shear stud connections. As mentioned in the beginning of the first chapter, the design of steel structures according to capacity design approach is demanded by many design codes (AISC 358-10(2010), AISC 341-10(2010)). Therefore, a capacity design approach for designing grouted shear stud beam to column connection is pursued in this study. The proposed design process is as follows:

1-The maximum possible plastic moment of the beam section at the plastic hinge region should be found from equation (2.1).

$$M_{pr} = C_{pr} R_y F_y Z_x \qquad (2.1)$$

where C_{pr} and R_y represent strength factors given by *AISC Seismic provision* (2010); F_y is the yield strength of steel material used; and Z_x is the plastic section modulus of the given beam section. C_{pr} can be found by using equation (2.2):

$$C_{pr} = \frac{F_y + F_u}{2F_y} \qquad (2.2)$$

where *Fu* is the tensile strength of steel material adopted.

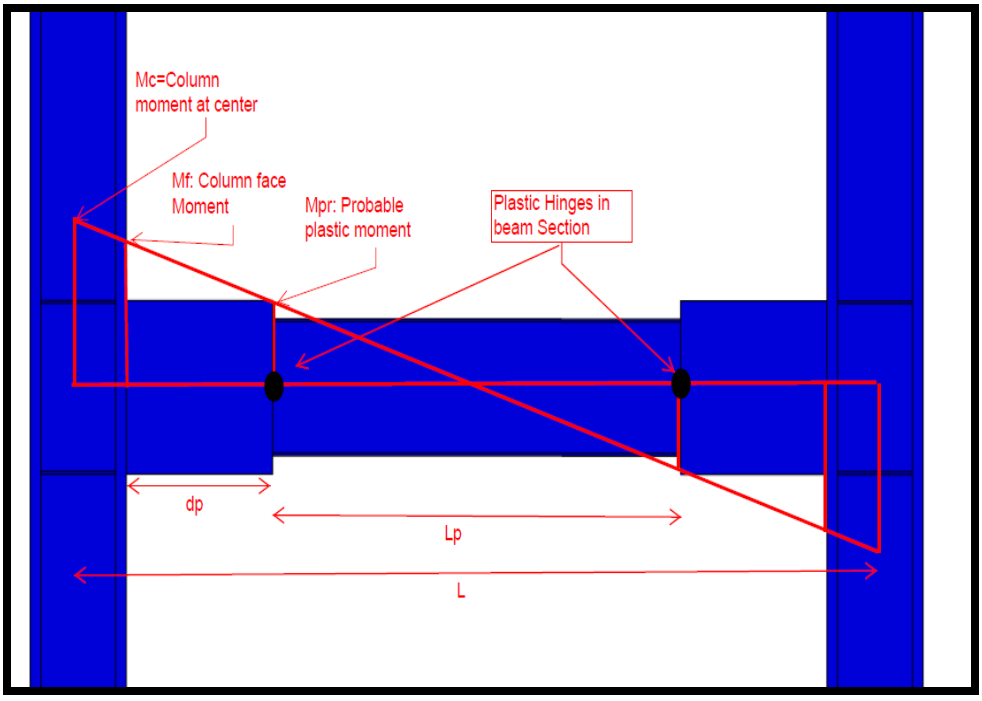

Figure 2-7: Moment Distribution Based on Plastic Demand in Beam Section

2-In order to determine the required size of the stub section, moment demand on the column face where the beam is joined to the column, is found by using equation (2.3):

$$M_f = M_{pr} + V_{pr} d_p \qquad (2.3)$$

where V_{pr} represents shear force resulting from plastic deformation in the beam, and d_p is the distance between the plastic hinge and the column face. V_{pr} (effect of gravity loading ignored because it is a comparatively small value) is given by equation (2.4):

$$V_{pr} = \frac{2M_{pr}}{L_p} \qquad (2.4)$$

where L_p is the distance between the plastic hinges in the beam section.

3-The welded interfaces of beams to columns are capacity protected regions. Therefore, any inelastic action caused by bending moment demand at these locations should be prevented. The section size of the stub is selected such that demand induced by seismic activity will not cause any yielding; in other words, the topmost fiber of the stub will not reach its yielding strength. Based on this reasoning, required section modulus can be found with equation (2.5):

$$S_x = \frac{M_f}{F_y} \qquad (2.5)$$

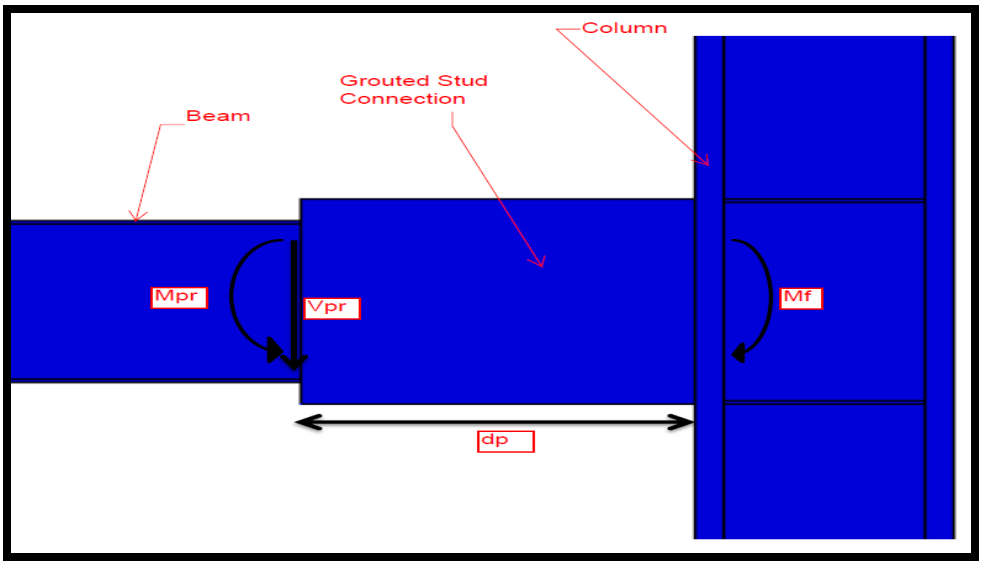

Figure 2-8: Forces Acting on Connection

4-In order to determine the necessary number of shear studs, a simple design assumption is made based on an adopted strength model for the shear studs. The assumption is that the total nominal strength of shear studs located on the flange faces of the beam section should be adequate for allowing the beam section to develop its full plastic moment capacity. In addition, the number of shear studs can be associated with stub length. In order to associate the number of shear studs with stub length, tension or compression forces, which are found by dividing column face moment by the height of the beam section, are divided by the nominal capacity of one shear stud. Furthermore, the number of shear studs required by the plastic moment of the beam should be smaller than the number of shear studs required by the column face moment. Put another way, the number of shear studs that resist forces produced by the column face moment should be more than the number of shear studs that resist forces produced by the plastic moment of that beam. As a result, length of stub will be

limited to a certain value to accommodate the number of shear studs to resist the plastic beam moment. In this study, the maximum length of the stub is limited to the height of the beam employed. Equation (2.6) produces find the needed number of shear studs:

$$N_{sc} = \frac{\frac{M_f}{(d_b - t_f)}}{Q_n} \geq \frac{\frac{M_{pr}}{(d_b - t_f)}}{Q_n} \qquad (2.6)$$

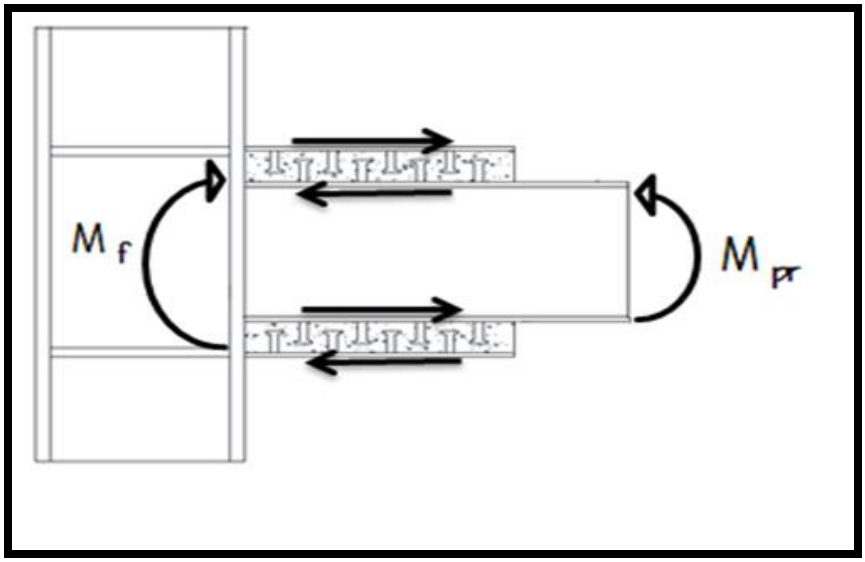

Figure 2-9: Forces Acting on Shear Studs

In this equation, N_{sc} represents the required number of shear studs; d_b is the beam depth; t_f is the beam flange thickness; and Q_n is shear stud nominal strength. Similar to the study conducted by Fulmer et al. (2012), shear stud nominal strength is based on the *AISC*

Seismic Provision (2010) model. The force produced by one shear stud can be found by equation (2.7):

$$Q_n = 0.5A_{sc}\sqrt{f_c^{'}E_c} \le A_{sc}F_u \qquad (2.7)$$

In this equation, A_{sc} represents the shear stud shank area; $f_c^{'}$ is the compressive strength of the grout; E_c is Young's Modulus of grout; and F_u is tensile strength of a shear stud.

4-Design of other parts such as columns, stiffener plates and panel zones can be done by following *AISC seismic provision* (2010) design criteria.

2.6.Shear Stud Location

The location of shear studs is determined based on the tension and compression forces developed by bending action. As is expected, maximum tension and compression forces develop at the outermost fiber of the beam section. Therefore, in order to take full advantage of the capacity of the shear studs included in the connection, the shear studs are located far from the neutral axis of the beam. Since bending of the beam is governing behavior caused by the applied loading, and axial forces are not large in beam sections, installment of shear studs near the neutral axis of the beam web will not provide significant advantage. Four different shear stud configurations, which are based on this reasoning and given beam sizes, are employed in this study. Among the suggested shear stud configurations, some number of shear studs is located on the beam web, as far removed from the neutral axis as practical, for one of the suggested configurations. In order to avoid causing stress concentration at the interface of the beam web and beam flange, the shear studs are located below the flange, where the distance is taken equal to k_{des}, the design value

of given beam section. The two beam sizes used in this study are W24x62 and W30x108. The length of the stub and the number of shear studs required for each beam determines the location of the shear studs. Shear studs are located such that a shear stud on a beam can be followed by another shear stud on a stub, as shown in Figure 2.10.

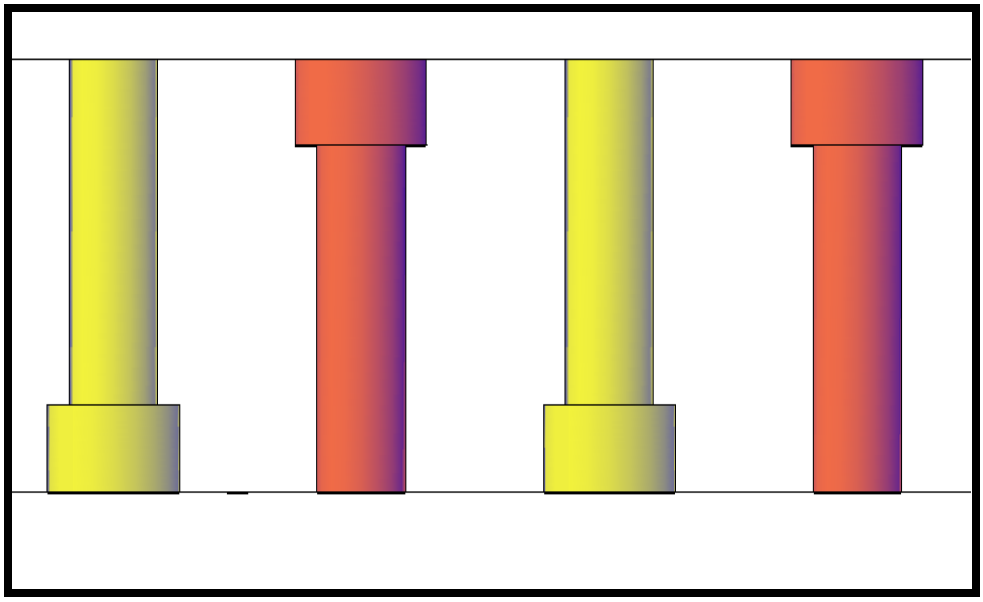

Figure 2-10: Shear Stud Positions

For beam section W24x62, four different configurations are shown in Figure 2.11. Blue circles represent shear studs on the beam and red circles represent shear studs on the stub. In the first configuration, the shear studs are located near the edge of the flange of the beam. Similarly, in the 4th configuration, half of the shear studs are located near the edge of the beam flange, and the remaining shear studs are located on the web near the flange faces.

The other two configurations, configurations 2 and 3, are slightly different; unlike configurations 1 and 4, the shear studs are distributed on the entire surface area of the beam flanges. The reason for this distribution of shear studs on the surface is to increase the amount of grout surrounding shear studs and to reduce stress in the surrounding grout.

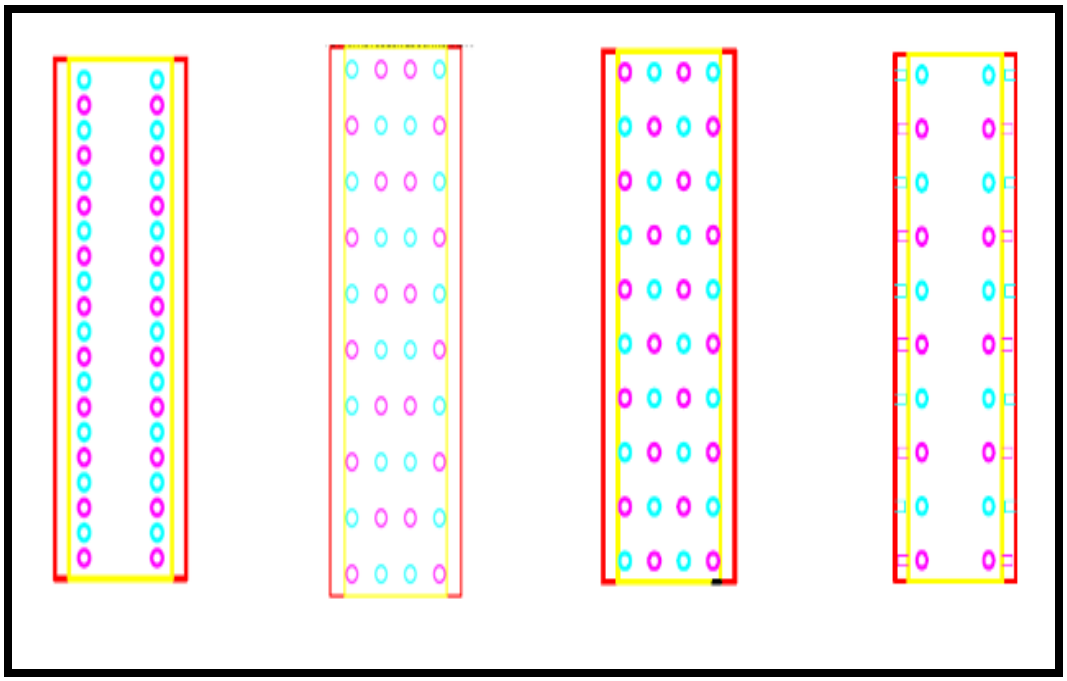

Figure 2-11: Shear Stud Configurations for Beam W24x62 (1st, 2nd, 3rd, 4th left to right)

For beam section W30x108, there is a slight difference in configuration 1. Instead of locating the shear studs in two lines, the shear studs are located in three lines to increase the surrounding grout, as shown in Figure 2.12. Additionally, stub length is not adequate for accommodating all shear studs in two lines.

In this study, the chosen diameter of shear studs is 3/4 in for all beam sizes. A parametric study on size of the shear studs will not be conducted. It is assumed that shear stud diameter will not have a significant effect on behavior of a beam section since behavior is dominated by a beam section. In addition, the strength model for determining the required shear stud number is dependent on the shear stud shank area because a change in shear stud shank diameter will cause a change in the required number of shear studs. Change in the required number of shear studs can cause difficulties in locating shear studs due to limitations on the stub length for a given beam section. Moreover, for different shear stud diameters, a change in the number may require a change in configuration. As a result, shear stud diameter is not taken as a parameter in this study.

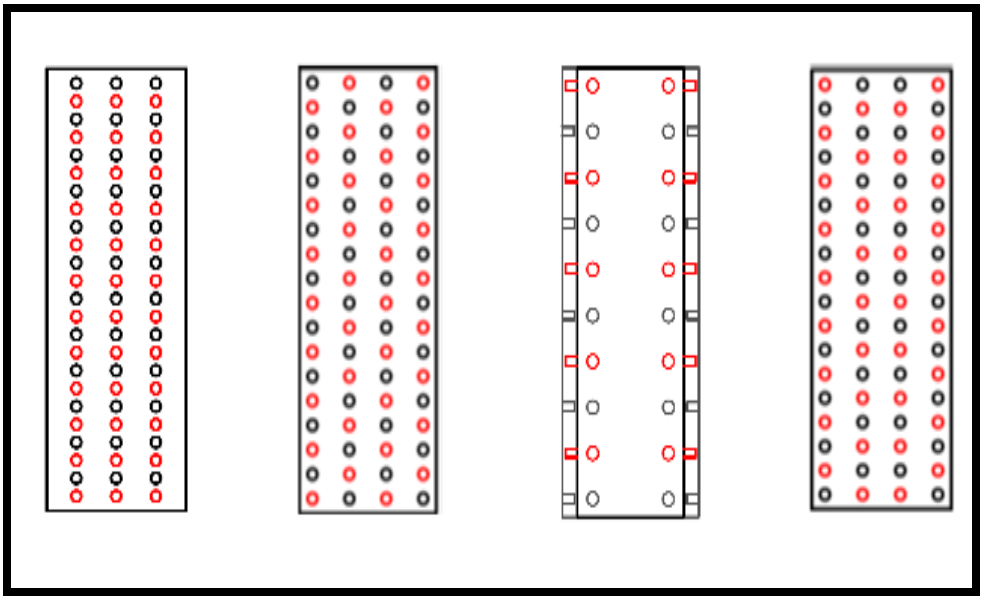

Figure 2-12: Shear Stud Configuration for Beam W30x108 (1st, 2nd, 3rd, 4th left to right)

CHAPTER 3

3. Literature Review

3.1.Overview

In this chapter, the focus will be on studies that incorporate different methods to connect beams to columns, to relocate the plastic action of a beam distant from the face of a column. Since the grouted shear stud connection is a novel connection type only applied to steel bridge bents (Fulmer et al., 2012), no application of grouted shear stud connection in steel moment frame connections has been discovered. On the other hand, research on different methods that provide an understanding of beam to column connections such as side plate moment connections (Deylami and Ashraf, 2004), flange plate moment connections (Gholami et al., 2013) and tapered beam moment connections (Chen and Lin, 2013) are summarized to provide insight into strengthening methods that allow relocation of plastic deformation far from the critical weld region and generate ductile beam to column connections.

3.2.Study by Gholami et al. (2013)

In this research, the authors essentially focused on seismic behavior of the connection where plates were used to connect an I-beam flange to a box column flange face by considering the effects of different parameters such as size of the flange plate and weld configuration. Details about experimentally and analytically studied moment connections are shown in Figure 3.1 where beams were not welded to columns. It can be seen from Figure 3.1 that transfer of forces, which are created by beam bending action, takes place through flange plates. Construction of this connection essentially depends on field welding. Three

samples with flange plates of different lengths and thicknesses, as well as various weld arrangements, given in Table 3.1, were tested. To avoid probable effects of beams and columns on performance of connections, the same size box column (built-up 400x400x20x20) and beam section (I-380x200x8x12) were used for all specimens.

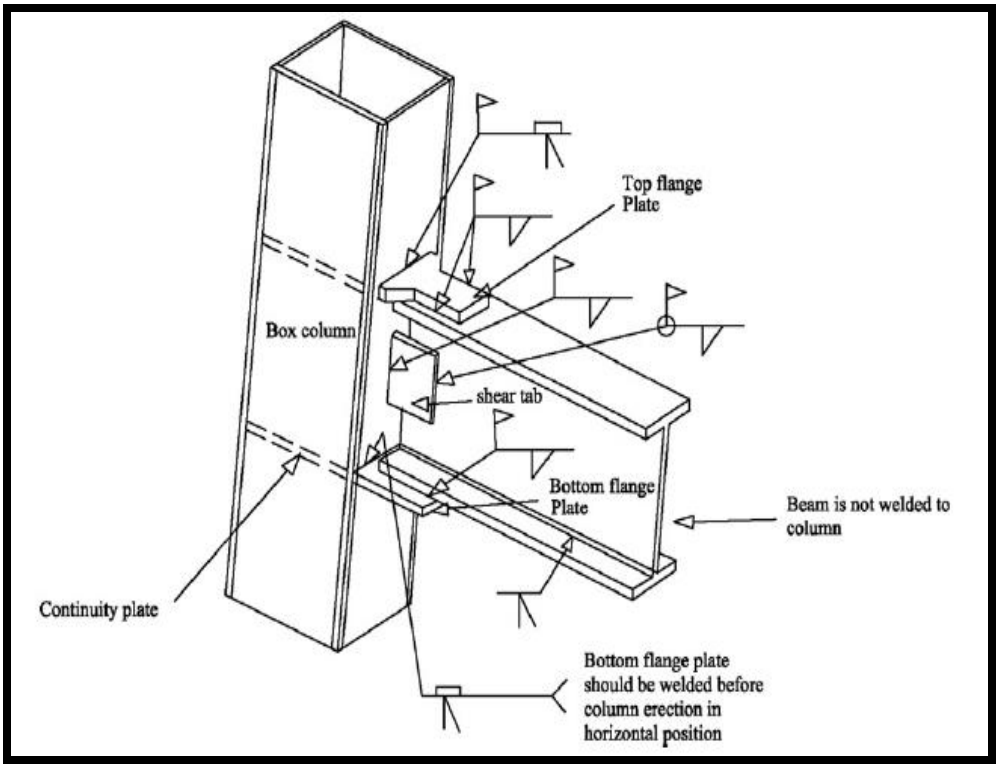

Figure 3-1: Details of Connections Studied (from Gholami et al., 2013)

Top and bottom flange plates were additionally welded to the beam from their unrestrained edge for specimen LF50-T. All specimens were loaded at the tip of the beams with the cyclic loading protocol suggested by AISC Seismic Provision (2005). Beams were loaded up to tip displacement corresponding to a 5% story drift angle.

Table 3-1: Details of Tested Samples (from Gholami et al., 2013)

Summary information on specimens.

Specimen	Flange-plate length	Top flange-plate thickness	Bottom flange-plate thickness	Longitudinal fillet weld	Transverse fillet weld	$M_{j,cap}/M_{j,dem}$ at column face
LF30	300	20	20	10	-	1.16
LF50	500	25	20	10	-	1.04
LF50-T	500	25	20	8	8	1.04

Note: All dimensions in mm.

Examination of experimental outcomes showed that the connections tested yielded similar plastic action shown in Figure 3.3, such that beam local buckling took place close to the tip of the flange plate. The moment generated at the column face at a 4% story drift was not less than 80% of nominal moment capacity of that beam. Consequently, the requirement of AISC seismic provision was satisfied for all connections. Moreover, 3D finite element models of each test specimen were produced by finite element software ABAQUS to enhance understanding of connection behavior. Under the same loading conditions, experimental results of all three specimens and their corresponding finite element models yielded similar hysteretic curves shown in Figure 3.2.

Experiments and finite element models showed that inducing plastic action into the intended region of beams without experiencing any failure at connections, which might affect ductility of connections, was satisfied with these three different configurations of flange plate connections. In addition, it was noted that when longer plates were used to connect beam flanges to columns, the welded interfaces between the flanges and the web of those beams

experienced rupture due to increased strain demand. In order to prevent this rupture, it was recommended that the length of flange plates used should be limited to the shortest reasonable length.

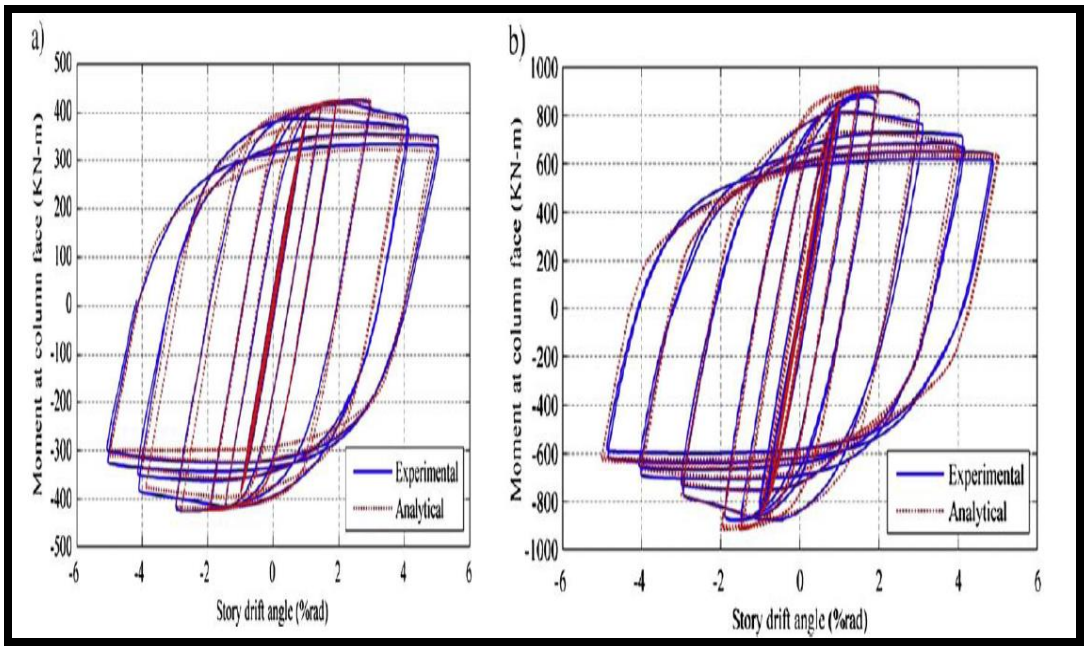

Figure 3-2: Finite Element Analysis and Experimental Comparison of a) LF30 and b) LF50 (from Gholami et al., 2013)

Figure 3-3: Plastic Deformation in the Beam (from Gholami et al., 2013)

3.3.Study by Chen and Lin (2013)

Chen and Lin (2013) enhanced a method for moment connections by gradually increasing the width of beam flanges at the vicinity column flange faces to increase connection ductility capacity, as shown in Figure 3.4. Both experimental and finite element modeling studies were conducted to interpret how connections behave under cyclic loading. Gradually increasing beam flange width close to column flange faces was intended to diminish seismically induced demand at the welded region. Furthermore, in order to prevent sudden change in geometry that may cause stress accumulation in the critical weld region, a curved part was added to efficiently transmit forces.

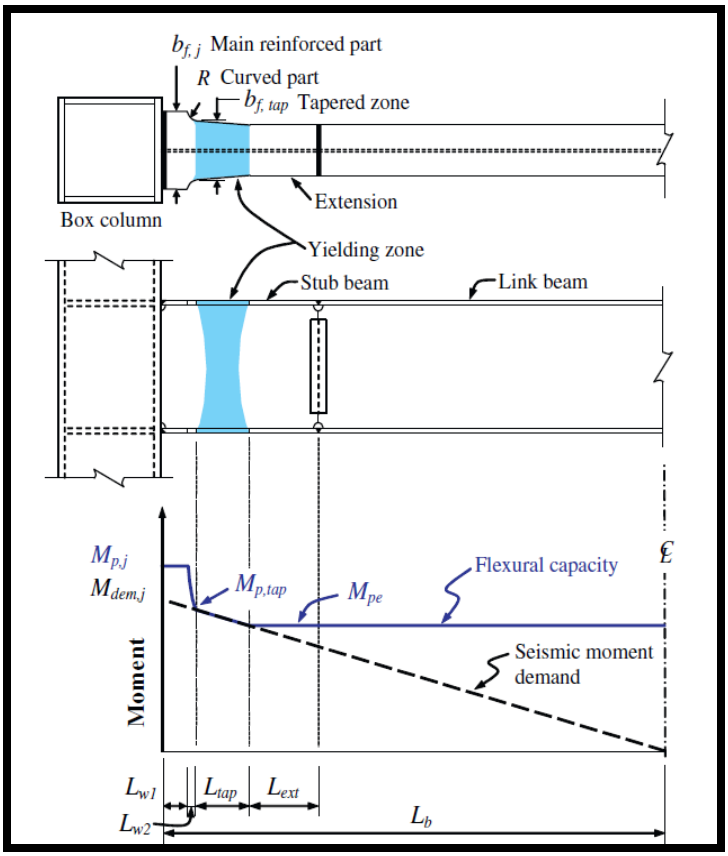

Figure 3-4: Design Configuration of Connection (Chen and Lin, 2013)

Two parameters were chosen with the aim of controlling behavior of the connections. The first parameter was the length of the tapered zone (L_{tap}). The second one was reinforcement ratio (β_j) defined as moment capacity of beams at column faces divided by moment demand induced by seismic event at column faces. Other parameters as seen in Figure 3.4 such as L_{w1}, L_{w2} were found to have less impact on behavior of connections; as a result, they were assumed to be constant. Table 3.2 gives tested specimen details in terms of reinforcement ratio and tapered zone length.

Table 3-2: Details for Specimens Tested (Chen and Lin, 2013)

Summary of test specimens.

Specimen designation	Reinforcement ratio β_j	Tapered zone length L_{tap} ($\times d_b$)	Connection details
PK	–	–	Column-tree connection, beam web welded
W1-L05	1.20	0.5	Column-tree connection, beam web welded
W1-L03	1.20	0.3	
W2-L03	1.10	0.3	
W3-L03	1.05	0.3	
B1-L03	1.20	0.3	Pre-Northridge connection, web-bolted flange-welded
B2-L03	1.10	0.3	

ASTM A572 Grade 50 steel material property was adopted for beams and columns used in this experimental program. 550x550x28x28 box columns and H700x300x13x24 beam sections were used for all specimens. Based on the given details in Table 3.2, five different beam-to-column connections were prepared with dimensions given in Figure 3.5.

Beam to column connections were loaded at the beam tip up to associated displacement with a 5% story drift angle, based on the AISC seismic provision suggested loading sequence for testing connection reliability. All modified welded connections, with the exception of the connection named W3-L03, performed in similar ways under given cyclic loading without any damage. For W3-L03, at a story drift of 4%, rupture was observed at the beam flange near the critical weld region. Rupture in the W3-L03 showed that a 1.05 reinforcement ratio did not provide adequate strength. Amounts of absorbed energy are shown in Figure 3.6; notably, all connections absorbed more energy than the Pre-Kobe connection.

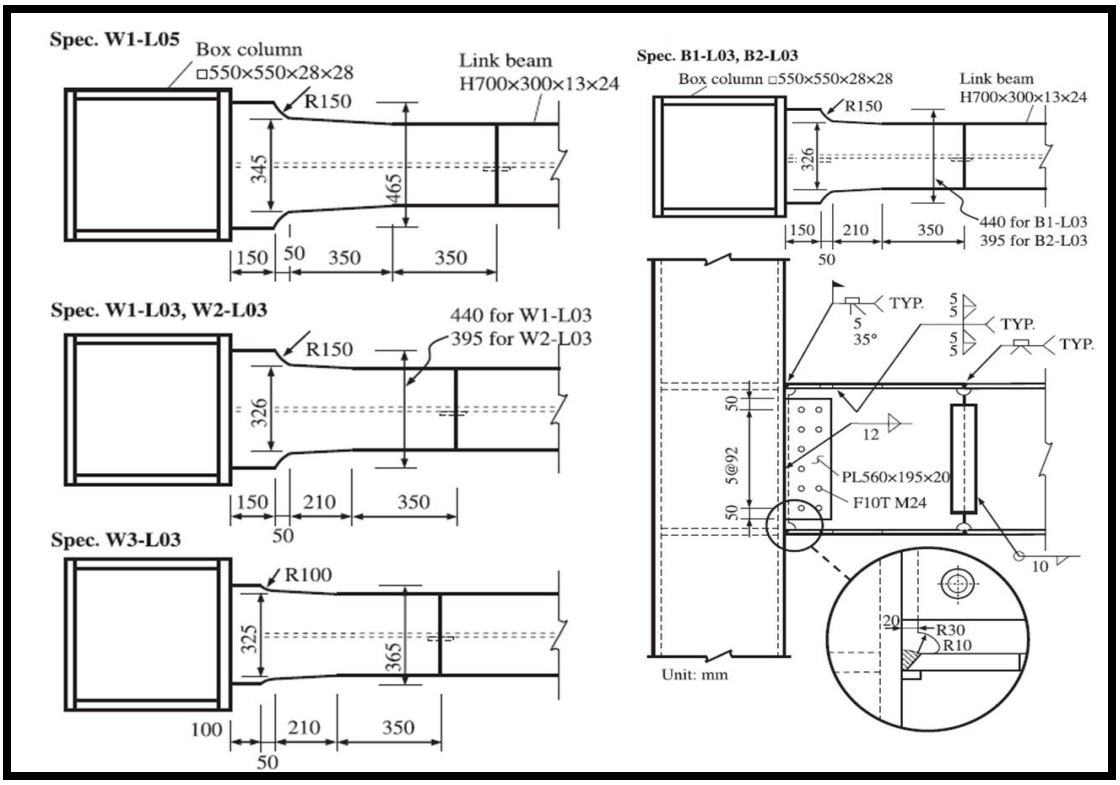

Figure 3-5: Details for Experimented Connections (Chen and Lin, 2013)

In the study, experimentally tested connections and also many connections with different design parameters, such as β_j and L_{tap}, were modeled and analyzed. For specimen W1-L03, force-displacement hysteresis curves of experiment and finite element models produced similar hysteretic behavior shown in Figure 3.7. As a result, finite element models were validated. In comparing performance of models with different design parameters, equivalent plastic strain (PEEQ) index, which is the ratio of plastic strain to yield strain of the material, was obtained at the welded regions through beam flange width near to welded interface of beams and columns, shown in Figure 3.8.

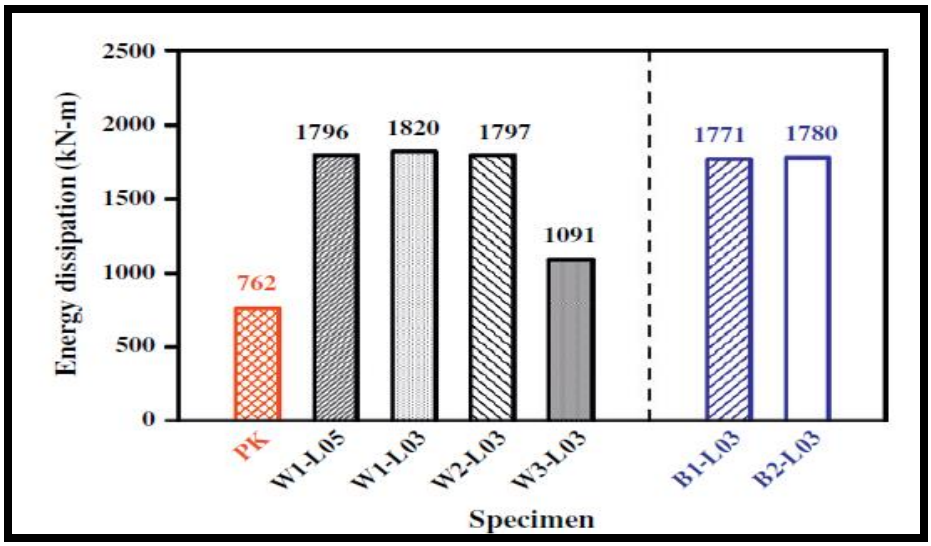

Figure 3-6: Comparison of Absorbed Energy (Chen and Lin, 2013)

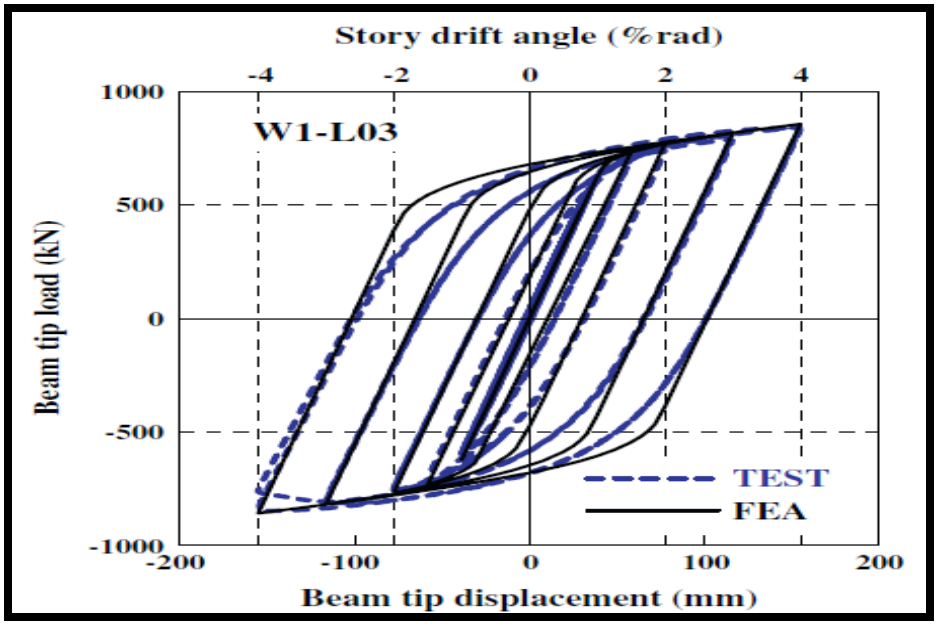

Figure 3-7: Comparison of finite element model and experiment of W1-L03 (Chen and Lin, 2013)

Figure 3.8 clearly shows that tapered beam connections lowered strain demand at the welded interface of beams and columns, and generated a stronger connection. Thus, increasing flange width near to column faces to force the plastic hinge into the tapered zone was confirmed.

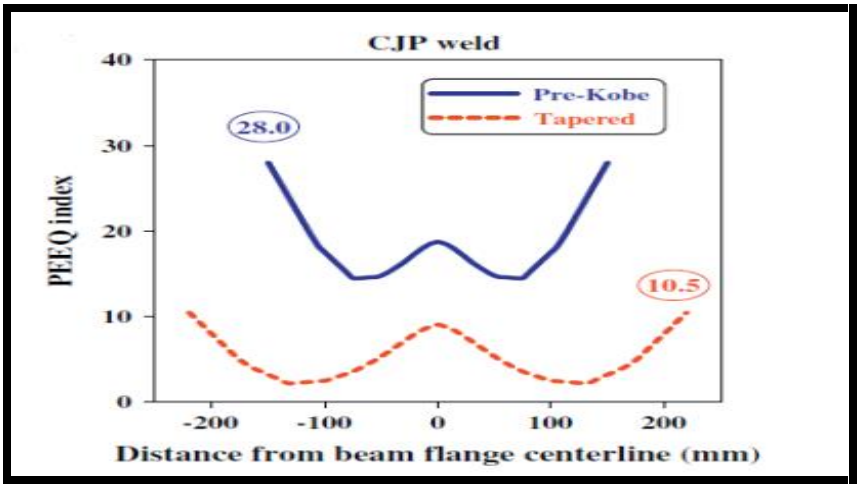

Figure 3-8: Equivalent Plastic Strain (PEEQ) Index at Groove Weld (Chen and Lin, 2013)

3.4.Study by Deylami and Ashraf (2004)

In this study, the researchers analytically explored how different geometric properties of plates, which were used to construct side plate connections, have an influence on the performance of the connection itself under monotonic and cyclic loading. The side plate connection was first introduced by Houghton (1998) to eliminate concerns generated by the Northridge. The idea was to connect beams to columns with side and flange plates as shown

in Figure 3.9. Welds between columns and beams were eliminated in this connection; therefore, forces were carried by plates connecting beams to columns.

In the study, eight finite element models, which have various beam and column sections, were taken into account with varying geometric properties of connecting plates. Moreover, connections designed with the same beam and column sections with side plates of various thicknesses, were also analyzed to investigate the influence of plate thicknesses on performance. The model details given in Table 3.3 and Table 3.4 are the vertical plate thickness utilized to resist shear, the plate thickness of the top and bottom flange of connections (c), and the plate thickness used on side (T).

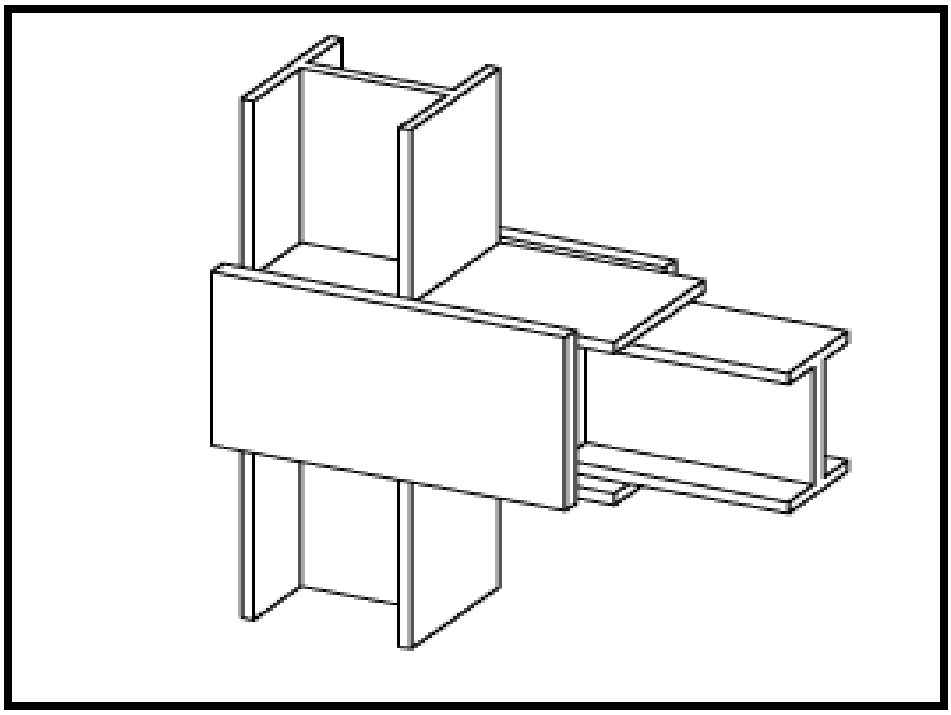

Figure 3-9: Side Plate Connection (from Deylami and Ashraf, 2004)

Table 3-3: Geometric Aspects of Models (from Deylami and Ashraf, 2004)

Model Name	Column Profile	Beam Profile	T (mm)	s (mm)	c (mm)
SPT1-1	IPB300	IPE300	15	10	10
SPT1-2	IPB300	IPE400	20	10	14
SPT1-3	IPB300	IPE500	25	10	15
SPT1-4	IPB300	IPE600	25	12	20
SPT1-5	IPB400	IPE300	15	10	10
SPT1-6	IPB400	IPE400	20	10	14
SPT1-7	IPB400	IPE500	25	10	15
SPT1-8	IPB400	IPE600	25	12	20

Table 3-4: Connections with Different Side Plate Thicknesses (from Deylami and Ashraf, 2004)

Model Name	Column Profile	Beam Profile	T (mm)	s (mm)	c (mm)
SPT1-1	IPB300	IPE300	15	10	10
SPT1-1a	IPB300	IPE300	10	10	10
SPT1-1b	IPB300	IPE300	20	10	10
SPT1-1c	IPB300	IPE300	25	10	10

Under monotonic loading, the finite element models of all connections had plastic hinging in the beam sections, as shown in Figure 3.11. Here, panel zones remained in the elastic range with the exception of specimen SPT-4, which had a column section much weaker than the beam section. As a result of the weaker column, the column web developed plastic deformation. For all models excluding the model SPT-4, the impact of size of columns on plastic behavior was insignificant because of the fact that hinging was successfully located in the beams.

Cyclic loading was applied to models given in Table 3.4. The study showed that when a thinner plate was used as a side plate, a large amount of plastic deformation took place in the side plate as shown in Figure 3.11. The connection with thicker side plates developed a plastic rotation twice as large as the connection with thinner side plates, as shown in Figure 3.10.

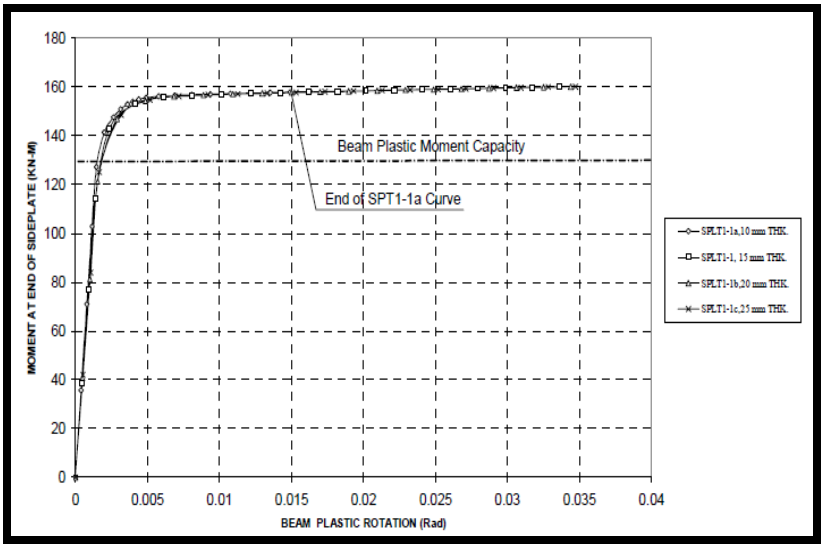

Figure 3-10: Moment-Rotation Curve for SPT1 Series (from Deylami and Ashraf, 2004)

Without including model SPT1-4, all side plate connections shown in Tables 3.3 and 3.4 had moment strengths exceeding those of the connected beam sections. The amount of dissipated energy by side plate connections, after repositioning plastic deformation into beams, revealed that side plate connection provides significant ductile capacity.

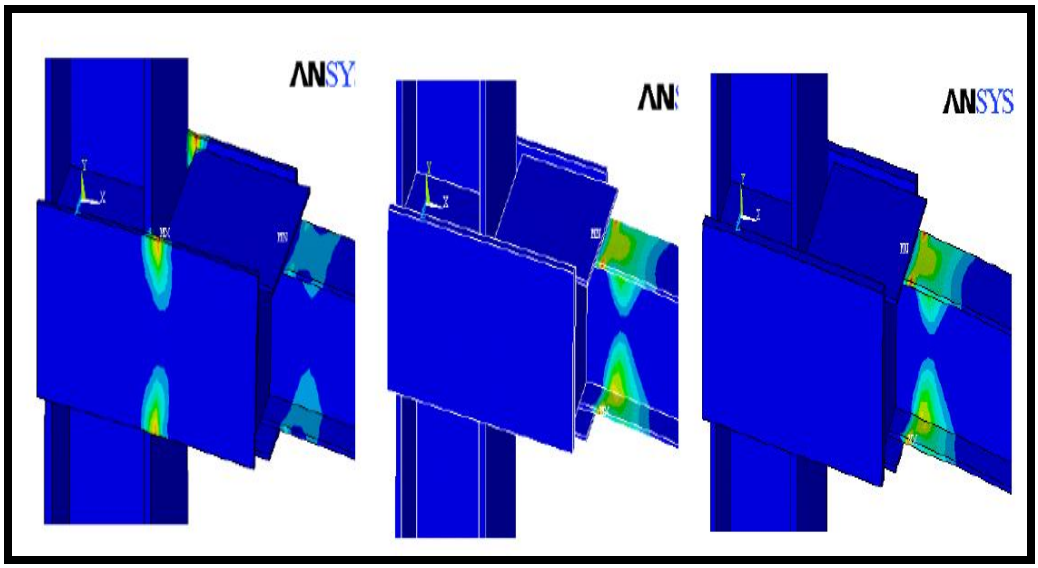

Figure 3-11: Plastic Deformation in Connection with Different Side Plate Thickness (10mm, 15mm, 25mm, respectively) (from Deylami and Ashraf, 2004)

CHAPTER 4

4. Modeling of Grouted Shear Stud Beam to Column Connections

4.1.Overview

Numerical modeling of structural systems gives engineers a better understanding of structural behavior and provides an opportunity to reduce the cost of generating effective design scenarios. Finite element modeling of structural systems is a computational modeling technique which has broad uses in the field of structural engineering. Since numerical models are representations of real structures, they can be a very effective way to conduct preliminary analyses in order to determine parameters, which may influence an intended design, before conducting an experimental program.

This chapter will focus on the detailed finite element modeling of grouted shear stud (GSS) beam to column connections by using ABAQUS 6.13. Overall, the modeling process does not change substantially from one connection type to another; therefore, a similar process can be followed for other possible applications of grouted shear stud connections in moment frames. In this study, many aspects of finite element models, such as material models of each component, element types, model geometry, and modeling assumption of shear studs will be discussed. In order to provide greater insight into the grouted shear stud beam to column connection, 3D finite element models were developed including both material and geometric nonlinearity except for the grout material.

This Chapter is organized as follows: first, section 4.2 discusses element type and meshing of models; section 4.3 incorporates a discussion of boundary conditions and loading; section 4.4 describes a modeling assumption of shear studs; section 4.5 discusses the

material models adopted in this study; section 4.6 discusses modeling of Pre-Northridge connections; section 4.7 discusses constraints and contacts adopted for modeling of structural systems; and finally, section 4.8 discusses indices for evaluating behavior of connections.

4.2.Element Type and Meshing

In order to better predict the behavior and decrease computational time of analysis, linear solid 8 node brick elements called C3D8 (ABAQUS 2013) were used for all components in the connection such as the beam, column, stub, and grout.

The meshing process of finite element models is one of the key aspects that may generate undesirable results if the meshes are not created adequately based on the element type. The beam to column connection, as shown in Figure 4.2, does not have complicated geometry that could generate difficulties for mesh matching. However, connected solid parts, which do not have similar dimensions, require partitioning. Partition tools offered by ABAQUS (2013) can be used to produce partitions that may help to generate a simpler geometry to match the mesh generated on different faces of connected solid members. As shown in Figure 4.1, mesh fineness is changed from coarse to fine to better predict behavior and reduce computational efforts of modeling where stress and strain gradients vary significantly. The structured mesh technique was used with the help of the partitioning tool to generate a smooth transition. The aspect ratio of the mesh was intended to become close to 1.0 near the welded region.

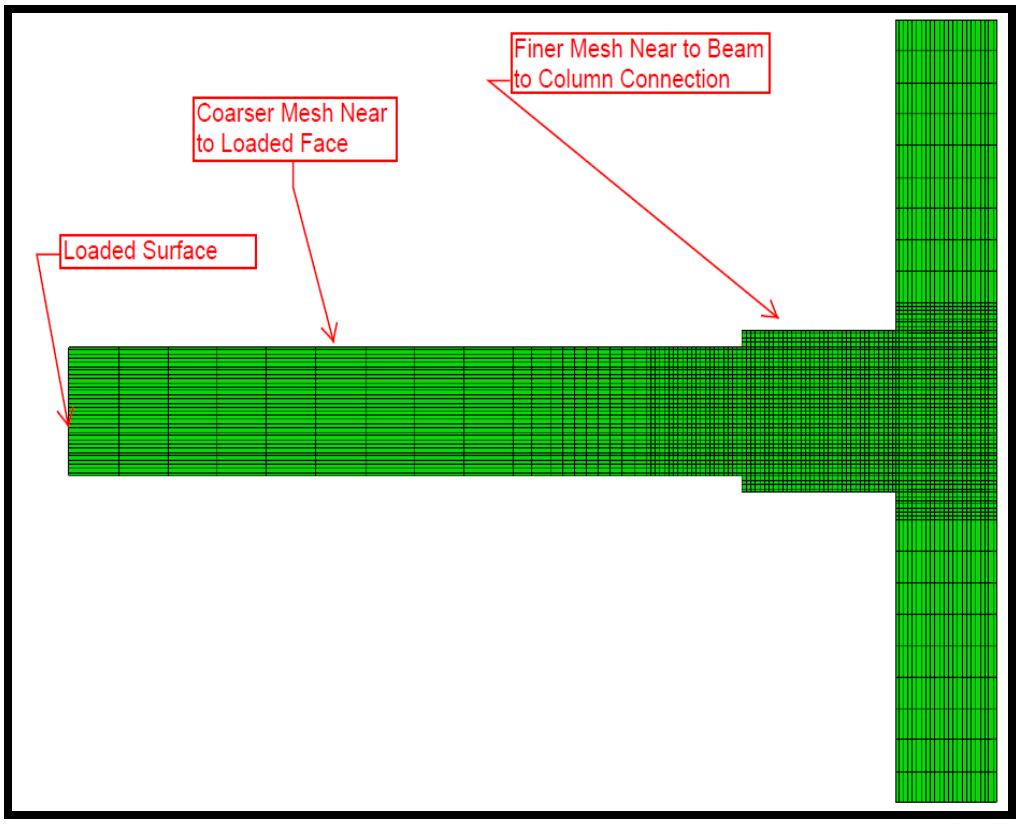

Figure 4-1: Mesh Quality

As can be seen in Figure 4.2, the column member was partitioned to employ the structured mesh technique, as well as some lengths below and above the panel zone. Instead of having a smooth transition of the mesh from the top and bottom end to the panel zone, the column is assumed to have coarser mesh near to a certain distance (6 inches) above and below the panel zone; this does not have a significant effect on the results mainly because the interaction between the stub and column occurs at the column flange face. Furthermore, the column is large enough to prevent any effect caused by panel zone yielding.

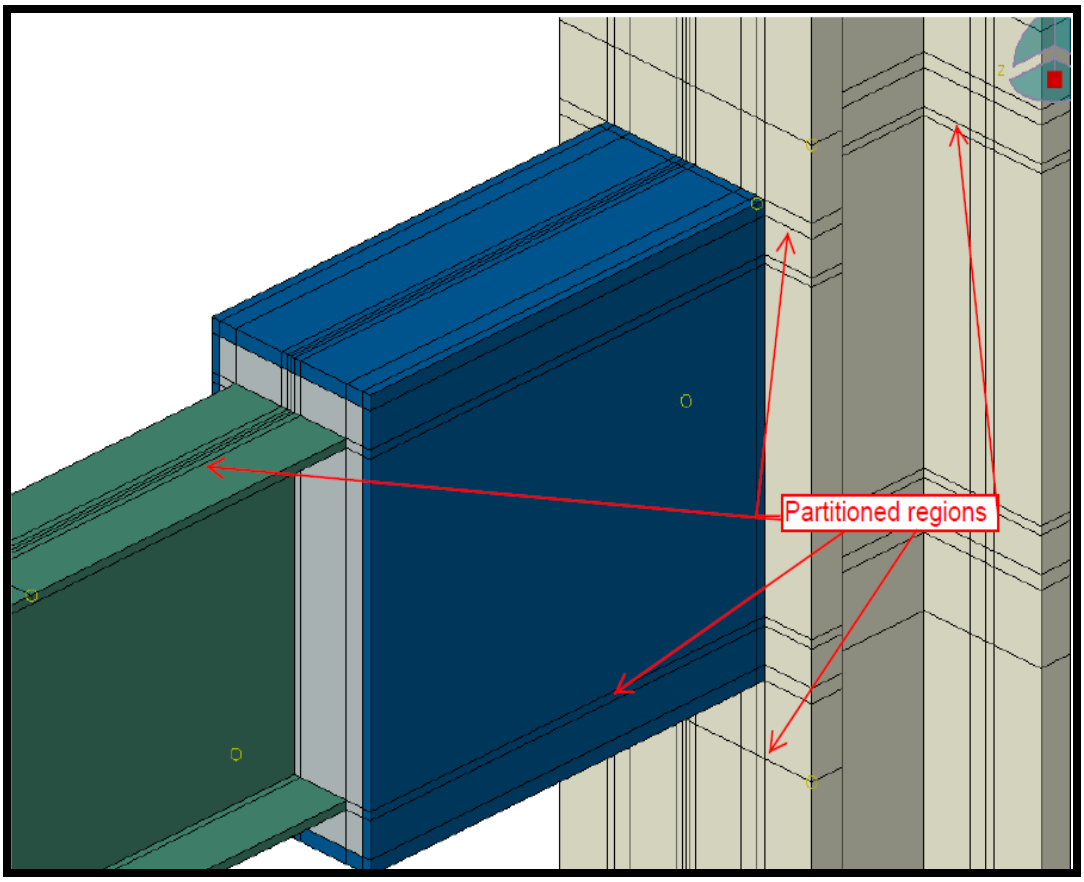

Figure 4-2: Geometry of Connection and Partitioned Regions

A case study of a beam section W24x62 was conducted to understand the effect of meshing on the results. As stated before, the mesh close to the welded region was intended to have an aspect ratio close to 1.0. For evaluating the effect of the mesh on behavior, varying edge lengths of elements was taken into account. The largest edge lengths of the element were 1, 0.85, 0.75 and 0.65 inches. Figure 4.3 shows that when the length of the largest edge of the element was changed, local buckling behavior of the beam elements show dissimilarities.

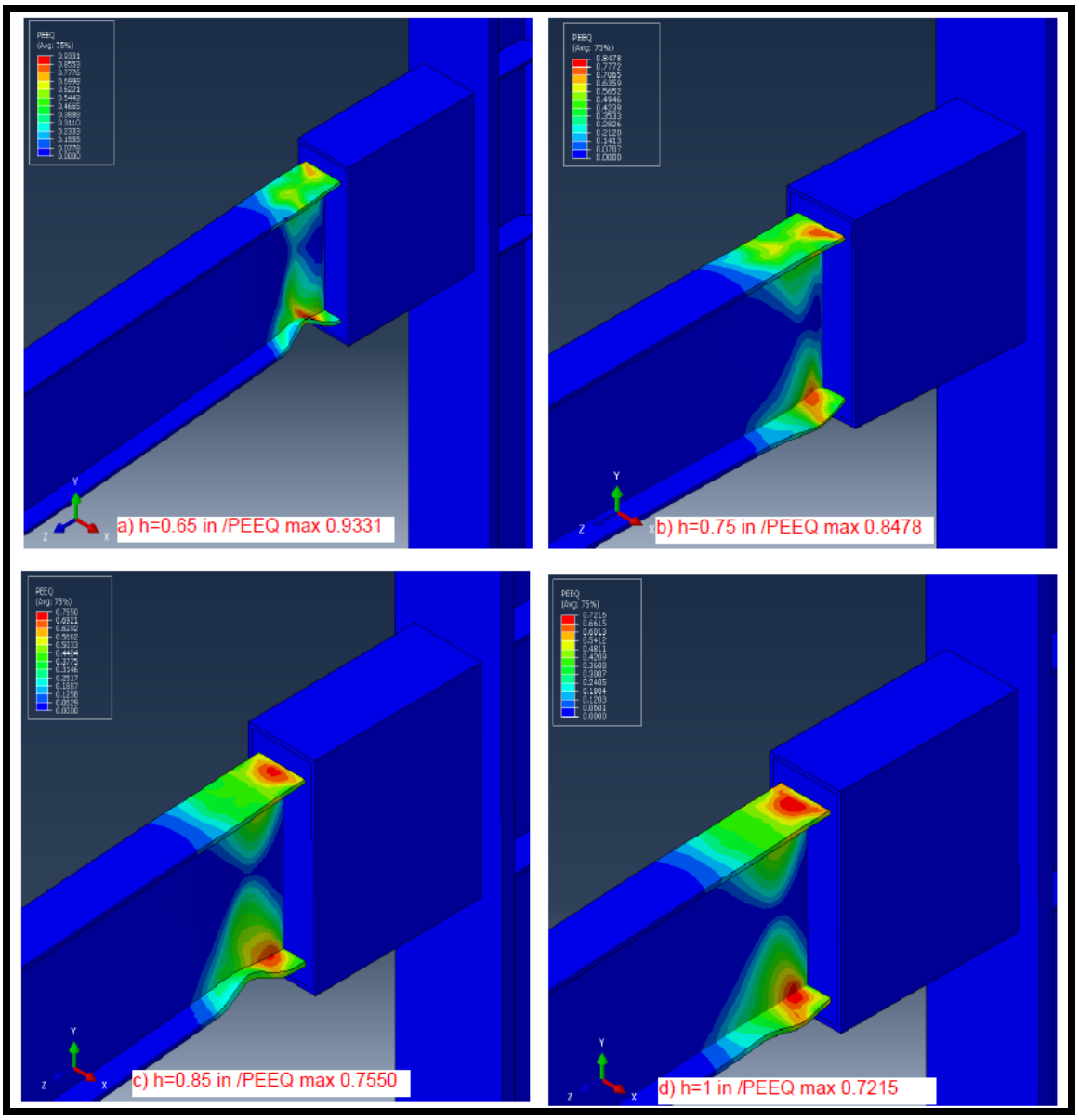

Figure 4-3: Effect of Mesh refinement on Buckling Behavior and Plastic Deformation

A change in local buckling behavior leads to a change in the hysteresis loops and maximum equivalent plastic strain (PEEQ). It can be seen in Figure 4.4 that when the mesh was refined from a size of 0.75 inches to 0.65 inches, the beam experiences additional

strength degradation at negative cycles of 0.05 rad story drift. However, the overall behavior of the models with mesh size of 0.75 inches and 0.65 inches was similar.

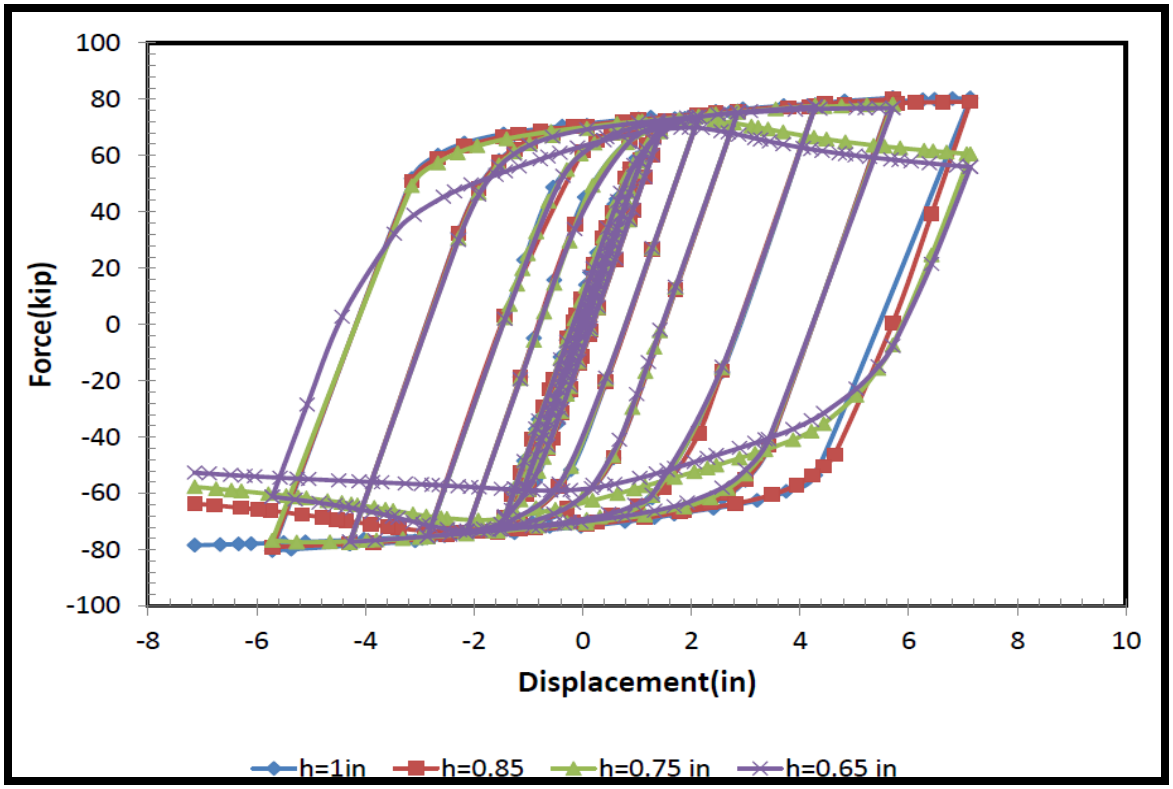

Figure 4-4**:** Force-Displacement Curves with Different Mesh Sizes

The computational cost of each model with the same computer capacity is shown in Figure 4.5. As shown in Figure 4.5, refining the mesh increases the demand for computational capacity. While mesh sizes of h=1 inch, h=0.85 inches and h=0.75 inches required similar amounts of time (about 5-7 hours), the relatively refined mesh size of h=0.65 inches requires 16 hours. Due to computer capacity limitations, the study cannot be

continued for lengths smaller than 0.65 inches. Therefore, the largest edge of an element was taken as 0.75 inches throughout this study.

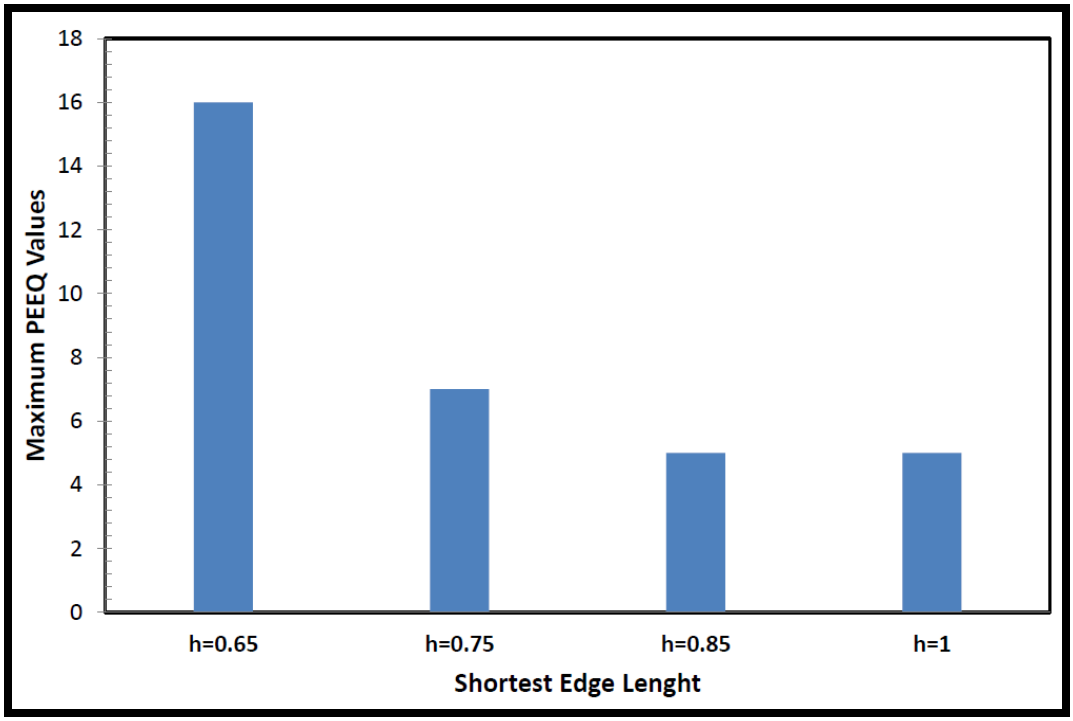

Figure 4-5: Required Time vs. Mesh Size

4.3.Boundary Conditions, Geometry and Loading

A likely setup for conducting an experimental program is shown in Figure 4.6. In this configuration, the movement of the bottom part of the column is restrained in the Z and Y directions. The top of the column is only supported in the Y direction. However, the boundary conditions adopted for modeling purposes are shown in Figure 4.7, where the top and bottom surfaces of the column are modeled as pinned supports. For a similar

experimental set up shown in Figure 4.6, El-Twail et al. (1998) took different configurations of boundary conditions into account. They found a 6% variation in tip displacement for different boundary conditions modeled.

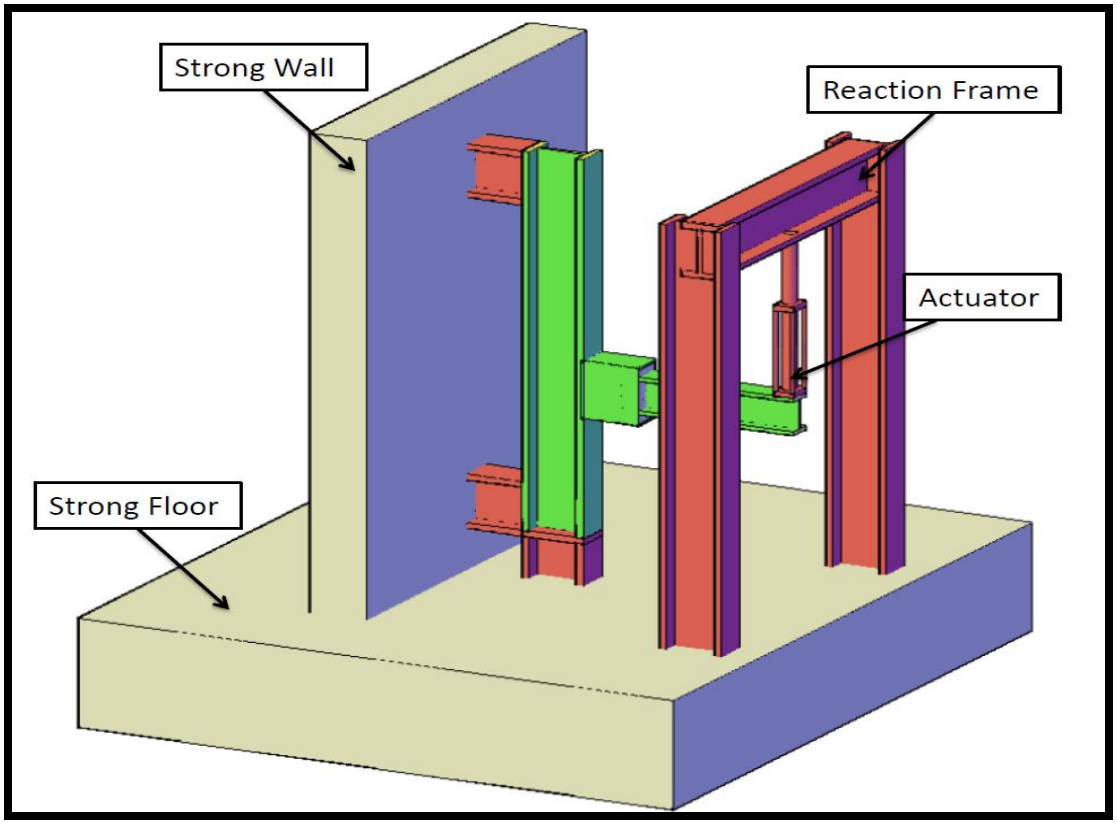

Figure 4-6: Experimental Setup

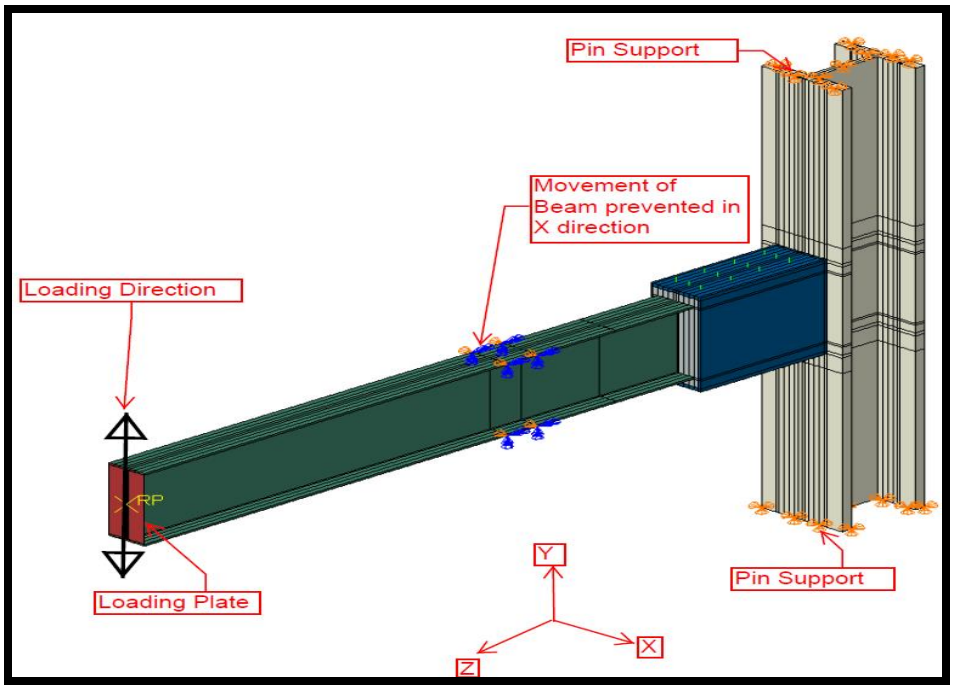

Figure 4-7: Boundary Conditions

As a result, the given boundary conditions are assumed to be appropriate for finite element modeling, and further investigation of the effects of different boundary conditions will not be studied in this research. Furthermore, for reaching the fully plastic moment (M_p) capacity of the beam, the top and bottom flanges of the beam member are supported against movement in X direction at a specific distance from the stub open end. Position of the support to prevent lateral movement of the beam in the X direction can be found with the equation (4.1) given by AISC 360-10(2010) as follows:

$$L_p = 1.76 r_y \sqrt{E_s / F_y} \qquad (4.1)$$

In this equation, L_p is the braced length required for achieving full moment capacity of beam, r_y is the radius of gyration in the weak axis, E_s is the Young's modulus and F_y is the

yield strength of the beam. Tip displacements are applied vertically to the reference Point (RP) shown in Figure 4.7 where an infinitely rigid loading plate is attached to the beam surface to move each corner of the beam equally. AISC Seismic Provisions (2010) suggests a cyclic loading protocol for qualifying beam to column connections. Tip displacements can be calculated from story drift angle given in Table 4.1.

Cycles can be continued after a 0.04 rad story drift angle with 2 additional cycles of ±0.01 rad for each increment. Story drift angle can be transformed to tip displacement by the equation (4.2) given as follows:

$$\theta = \frac{d_t}{L} \qquad (4.2)$$

In this equation, L is the length from the column center line to the beam tip, θ is the story drift angle and d_t is the tip displacement in the direction of the given rotation of the end of the beam. Beam and column heights were taken as 135 inches and 145 inches, respectively. For the given dimensions of beams and columns, tip displacements for beam section W24x62 and W30x108 were calculated. Tip displacements were calculated up to a 5 % rad story drift angle. Tip displacements for given beam sections are shown in Appendix A.

Table 4-1: Loading Sequence

Step	Cycle	Story Drift Angle (rad), θ
1	6	± 0.00375
2	6	± 0.005
3	6	± 0.0075
4	4	± 0.01
5	2	± 0.015
6	2	± 0.02
7	2	± 0.03
8	2	± 0.04

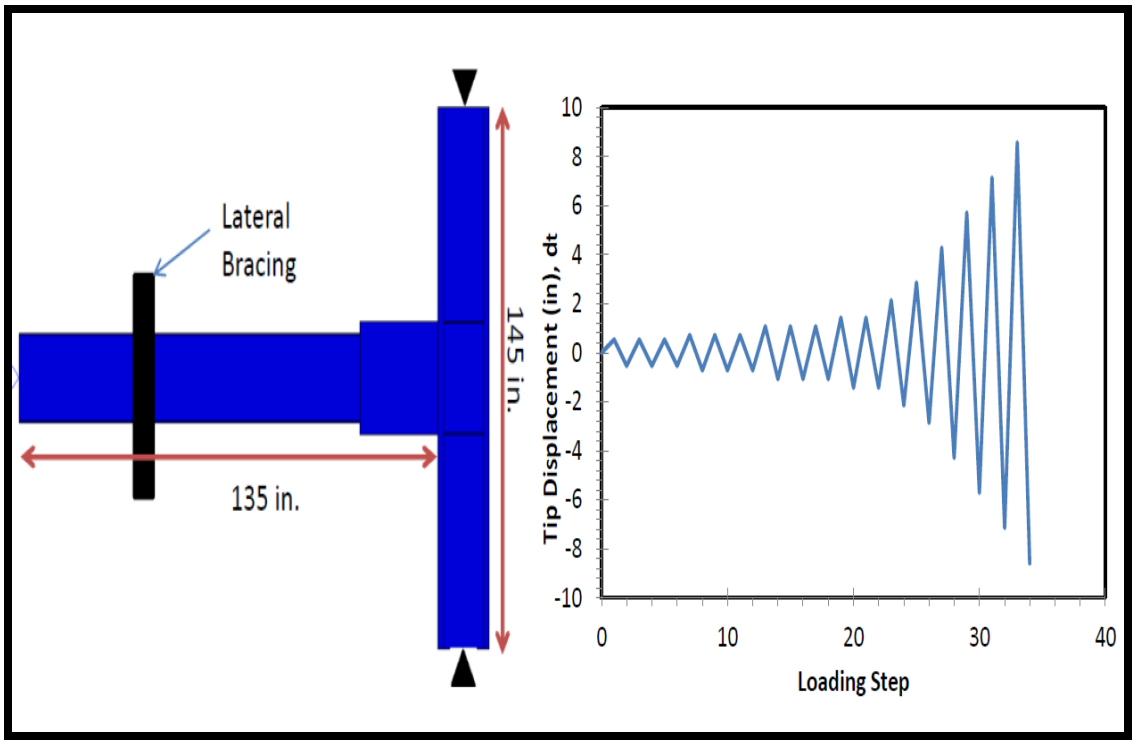

Figure 4-8: Model Geometry and Applied Tip displacement

4.4.Shear Stud Modeling

Shear studs eliminate the need for welding between the beam and column by locking the beam into the stub. Hence, forces will be transferred through the grout that fills the gap between beam and stub sections. Shear studs are small construction members compared to others such as beams and columns; therefore, modeling of such smaller elements may increase computational effort. Modeling of shear studs will increase the number of elements and hence the number of degrees of freedom. In addition, interaction between shear studs and grout will increase computational effort when shear studs are included in models. Considering the finite element method to be the most effective in predicting the overall behavior of a structural model, simplifications can be made based on engineering judgment. ABAQUS 6.13 (2013) provides a point-based fastener option which can be utilized to connect two surfaces at predetermined locations and to move connected nodes equally; additionally, this option enables the modeling of welds and bolts. This feature was used to model shear studs.

Predefined attachment points on the face of the beam and inside surface of the stub member shown in Figure 4.9 were used to model shear studs. These points were used at the location of the shear studs where two touching surfaces were connected together with rigid beam elements. These attachments points connect the beam section to the grout and the grout to the stub section. Only the radius of a shear stud can be assigned to these attachment points; therefore, the behavior of the shear studs cannot be investigated. It is believed that the fastener feature of ABAQUS (2013) provides an effective and easy method of modeling shear studs for the study of the overall performance of the grouted shear stud connection.

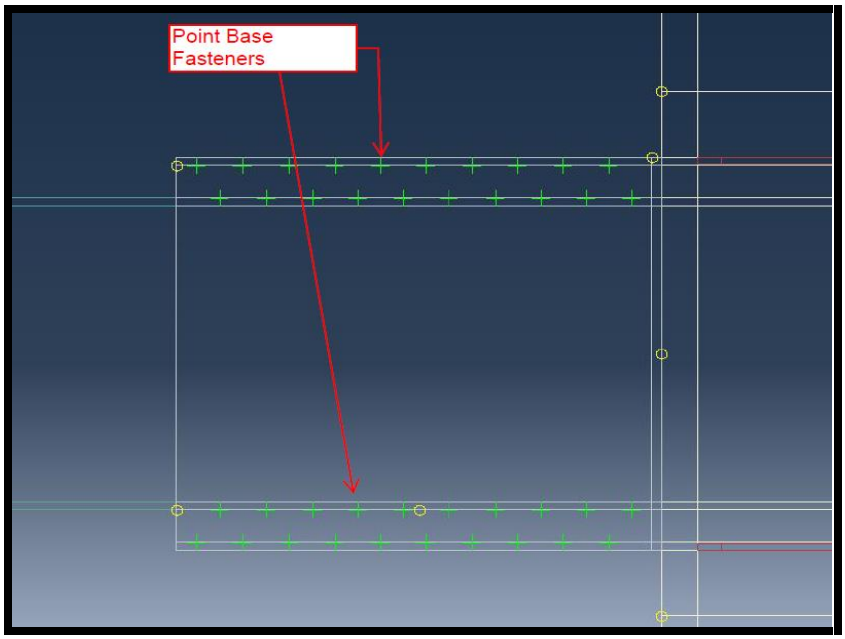

Figure 4-9: Point Based Fasteners

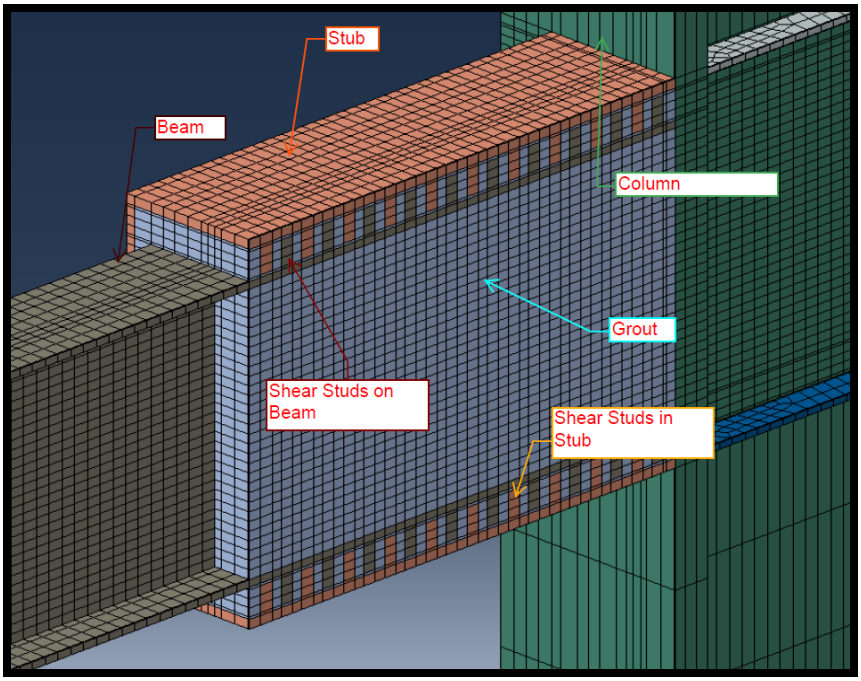

Figure 4-10: 3D Shear Stud Modeling

To examine the behavior of the shear studs embedded in the grout, a case study was conducted using a W24x62 beam section. Instead of modeling shear studs with their real geometry, which is of circular cross section, the study used rectangular geometries to provide more efficiency in regards to computational time and capacity. Rectangular geometries may reduce the mesh size because they are less complex than circular geometries. Circular geometries would require additional effort to partition the model in order to create simple geometries and would consequently create an undesirable increase in the number of elements and degrees of freedom. As shown in Figure 4.10, the shear stud heads were not included in the models. This is for two reasons: 1) including shear stud heads would lead to an increase in the number of elements and degrees of freedom; 2) shear studs embedded in the grout cannot be easily pulled out since they are encased by beam and stub sections.

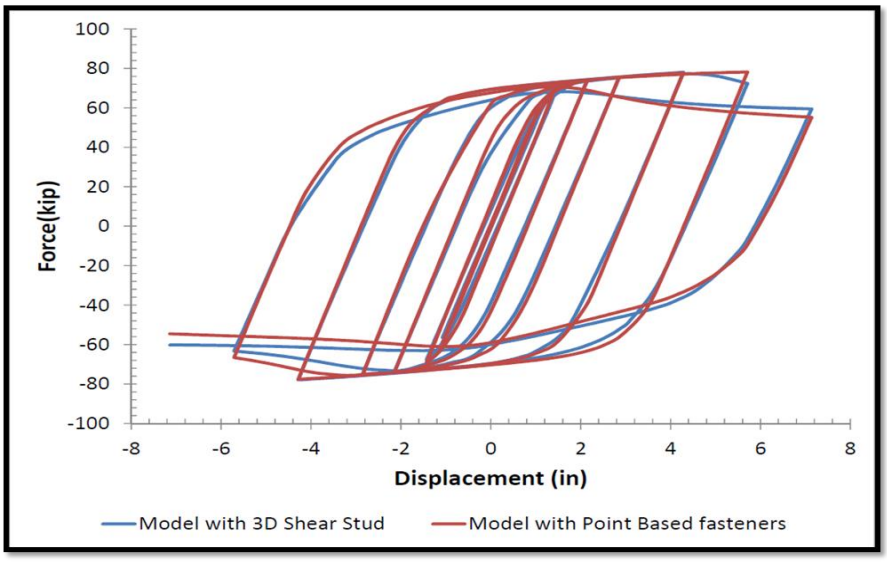

Figure 4-11: Force-Displacement Curves for Two Comparison Models

Figure 4.11 shows the force-displacement hysteretic loops of two models with shear studs, using the point-based fastener approach. As can be seen, the modeling approach of shear studs does not cause a significant difference in force-displacement behavior. As a result, the point-based fastener modeling approach can be used to observe global behavior of models.

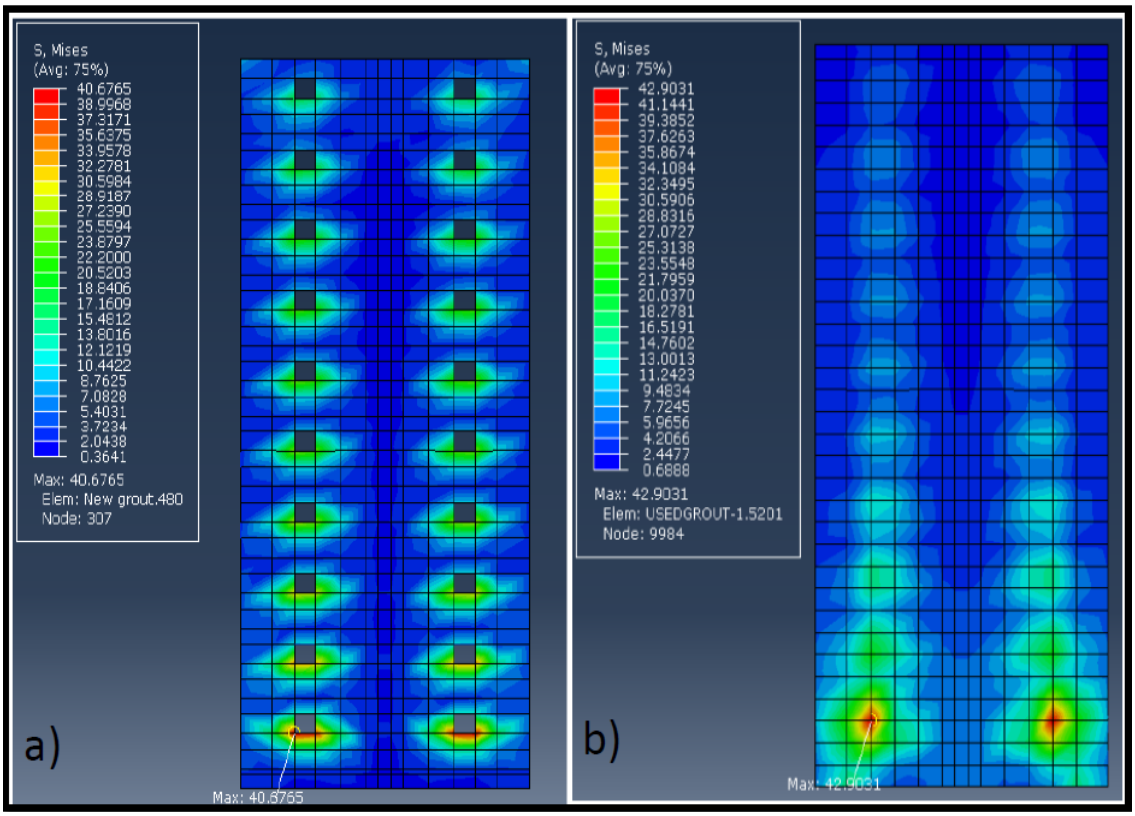

Figure 4-12: Von Mises Stress in Grout with a) 3d Model and b) Point Based Fastener Model

Figure 4.12 shows Von Mises stresses around the shear studs when the beam reaches its maximum moment capacity. Maximum Von Mises stress are 40.6 ksi and 42.9 ksi for the rectangular shear studs and point-based fastener approaches, respectively. The difference in stress distribution is largely due to geometry. The use of rectangular shear studs causes stress distribution in the grout unlike the point-based fastener as shown in Figure 4-12. As mentioned before, grout material is assumed to be elastic, and thus observation should be done based on this feature. These stress results could be used as an indicator to understand the possible failure mechanism of the grout.

4.5.Material Models Adopted for Analyses

With regard to steel members, a kinematic hardening material model was employed in this research to account for material nonlinearity. For the grout material a model was not adopted because grout material was assumed to be elastic. ABAQUS (2013) utilizes the logarithmic (true) stress and corresponding plastic strain to conduct the analyses. Calculation of logarithmic stress and plastic strain can be calculated by the following equations (4.3 and 4.4) and, respectively:

$$\sigma^{true} = \sigma^{nom}(1+\varepsilon^{nom}) \tag{4.3}$$

$$\varepsilon^{plastic} = \ln(1+\varepsilon^{nom}) - \sigma^{nom}/E \tag{4.4}$$

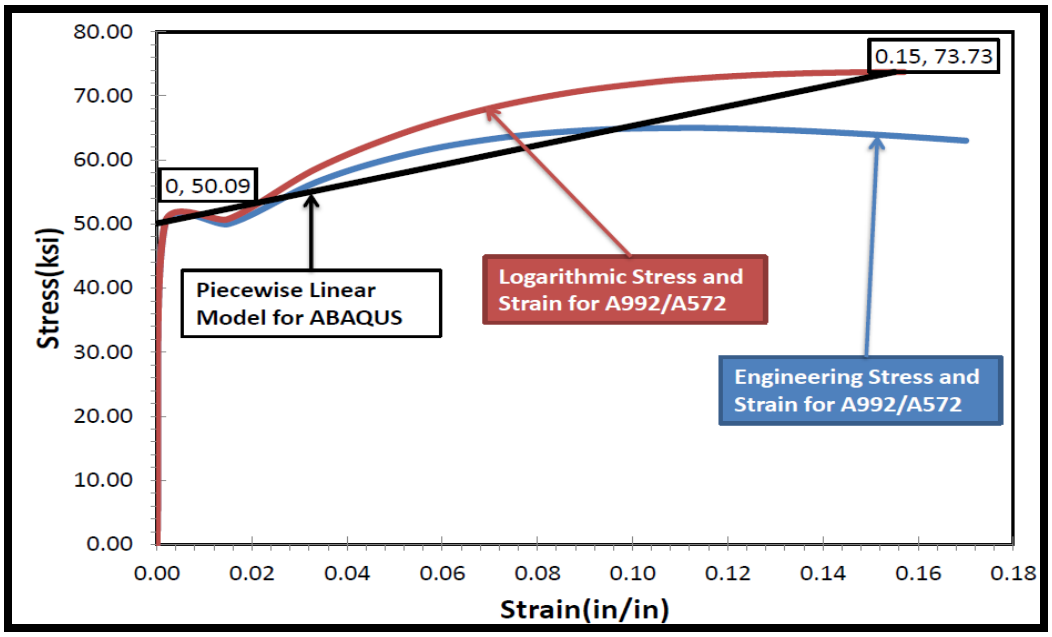

Figure 4-13: Stress-Strain Curve for A992/A572 Steel Material (from Sap2000 (2014))

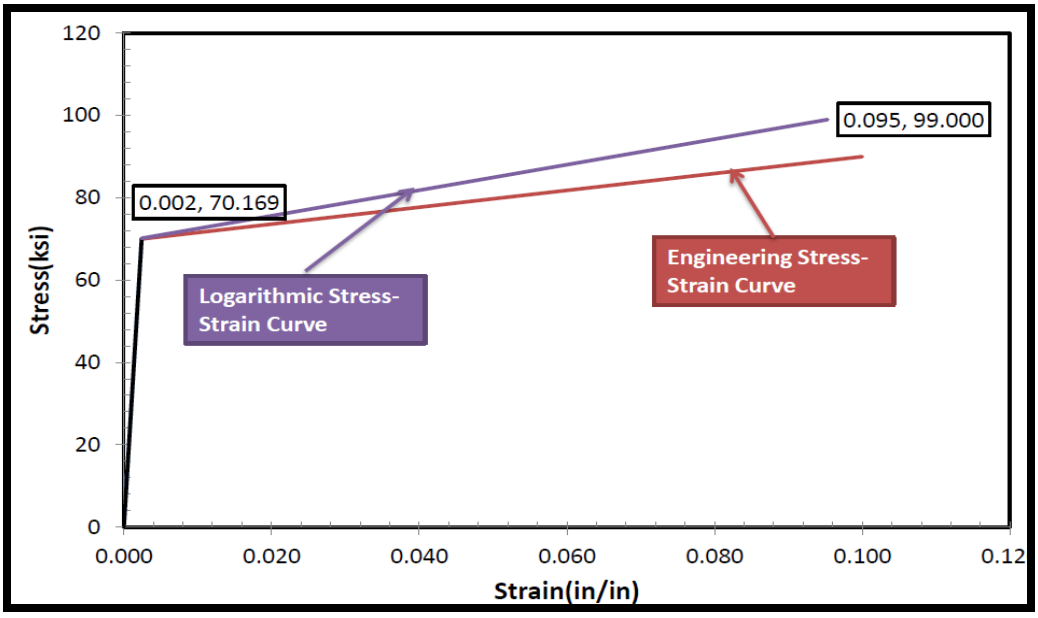

Figure 4-14: Stress-Strain Curve for E70 Weld (Ricles et al., 2000)

In this equation, σ^{nom}, σ^{true}, ε^{nom}, $\varepsilon^{plastic}$, and E are the nominal stress, logarithmic stress, nominal strain, plastic strain, and Young's modulus, respectively. The material properties adopted for steel components were taken from commonly used structural engineering software SAP2000 (2014) in which generic stress-strain curves for material A992 and A572 Gr. 50 are given.

A generic engineering stress-strain curve is shown in Figure 4.13. For the plates of the stub section, and for both beam and column elements, the materials employed were A572 and A992 steel, respectively. Taking material properties given in Figure 4.13 into account, it was inferred that using the same material properties for the A992 and A572 steel will not cause a significant difference in the outcomes from the numerical analysis since in SAP2000A992 and A572 Gr.50 steel have similar stress-strain behavior (Sap2000, 2014).

For the nonlinear branch of the stress-strain curve, a piecewise linear model was used in which true ultimate and true yield stresses were 73 ksi and 50 ksi, respectively; the true ultimate strain and yield strains were 0.1570 and 0.00172, respectively. Corresponding plastic strains for the true yield and true ultimate stresses were 0 and 0.155, respectively.

Table 4-2: Summary of Material Properties Used for Numerical Analysis

	Beam	Column	Weld
E (ksi)	29000	29000	29000
Yield Stress(ksi)	50	50	70
Yield Strain(in/in)	0.0017	0.0017	0.0024
Ultimate Stress(ksi)	63	63	90
Ultimate Strain(in/in)	0.17	0.17	0.1
True Yield Stress(ksi)	50.09	50.09	70.17
True Yield Strain(in/in)	0.0017	0.0017	0.0024
True Ultimate Stress(ksi)	73.73	73.73	99.00
True Ultimate Strain(in/in)	0.157	0.157	0.205
Plastic strain(in/in) at ultimate	0.155	0.155	0.095

Regarding the grout in the connections, the elastic material model is used to reduce computational cost given that the study performed by Fulmer (2012) showed that this model works well for predicting structural behavior. The Young's modulus E_c (in ksi units) is calculated by the following equation (4.5) (AISC 360-10(2010)):

$$E_c = 1746\sqrt{f_c'} \qquad \text{(ksi)} \qquad (4.5)$$

In this equation, f_c' is the compressive strength of the grout used.

The stress-strain curve of E70 weld material, which was a generic engineering stress-strain curve produced by Ricles et al. (2000) shown in Figure 4.14, was adopted for numerical analyses. The yield stress and ultimate stress were given as 70 ksi and 90 ksi, respectively. Young's modulus E was taken as 29000 ksi. Consequently, the yield and ultimate strains were 0.0024 and 0.1, respectively. Plastic strain associated with ultimate tensile (true) stress is 0.095, calculated from the given equation. Table 4.2 summarizes the material properties used in the structural model. The material models described above are assumed to be valid for all beam and column sections included in this study.

4.6.Modeling of Pre-Northridge Connection

In order to compare the effect of different parameters on the behavior of the grouted shear stud connection, simple moment connection (Flange welded- web bolted) models using W24x62 and W30x108 beams were developed. The models had similar dimensions to those for grouted shear stud beam to column connection models, shown in Figure 4.15, in which the height of column and length of beam are 145 inches and 135 inches, respectively.

The column sizes for these connections are identical to the column sizes used for the Grouted Shear Stud connection in order to avoid possible effects of the column on the performance of the connections. In fact, the beam sizes employed require smaller column sizes in comparison to beams connected to columns using a Grouted Shear Stud Connection.

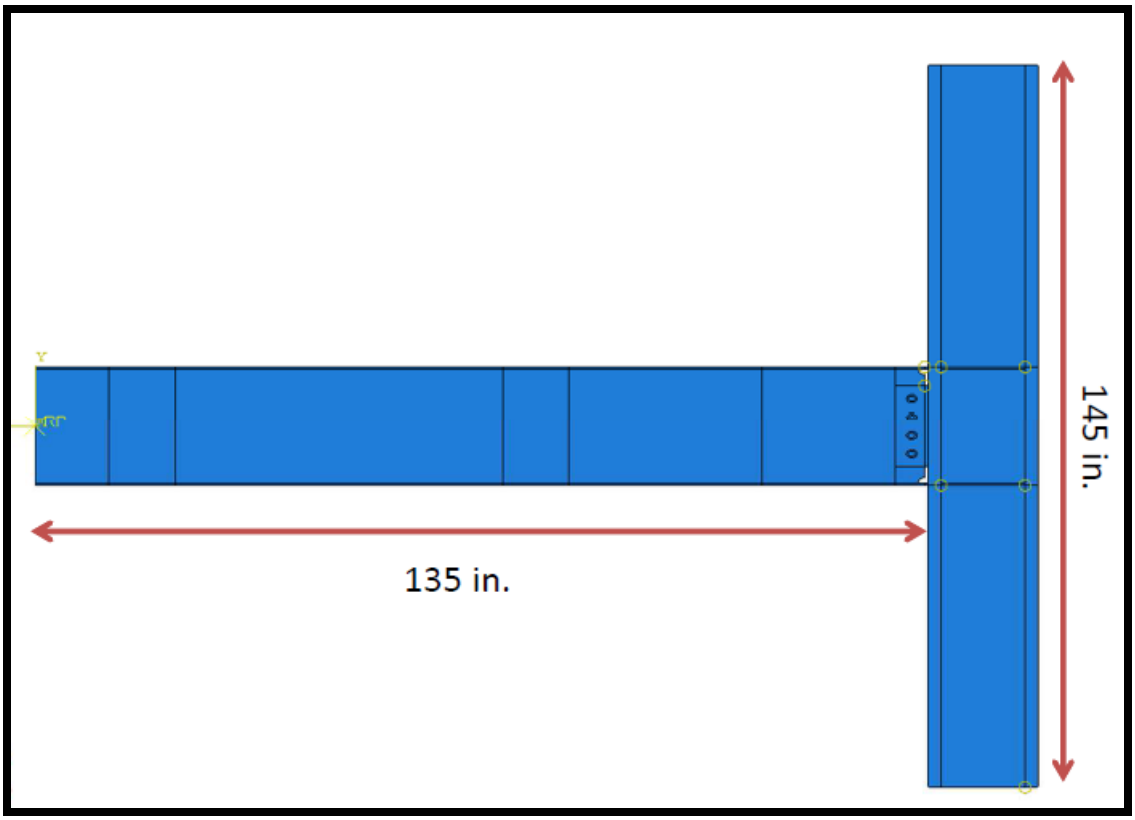

Figure 4-15: Model Geometry

Column sections used were W14x257 and W14x370; for the W24x62 beam section, the shear tab plate thickness, width, and height are 0.5 inches, 5 inches, and 16 inches, respectively. For the beam section W30x108, the shear tab plate thickness, width, and height are 0.6 inches, 5 inches and 24 inches, respectively. The material properties used for the shear tab are similar to the material model used for the stub of the grouted shear stud connection. As shown in Figure 4.16, complete joint penetration welds are explicitly modeled with a similar material model used for welding of the grouted shear stud stub section.

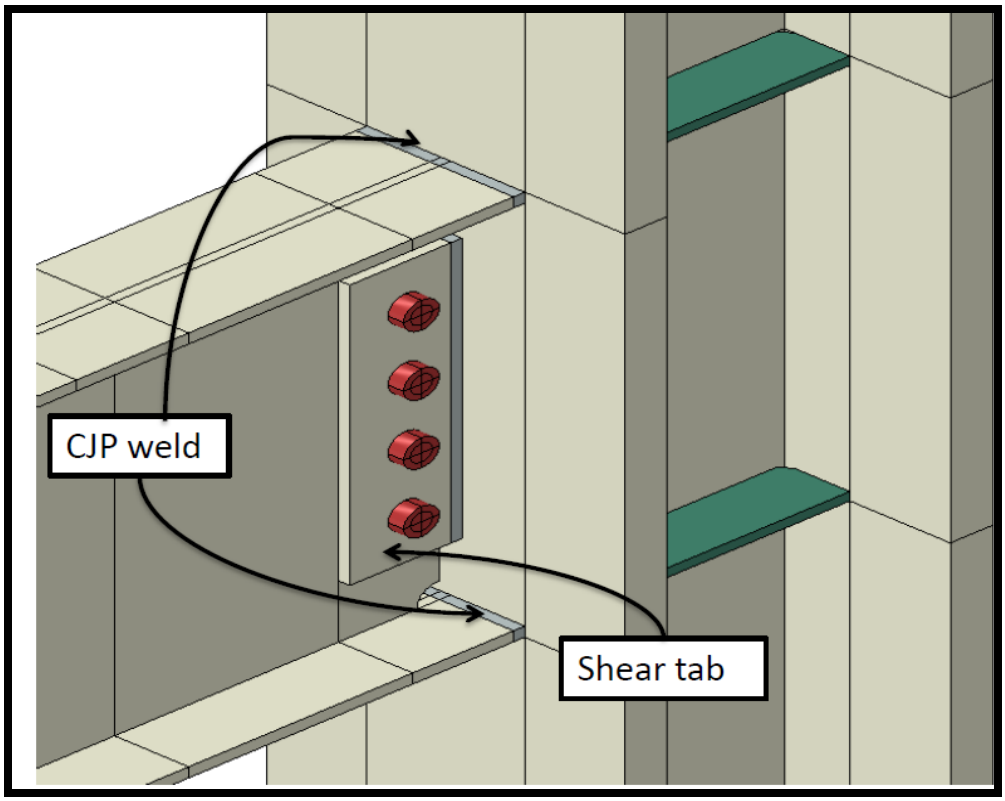

Figure 4-16: Web Bolted-Flange Welded Moment Connection

The required number of high-strength bolts is four for the W24x62 beam section and seven for the W30x108 beam section. Details of the calculation are given in the Appendix B. The bolt nut and threads are not included in the model. Instead of a nut, both bolt ends were modeled as circular heads. The thickness of the head was taken as 0.7 inches and the diameter of head as 1.6 inches; a washer is not included in the model. The distance between head inner surfaces is taken equal to the thickness of the shear tab plate plus the thickness of the beam web. Friction between faying surfaces was also included in the model. The associated friction coefficient was taken as 0.3 based on the results obtained by Hu (2008).

For reference, Tao et al. (2013) used 0.45 for friction coefficient. Additionally, hard contact behavior was assigned between bolts and plates that interact. Hard contact behavior implies that modeled parts come into interaction and get separated without entering each other (ABAQUS, 2013).

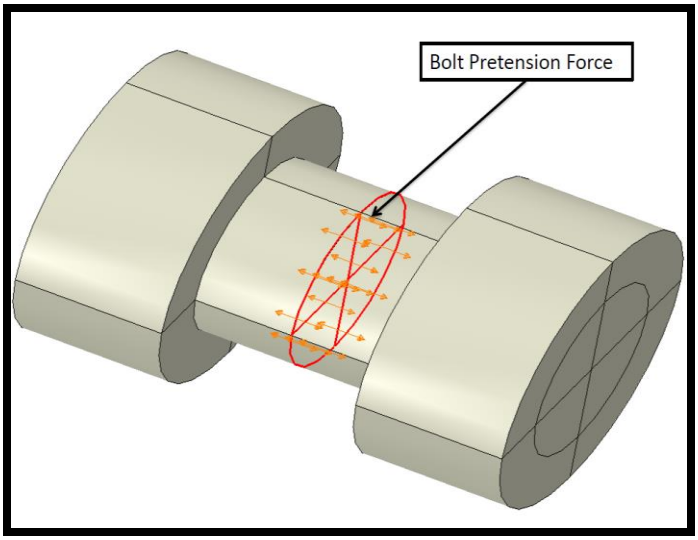

Figure 4-17: Bolt Pre-Tension Force

The *AISC Steel Construction Manual 14th Edition* presents the pretension forces for different shank diameters of bolts. For a 1 inch shank diameter, the minimum applied force is 51 kips; this was taken into account in the model, as ABAQUS (2013) has an option for defining pretension bolt loads. Bolt pretension loads were applied to a pre-created plane, which cuts the bolt into two halves, in the direction of the longitudinal axis. The pretension force will remain constant during analysis. It should be noted that bearing type bolts are employed.

The material model for high-strength bolts was adopted from a study by Sherbourne et al. (1994); the stress-strain curve for the adopted material model is shown in Figure 4.18. The curve consists of three piecewise linear parts. The ultimate engineering stress and corresponding strain are 121 ksi and 0.019, respectively. The yield stress and strain of the bolt are 89.9 ksi and 0.004, respectively. Unlike other components such as beams, columns and shear tabs, an isotropic hardening material model was adopted for bolts. It is believed that under cyclic loading, the impact of bolts on overall connection behavior is comparatively less important than other components.

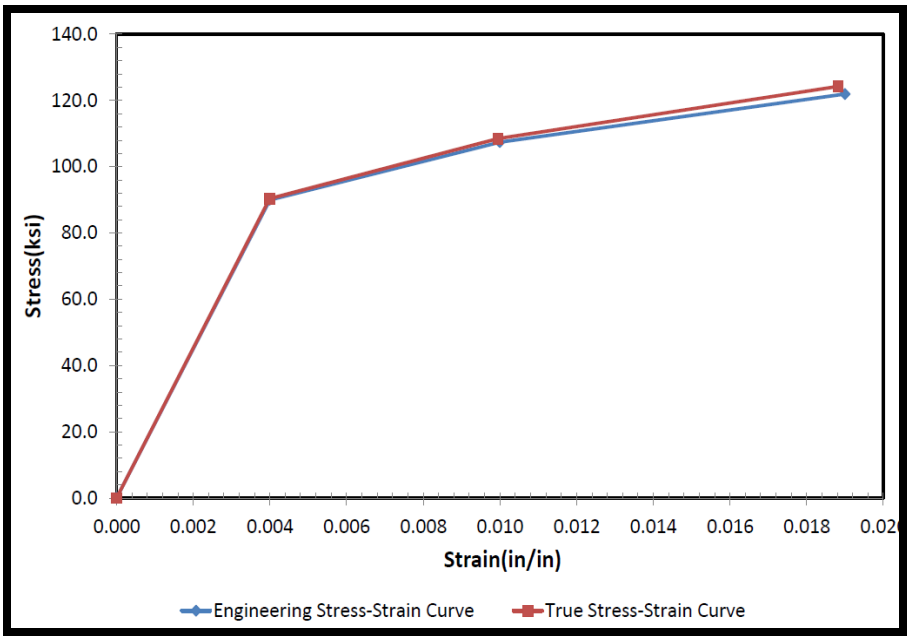

Figure 4-18: Stress-Strain Curve for High-Strength Bolt (Sherbourne et al., 1994)

Mesh sizes employed for Pre-Northridge connections are similar to those used for the Grouted Shear Stud beam to column connections in order to avoid possible effects caused by

differing mesh sizes. Varying mesh sizes would lead to unreliable comparisons in the outcomes of the two beam to column connections; therefore, minimum mesh sizes of 0.75 inches were adopted in the two connections, near the welded region. Similarly, the aspect ratio around the welded region and panel zone was adjusted close to 1.0.

The loading protocol adopted for the Grouted Shear Stud beam to column connection is also employed for the Pre-Northridge connections. Tip displacements for given loading steps are the same because the length of the beam from tip to column center was not modified.

4.7.Constraint and Contact between Modeled Parts

ABAQUS allows for modeling every part of the connection separately. Therefore, contact and constraint between parts must be explicitly included in the models; otherwise, ABAQUS (2013) will not identify the interaction between parts. Behavior between parts which are not connected may have contact during analysis; this was accounted for through use of the "hard contact" option available in ABAQUS (2013) which permits modeled parts to come into contact during the analysis but does not let them enter each other (ABAQUS (2013)). Possible friction between modeled parts was ignored for GSS connections. The reason is that the chemical bond created by dry grout is not known for certain, and cracking behavior of grout due to interaction of parts was not modeled. In addition, there are no sources available to calibrate this behavior. Therefore, only hard contact behavior was utilized between parts such as beam, grout, column and stub.

In order to define the constraint between two model components, available options such as “tie constraint” (ABAQUS 2013) and “shell-to-solid coupling” (ABAQUS 2013) were used between two connected parts. Tie constraint was used to represent the connection between the stub, column flange face, and stiffeners as shown in Figure 4.19. A “tie constraint” displaces nodes on two connected surfaces equally in transition and rotation (ABAQUS 2013). A “shell-to-solid coupling” works in the same manner except that a tie constraint can be used for connecting 2D-to-3D, 2D-to-2D, or 3D-to-3D elements whereas a shell-to-solid coupling constraint can only be used for a connection between shell-to-solid elements.

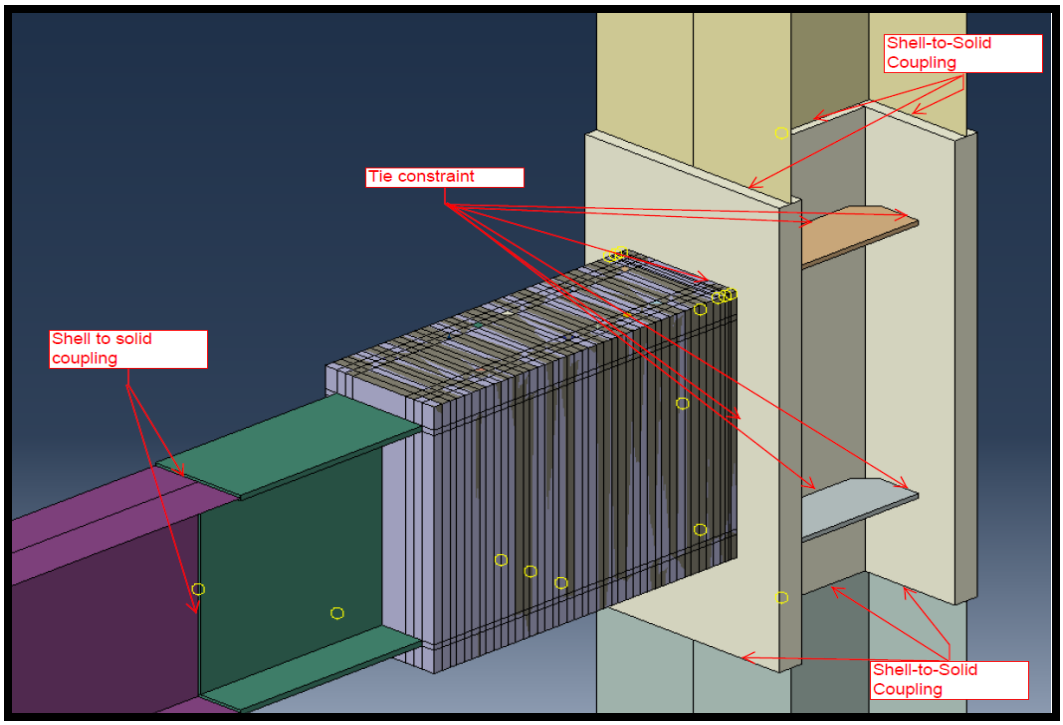

Figure 4-19: Contact and Constraint in the Model

Shell elements were used to model parts that are far from high-stress regions of the connection, as shown in Figure 4.19. Shell elements were used to reduce the degrees of freedom in the models, thereby reducing computational effort. Shell-to-solid couplings were used to simulate the behavior between parts of beams and columns where shell and solid elements were used together.

4.8.Tools for Evaluation of Behavior of Connections

Several indices and one dissipated energy indicator are adopted in this study to investigate the performance of grouted shear stud beam to column connections. The cumulative Equivalent Plastic Strain (PEEQ) index and the Failure Index (FI) are the two indices adopted in this study. Dissipated plastic energy was also extracted from ABAQUS for the purpose of comparison. The details of those indices and energy dissipation levels are discussed in the following subsections.

4.8.1.PEEQ Index

The PEEQ index is calculated as the cumulative equivalent plastic strain of the region of interest, divided by the yield strain of the material:

$$PEEQ^{index} = PEEQ \Big/ \varepsilon_y \qquad (4.6)$$

In this equation (4.6), ε_y is the yielding strain of the material and PEEQ is the cumulative equivalent plastic strain. The cumulative plastic strain (PEEQ) is calculated as

$$PEEQ = \sqrt{\frac{2}{3}\varepsilon_{ij}\varepsilon_{ij}} \qquad (4.7)$$

where ε_{ij} is the component of plastic strain in the global direction of $i,j = 1,2,3$.

PEEQ index is an indicator of the local strain demand of the region of interest; a higher PEEQ index indicates greater possibility of having ductile fracture (El-Tawil et al (1998)). El-Tawil et al. (1998) employed this index to compare the performance of Pre-Northridge beam to column connections with different sizes of weld access holes (WAH).

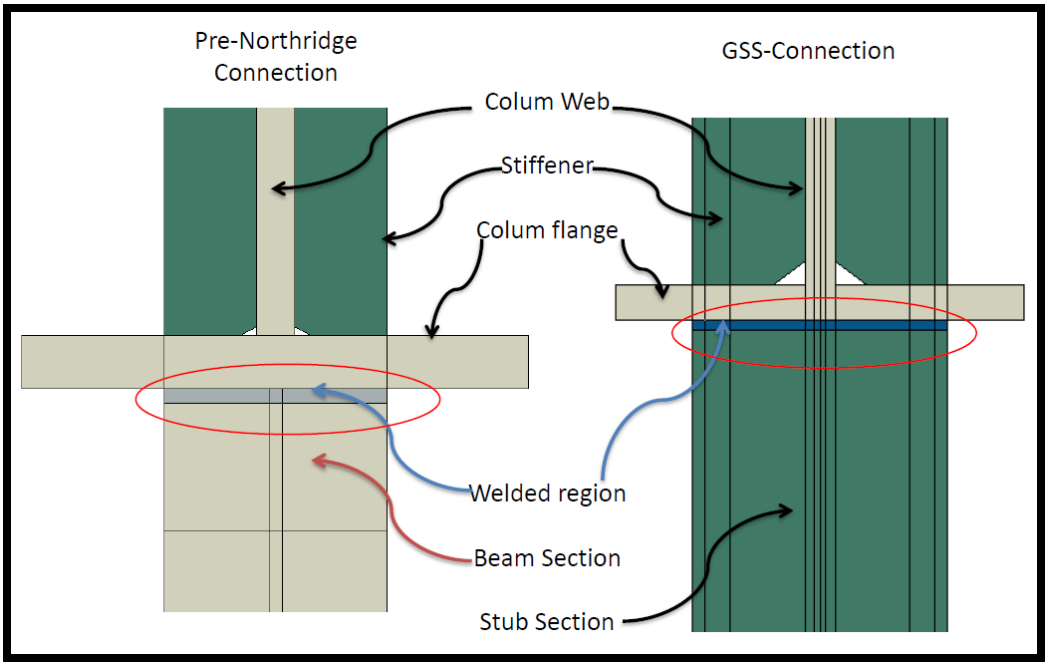

Figure 4-20: PEEQ Index Comparison Location (Plan View of Connections)

In this research, the PEEQ index is also utilized to compare grouted shear stud beam to column connections modeled with different parameters. Additionally, the same index is used for comparison between grouted shear stud beam to column connections to Pre-Northridge connections. The location of the PEEQ index for comparison purposes is shown

in Figure 4.20, in which the red circle shows the critical weld region at the column flange face. ABAQUS (2013) provides instantaneous strain, stress and displacement data at nodes or regions. With the help of this feature, the maximum PEEQ data in critical regions was extracted and divided by the yield strain of steel material in order to make a quick comparison of different models (see Figure 4.20).

4.8.2.Failure Index

A "failure index", which is based on a stress-modified critical strain principal (SMCS), was adopted to determine low cycle fatigue damage in the critical weld region of the beam to column connection, and also in the shear studs. Several researchers adopted a "failure index" to predict ductile fracture initiation in steel structures (Chi et al., 2006; Fell et al., 2006; Richards and Prinz, 2007; Prinz and Richards, 2009).

The failure index is defined as the ratio of the cumulative equivalent plastic strain to the critical plastic strain:

$$FailureIndex(FI) = PEEQ / \varepsilon_p^{\ critical} \tag{4.8}$$

(Prinz and Richards, 2009). PEEQ is the cumulative equivalent plastic strain at the region under consideration, and $\varepsilon_p^{critical}$ is the critical plastic strain defined by Hancock and Mackenzie (1976) as

$$\varepsilon_p^{critical} = \alpha \exp(-1.5\frac{\sigma^m}{\sigma^e}) \tag{4.9}$$

where α,σ^m and σ^e are the material constant, hydrostatic stress, and von Mises stress, respectively.

Determination of the critical plastic strain necessitates two parameters: a characteristic length (l), and a material constant (α). Determination of the characteristic length (l) requires full understanding of the coupon's fracture surfaces which can be usually determined from fractographic images (Kanvinde and Deierlein, 2006). Kanvinde and Deierlein (2006) determined a characteristic length of 0.20 mm for a notched bar with material A572 Grade 50. By conducting a mesh refinement study, Prinz and Richards (2009) determined that 3.175 mm is the characteristic length for link beams with reduced web sections. Through this work, researchers were able to determine the appropriate mesh size for critical regions. Details of this mesh refinement study will be discussed in subsection 4.8.3. Kanvinde and Deierlein (2004) and Chi et al. (2006) took α value of 2.6 for A572 Grade 50 steel. In this study, a value of 2.6 was also adopted as the material constant.

Kanvinde and Deierlein (2004) stated that under cyclic loading, the prediction of fracture initiation using SMCS becomes less accurate than predictions which are made when monotonic loading is applied. Moreover, Kanvinde and Deierlein (2004) stated that the stress modified critical strain model (SMCS) does not account for changes in the type of applied forces which have an effect on the size of voids in the steel material; therefore, under tension and compression loading, this model produces less accurate results. In addition, Kanvinde and Deierlein (2004) observed that under cyclic loading, where triaxial stress generally shows large differences, SMCS estimation for fracture initiation is comparatively conservative, the exact level of which was not evaluated. Prinz and Richards (2009) also showed that the failure index with SCMS prediction is conservative under reversed cyclic loading conditions.

Fell et al. (2006), Prinz and Richards (2007), and Prinz and Richards (2009) predicted ductile fracture initiation in regions of a structure where the failure index reaches a value larger than 1.0. In this study, the failure index at the critical weld region and in the shear studs was calculated based on the observations discussed above. Rupture initiation is predicted whenever the failure index exceeds 1.0 in the critical weld region and in the shear studs. Since the level of conservatism is not clearly known, the failure index can be used to compare models with different parameters in this research.

4.8.3.Mesh Refinement Study

A mesh refinement study similar to that of Cook et al. (2001) was conducted to determine the appropriate mesh size for calculation of the failure index. This study was conducted at the critical weld region, near the column face, as shown in Figure 4.21.

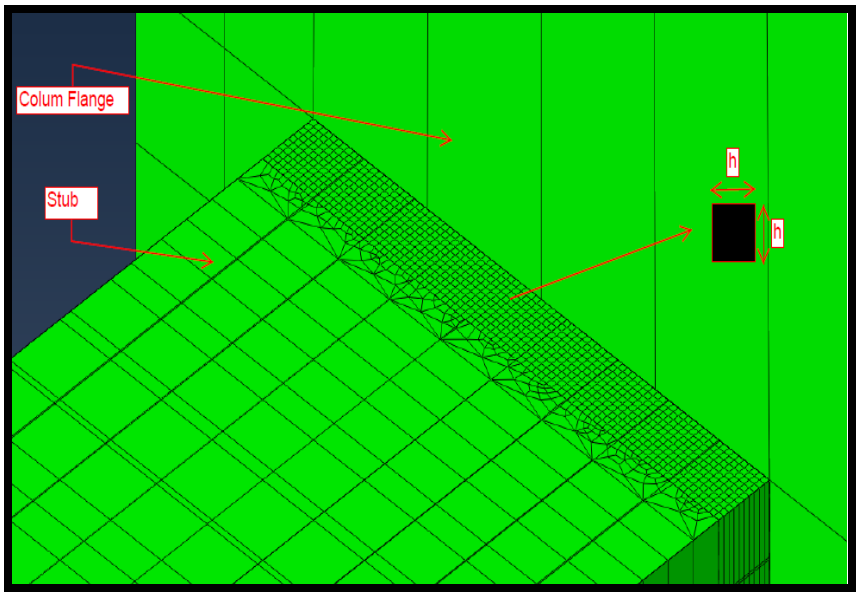

Figure 4-21: Refined Mesh at Critical Weld Region

In this study, the stub was modeled with Quadrilateral linear shell elements in order to predict fracture initiation in the critical weld region. Mesh size versus maximum longitudinal stress at the critical weld region was plotted, as shown in Figure 4.22. With the help of curve fitting, a trend line for a number of data points was determined. Using the given equation, the stress after the last point of the linear line was predicted. Mesh sizes of 0.2 inches, 0.1 inches and 0.05 inches were used, and the model loaded to achieve a drift of 5%. The maximum longitudinal stresses were 63.52 ksi, 70.41 ksi and 74.11 ksi for mesh sizes of 0.2 inches, 0.1 inches and 0.05 inches, respectively. The mesh refinement started with a mesh size of 0.2 inches and was reduced by half until the mesh size was 0.025 inches was attained. The maximum longitudinal stress was predicted using the given equation and compared to the finite element result at a mesh size of 0.025 inches.

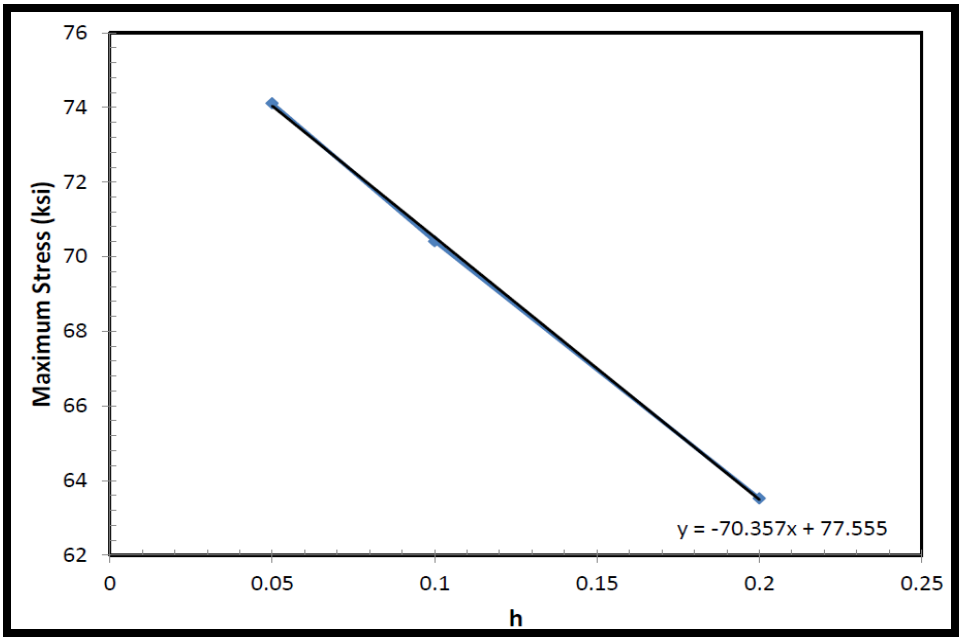

Figure 4-22: Mesh Size versus Maximum Stress

The maximum longitudinal stress predicted by the equation was 75.79 ksi whereas the maximum longitudinal stress from the finite element analysis for a mesh size of 0.025 inches was 76.92 ksi. The relative error between the predicted and finite element analysis was -1.47%, a reasonable and acceptable result. Mesh sizes smaller than 0.025 inches were not considered due to computer capacity used at the time of the analysis.

Figure 4.23 shows the failure index, calculated at the critical weld region for several mesh sizes. It can be seen that the lower the mesh size used, the higher the failure index calculated. Therefore, while the failure index cannot be used for conclusive results, it can be used for comparison of models with different parameters.

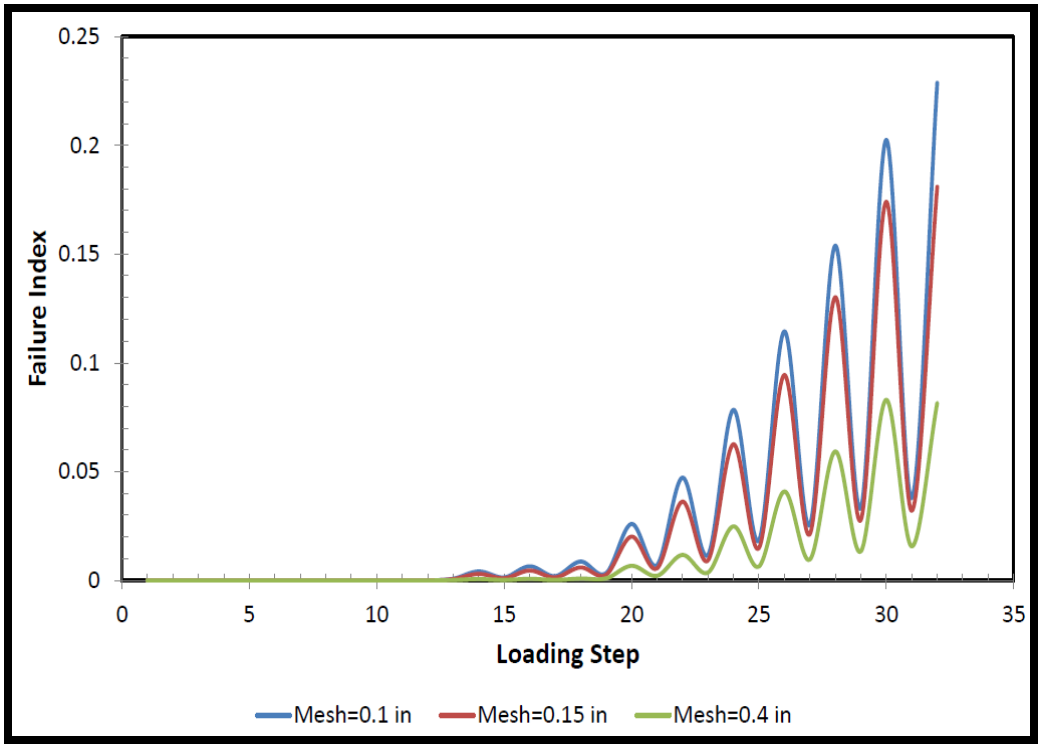

Figure 4-23: Failure Index for Different Mesh Sizes

For the sake of completeness and due to the capacity of the computer used throughout this research, this study used a mesh size of 0.15 inches to predict failure index. Using a smaller mesh size than 0.15 inches prevents analyzing models with large amount of shear studs. Therefore, the same mesh size was used for the shear studs and critical weld region, regardless of the element type used in the models.

4.8.4.Dissipated Plastic Energy

ABAQUS (2013) provides the amount of plastic energy dissipated when a material goes into an inelastic state during analyses. Calculation of dissipated plastic energy is given by ABAQUS (2013) as

$$ALLPD = \int \varepsilon^{p}{}_{ij}\sigma_{ij}d\varepsilon \qquad (4.10)$$

where ε_{ij}^{p} is plastic strain, and σ_{ij} is stress in the global direction of $i,j=1,2,3$.

Dissipated plastic energy can be a good quantity to compare for different connections or connections with different parameters. The level of dissipated energy can give an indication of performance of the connection.

CHAPTER 5

5. Parametric Study for Grouted Shear Stud Beam to Column Connections

5.1.Introduction

This chapter will focus on the effects of various parameters on the performance of grouted shear stud (GSS) beam to column connections. These include the presence or absence of stiffener plates, shear stud configuration, thickness of stub flange plates, height of the stub, and the number of shear studs.

For comparison purposes, two different beam sections (W24x62 and W30x108) were incorporated and the connections were modeled using the point based fastener approach to account for shear studs. The process of designing the connection with these two beam sections, outlined in Chapter 2, was determined by the capacity design approach. Appendix B presents details of the design process. In order to evaluate the effects of different parameters, six parametric study matrices are proposed for each beam section. In addition, in order to assess the performance of grouted shear stud (GSS) beam to column connections, two typical Pre-Northridge connections are modeled with the same beam sections (W24x62 and W30x108). For comparison of the results between GSS beam to column and pre-Northridge connections, different performance indicators are considered which include moment-rotation curves (at the column face), normalized longitudinal stress, normalized longitudinal strain, cumulative equivalent plastic strain index (PEEQ index) at the critical weld region, and the amount of plastic energy dissipated at the connection level.

In order to evaluate the effects of the number and configuration of shear studs, detailed finite element models for the W24x62 beam section of several configurations were constructed. The reason for only modeling this beam is that the results are expected to be similar for all beam sizes. The shear studs are modeled as rectangular members in order to make a quick comparison of configurations and also to avoid meshing when modeling elements with circular cross sections.

The effects of shear studs location on their behavior were analyzed using the failure index, which was discussed in Chapter 4. For configurations 1 and 2 (see Figure 2.11), the effect of the number of studs was also examined using the failure index. Moreover, the failure index was adopted to evaluate fracture initiation at the critical weld region; for this evaluation, three models for the W24x62 beam section with increasing stub flange thicknesses were developed with the point based fastener approach.

5.2.Parametric Study Matrices for Models with Point Based Fasteners

As mentioned in Chapter 6, parametric study matrices for each beam section were provided. Each matrix includes one beam section and one parameter for each of the four configurations of shear studs (discussed in Chapter 2). As stated earlier, parameters that have an effect on the performance of the connections, such as shear stud configuration, stub flange plate thickness and stub height were considered. In addition, a parametric study matrix, which includes only configuration 1 (see Figure 2.11), was provided in this chapter to examine the effects of stiffeners on the performance of connections.

Model Name	Beam- Column properties			Stub Properties			Shear Stud Config1	Shear Stud number	Stiffener			Grout Strength fc'(ksi)
		w24x62	w14x257									
Model1	height(in)	23.7	16.4	Height(ht)	28.7	in		80	Thickness	0.5	in	6
	width(in)	7.04	16	Flange (ttf)	0.6	in			width	3.91	in	
	flange thic(in)	0.59	1.89	Side(tts)	0.5	in			length	12.62	in	
	web thick(in)	0.43	1.18	width(bt)	9	in						
	Zx(in3)	153	487	Length	25	in						
	Sx(in3)	131	415									
Model Name	Beam- Column properties			Stub Properties			Shear Stud Config2	Shear Stud number	Stiffener			Grout Strength fc'(ksi)
		w24x62	w14x257									
Model2	height(in)	23.7	16.4	Inside height(ht)	28.7	in	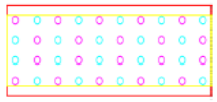	80	Thickness	0.5	in	6
	width(in)	7.04	16	Flange (ttf)	0.6	in			width	3.91	in	
	flange thic(in)	0.59	1.89	Side(tts)	0.5	in			length	12.62	in	
	web thick(in)	0.43	1.18	width(bt)	9	in						
	Zx(in3)	153	487	Length	25	in						
	Sx(in3)	131	415									
Model Name	Beam- Column properties			Stub Properties			Shear Stud Config3	Shear Stud number	Stiffener			Grout Strength fc'(ksi)
		w24x62	w14x257									
Model3	height(in)	23.7	16.4	Inside height(ht)	28.7	in	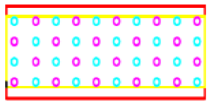	80	Thickness	0.5	in	6
	width(in)	7.04	16	Flange (ttf)	0.6	in			width	3.91	in	
	flange thic(in)	0.59	1.89	Side(tts)	0.5	in			length	12.62	in	
	web thick(in)	0.43	1.18	width(bt)	9	in						
	Zx(in3)	153	487	Length	25	in						
	Sx(in3)	131	415									
Model Name	Beam- Column properties			Stub Properties			Shear Stud Config4	Shear Stud number	Stiffener			Grout Strength fc'(ksi)
		w24x62	w14x257									
Model4	height(in)	23.7	16.4	Inside height(ht)	28.7	in	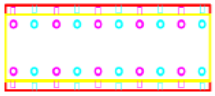	80	Thickness	0.5	in	6
	width(in)	7.04	16	Flange (ttf)	0.6	in			width	3.91	in	
	flange thic(in)	0.59	1.89	Side(tts)	0.5	in			length	12.62	in	
	web thick(in)	0.43	1.18	width(bt)	9	in						
	Zx(in3)	153	487	Length	25	in						
	Sx(in3)	131	415									

Figure 5-1: Parametric Study Matrix 1 for Beam Section W24x62 (Stub: Inside Height=28.7 inches; Flange Thickness=0.6 inches)

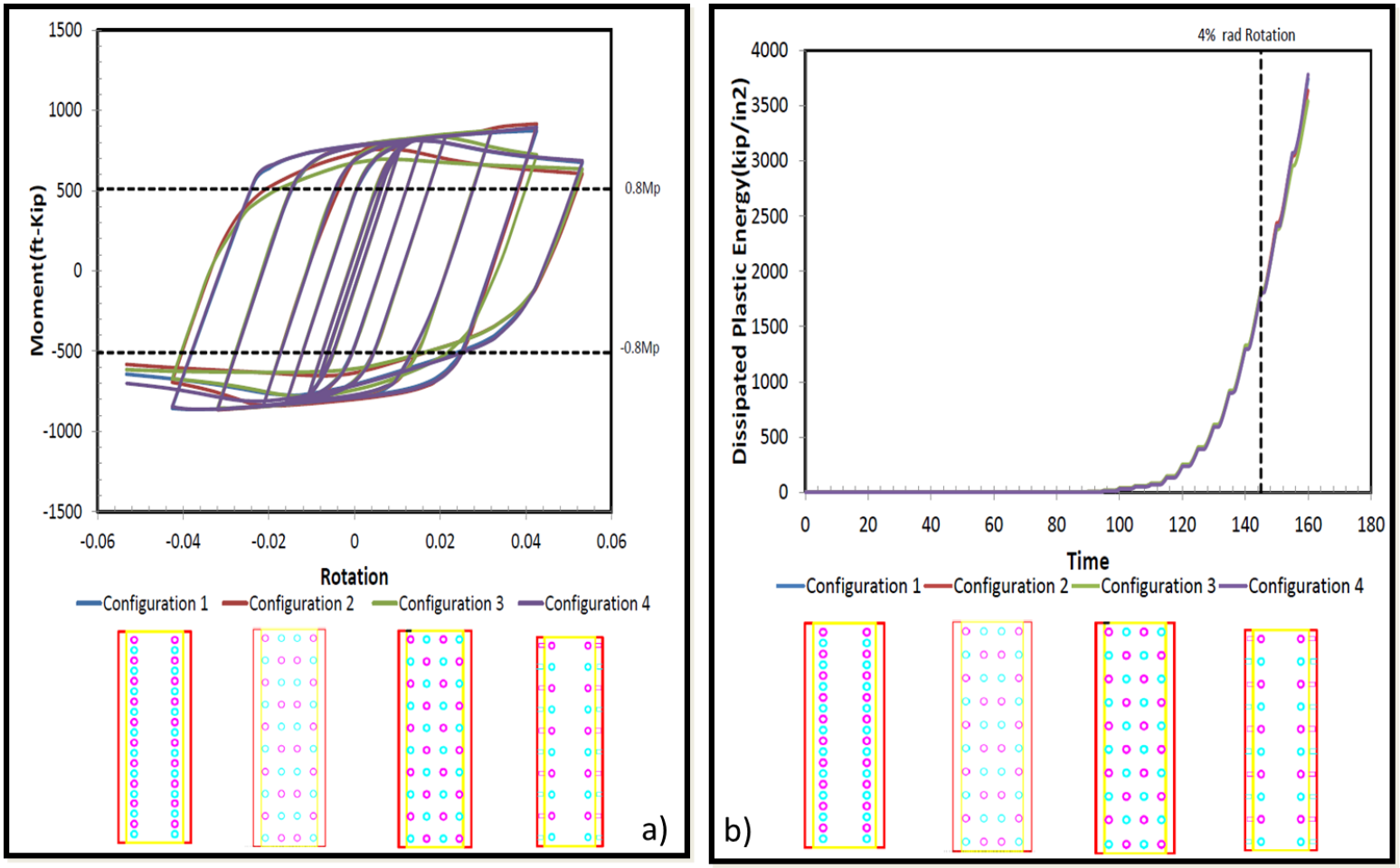

Figure 5-2: a) Moment-Rotation Curves and b) Dissipated Energy Levels for Matrix 1

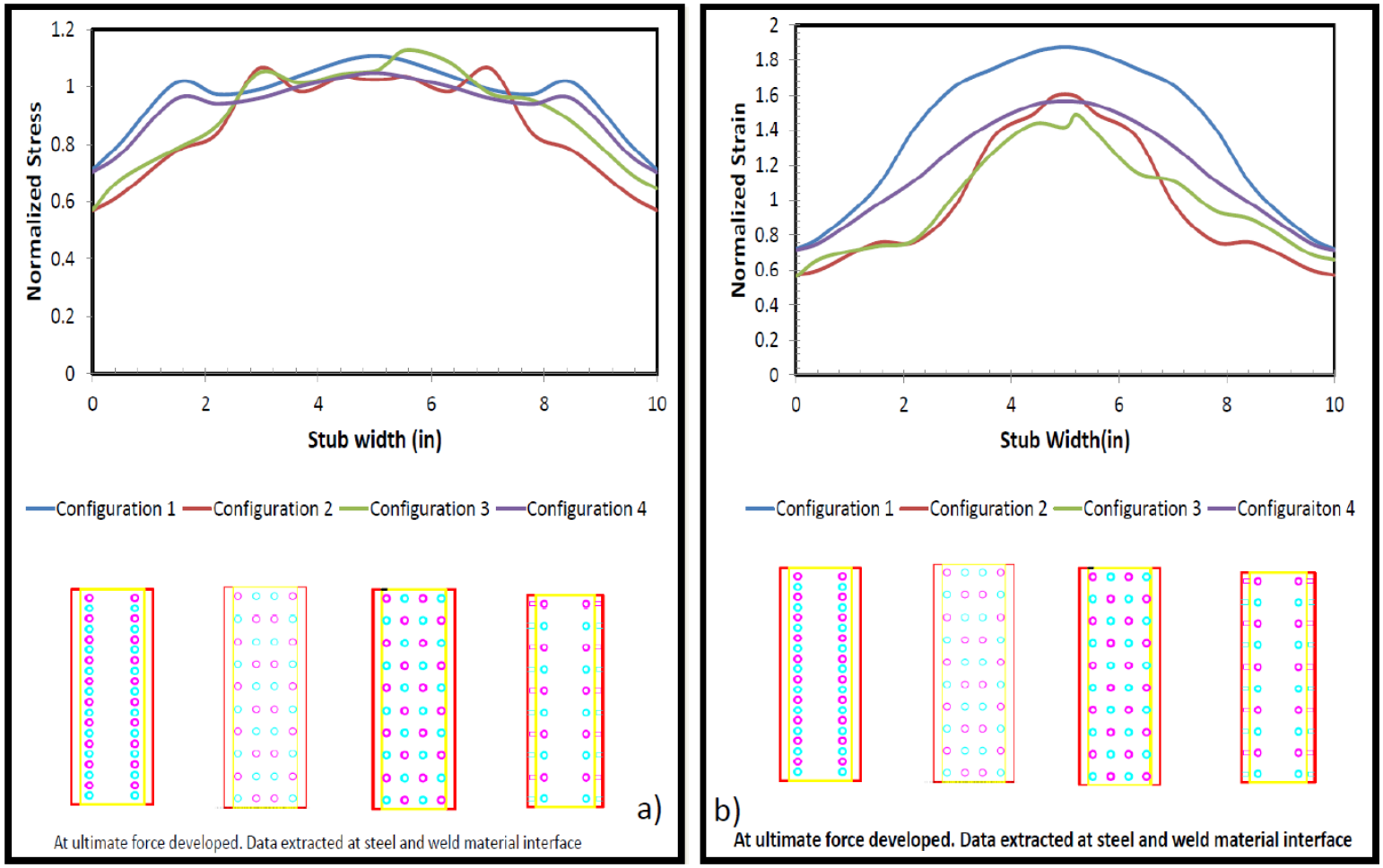

Figure 5-3: a) Normalized Longitudinal Stress and b) Normalized Longitudinal Strain at Welded Region for Matrix 1

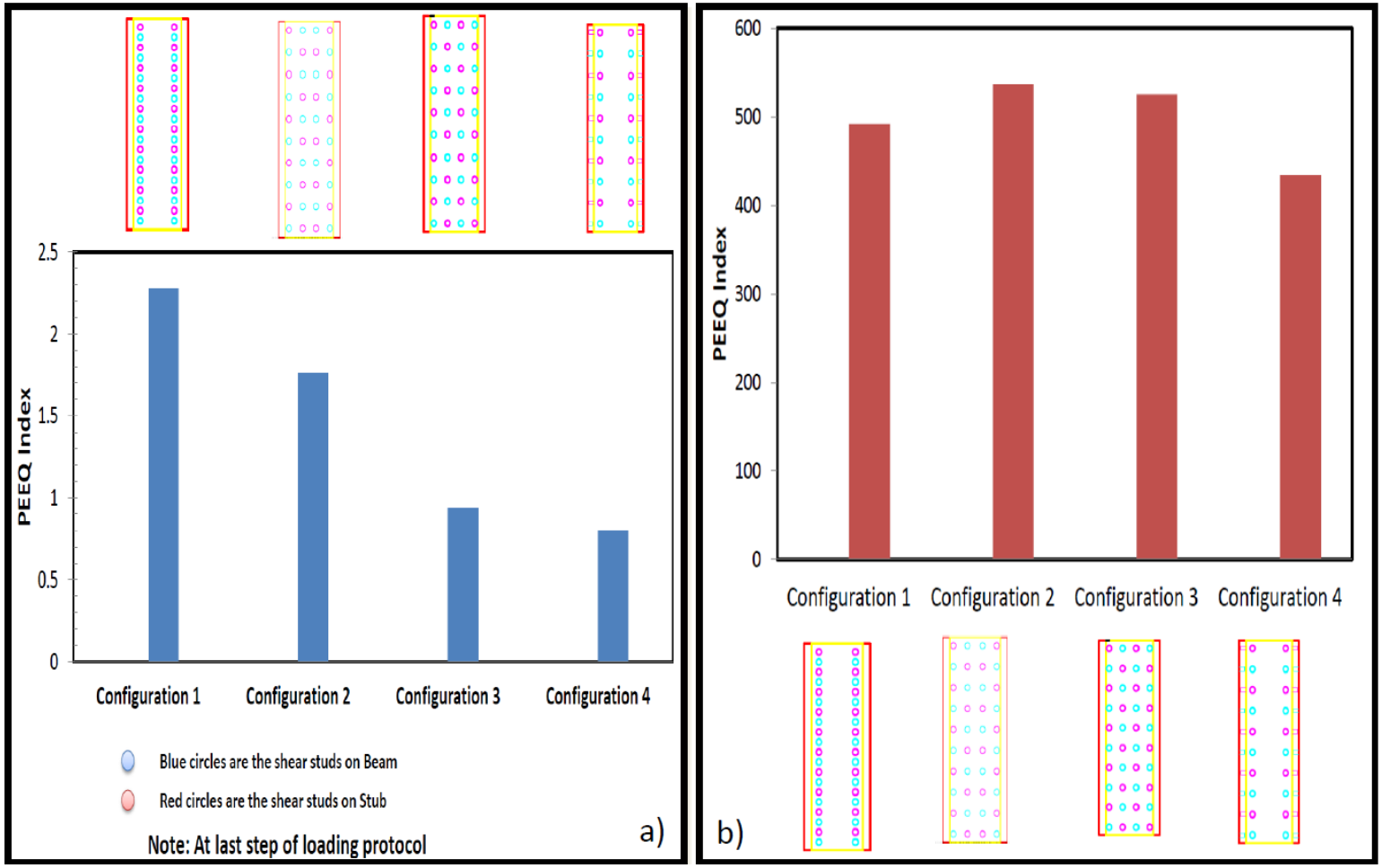

Figure 5-4: a) PEEQ Index at the Welded Region and b) PEEQ Index at Plastic Hinge Region for Matrix 1

Model Name	Beam- Column properties			Stub Properties			Shear Stud Config1	Shear Stud number	Stiffener			Grout Strength fc'(ksi)
		w24x62	w14x257									
Model1	height(in)	23.7	16.4	Height(ht)	28.7	in		80	Thickness	0.5	in	6
	width(in)	7.04	16	Flange (ttf)	0.75	in			width	3.91	in	
	flange thic(in)	0.59	1.89	Side(tts)	0.5	in			length	12.62	in	
	web thick(in)	0.43	1.18	width(bt)	9	in						
	Zx(in3)	153	487	Length	25	in						
	Sx(in3)	131	415									
Model Name	Beam- Column properties			Stub Properties			Shear Stud Config2	Shear Stud number	Stiffener			Grout Strength fc'(ksi)
		w24x62	w14x257									
Model2	height(in)	23.7	16.4	Inside height(ht)	28.7	in	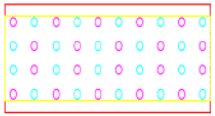	80	Thickness	0.5	in	6
	width(in)	7.04	16	Flange (ttf)	0.75	in			width	3.91	in	
	flange thic(in)	0.59	1.89	Side(tts)	0.5	in			length	12.62	in	
	web thick(in)	0.43	1.18	width(bt)	9	in						
	Zx(in3)	153	487	Length	25	in						
	Sx(in3)	131	415									
Model Name	Beam- Column properties			Stub Properties			Shear Stud Config3	Shear Stud number	Stiffener			Grout Strength fc'(ksi)
		w24x62	w14x257									
Model3	height(in)	23.7	16.4	Inside height(ht)	28.7	in	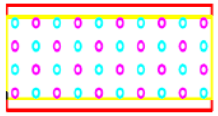	80	Thickness	0.5	in	6
	width(in)	7.04	16	Flange (ttf)	0.75	in			width	3.91	in	
	flange thic(in)	0.59	1.89	Side(tts)	0.5	in			length	12.62	in	
	web thick(in)	0.43	1.18	width(bt)	9	in						
	Zx(in3)	153	487	Length	25	in						
	Sx(in3)	131	415									
Model Name	Beam- Column properties			Stub Properties			Shear Stud Config4	Shear Stud number	Stiffener			Grout Strength fc'(ksi)
		w24x62	w14x257									
Model4	height(in)	23.7	16.4	Inside height(ht)	28.7	in	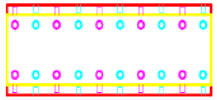	80	Thickness	0.5	in	6
	width(in)	7.04	16	Flange (ttf)	0.75	in			width	3.91	in	
	flange thic(in)	0.59	1.89	Side(tts)	0.5	in			length	12.62	in	
	web thick(in)	0.43	1.18	width(bt)	9	in						
	Zx(in3)	153	487	Length	25	in						
	Sx(in3)	131	415									

Figure 5-5: Parametric Study Matrix 2 for Beam Section W24x62 (Stub: Inside Height=28.7 inches; Flange Thickness=0.75 inches)

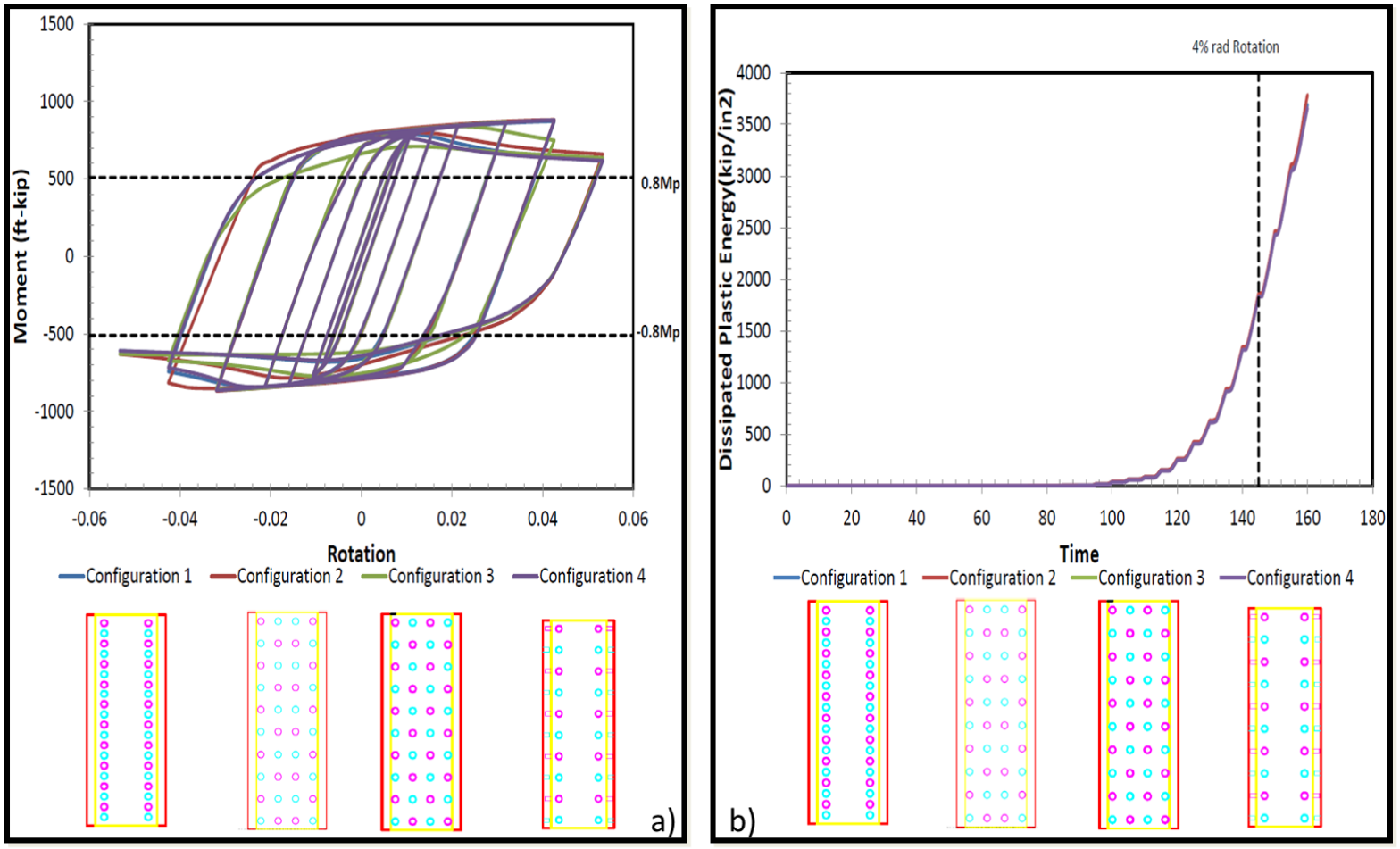

Figure 5-6: a) Moment-Rotation Curves and b) Dissipated Energy Levels for Matrix 2

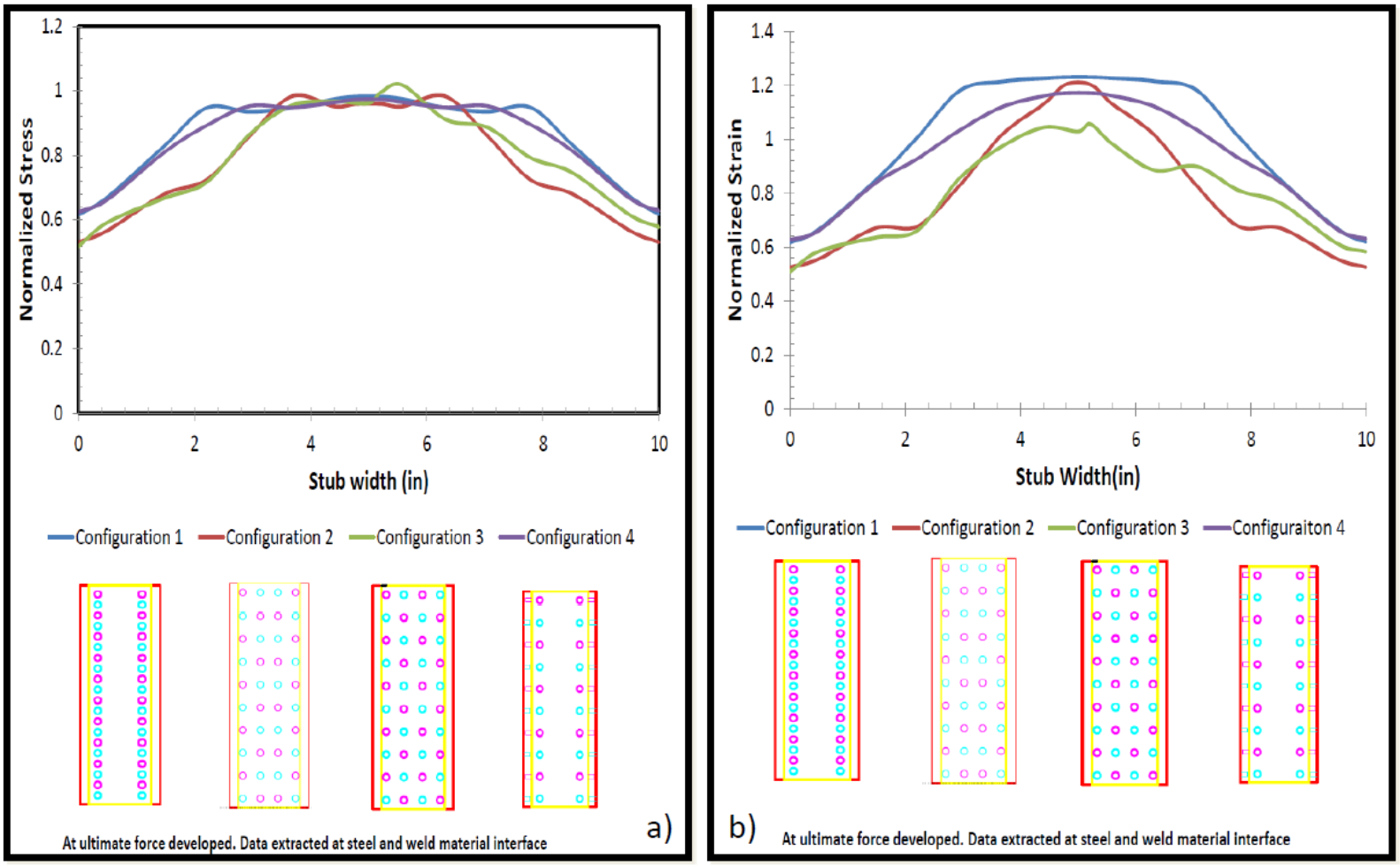

Figure 5-7: a) Normalized Longitudinal Stress and b) Normalized Longitudinal Strain at the Welded Regions for Matrix 2

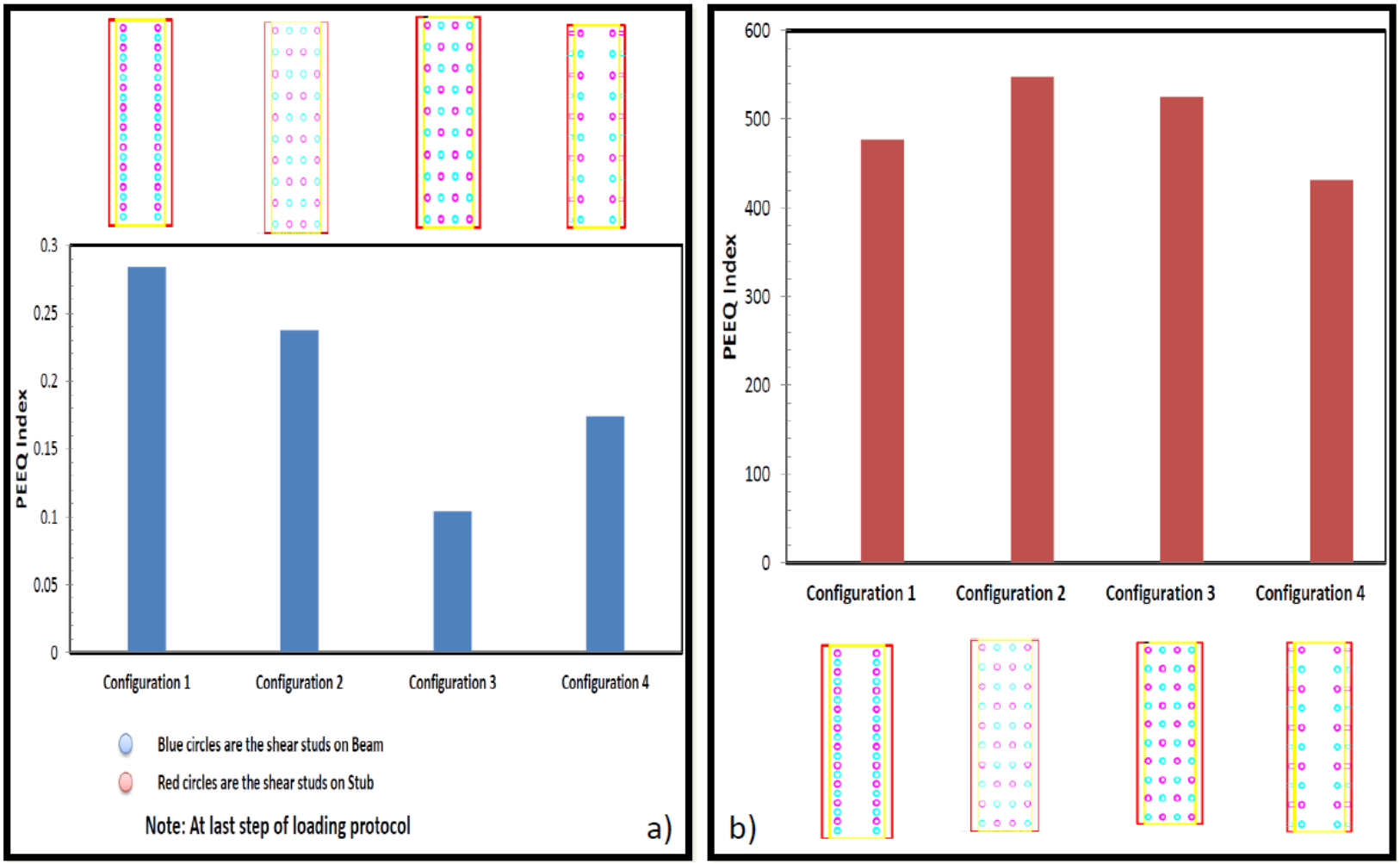

Figure 5-8: a) PEEQ Index at the Welded Regions and b) PEEQ Index at Plastic Hinge Regions for Matrix 2

Model Name	Beam- Column properties			Stub Properties			Shear Stud Config1	Shear Stud number	Stiffener			Grout Strength fc'(ksi)
		w24x62	w14x257									
Model1	height(in)	23.7	16.4	Height(ht)	28.7	in		80	Thickness	0.5	in	6
	width(in)	7.04	16	Flange (ttf)	1	in			width	3.91	in	
	flange thic(in)	0.59	1.89	Side(tts)	0.5	in			length	12.62	in	
	web thick(in)	0.43	1.18	width(bt)	9	in						
	Zx(in3)	153	487	Length	25	in						
	Sx(in3)	131	415									
Model Name	Beam- Column properties			Stub Properties			Shear Stud Config2	Shear Stud number	Stiffener			Grout Strength fc'(ksi)
		w24x62	w14x257									
Model2	height(in)	23.7	16.4	Inside height(ht)	28.7	in	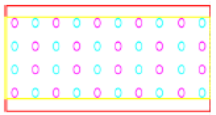	80	Thickness	0.5	in	6
	width(in)	7.04	16	Flange (ttf)	1	in			width	3.91	in	
	flange thic(in)	0.59	1.89	Side(tts)	0.5	in			length	12.62	in	
	web thick(in)	0.43	1.18	width(bt)	9	in						
	Zx(in3)	153	487	Length	25	in						
	Sx(in3)	131	415									
Model Name	Beam- Column properties			Stub Properties			Shear Stud Config3	Shear Stud number	Stiffener			Grout Strength fc'(ksi)
		w24x62	w14x257									
Model3	height(in)	23.7	16.4	Inside height(ht)	28.7	in	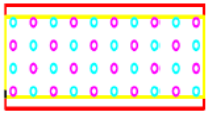	80	Thickness	0.5	in	6
	width(in)	7.04	16	Flange (ttf)	1	in			width	3.91	in	
	flange thic(in)	0.59	1.89	Side(tts)	0.5	in			length	12.62	in	
	web thick(in)	0.43	1.18	width(bt)	9	in						
	Zx(in3)	153	487	Length	25	in						
	Sx(in3)	131	415									
Model Name	Beam- Column properties			Stub Properties			Shear Stud Config4	Shear Stud number	Stiffener			Grout Strength fc'(ksi)
		w24x62	w14x257									
Model4	height(in)	23.7	16.4	Inside height(ht)	28.7	in	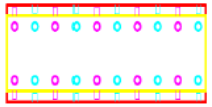	80	Thickness	0.5	in	6
	width(in)	7.04	16	Flange (ttf)	1	in			width	3.91	in	
	flange thic(in)	0.59	1.89	Side(tts)	0.5	in			length	12.62	in	
	web thick(in)	0.43	1.18	width(bt)	9	in						
	Zx(in3)	153	487	Length	25	in						
	Sx(in3)	131	415									

Figure 5-9: Parametric Study Matrix 3 for Beam Section (Stub: Inside Height=28.7 inches; Flange Thickness=1 inch)

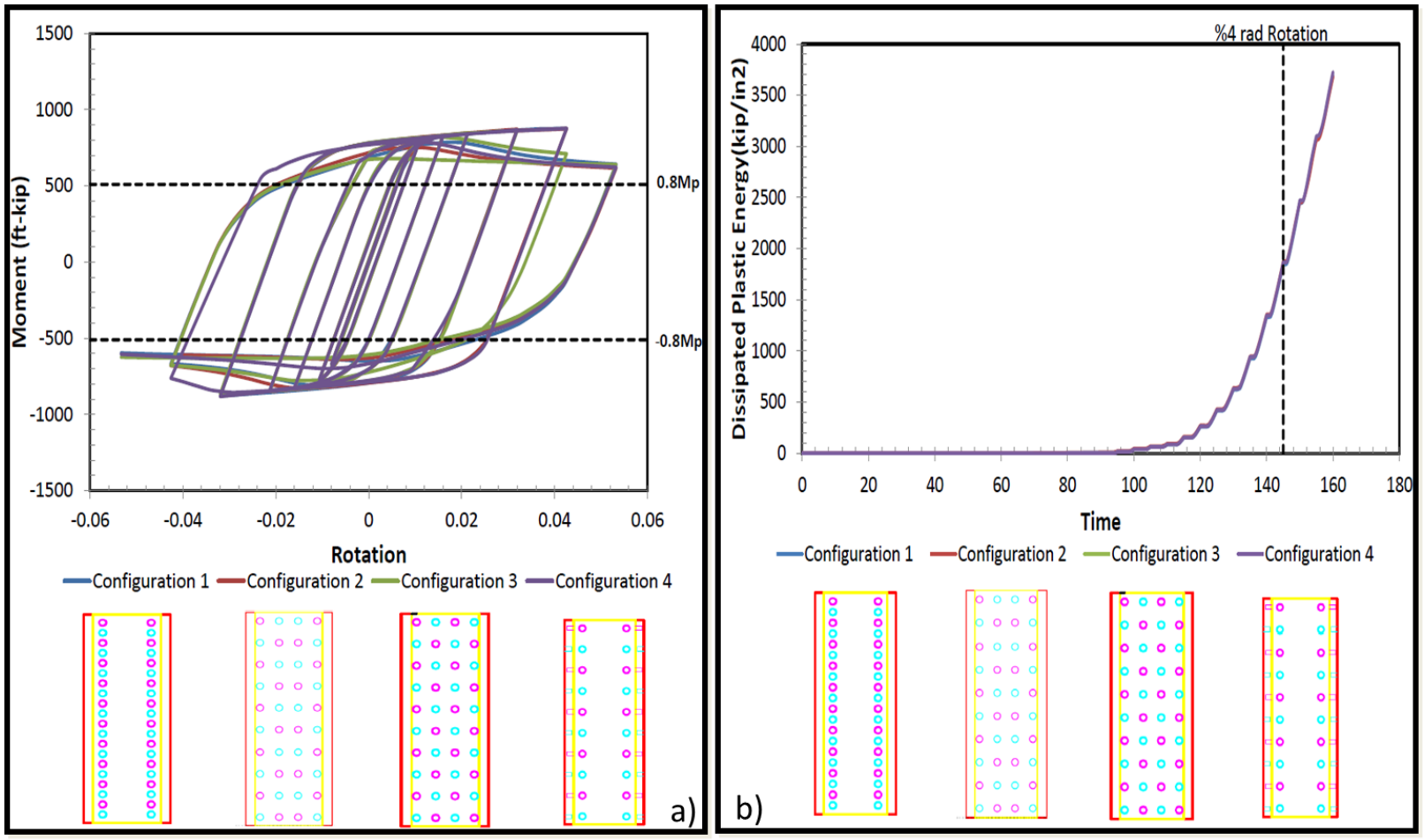

Figure 5-10: a) Moment-Rotation Curves and b) Dissipated Energy Levels for Matrix 3

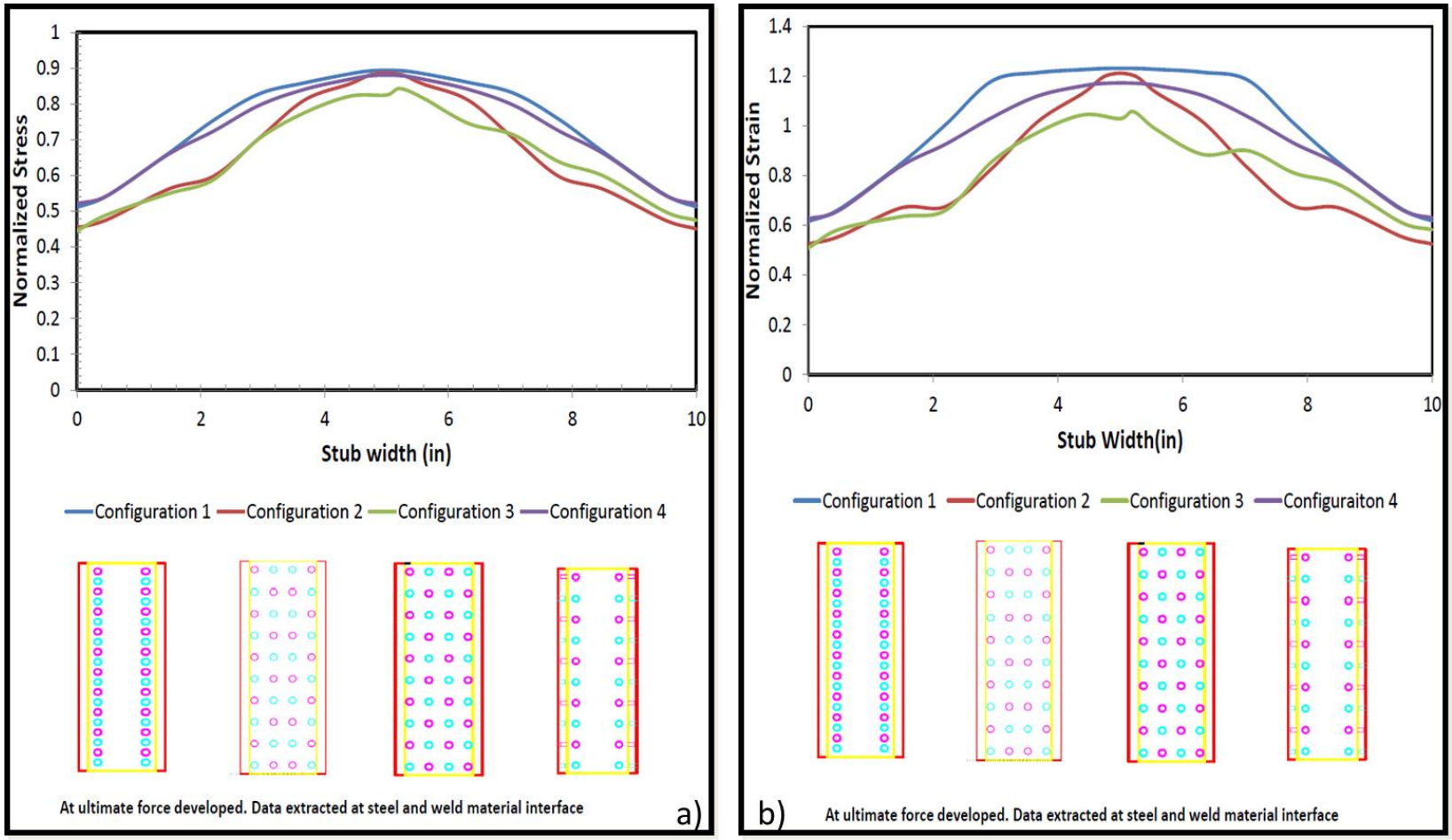

Figure 5-11: a) Normalized Longitudinal Stress and b) Normalized Longitudinal Strain at the Welded Regions for Matrix 3

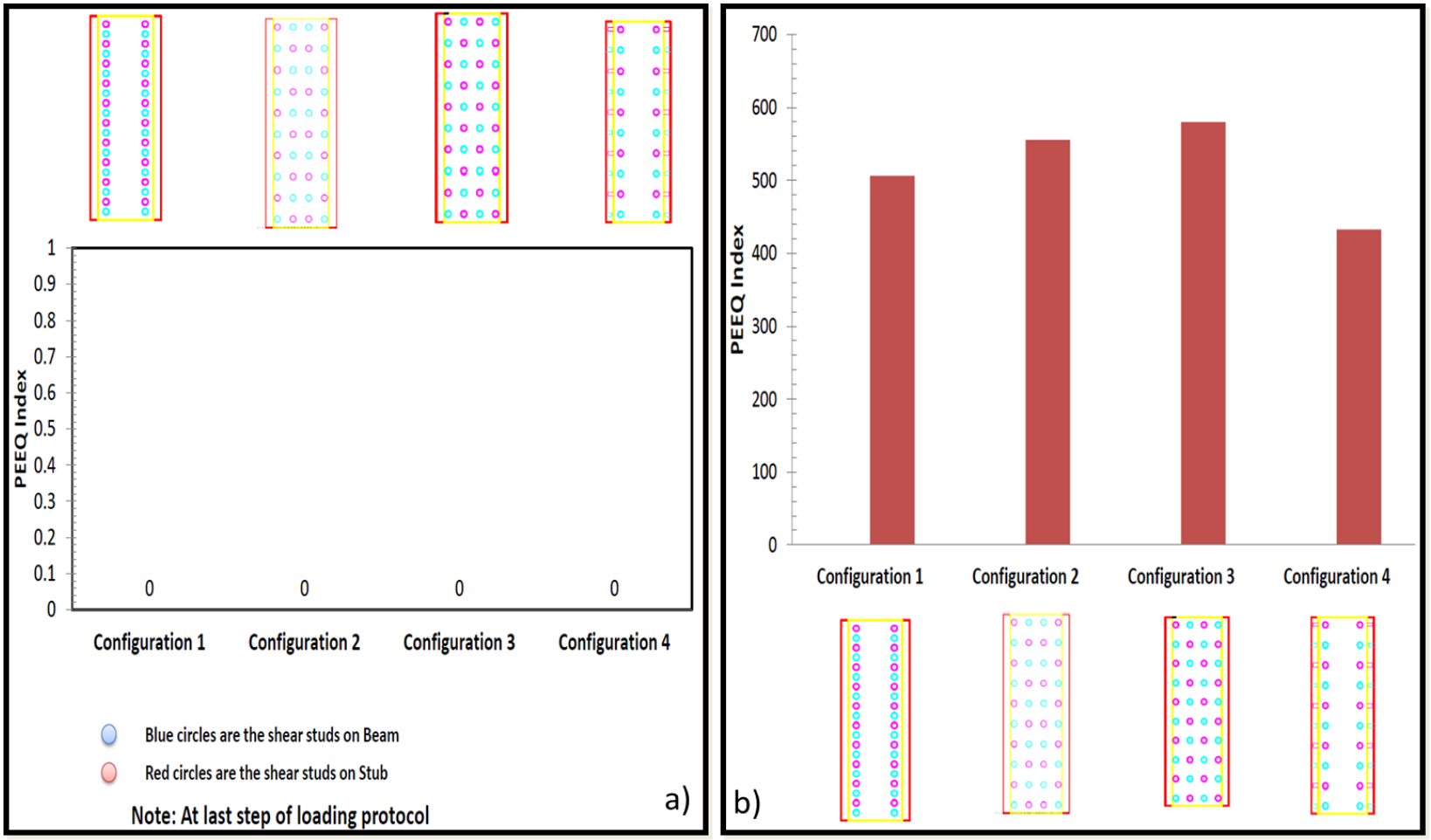

Figure 5-12: a) PEEQ Index at the Welded Regions and b) PEEQ Index at Plastic Hinge Regions for Matrix 3

Model Name	Beam- Column properties			Stub Properties			Shear Stud Config1	Shear Stud number	Stiffener			Grout Strength fc'(ksi)
		w24x62	w14x257									
Model1	height(in)	23.7	16.4	Height(ht)	32	in		80	Thickness	0.5	in	6
	width(in)	7.04	16	Flange (ttf)	0.6	in			width	3.91	in	
	flange thic(in)	0.59	1.89	Side(tts)	0.5	in			length	12.62	in	
	web thick(in)	0.43	1.18	width(bt)	9	in						
	Zx(in3)	153	487	Length	25	in						
	Sx(in3)	131	415									
Model Name	Beam- Column properties			Stub Properties			Shear Stud Config2	Shear Stud number	Stiffener			Grout Strength fc'(ksi)
		w24x62	w14x257									
Model2	height(in)	23.7	16.4	Inside height(ht)	32	in	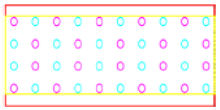	80	Thickness	0.5	in	6
	width(in)	7.04	16	Flange (ttf)	0.6	in			width	3.91	in	
	flange thic(in)	0.59	1.89	Side(tts)	0.5	in			length	12.62	in	
	web thick(in)	0.43	1.18	width(bt)	9	in						
	Zx(in3)	153	487	Length	25	in						
	Sx(in3)	131	415									
Model Name	Beam- Column properties			Stub Properties			Shear Stud Config3	Shear Stud number	Stiffener			Grout Strength fc'(ksi)
		w24x62	w14x257									
Model3	height(in)	23.7	16.4	Inside height(ht)	32	in	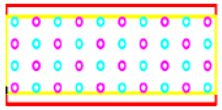	80	Thickness	0.5	in	6
	width(in)	7.04	16	Flange (ttf)	0.6	in			width	3.91	in	
	flange thic(in)	0.59	1.89	Side(tts)	0.5	in			length	12.62	in	
	web thick(in)	0.43	1.18	width(bt)	9	in						
	Zx(in3)	153	487	Length	25	in						
	Sx(in3)	131	415									
Model Name	Beam- Column properties			Stub Properties			Shear Stud Config4	Shear Stud number	Stiffener			Grout Strength fc'(ksi)
		w24x62	w14x257									
Model4	height(in)	23.7	16.4	Inside height(ht)	32	in	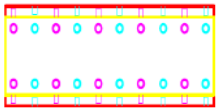	80	Thickness	0.5	in	6
	width(in)	7.04	16	Flange (ttf)	0.6	in			width	3.91	in	
	flange thic(in)	0.59	1.89	Side(tts)	0.5	in			length	12.62	in	
	web thick(in)	0.43	1.18	width(bt)	9	in						
	Zx(in3)	153	487	Length	25	in						
	Sx(in3)	131	415									

Figure 5-13: Parametric Study Matrix 4 for Beam Section W24x62 (Stub: Inside Height=32 inches; Flange Thickness=0.6 inches)

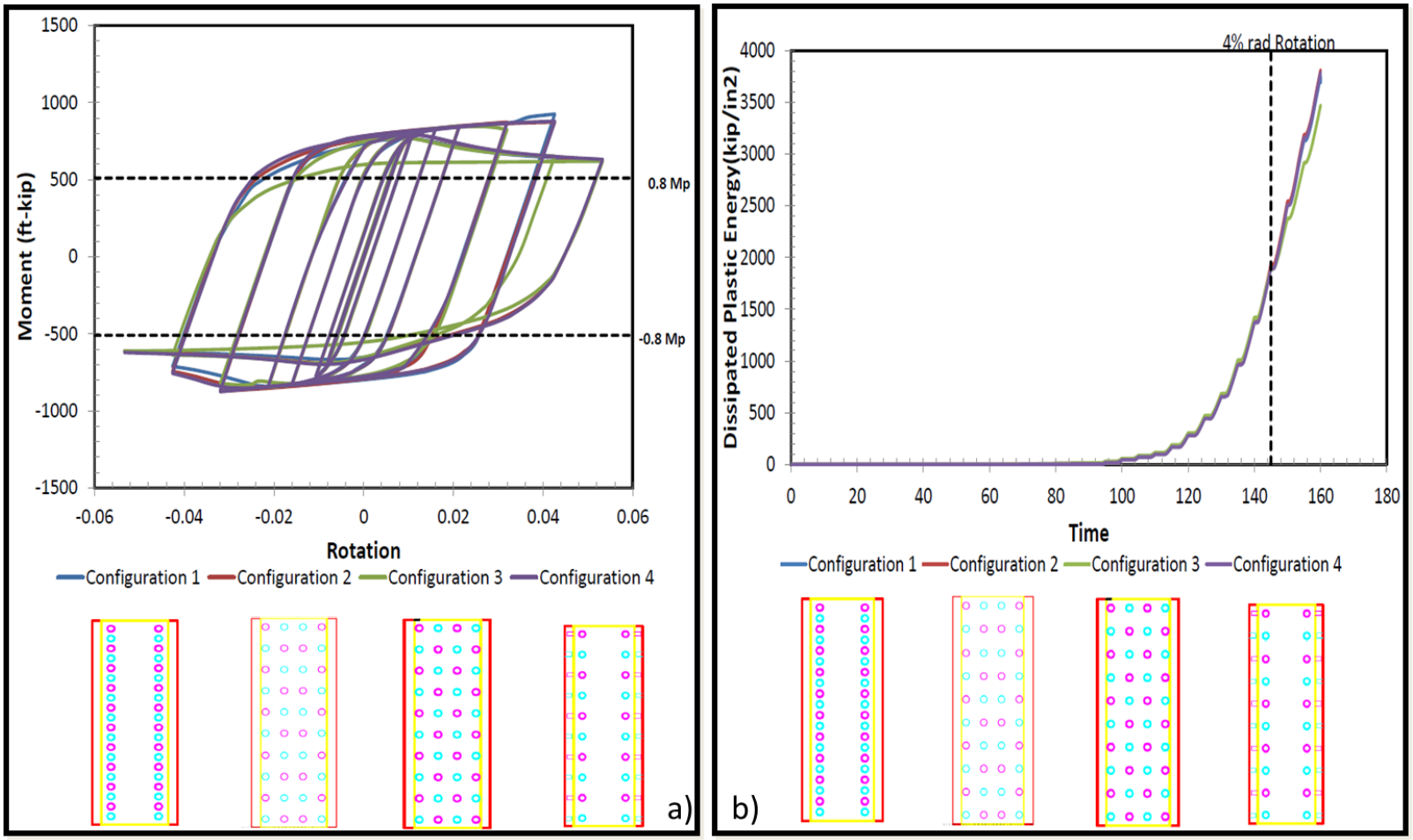

Figure 5-14: a) Moment-Rotation Curves and b) Dissipated Energy Levels for Matrix 4

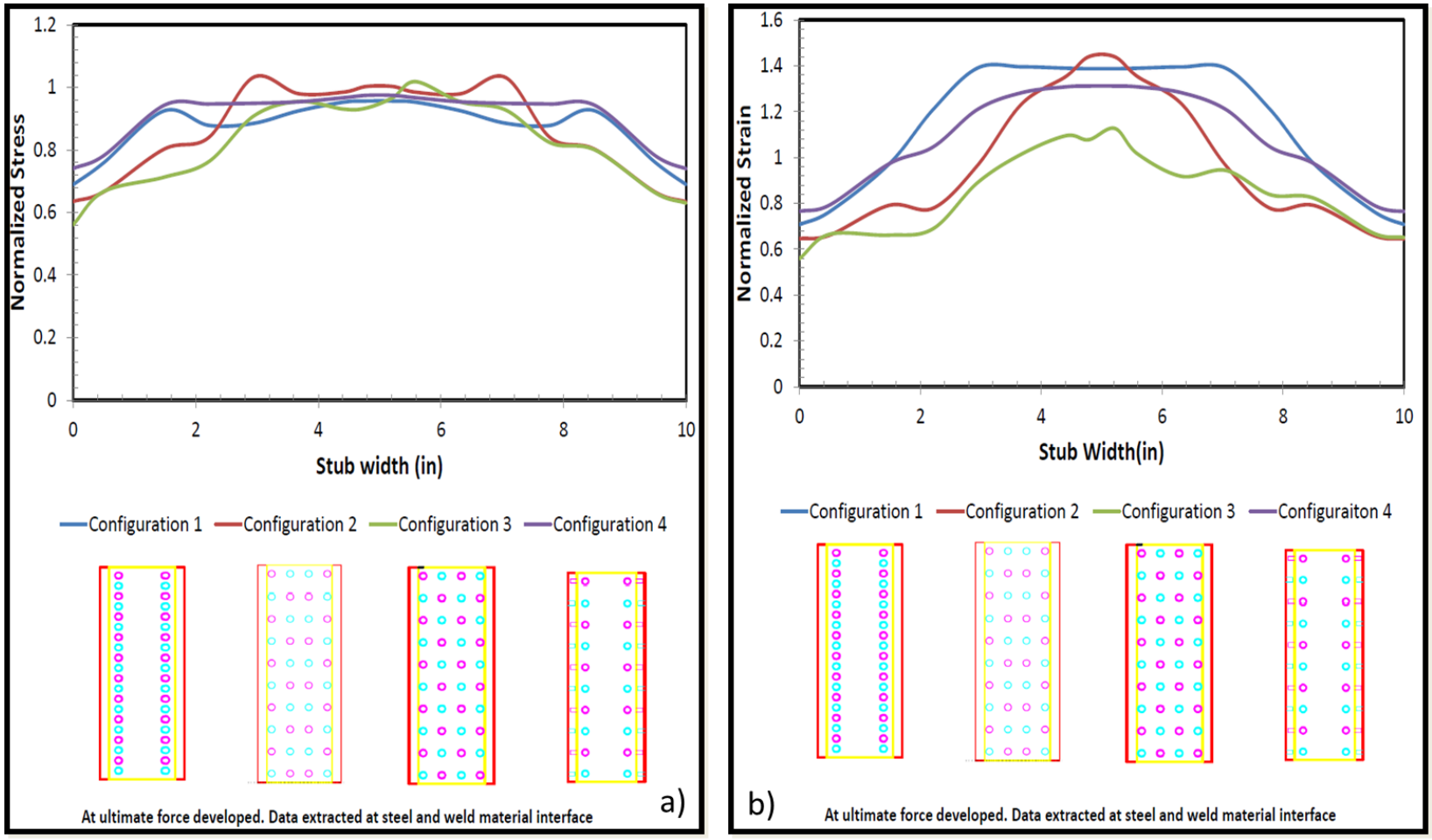

Figure 5-15: a) Normalized Longitudinal Stress and b) Normalized Longitudinal Strain at the Welded Regions for Matrix4

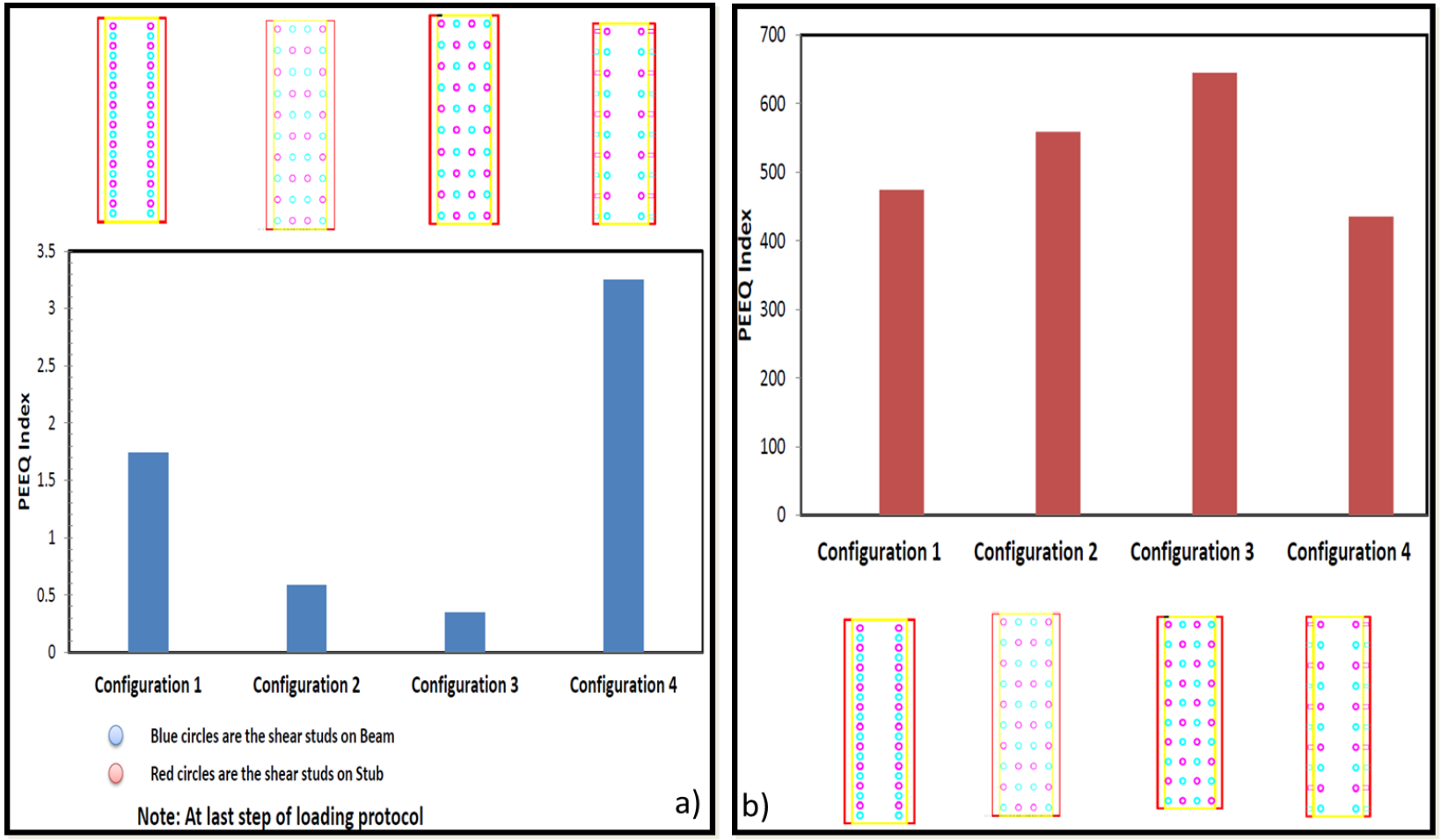

Figure 5-16: a) PEEQ Index at the Welded Regions and b) PEEQ Index at Plastic Hinge Regions for Matrix 4

Model Name	Beam- Column properties			Stub Properties			Shear Stud Config1	Shear Stud number	Stiffener			Grout Strength fc'(ksi)
		w24x62	w14x257									
Model1	height(in)	23.7	16.4	Height(ht)	32	in		80	Thickness	0.5	in	6
	width(in)	7.04	16	Flange (ttf)	0.75	in			width	3.91	in	
	flange thic(in)	0.59	1.89	Side(tts)	0.5	in			length	12.62	in	
	web thick(in)	0.43	1.18	width(bt)	9	in						
	Zx(in3)	153	487	Length	25	in						
	Sx(in3)	131	415									
Model Name	Beam- Column properties			Stub Properties			Shear Stud Config2	Shear Stud number	Stiffener			Grout Strength fc'(ksi)
		w24x62	w14x257									
Model2	height(in)	23.7	16.4	Inside height(ht)	32	in	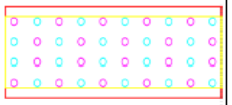	80	Thickness	0.5	in	6
	width(in)	7.04	16	Flange (ttf)	0.75	in			width	3.91	in	
	flange thic(in)	0.59	1.89	Side(tts)	0.5	in			length	12.62	in	
	web thick(in)	0.43	1.18	width(bt)	9	in						
	Zx(in3)	153	487	Length	25	in						
	Sx(in3)	131	415									
Model Name	Beam- Column properties			Stub Properties			Shear Stud Config3	Shear Stud number	Stiffener			Grout Strength fc'(ksi)
		w24x62	w14x257									
Model3	height(in)	23.7	16.4	Inside height(ht)	32	in	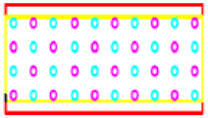	80	Thickness	0.5	in	6
	width(in)	7.04	16	Flange (ttf)	0.75	in			width	3.91	in	
	flange thic(in)	0.59	1.89	Side(tts)	0.5	in			length	12.62	in	
	web thick(in)	0.43	1.18	width(bt)	9	in						
	Zx(in3)	153	487	Length	25	in						
	Sx(in3)	131	415									
Model Name	Beam- Column properties			Stub Properties			Shear Stud Config4	Shear Stud number	Stiffener			Grout Strength fc'(ksi)
		w24x62	w14x257									
Model4	height(in)	23.7	16.4	Inside height(ht)	32	in	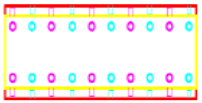	80	Thickness	0.5	in	6
	width(in)	7.04	16	Flange (ttf)	0.75	in			width	3.91	in	
	flange thic(in)	0.59	1.89	Side(tts)	0.5	in			length	12.62	in	
	web thick(in)	0.43	1.18	width(bt)	9	in						
	Zx(in3)	153	487	Length	25	in						
	Sx(in3)	131	415									

Figure 5-17: Parametric Study Matrix 5 for Beam Section W24x62 (Stub: Inside Height=32 inches; Flange Thickness=0.75 inches)

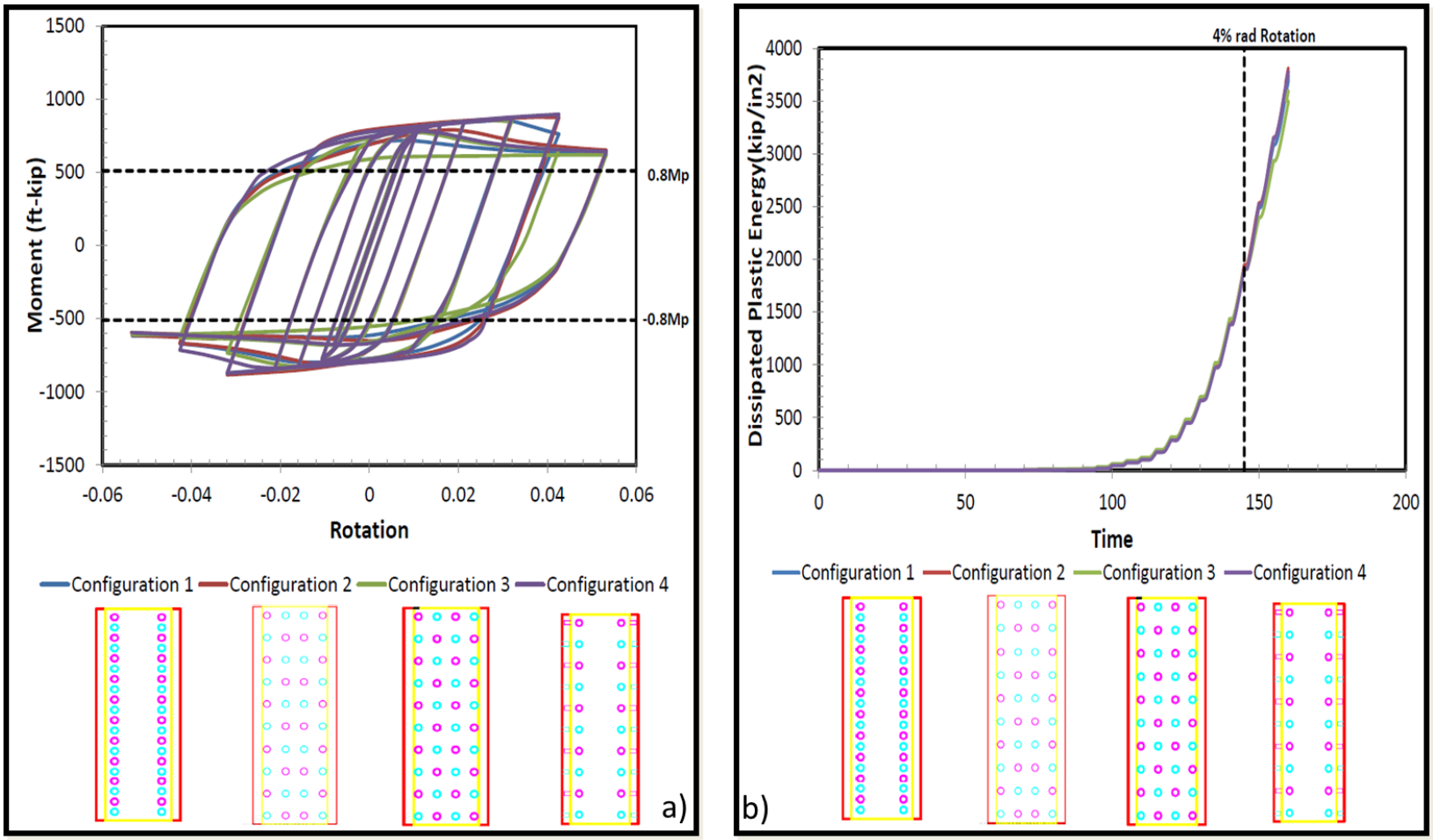

Figure 5-18: a) Moment-Rotation Curves and b) Dissipated Energy Levels for Matrix 5

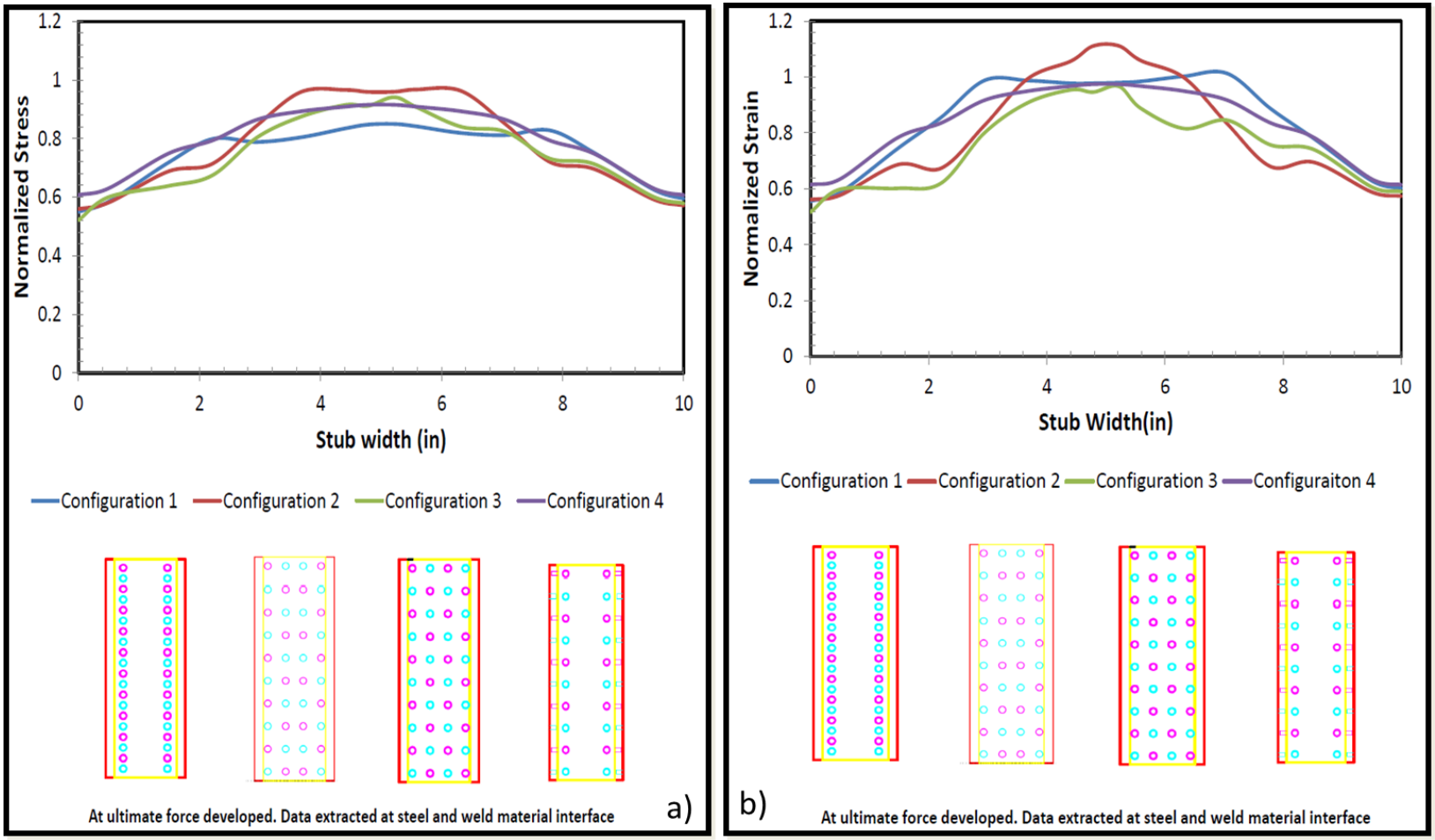

Figure 5-19: a) Normalized Longitudinal Stress and b) Normalized Longitudinal Strain at the Welded Regions for Matrix 5

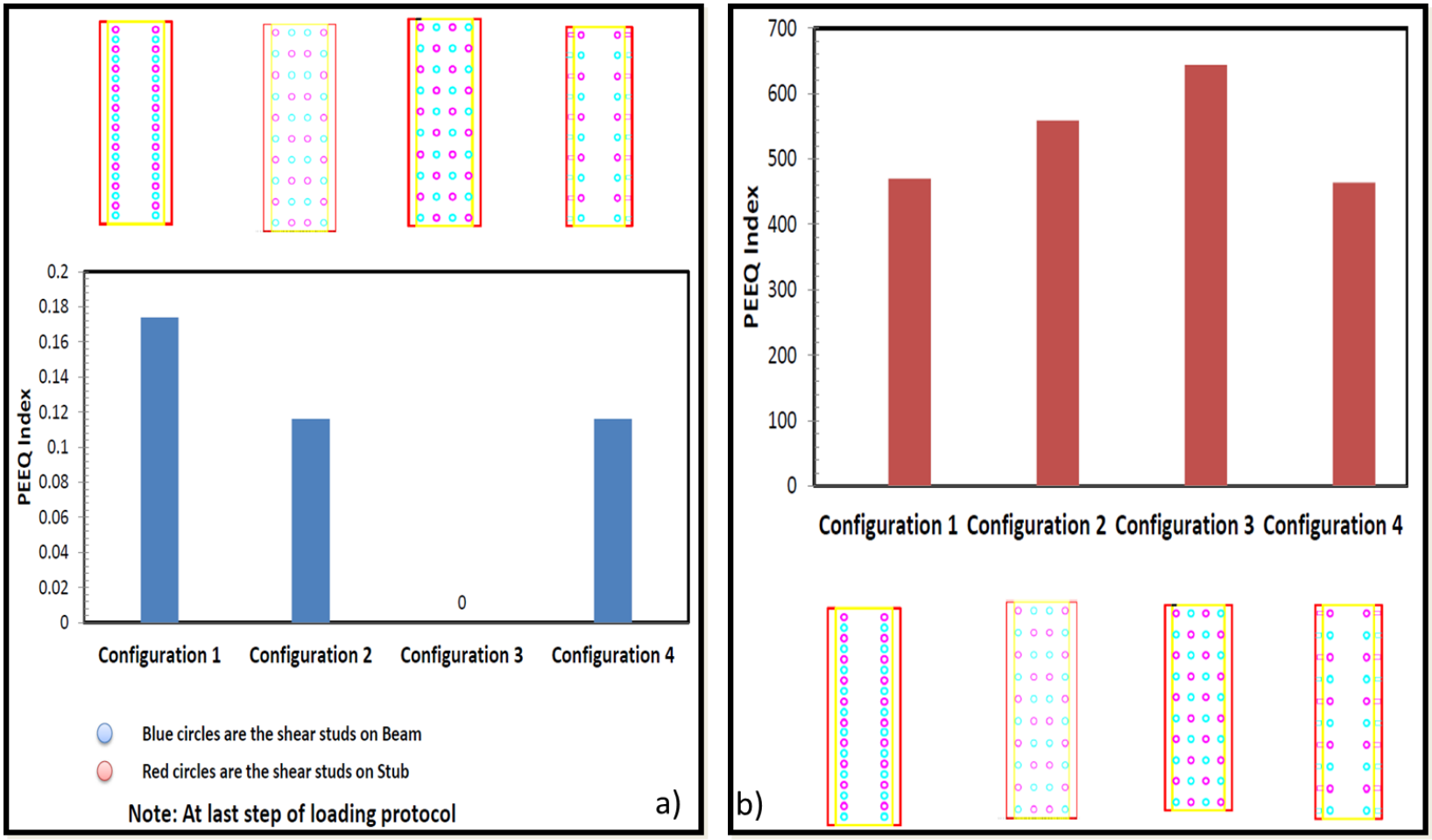

Figure 5-20: a) PEEQ Index at the Welded Regions and b) PEEQ Index at Plastic Hinge Regions for Matrix 5

Model Name	Beam- Column properties			Stub Properties			Shear Stud Config1	Shear Stud number	Stiffener			Grout Strength fc'(ksi)
		w24x62	w14x257									
Model1	height(in)	23.7	16.4	Height(ht)	32	in		80	Thickness	0.5	in	6
	width(in)	7.04	16	Flange (ttf)	1	in			width	3.91	in	
	flange thic(in)	0.59	1.89	Side(tts)	0.5	in			length	12.62	in	
	web thick(in)	0.43	1.18	width(bt)	9	in						
	Zx(in3)	153	487	Length	25	in						
	Sx(in3)	131	415									
Model Name	Beam- Column properties			Stub Properties			Shear Stud Config2	Shear Stud number	Stiffener			Grout Strength fc'(ksi)
		w24x62	w14x257									
Model2	height(in)	23.7	16.4	Inside height(ht)	32	in	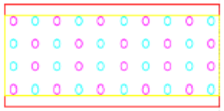	80	Thickness	0.5	in	6
	width(in)	7.04	16	Flange (ttf)	1	in			width	3.91	in	
	flange thic(in)	0.59	1.89	Side(tts)	0.5	in			length	12.62	in	
	web thick(in)	0.43	1.18	width(bt)	9	in						
	Zx(in3)	153	487	Length	25	in						
	Sx(in3)	131	415									
Model Name	Beam- Column properties			Stub Properties			Shear Stud Config3	Shear Stud number	Stiffener			Grout Strength fc'(ksi)
		w24x62	w14x257									
Model3	height(in)	23.7	16.4	Inside height(ht)	32	in	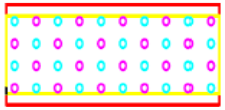	80	Thickness	0.5	in	6
	width(in)	7.04	16	Flange (ttf)	1	in			width	3.91	in	
	flange thic(in)	0.59	1.89	Side(tts)	0.5	in			length	12.62	in	
	web thick(in)	0.43	1.18	width(bt)	9	in						
	Zx(in3)	153	487	Length	25	in						
	Sx(in3)	131	415									
Model Name	Beam- Column properties			Stub Properties			Shear Stud Config4	Shear Stud number	Stiffener			Grout Strength fc'(ksi)
		w24x62	w14x257									
Model4	height(in)	23.7	16.4	Inside height(ht)	32	in	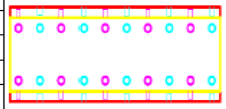	80	Thickness	0.5	in	6
	width(in)	7.04	16	Flange (ttf)	1	in			width	3.91	in	
	flange thic(in)	0.59	1.89	Side(tts)	0.5	in			length	12.62	in	
	web thick(in)	0.43	1.18	width(bt)	9	in						
	Zx(in3)	153	487	Length	25	in						
	Sx(in3)	131	415									

Figure 5-21: Parametric Study Matrix 6 for Beam Section W24x62 (Stub: Inside Height=32inches Flange Thickness=1inch)

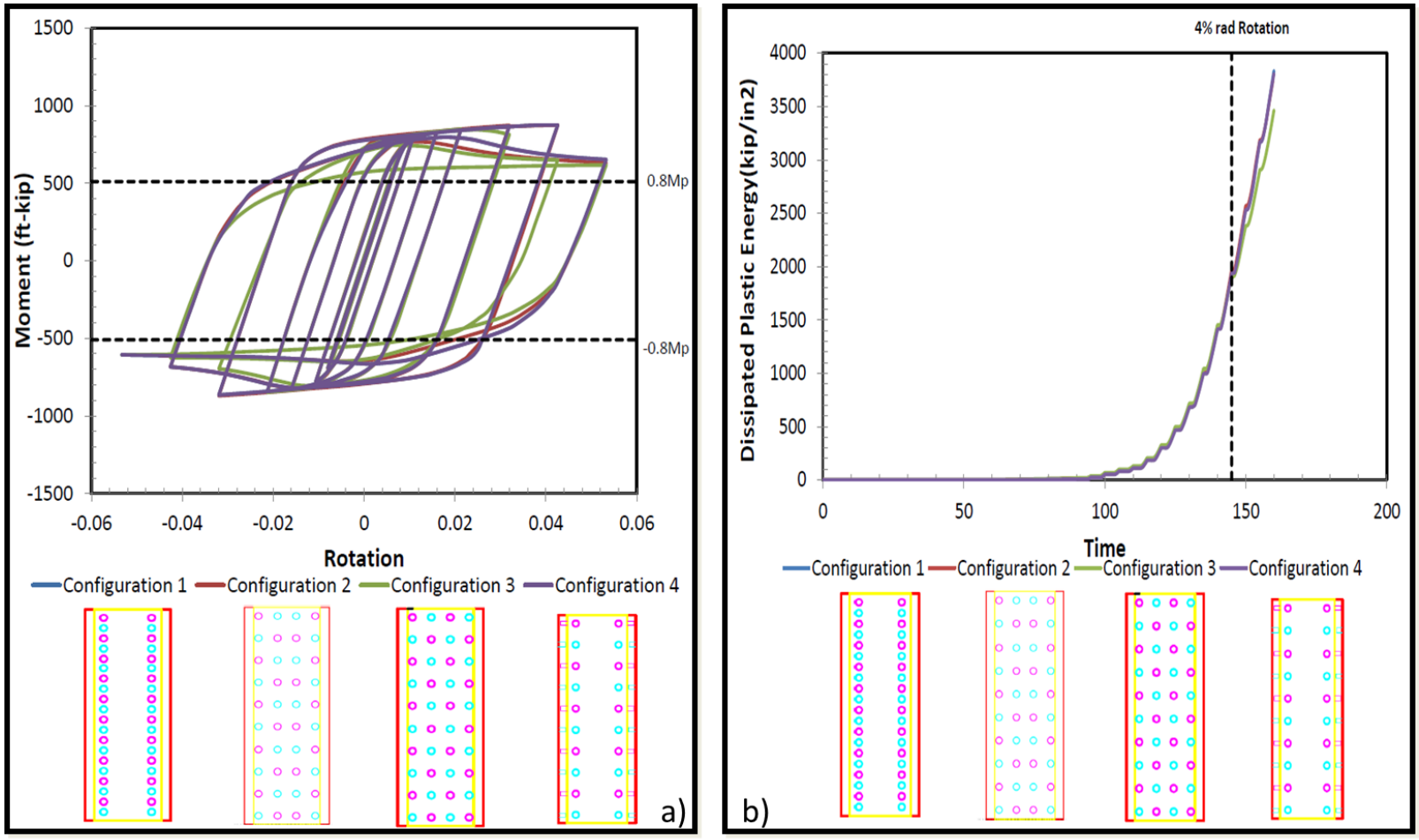

Figure 5-22: a) Moment-Rotation Curves and b) Dissipated Energy Levels for Matrix 6

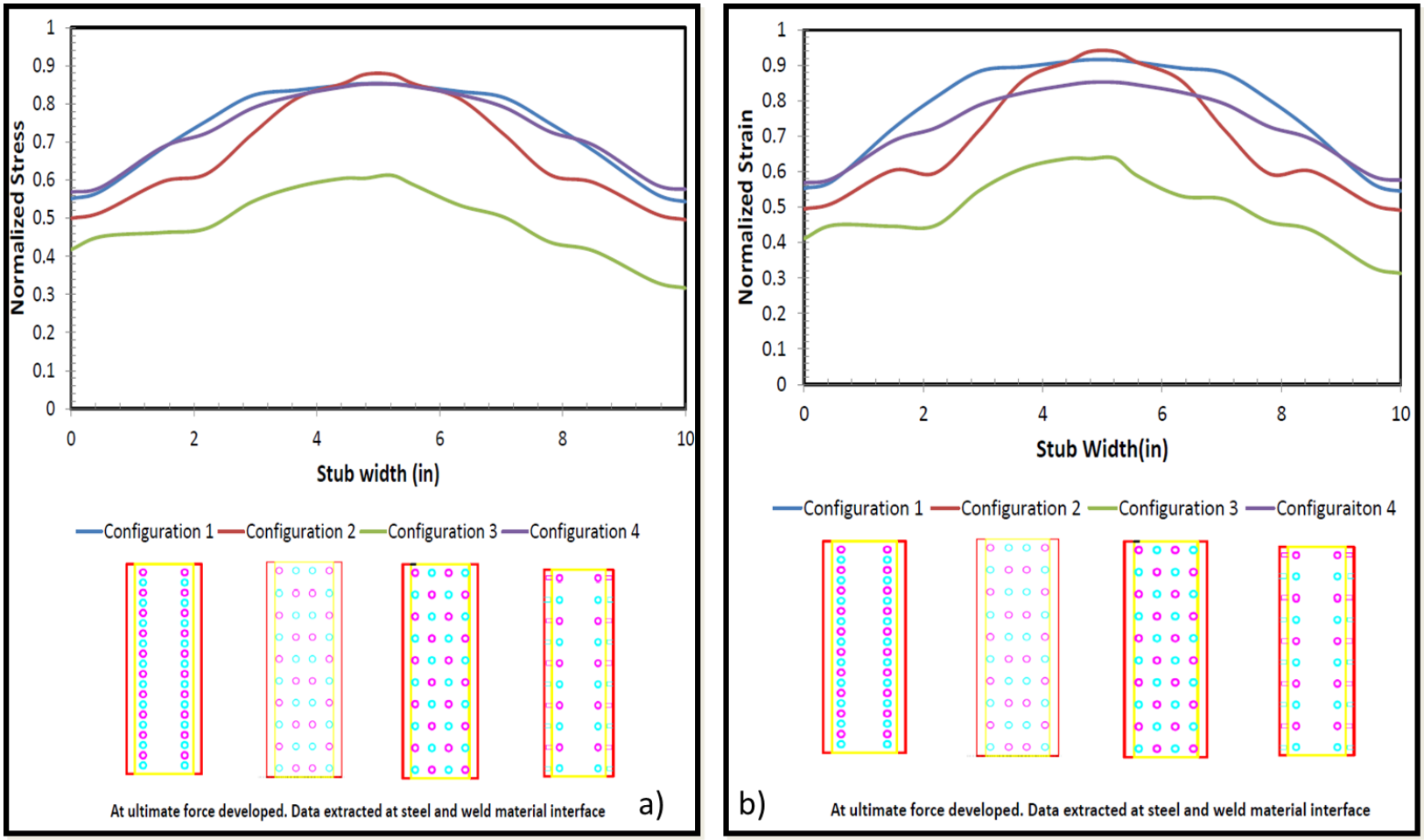

Figure 5-23: a) Normalized Longitudinal Stress and b) Normalized Longitudinal Strain at the Welded Regions for Matrix 6

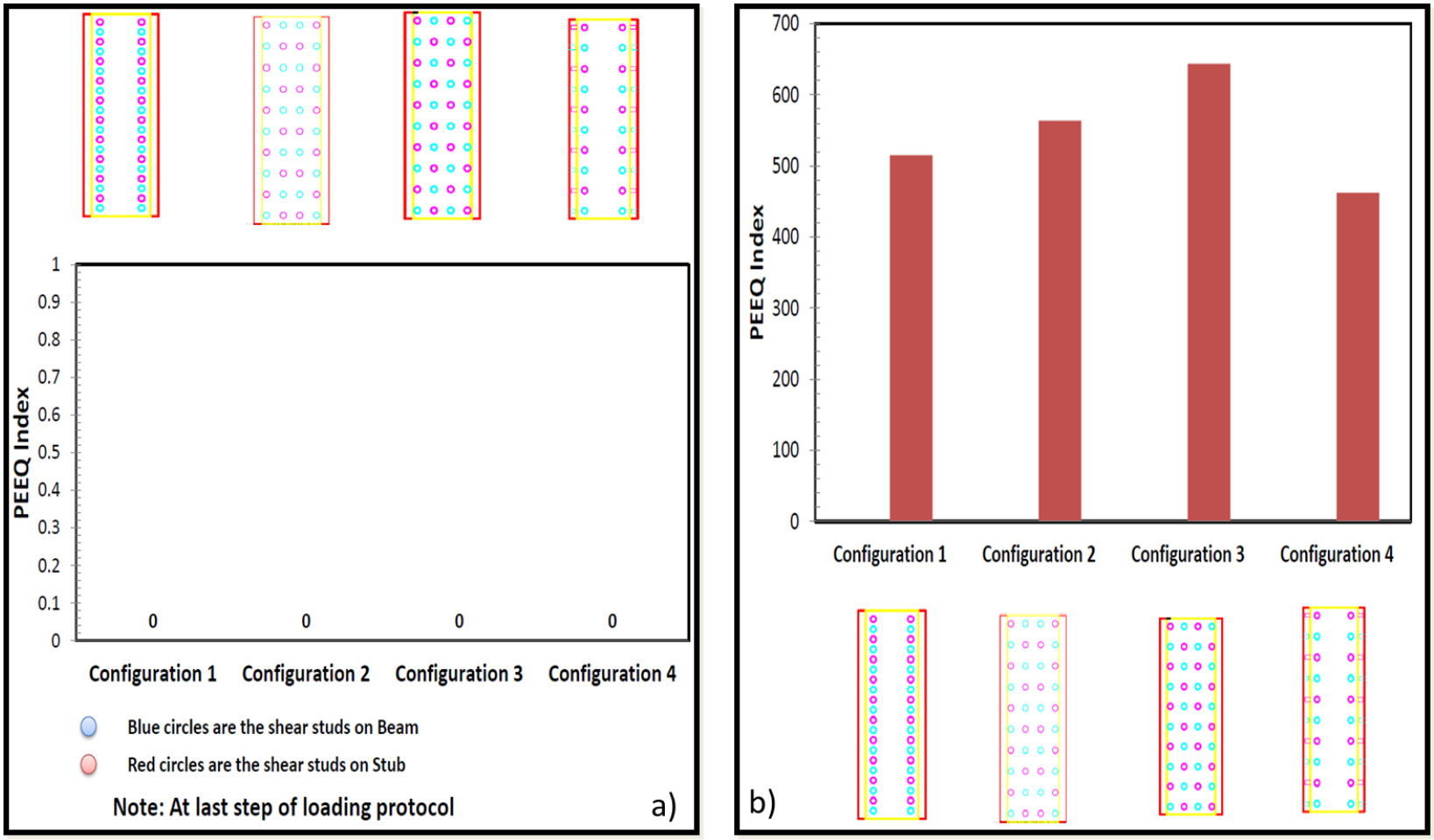

Figure 5-24: a) PEEQ Index at the Welded Regions and b) PEEQ Index at Plastic Hinge Regions for Matrix 6

Model Name	Beam- Column properties			Stub Properties			Shear Stud Config1	Shear Stud number	Stiffener			Grout Strength fc'(ksi)
		w30x108	w14x370									
Model1	height	29.8	17.9	Inside height(ht)	35	in	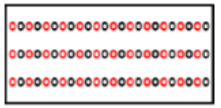	144	Thickness	0.5	in	6
	width	10.5	16.5	Flange (ttf)	0.8	in			width	5.52	in	
	flange thic	0.76	2.66	Side(tts)	0.6	in			length	12.58	in	
	web thick	0.545	1.66	width(bt)	12.7	in						
	Zx	346	736	Length	30	in						
	Sx	299	607									
Model Name	Beam- Column properties			Stub Properties			Shear Stud Config2	Shear Stud number	Stiffener			Grout Strength fc'(ksi)
		w30x108	w14x370									
Model2	height	29.8	17.9	Inside height(ht)	35	in	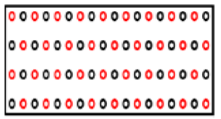	144	Thickness	0.5	in	6
	width	10.5	16.5	Flange (ttf)	0.8	in			width	5.17	in	
	flange thic	0.76	2.66	Side(tts)	0.6	in			length	12.58	in	
	web thick	0.545	1.66	width(bt)	12	in						
	Zx	346	736	Length	30	in						
	Sx	299	607									
Model Name	Beam- Column properties			Stub Properties			Shear Stud Config3	Shear Stud number	Stiffener			Grout Strength fc'(ksi)
		w30x108	w14x370									
Model3	height	29.8	17.9	Inside height(ht)	35	in	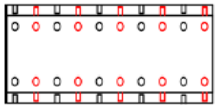	144	Thickness	0.5	in	6
	width	10.5	16.5	Flange (ttf)	0.8	in			width	5.17	in	
	flange thic	0.76	2.66	Side(tts)	0.6	in			length	12.58	in	
	web thick	0.545	1.66	width(bt)	12	in						
	Zx	346	736	Length	30	in						
	Sx	299	607									
Model Name	Beam- Column properties			Stub Properties			Shear Stud Config4	Shear Stud number	Stiffener			Grout Strength fc'(ksi)
		w30x108	w14x370									
Model4	height	29.8	17.9	Inside height(ht)	35	in	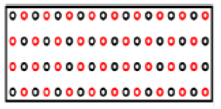	144	Thickness	0.5	in	6
	width	10.5	16.5	Flange (ttf)	0.8	in			width	5.17	in	
	flange thic	0.76	2.66	Side(tts)	0.6	in			length	12.58	in	
	web thick	0.545	1.66	width(bt)	12	in						
	Zx	346	736	Length	30	in						
	Sx	299	607									

Figure 5-25: Parametric Study Matrix 1 for Beam Section W30x108 (Stub: Inside Height=35 inches; Flange Thickness=0.8 inches)

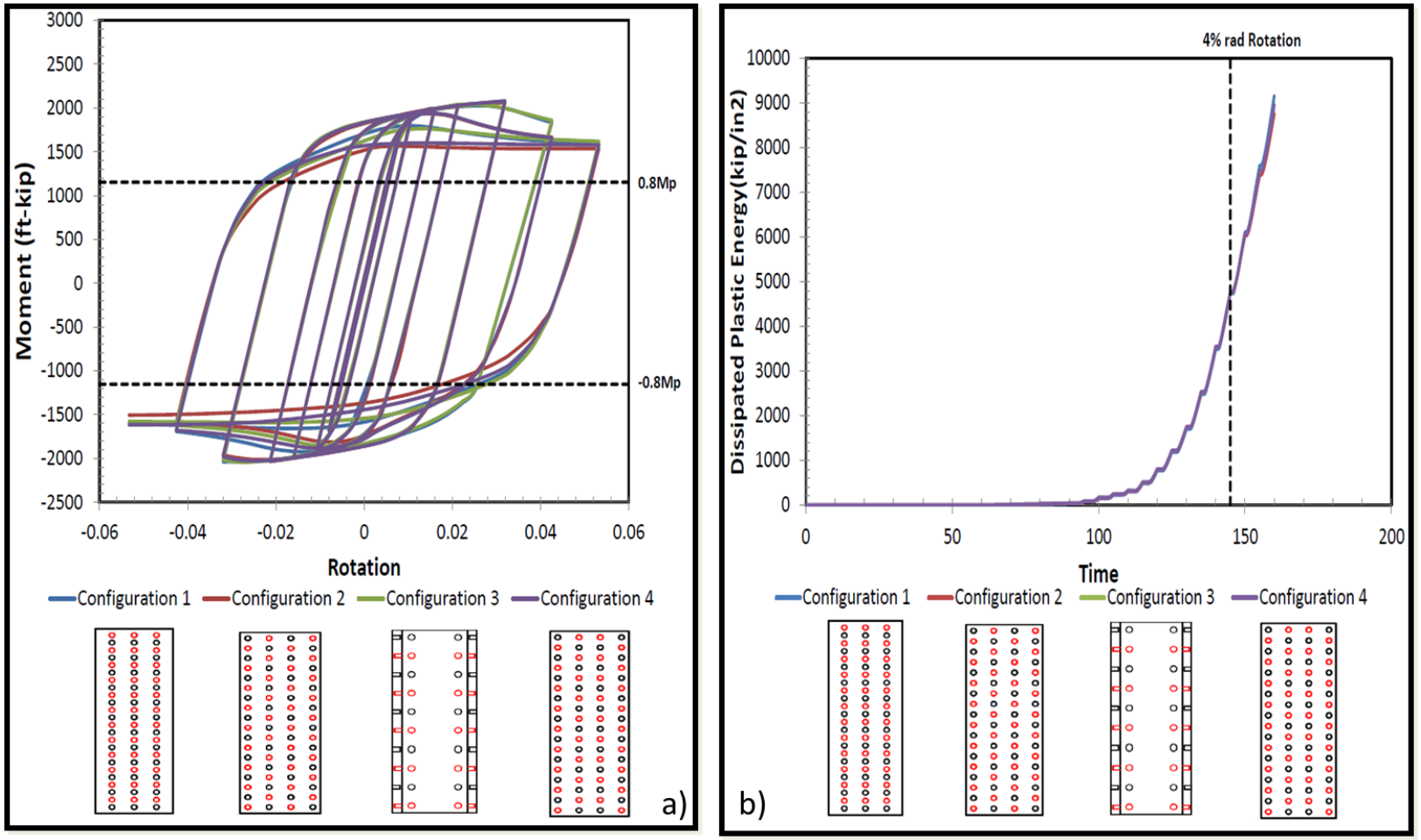

Figure 5-26: a) Moment-Rotation Curves and b) Dissipated Energy Levels for Matrix 1

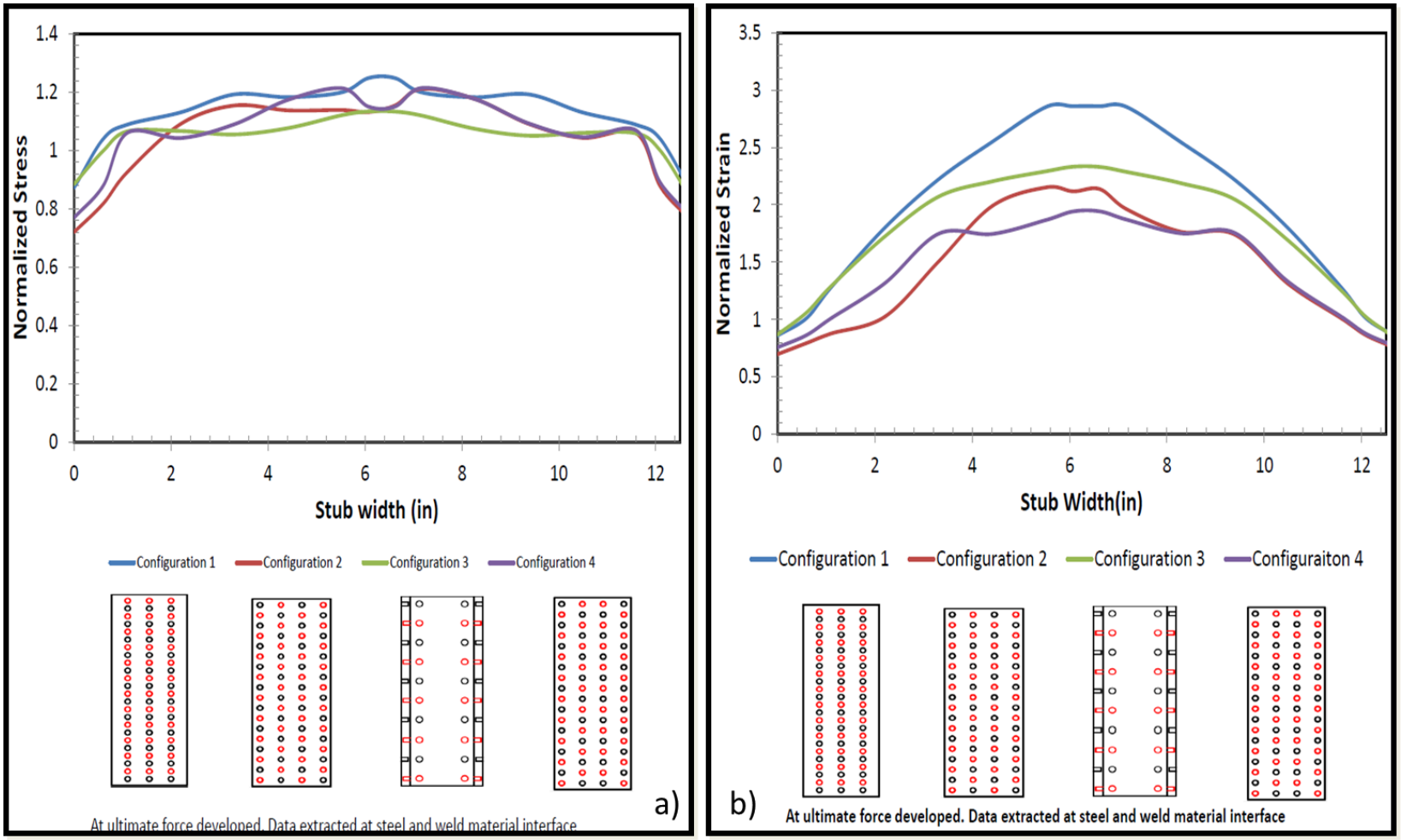

Figure 5-27: a) Normalized Longitudinal Stress and b) Normalized Longitudinal Strain at the Welded Regions for Matrix 1

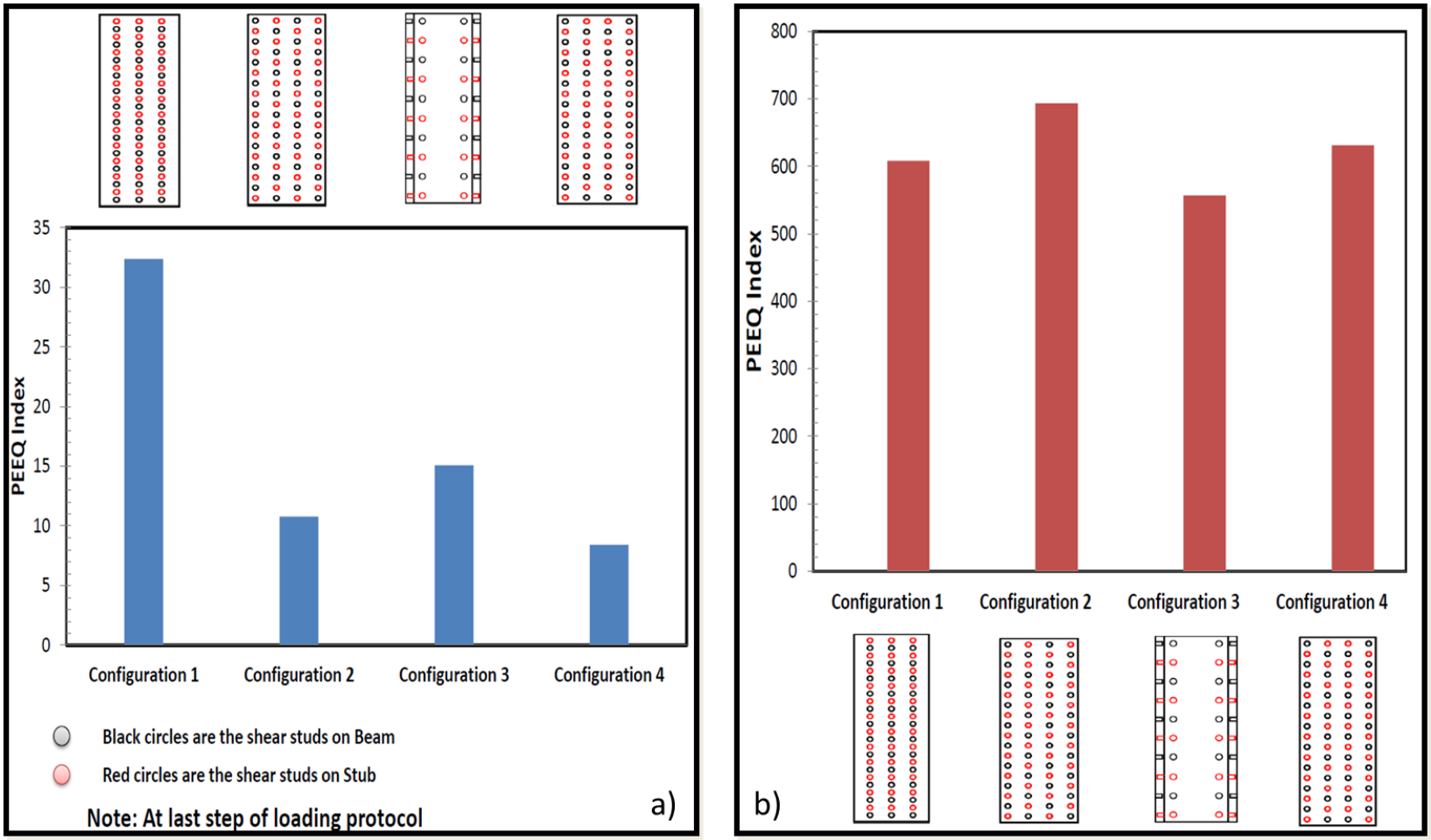

Figure 5-28: a) PEEQ Index at the Welded Regions and b) PEEQ Index at Plastic Hinge Regions for Matrix 1

Model Name	Beam- Column properties			Stub Properties			Shear Stud Config1	Shear Stud number	Stiffener			Grout Strength fc'(ksi)
		w30x108	w14x370									
Model1	height	29.8	17.9	Inside height(ht)	35	in		144	Thickness	0.5	in	6
	width	10.5	16.5	Flange (ttf)	1	in			width	5.52	in	
	flange thic	0.76	2.66	Side(tts)	0.6	in			length	12.58	in	
	web thick	0.545	1.66	width(bt)	12.7	in						
	Zx	346	736	Length	30	in						
	Sx	299	607									
Model Name	Beam- Column properties			Stub Properties			Shear Stud Config2	Shear Stud number	Stiffener			Grout Strength fc'(ksi)
		w30x108	w14x370									
Model2	height	29.8	17.9	Inside height(ht)	35	in	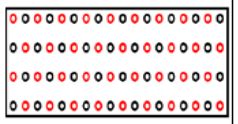	144	Thickness	0.5	in	6
	width	10.5	16.5	Flange (ttf)	1	in			width	5.17	in	
	flange thic	0.76	2.66	Side(tts)	0.6	in			length	12.58	in	
	web thick	0.545	1.66	width(bt)	12	in						
	Zx	346	736	Length	30	in						
	Sx	299	607									
Model Name	Beam- Column properties			Stub Properties			Shear Stud Config3	Shear Stud number	Stiffener			Grout Strength fc'(ksi)
		w30x108	w14x370									
Model3	height	29.8	17.9	Inside height(ht)	35	in	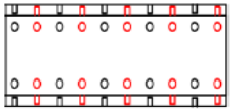	144	Thickness	0.5	in	6
	width	10.5	16.5	Flange (ttf)	1	in			width	5.17	in	
	flange thic	0.76	2.66	Side(tts)	0.6	in			length	12.58	in	
	web thick	0.545	1.66	width(bt)	12	in						
	Zx	346	736	Length	30	in						
	Sx	299	607									
Model Name	Beam- Column properties			Stub Properties			Shear Stud Config4	Shear Stud number	Stiffener			Grout Strength fc'(ksi)
		w30x108	w14x370									
Model4	height	29.8	17.9	Inside height(ht)	35	in	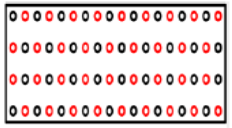	144	Thickness	0.5	in	6
	width	10.5	16.5	Flange (ttf)	1	in			width	5.17	in	
	flange thic	0.76	2.66	Side(tts)	0.6	in			length	12.58	in	
	web thick	0.545	1.66	width(bt)	12	in						
	Zx	346	736	Length	30	in						
	Sx	299	607									

Figure 5-29: Parametric Study Matrix 2 for Beam Section W30x108 (Stub: Inside Height=35 inches; Flange Thickness=1inch)

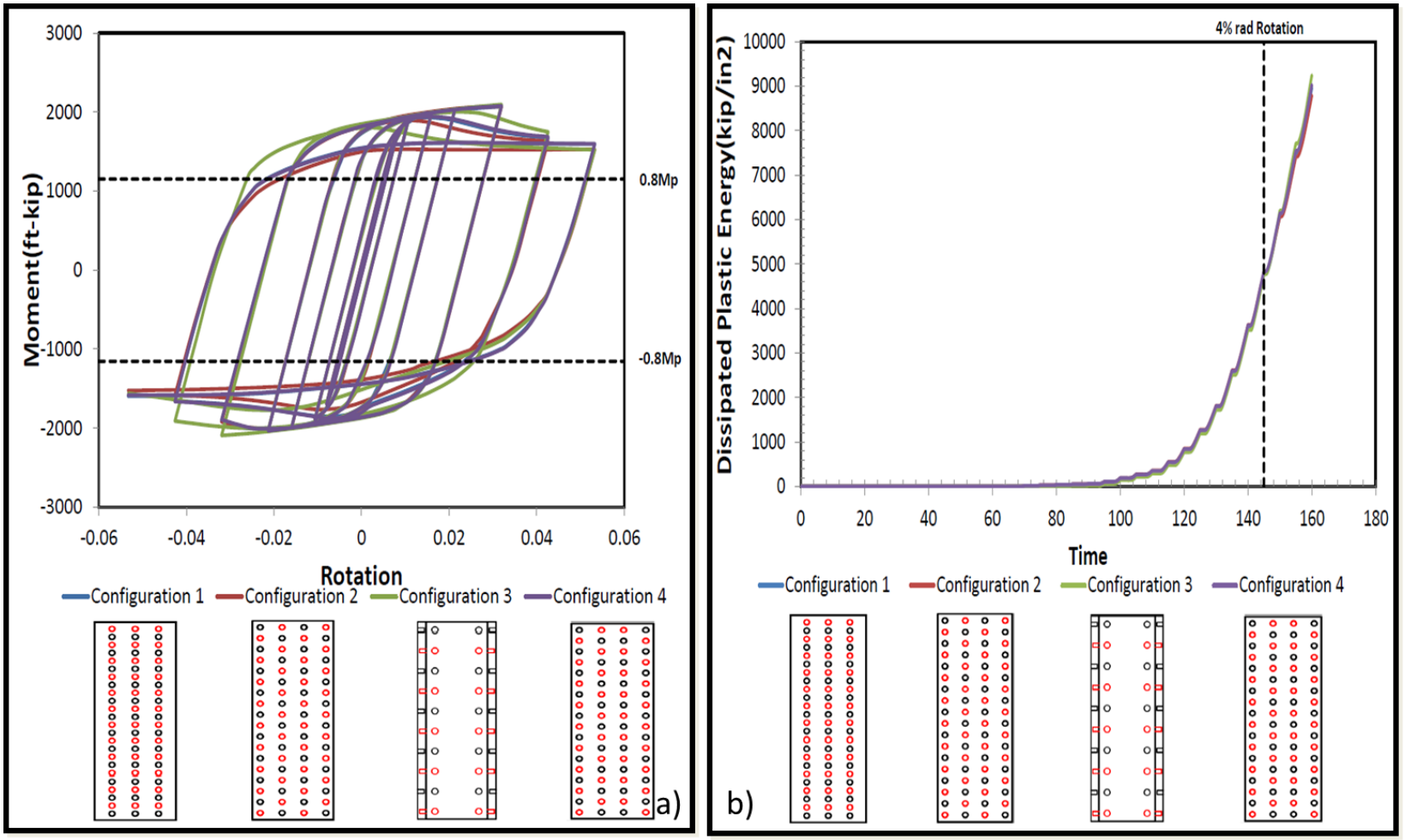

Figure 5-30: a) Moment-Rotation Curves and b) Dissipated Energy Levels for Matrix 2

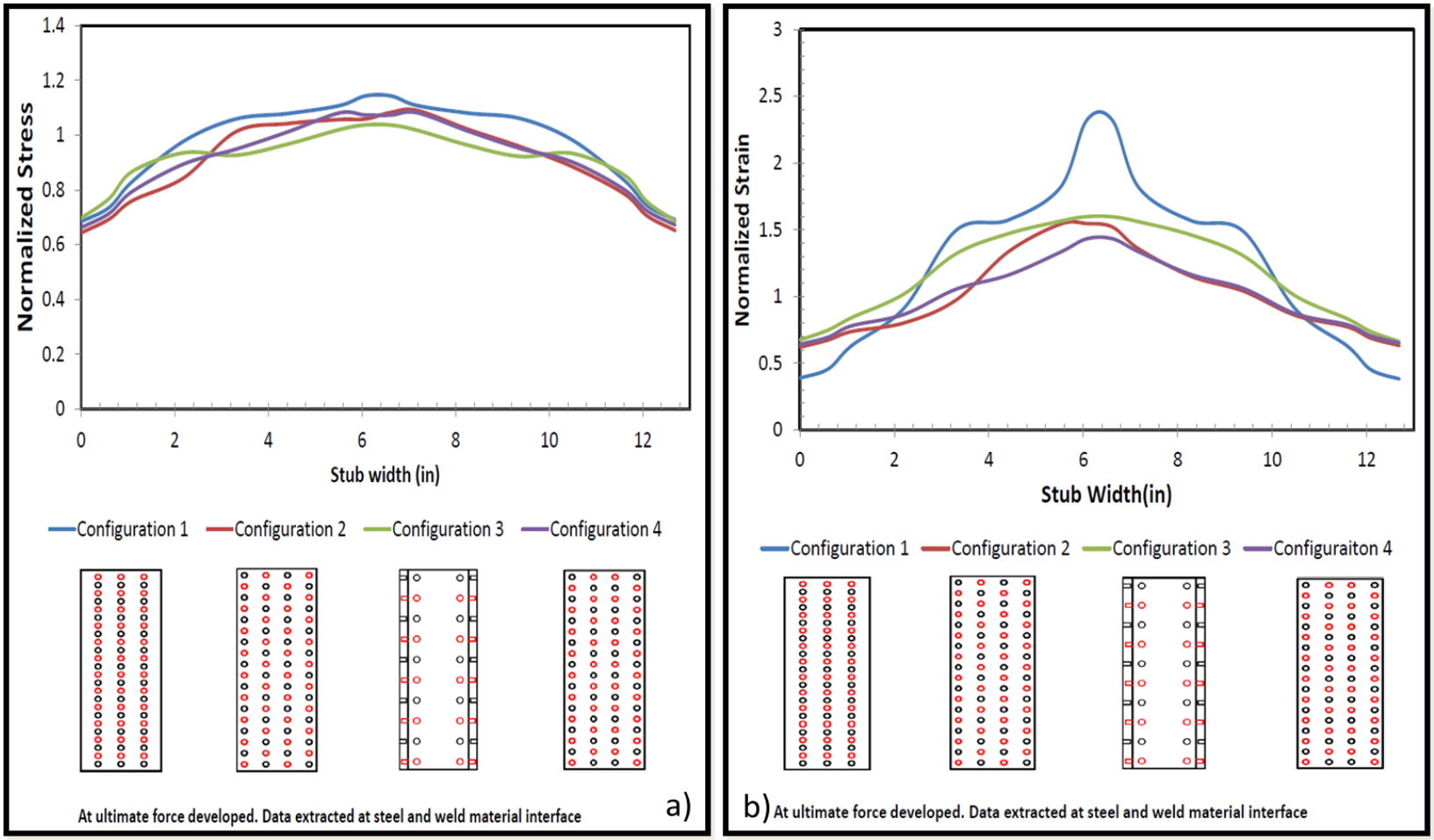

Figure 5-31: a) Normalized Longitudinal Stress and b) Normalized Longitudinal Strain at the Welded Regions for Matrix 2

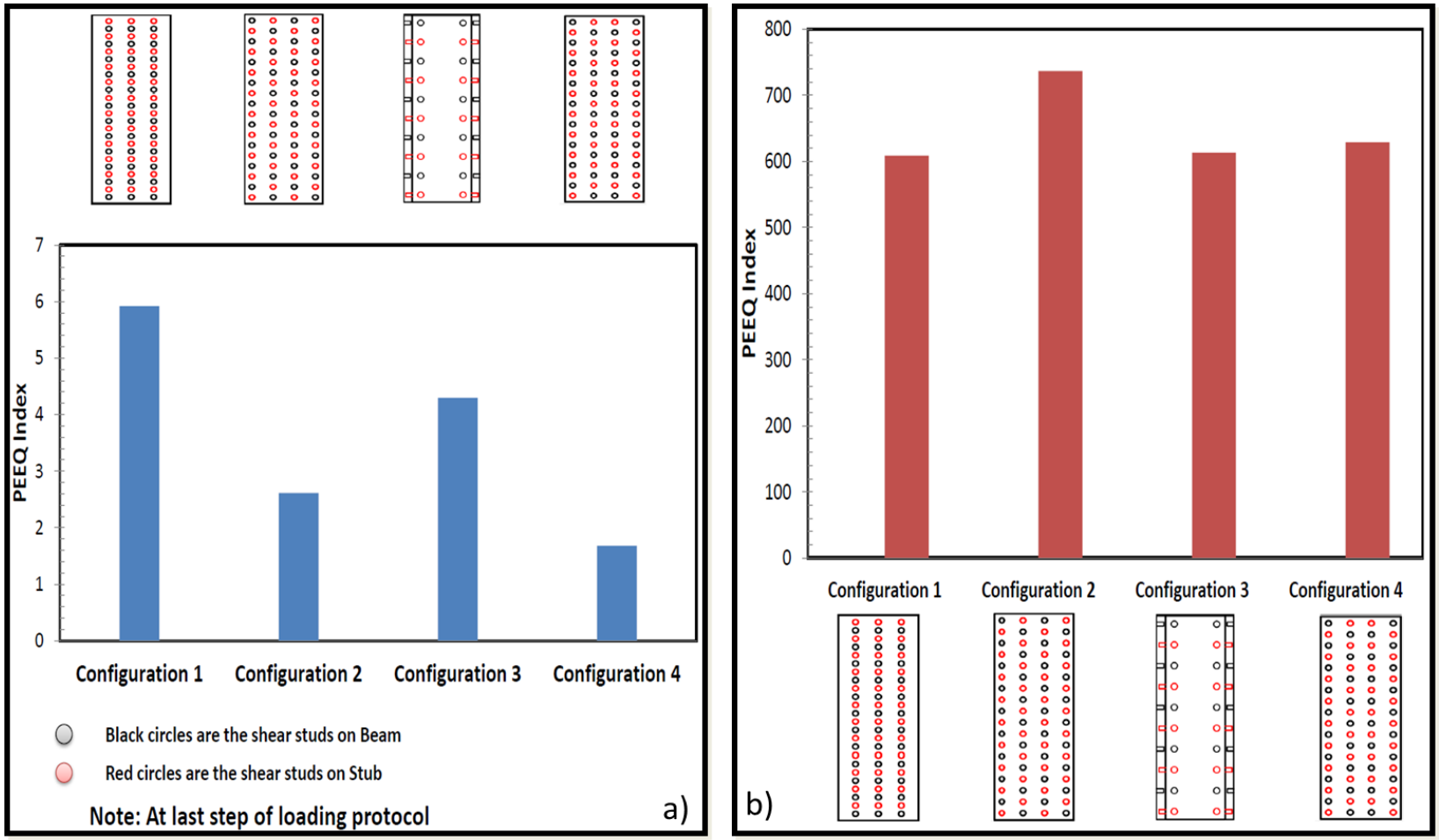

Figure 5-32: a) PEEQ Index at the Welded Regions and b) PEEQ Index at Plastic Hinge Regions for Matrix 2

Model Name	Beam- Column properties			Stub Properties			Shear Stud Config1	Shear Stud number	Stiffener			Grout Strength fc'(ksi)
		w30x108	w14x370									
Model1	height	29.8	17.9	Inside height(ht)	35	in		144	Thickness	0.5	in	6
	width	10.5	16.5	Flange (ttf)	1.25	in			width	5.52	in	
	flange thic	0.76	2.66	Side(tts)	0.6	in			length	12.58	in	
	web thick	0.545	1.66	width(bt)	12.7	in						
	Zx	346	736	Length	30	in						
	Sx	299	607									
Model Name	Beam- Column properties			Stub Properties			Shear Stud Config2	Shear Stud number	Stiffener			Grout Strength fc'(ksi)
		w30x108	w14x370									
Model2	height	29.8	17.9	Inside height(ht)	35	in	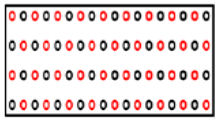	144	Thickness	0.5	in	6
	width	10.5	16.5	Flange (ttf)	1.25	in			width	5.17	in	
	flange thic	0.76	2.66	Side(tts)	0.6	in			length	12.58	in	
	web thick	0.545	1.66	width(bt)	12	in						
	Zx	346	736	Length	30	in						
	Sx	299	607									
Model Name	Beam- Column properties			Stub Properties			Shear Stud Config3	Shear Stud number	Stiffener			Grout Strength fc'(ksi)
		w30x108	w14x370									
Model3	height	29.8	17.9	Inside height(ht)	35	in	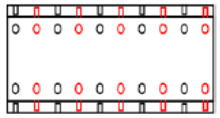	144	Thickness	0.5	in	6
	width	10.5	16.5	Flange (ttf)	1.25	in			width	5.17	in	
	flange thic	0.76	2.66	Side(tts)	0.6	in			length	12.58	in	
	web thick	0.545	1.66	width(bt)	12	in						
	Zx	346	736	Length	30	in						
	Sx	299	607									
Model Name	Beam- Column properties			Stub Properties			Shear Stud Config4	Shear Stud number	Stiffener			Grout Strength fc'(ksi)
		w30x108	w14x370									
Model4	height	29.8	17.9	Inside height(ht)	35	in	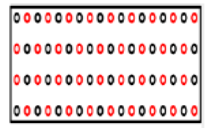	144	Thickness	0.5	in	6
	width	10.5	16.5	Flange (ttf)	1.25	in			width	5.17	in	
	flange thic	0.76	2.66	Side(tts)	0.6	in			length	12.58	in	
	web thick	0.545	1.66	width(bt)	12	in						
	Zx	346	736	Length	30	in						
	Sx	299	607									

Figure 5-33: Parametric Study Matrix 3 for Beam Section W30x108 (Stub: Inside Height=32 inches; Flange Thickness=1.25 inches)

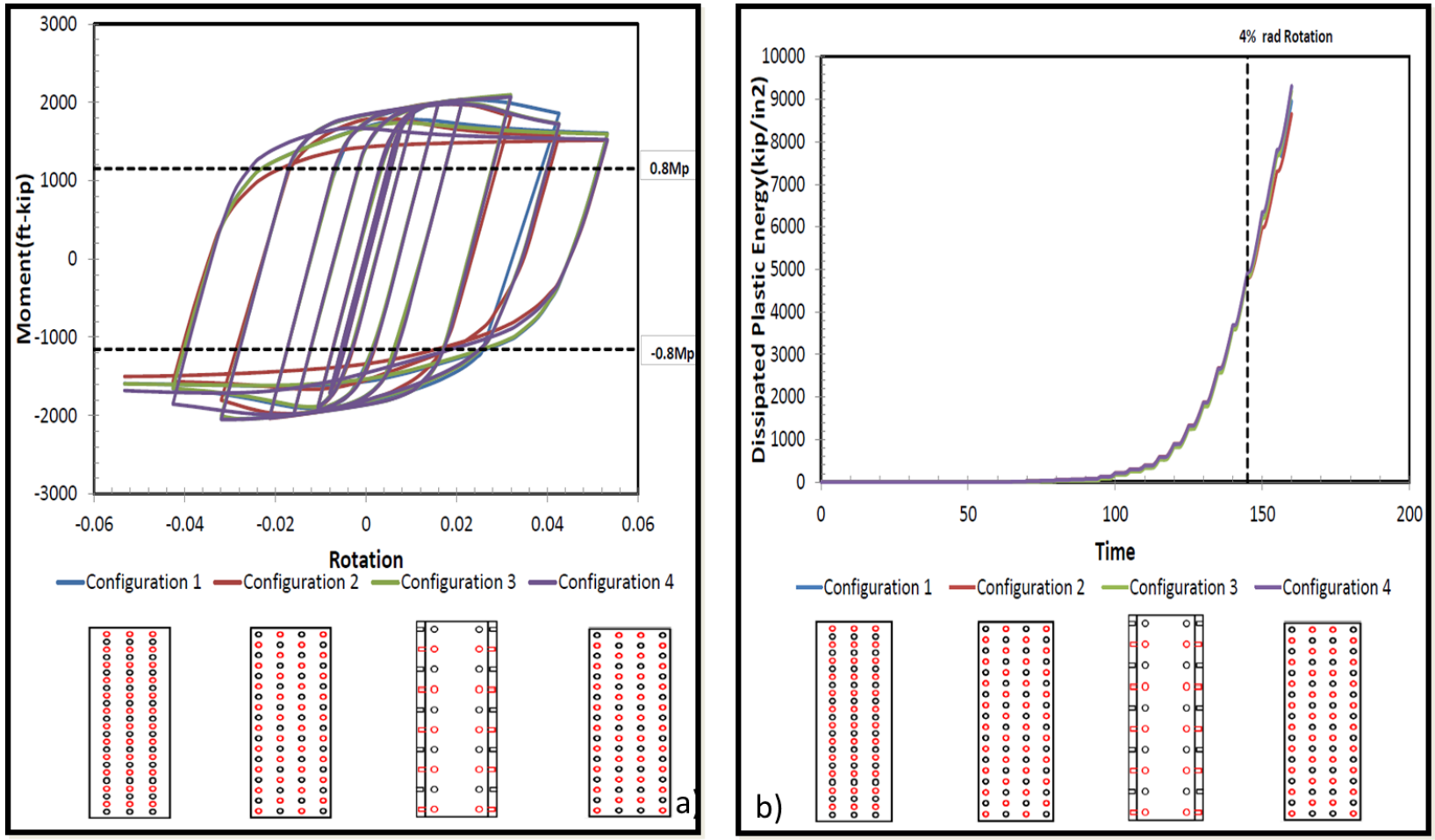

Figure 5-34: a) Moment-Rotation Curves and b) Dissipated Energy Levels for Matrix 3

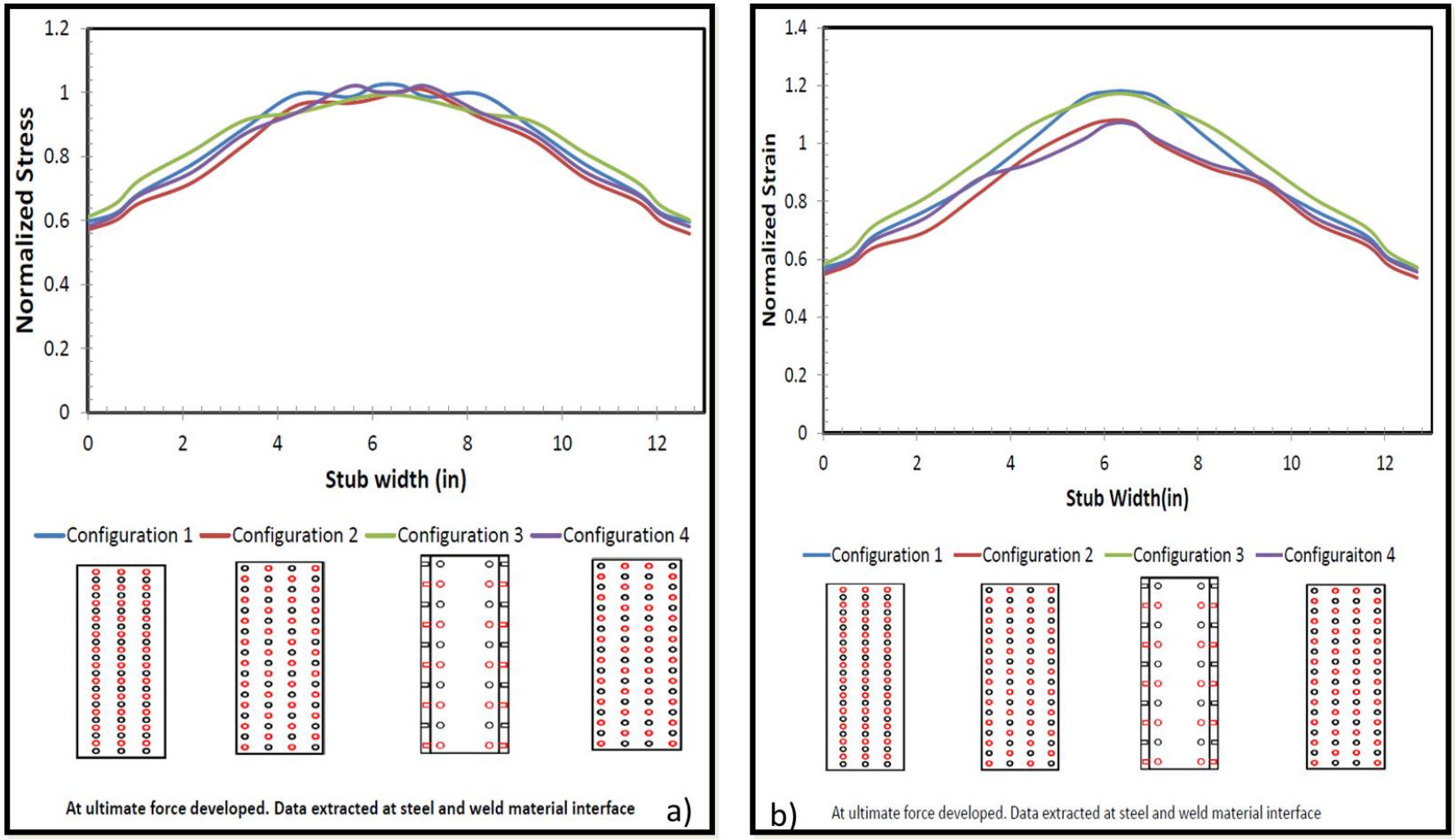

Figure 5-35: a) Normalized Longitudinal Stress and b) Normalized Longitudinal Strain at the Welded Regions for Matrix 3

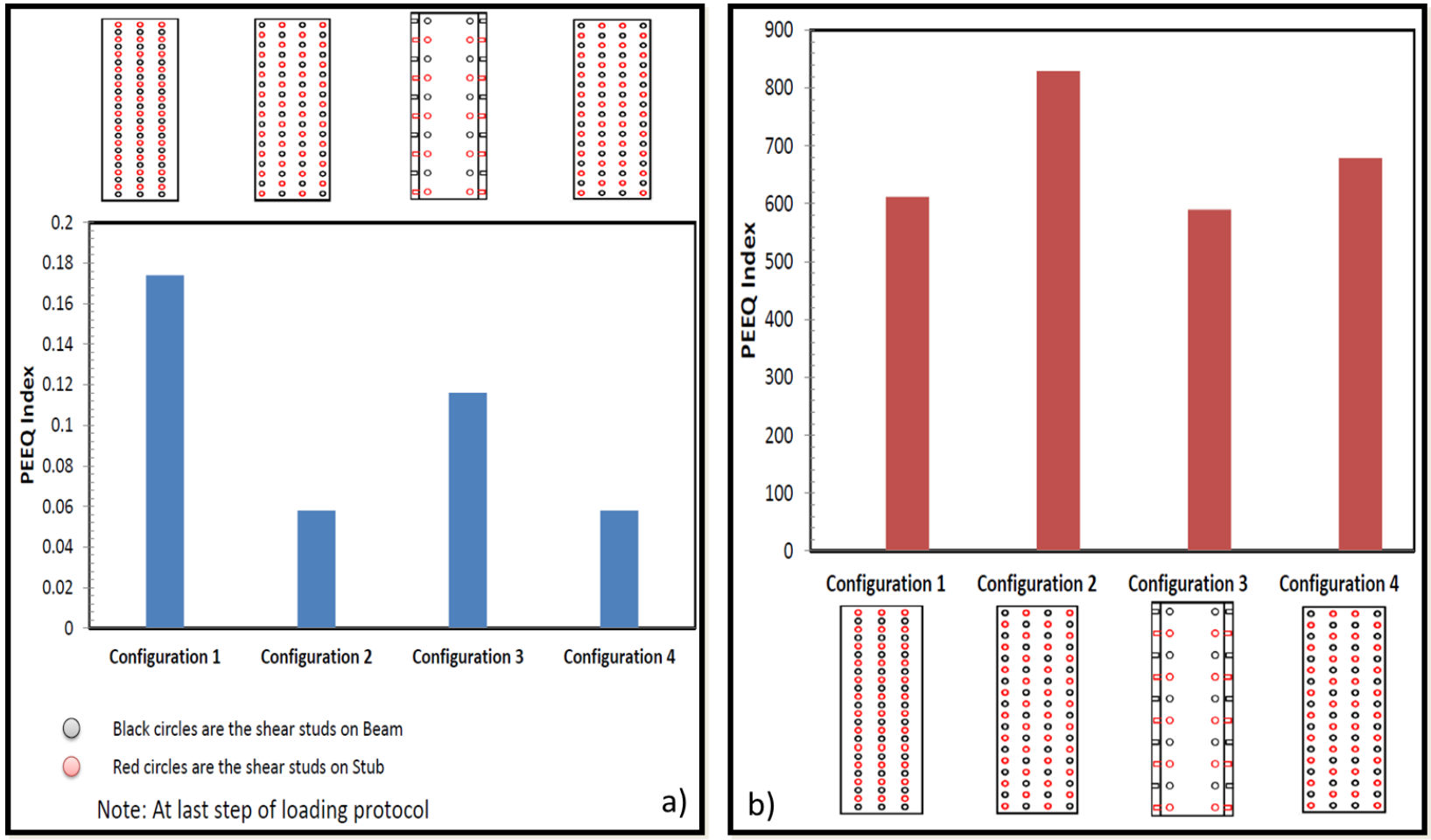

Figure 5-36: a) PEEQ Index at the Welded Regions and b) PEEQ Index at Plastic Hinge Regions for Matrix 3

Model Name	Beam- Column properties			Stub Properties			Shear Stud Config1	Shear Stud number	Stiffener			Grout Strength fc'(ksi)
		w30x108	w14x370									
Model1	height	29.8	17.9	Inside height(ht)	40	in		144	Thickness	0.5	in	6
	width	10.5	16.5	Flange (ttf)	0.8	in			width	5.52	in	
	flange thic	0.76	2.66	Side(tts)	0.6	in			length	12.58	in	
	web thick	0.545	1.66	width(bt)	12.7	in						
	Zx	346	736	Length	30	in						
	Sx	299	607									
Model Name	Beam- Column properties			Stub Properties			Shear Stud Config2	Shear Stud number	Stiffener			Grout Strength fc'(ksi)
		w30x108	w14x370									
Model2	height	29.8	17.9	Inside height(ht)	40	in	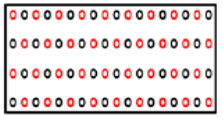	144	Thickness	0.5	in	6
	width	10.5	16.5	Flange (ttf)	0.8	in			width	5.17	in	
	flange thic	0.76	2.66	Side(tts)	0.6	in			length	12.58	in	
	web thick	0.545	1.66	width(bt)	12	in						
	Zx	346	736	Length	30	in						
	Sx	299	607									
Model Name	Beam- Column properties			Stub Properties			Shear Stud Config3	Shear Stud number	Stiffener			Grout Strength fc'(ksi)
		w30x108	w14x370									
Model3	height	29.8	17.9	Inside height(ht)	40	in	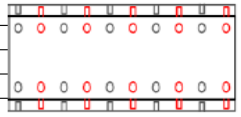	144	Thickness	0.5	in	6
	width	10.5	16.5	Flange (ttf)	0.8	in			width	5.17	in	
	flange thic	0.76	2.66	Side(tts)	0.6	in			length	12.58	in	
	web thick	0.545	1.66	width(bt)	12	in						
	Zx	346	736	Length	30	in						
	Sx	299	607									
Model Name	Beam- Column properties			Stub Properties			Shear Stud Config4	Shear Stud number	Stiffener			Grout Strength fc'(ksi)
		w30x108	w14x370									
Model4	height	29.8	17.9	Inside height(ht)	40	in	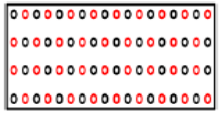	144	Thickness	0.5	in	6
	width	10.5	16.5	Flange (ttf)	0.8	in			width	5.17	in	
	flange thic	0.76	2.66	Side(tts)	0.6	in			length	12.58	in	
	web thick	0.545	1.66	width(bt)	12	in						
	Zx	346	736	Length	30	in						
	Sx	299	607									

Figure 5-37: Parametric Study Matrix 4 for Beam Section W30x108 (Stub: Inside Height=40 inches; Flange Thickness=0.8 inches)

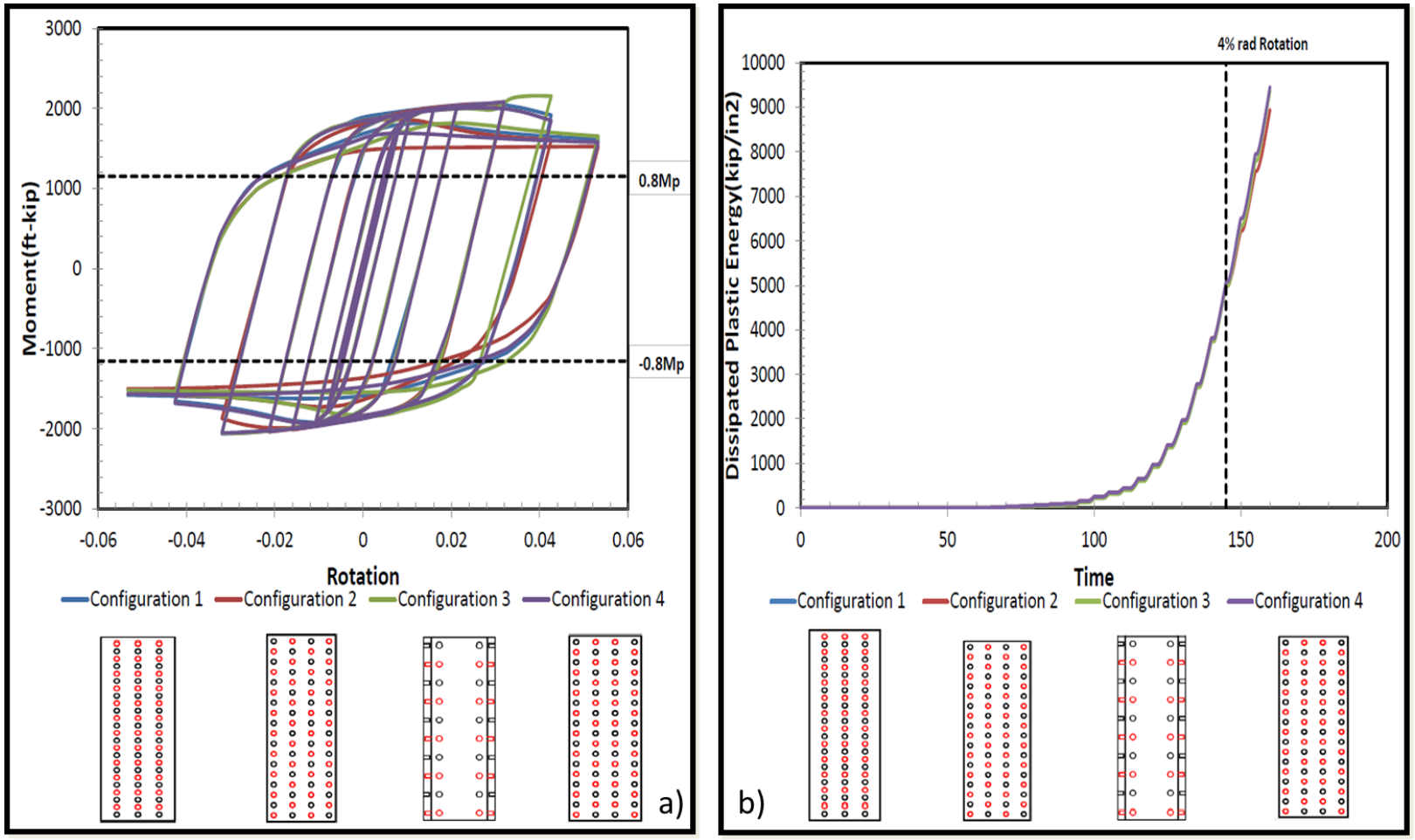

Figure 5-38: a) Moment-Rotation Curves and b) Dissipated Energy Levels for Matrix 4

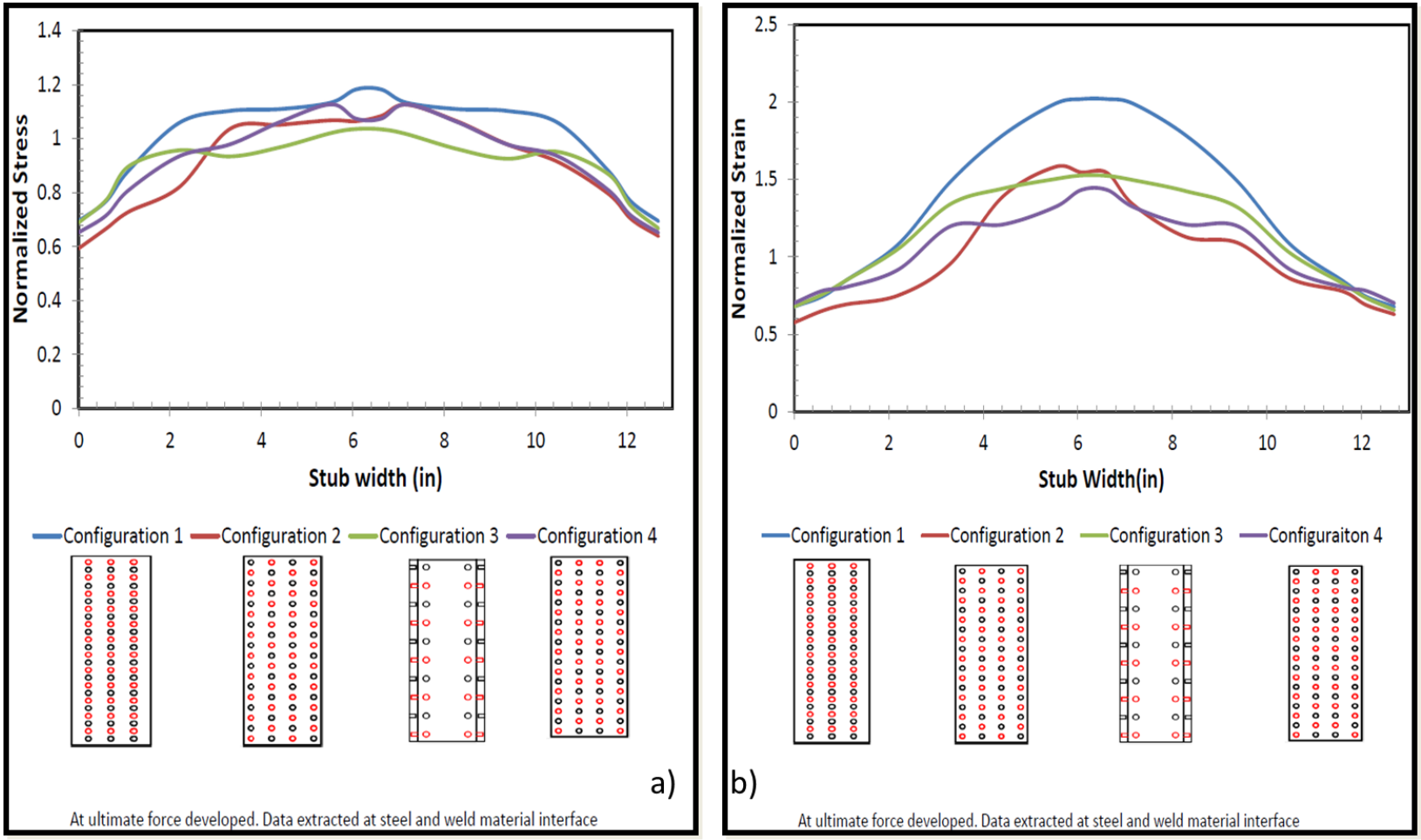

Figure 5-39: a) Normalized Longitudinal Stress and b) Normalized Longitudinal Strain at the Welded Regions for Matrix 4

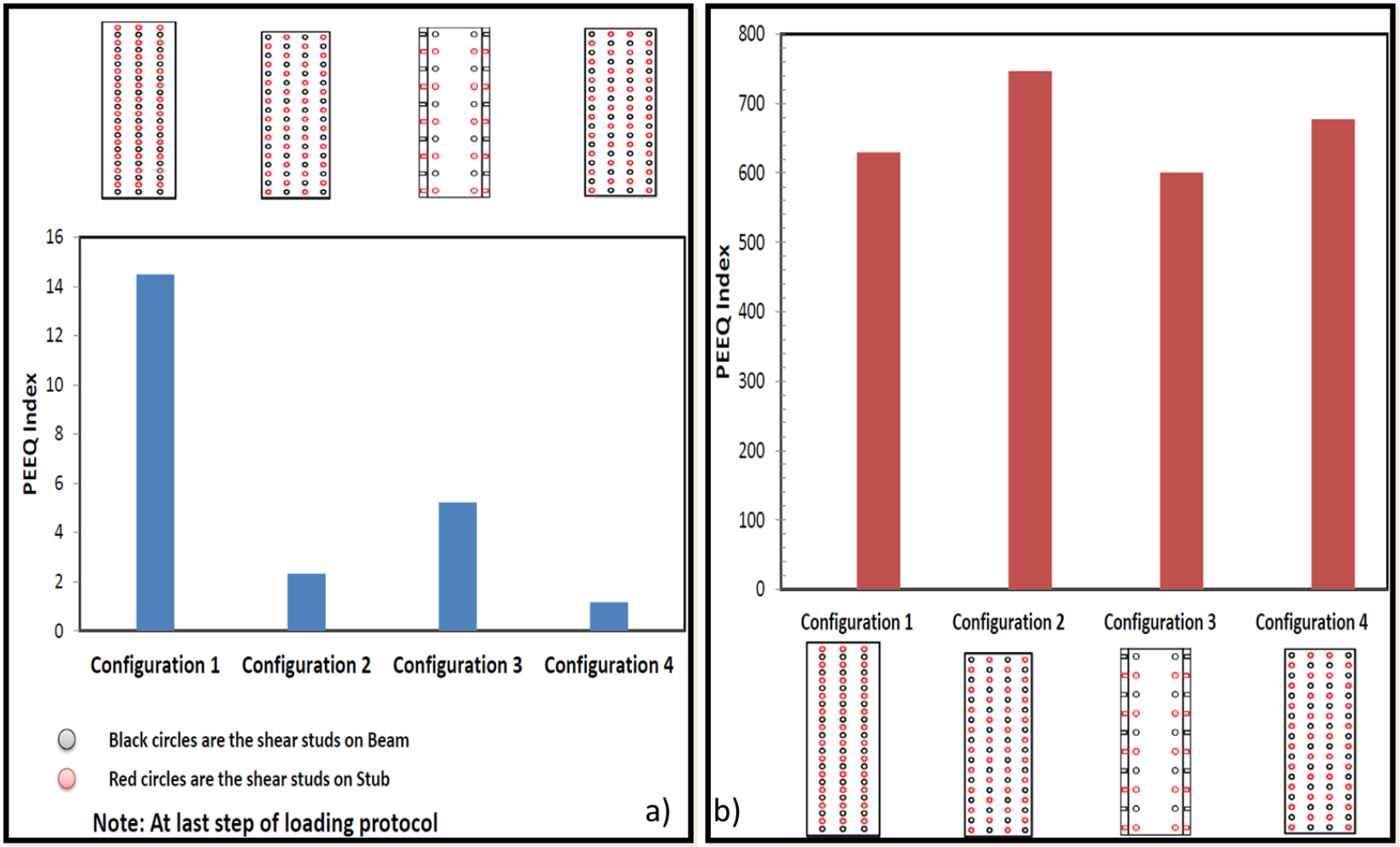

Figure 5-40: a) PEEQ Index at the Welded Regions and b) PEEQ Index at Plastic Hinge Regions for Matrix 4

Model Name	Beam- Column properties			Stub Properties			Shear Stud Config1	Shear Stud number	Stiffener			Grout Strength fc'(ksi)
		w30x108	w14x370									
Model1	height	29.8	17.9	Inside height(ht)	40	in	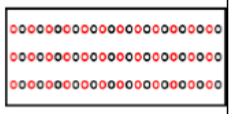	144	Thickness	0.5	in	6
	width	10.5	16.5	Flange (ttf)	1	in			width	5.52	in	
	flange thic	0.76	2.66	Side(tts)	0.6	in			length	12.58	in	
	web thick	0.545	1.66	width(bt)	12.7	in						
	Zx	346	736	Length	30	in						
	Sx	299	607									
Model Name	Beam- Column properties			Stub Properties			Shear Stud Config2	Shear Stud number	Stiffener			Grout Strength fc'(ksi)
		w30x108	w14x370									
Model2	height	29.8	17.9	Inside height(ht)	40	in	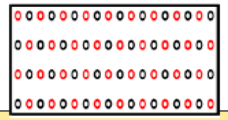	144	Thickness	0.5	in	6
	width	10.5	16.5	Flange (ttf)	1	in			width	5.17	in	
	flange thic	0.76	2.66	Side(tts)	0.6	in			length	12.58	in	
	web thick	0.545	1.66	width(bt)	12	in						
	Zx	346	736	Length	30	in						
	Sx	299	607									
Model Name	Beam- Column properties			Stub Properties			Shear Stud Config3	Shear Stud number	Stiffener			Grout Strength fc'(ksi)
		w30x108	w14x370									
Model3	height	29.8	17.9	Inside height(ht)	40	in	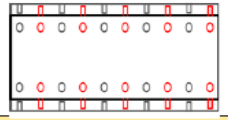	144	Thickness	0.5	in	6
	width	10.5	16.5	Flange (ttf)	1	in			width	5.17	in	
	flange thic	0.76	2.66	Side(tts)	0.6	in			length	12.58	in	
	web thick	0.545	1.66	width(bt)	12	in						
	Zx	346	736	Length	30	in						
	Sx	299	607									
Model Name	Beam- Column properties			Stub Properties			Shear Stud Config4	Shear Stud number	Stiffener			Grout Strength fc'(ksi)
		w30x108	w14x370									
Model4	height	29.8	17.9	Inside height(ht)	40	in	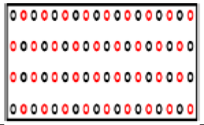	144	Thickness	0.5	in	6
	width	10.5	16.5	Flange (ttf)	1	in			width	5.17	in	
	flange thic	0.76	2.66	Side(tts)	0.6	in			length	12.58	in	
	web thick	0.545	1.66	width(bt)	12	in						
	Zx	346	736	Length	30	in						
	Sx	299	607									

Figure 5-41: Parametric Study Matrix 5 for Beam Section W30x108 (Stub: Inside Height=40 inches; Flange Thickness=1inch)

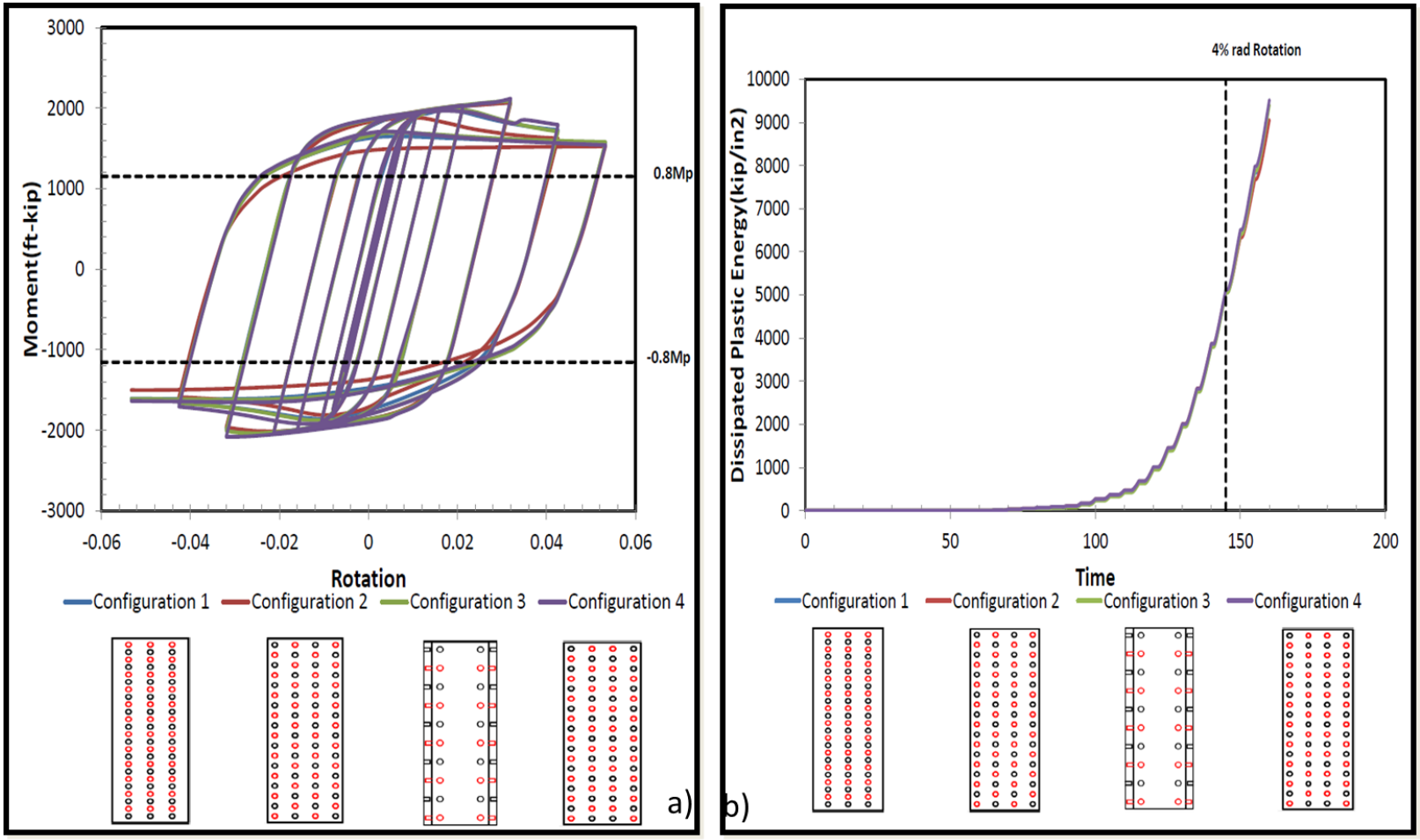

Figure 5-42: a) Moment-Rotation Curves and b) Dissipated Energy Levels for Matrix 5

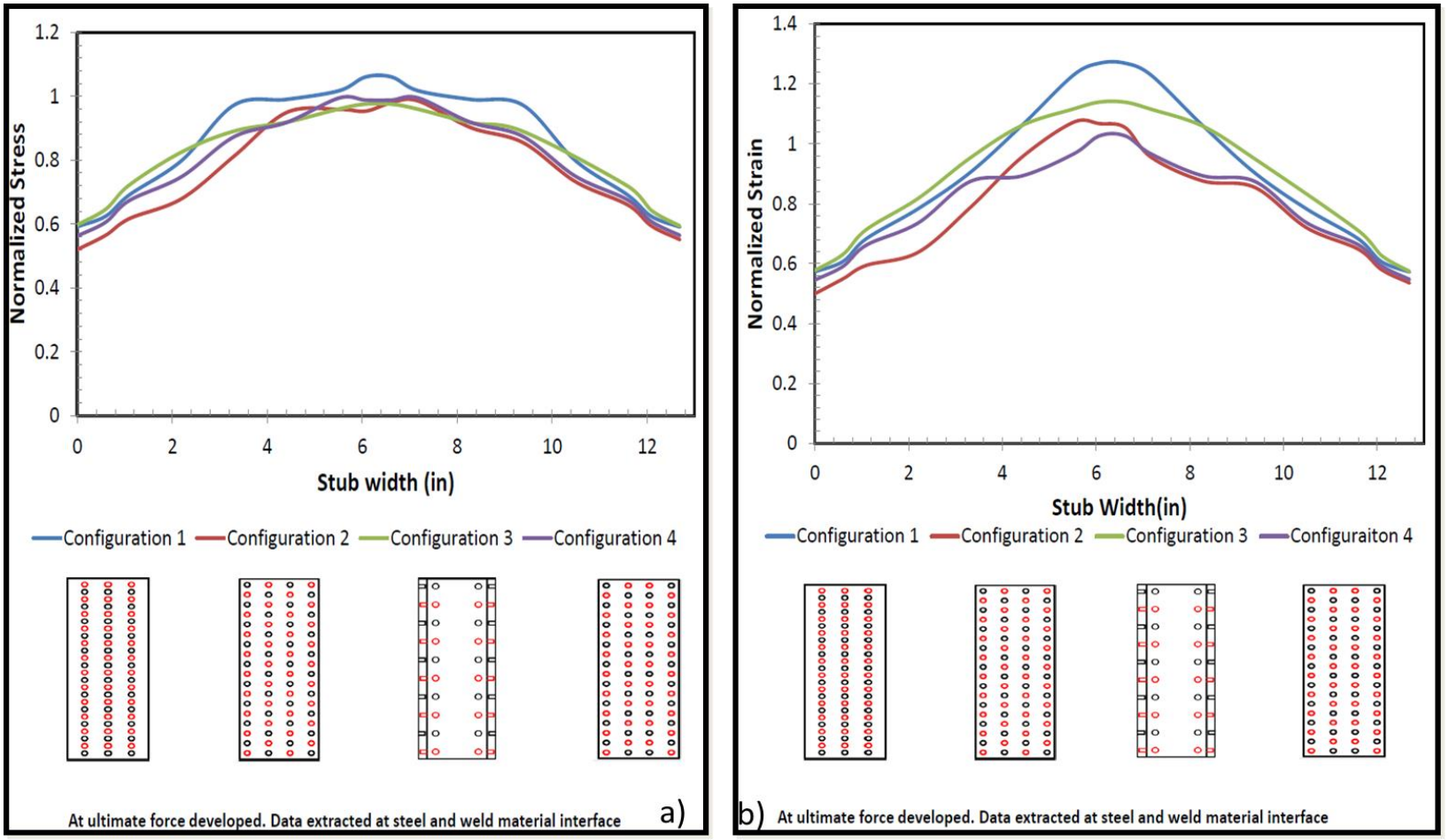

Figure 5-43: a) Normalized Longitudinal Stress and b) Normalized Longitudinal Strain at the Welded Regions for Matrix 5

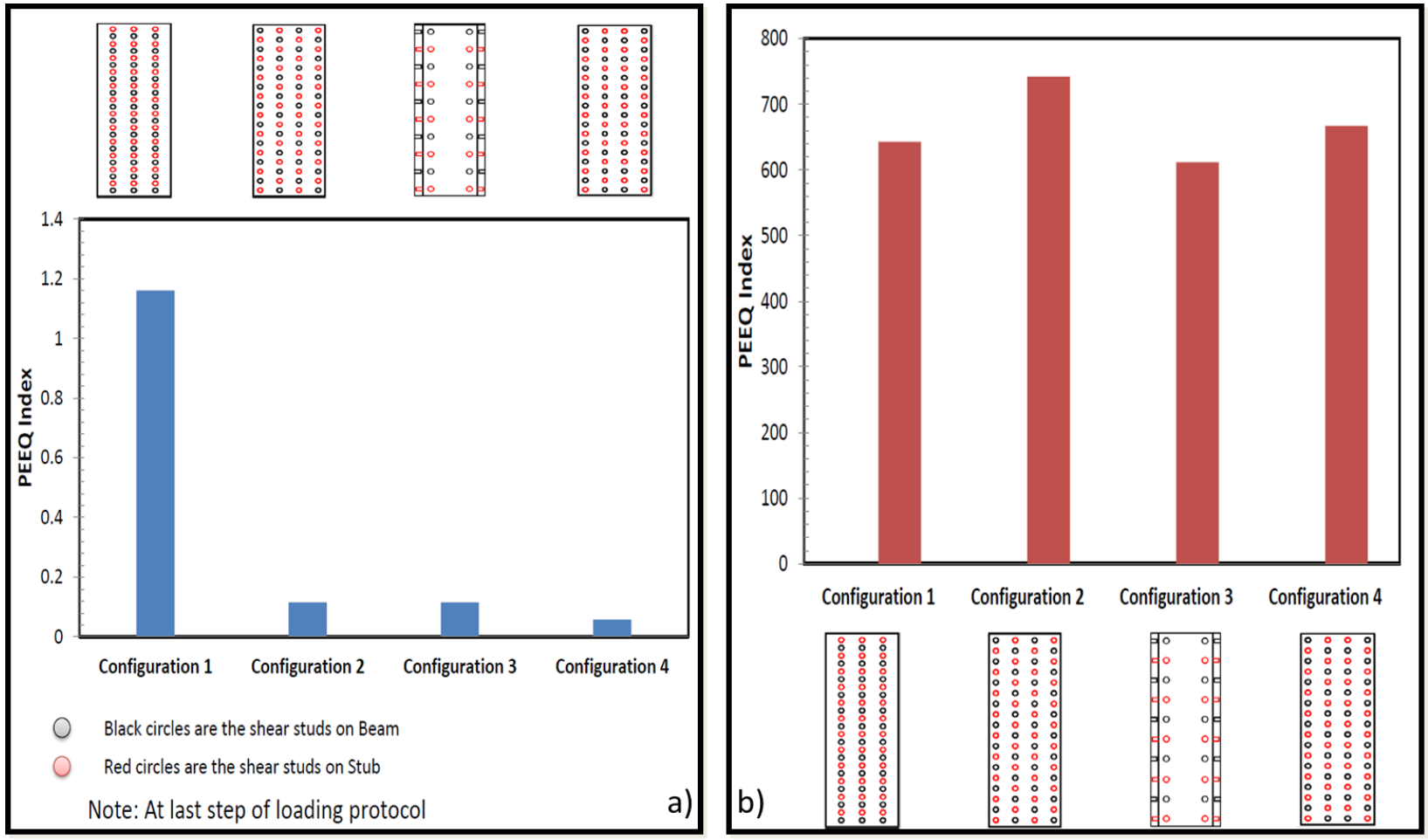

Figure 5-44: a) PEEQ Index at the Welded Regions and b) PEEQ Index at Plastic Hinge Regions for Matrix 5

Model Name	Beam- Column properties			Stub Properties			Shear Stud Config1	Shear Stud number	Stiffener			Grout Strength fc'(ksi)
		w30x108	w14x370									
Model1	height	29.8	17.9	Inside height(ht)	40	in		144	Thickness	0.5	in	6
	width	10.5	16.5	Flange (ttf)	1.25	in			width	5.52	in	
	flange thic	0.76	2.66	Side(tts)	0.6	in			length	12.58	in	
	web thick	0.545	1.66	width(bt)	12.7	in						
	Zx	346	736	Length	30	in						
	Sx	299	607									
Model Name	Beam- Column properties			Stub Properties			Shear Stud Config2	Shear Stud number	Stiffener			Grout Strength fc'(ksi)
		w30x108	w14x370									
Model2	height	29.8	17.9	Inside height(ht)	40	in	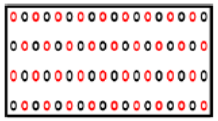	144	Thickness	0.5	in	6
	width	10.5	16.5	Flange (ttf)	1.25	in			width	5.17	in	
	flange thic	0.76	2.66	Side(tts)	0.6	in			length	12.58	in	
	web thick	0.545	1.66	width(bt)	12	in						
	Zx	346	736	Length	30	in						
	Sx	299	607									
Model Name	Beam- Column properties			Stub Properties			Shear Stud Config3	Shear Stud number	Stiffener			Grout Strength fc'(ksi)
		w30x108	w14x370									
Model3	height	29.8	17.9	Inside height(ht)	40	in	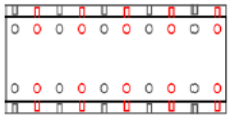	144	Thickness	0.5	in	6
	width	10.5	16.5	Flange (ttf)	1.25	in			width	5.17	in	
	flange thic	0.76	2.66	Side(tts)	0.6	in			length	12.58	in	
	web thick	0.545	1.66	width(bt)	12	in						
	Zx	346	736	Length	30	in						
	Sx	299	607									
Model Name	Beam- Column properties			Stub Properties			Shear Stud Config4	Shear Stud number	Stiffener			Grout Strength fc'(ksi)
		w30x108	w14x370									
Model4	height	29.8	17.9	Inside height(ht)	40	in	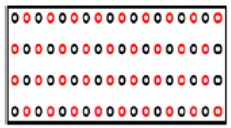	144	Thickness	0.5	in	6
	width	10.5	16.5	Flange (ttf)	1.25	in			width	5.17	in	
	flange thic	0.76	2.66	Side(tts)	0.6	in			length	12.58	in	
	web thick	0.545	1.66	width(bt)	12	in						
	Zx	346	736	Length	30	in						
	Sx	299	607									

Figure 5-45: Parametric Study Matrix 6 for Beam Section W30x108 (Stub: Inside Height=40 inches; Flange Thickness=1.25 inches)

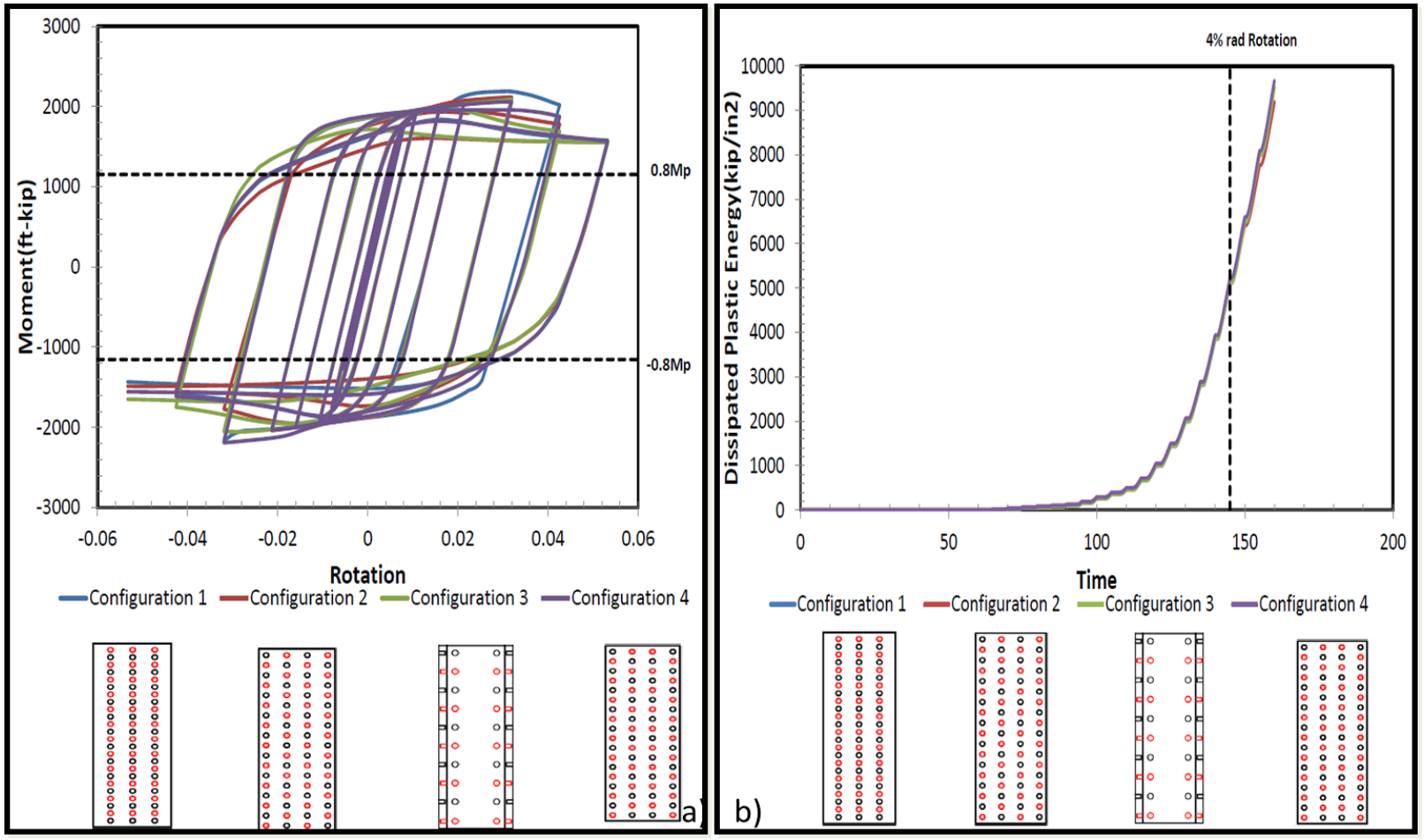

Figure 5-46: a) Moment-Rotation Curves and b) Dissipated Energy Levels for Matrix 6

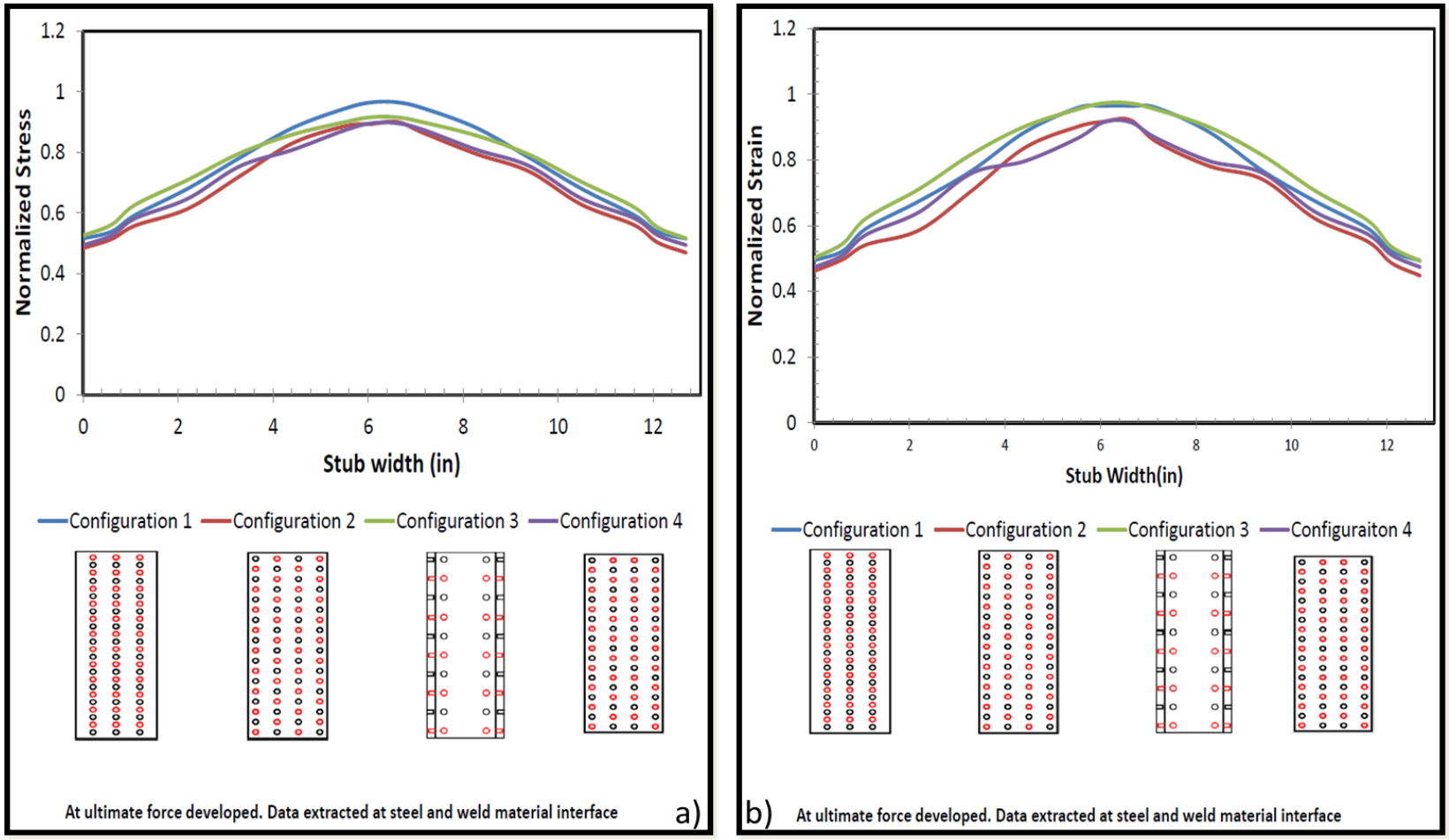

Figure 5-47: a) Normalized Longitudinal Stress and b) Normalized Longitudinal Strain at the Welded Regions for Matrix 6

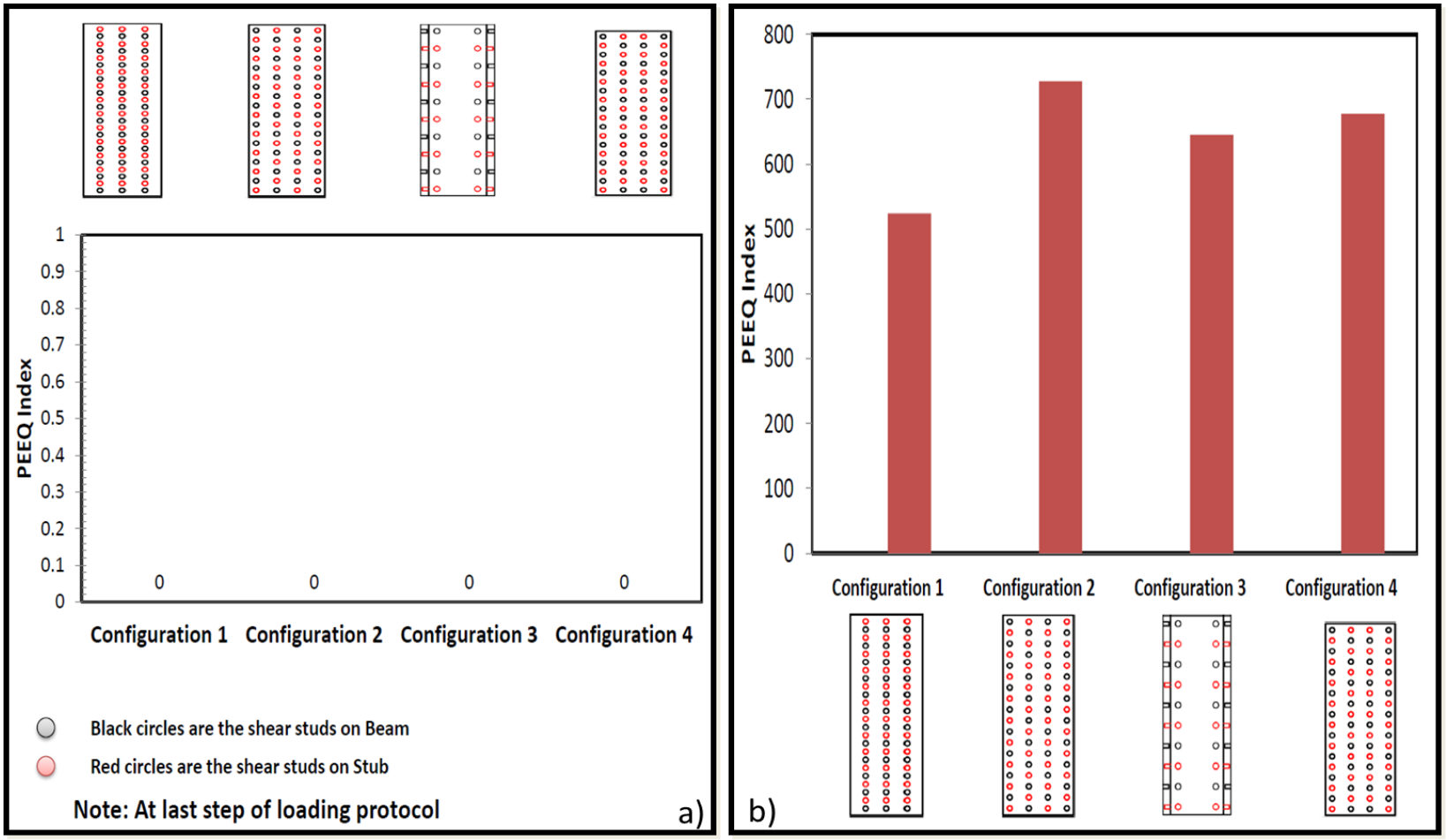

Figure 5-48: a) PEEQ Index at the Welded Regions and b) PEEQ Index at Plastic Hinge Regions for Matrix 6

Model Name	Beam- Column properties			Stub Properties			Shear Stud Config1	Shear Stud number	Stiffener			Grout Strength fc'(ksi)
		w24x62	w14x257									
No Stiffener	height(in)	23.7	16.4	Height(ht)	28.7	in		80	No Stiffener			6
	width(in)	7.04	16	Flange (ttf)	0.6	in						
	flange thic(in)	0.59	1.89	Side(tts)	0.5	in						
	web thick(in)	0.43	1.18	width(bt)	9	in						
	Zx(in3)	153	487	Length	25	in						
	Sx(in3)	131	415									
Model Name	Beam- Column properties			Stub Properties			Shear Stud Config	Shear Stud number	Stiffener			Grout Strength fc'(ksi)
		w24x62	w14x257									
Thickness 0.25	height(in)	23.7	16.4	Inside height(ht)	28.7	in		80	Thicknes	0.25	in	6
	width(in)	7.04	16	Flange (ttf)	0.6	in			width	3.91	in	
	flange thic(in)	0.59	1.89	Side(tts)	0.5	in			length	12.62	in	
	web thick(in)	0.43	1.18	width(bt)	9	in						
	Zx(in3)	153	487	Length	25	in						
	Sx(in3)	131	415									
Model Name	Beam- Column properties			Stub Properties			Shear Stud Config	Shear Stud number	Stiffener			Grout Strength fc'(ksi)
		w24x62	w14x257									
Thickness 0.5	height(in)	23.7	16.4	Inside height(ht)	28.7	in		80	Thicknes	0.5	in	6
	width(in)	7.04	16	Flange (ttf)	0.6	in			width	3.91	in	
	flange thic(in)	0.59	1.89	Side(tts)	0.5	in			length	12.62	in	
	web thick(in)	0.43	1.18	width(bt)	9	in						
	Zx(in3)	153	487	Length	25	in						
	Sx(in3)	131	415									

Figure 5-49: Parametric Study Matrix for Beam Section W24x62 to Examine Effects of Stiffeners

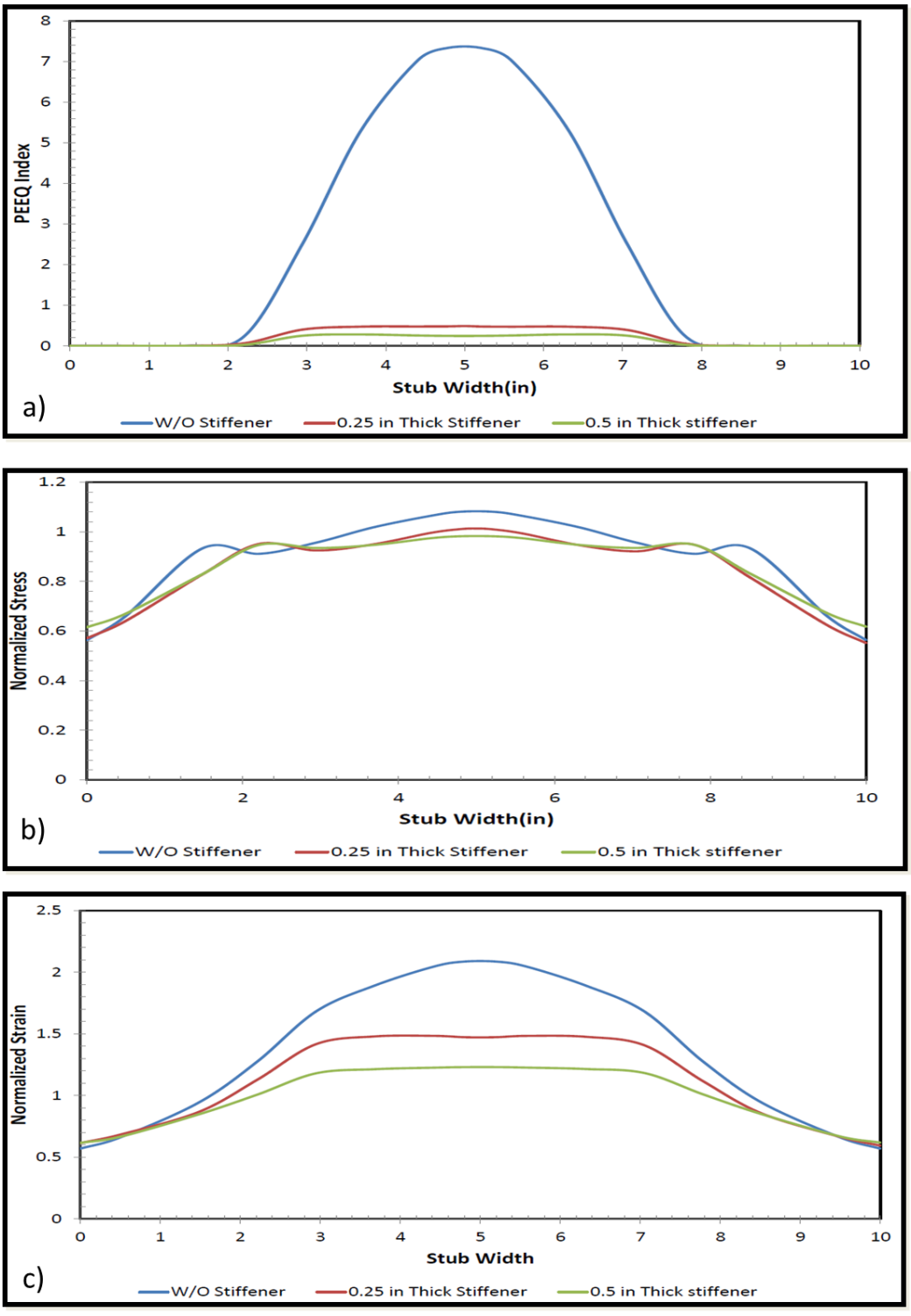

Figure 5-50: a) PEEQ Index at the Welded Region, b) Normalized Stress at the Welded Region , and c) Normalized Strain at the Welded Region

5.3.Parametric Study Matrix to Determine Effect of Configuration on Behavior of the Shear Studs

The parametric study matrix included in this section highlights four configurations that were discussed in Chapter 2. This parametric matrix is similar to the one shown in Figure 5.1 except for the modeling assumption of shear studs; in this matrix, the shear studs were modeled as 3-dimensional solid members instead of using the point based fasteners approach. The "failure index" based on the stress modified strain criterion was adopted in order to evaluate the effect of shear stud configuration on their behavior. The required number of shear studs was 20 on one of the flange surfaces of the beam section, based on the assumption discussed in Chapter 2. The failure index and corresponding loading steps are provided as plots in this chapter; failure initiations were marked out at the corresponding level of beam rotation. Failure initiations in the shear studs were expected earlier in those located near the plastic hinge region of the beam section; therefore, plots only include five rows which are in close proximity to the plastic hinge region. For configurations 1 and 2, only four rows of shear studs, which are near plastic hinge region, were provided in the plots. The shear studs on the stub experienced higher failure index values where they were close to the welded region of the stub; thus the model was designed to include three rows of shear studs (a total of 20) on the stub section (close to the welded region).

After comparing four different configurations of shear studs, two dissimilar configurations were chosen to investigate the effects of shear stud number on their behavior. The number of shear studs was reduced only for configurations 1 and 2; the number of shear studs on one flange face of the beam section was reduced to 16 and 10, respectively.

Recommendations for the most efficient configuration, found in Chapter 7, were based on the results of this comparison.

Model Name	Beam- Column properties			Stub Properties			Shear Stud Config1	Shear Stud number	Stiffener			Grout Strength fc'(ksi)
		w24x62	w14x257									
Model1	height(in)	23.7	16.4	Height(ht)	28.7	in		80	Thickness	0.5	in	6
	width(in)	7.04	16	Flange (ttf)	0.6	in			width	3.91	in	
	flange thic(in)	0.59	1.89	Side(tts)	0.5	in			length	12.62	in	
	web thick(in)	0.43	1.18	width(bt)	9	in						
	Zx(in3)	153	487	Length	25	in						
	Sx(in3)	131	415									
Model Name	Beam- Column properties			Stub Properties			Shear Stud Config2	Shear Stud number	Stiffener			Grout Strength fc'(ksi)
		w24x62	w14x257									
Model2	height(in)	23.7	16.4	Inside height(ht)	28.7	in	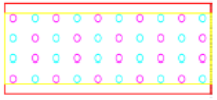	80	Thickness	0.5	in	6
	width(in)	7.04	16	Flange (ttf)	0.6	in			width	3.91	in	
	flange thic(in)	0.59	1.89	Side(tts)	0.5	in			length	12.62	in	
	web thick(in)	0.43	1.18	width(bt)	9	in						
	Zx(in3)	153	487	Length	25	in						
	Sx(in3)	131	415									
Model Name	Beam- Column properties			Stub Properties			Shear Stud Config3	Shear Stud number	Stiffener			Grout Strength fc'(ksi)
		w24x62	w14x257									
Model3	height(in)	23.7	16.4	Inside height(ht)	28.7	in	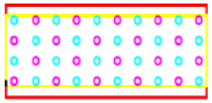	80	Thickness	0.5	in	6
	width(in)	7.04	16	Flange (ttf)	0.6	in			width	3.91	in	
	flange thic(in)	0.59	1.89	Side(tts)	0.5	in			length	12.62	in	
	web thick(in)	0.43	1.18	width(bt)	9	in						
	Zx(in3)	153	487	Length	25	in						
	Sx(in3)	131	415									
Model Name	Beam- Column properties			Stub Properties			Shear Stud Config4	Shear Stud number	Stiffener			Grout Strength fc'(ksi)
		w24x62	w14x257									
Model4	height(in)	23.7	16.4	Inside height(ht)	28.7	in	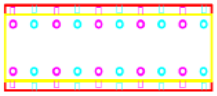	80	Thickness	0.5	in	6
	width(in)	7.04	16	Flange (ttf)	0.6	in			width	3.91	in	
	flange thic(in)	0.59	1.89	Side(tts)	0.5	in			length	12.62	in	
	web thick(in)	0.43	1.18	width(bt)	9	in						
	Zx(in3)	153	487	Length	25	in						
	Sx(in3)	131	415									

Figure 5-51: Parametric Study Matrix for Beam Section W24x62 with 3D Shear Stud Models

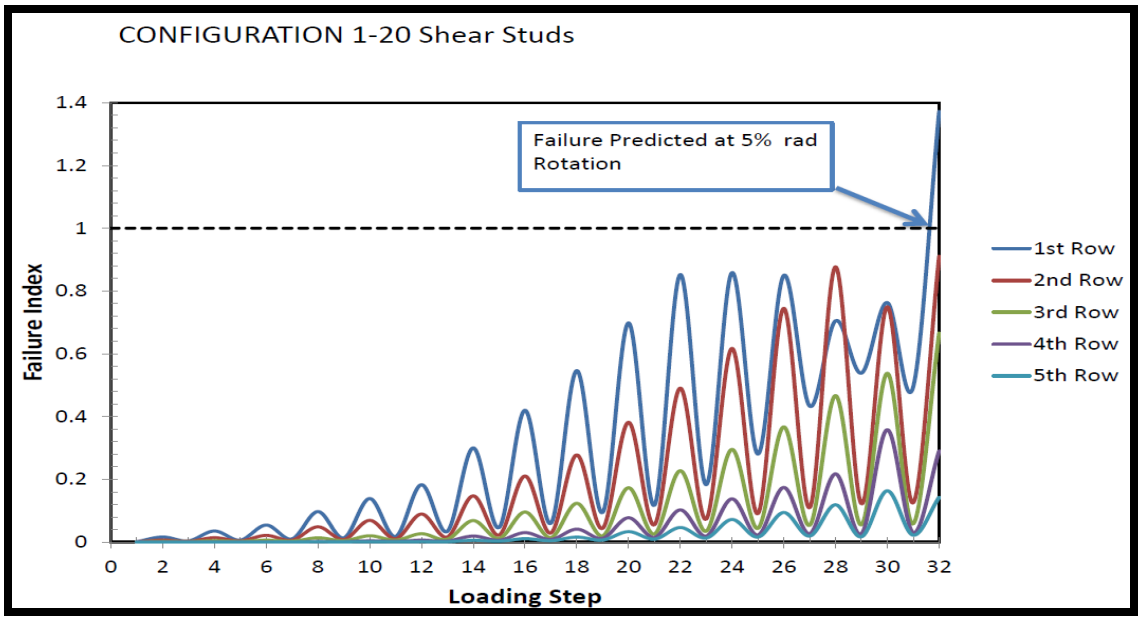

Figure 5-52: Failure Index for Shear Stud Configuration 1(for Shear Studs, on Beam, near the plastic hinge region)

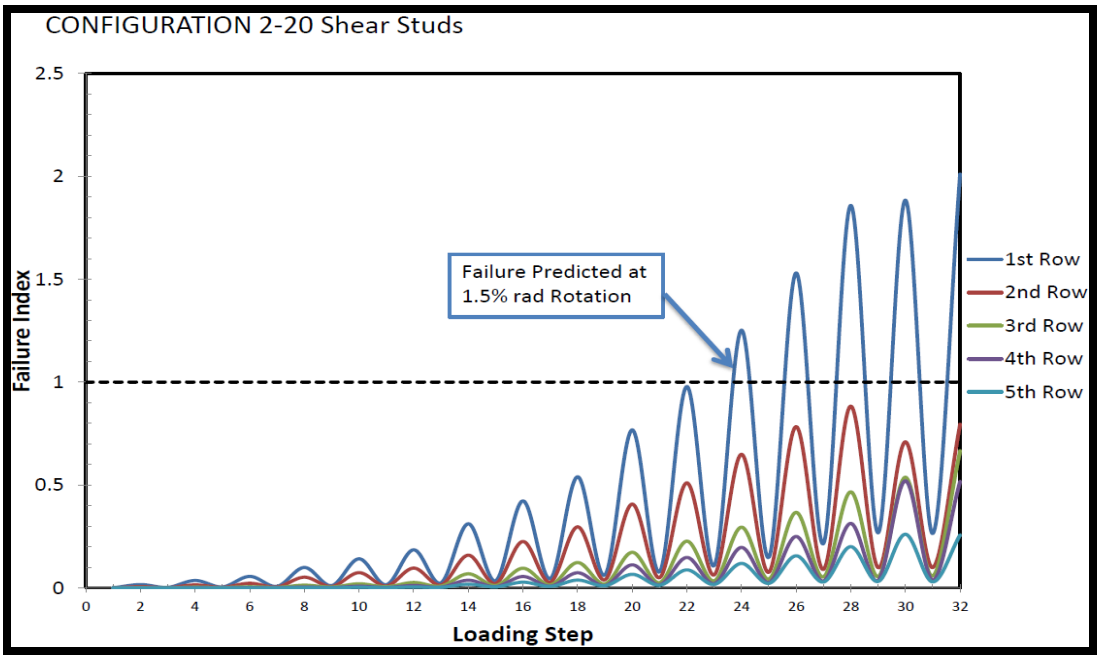

Figure 5-53: Failure Index for Shear Stud Configuration 2(for Shear Studs, on Beam, near the plastic hinge region)

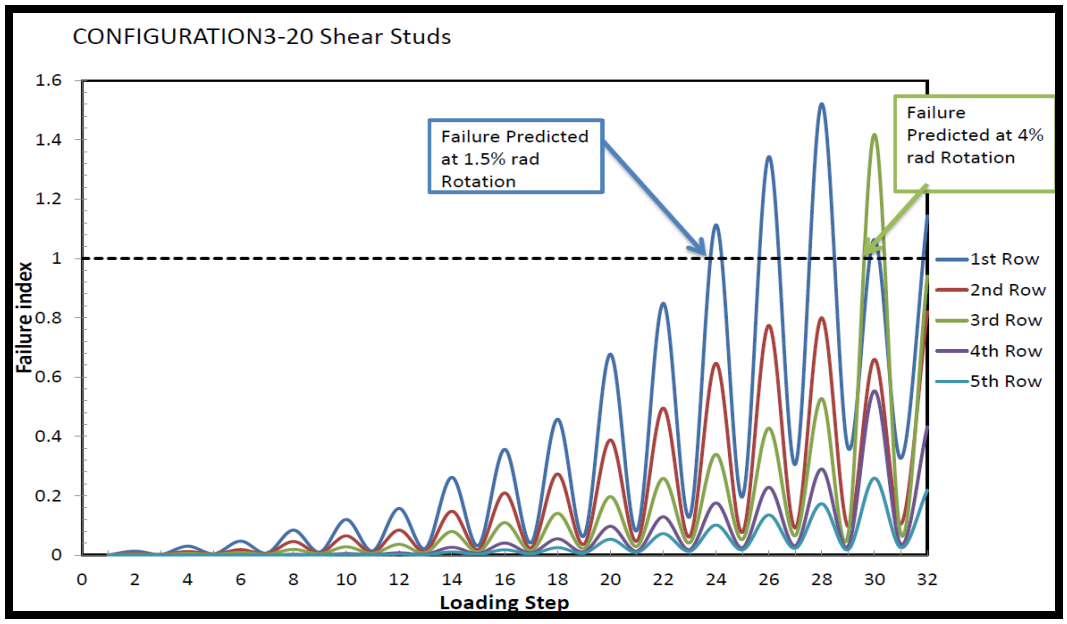

Figure 5-54: Failure Index for Shear Stud Configuration 3(for Shear Studs, on Beam, near the plastic hinge region)

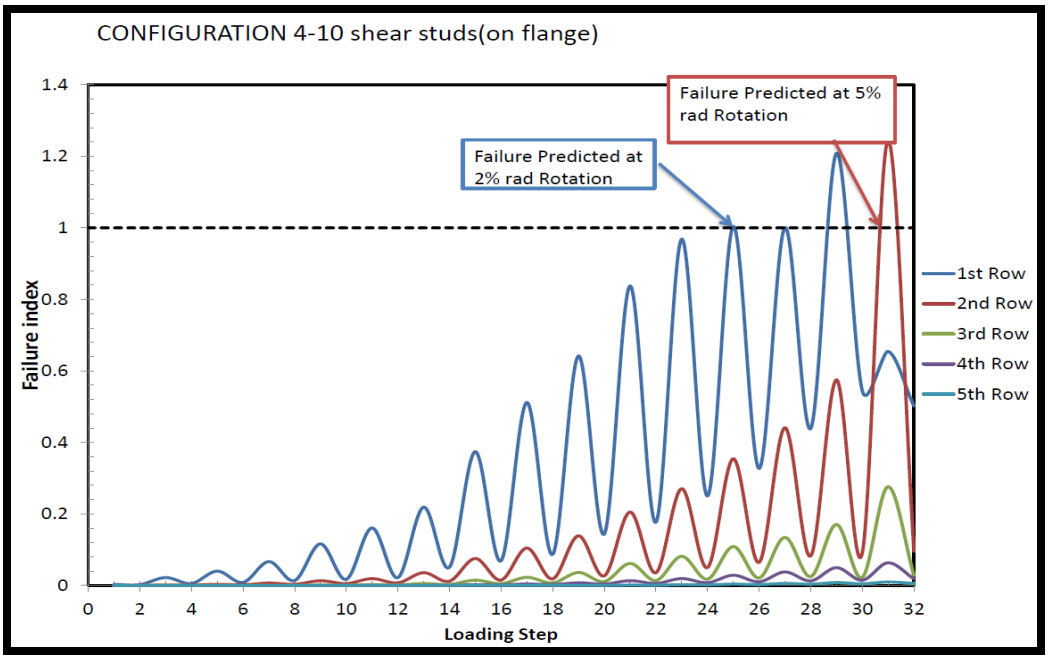

Figure 5-55: Failure Index for Shear Stud Configuration 4 (for Shear Studs, on Beam flange, near the plastic hinge region)

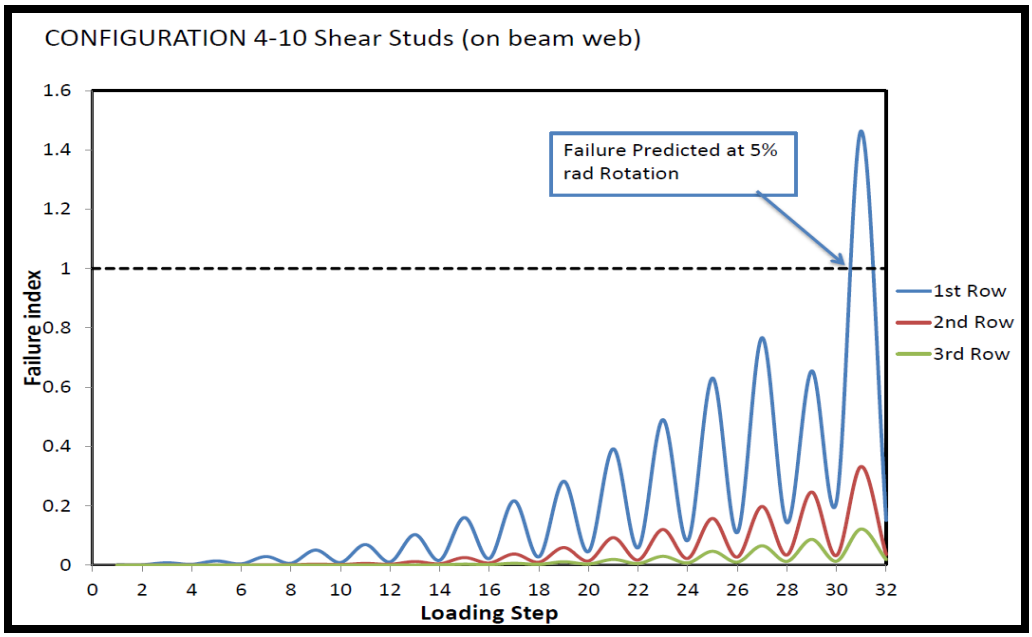

Figure 5-56: Failure Index for Shear Stud Configuration 4 (for Shear Studs, on Beam web, near the plastic hinge region)

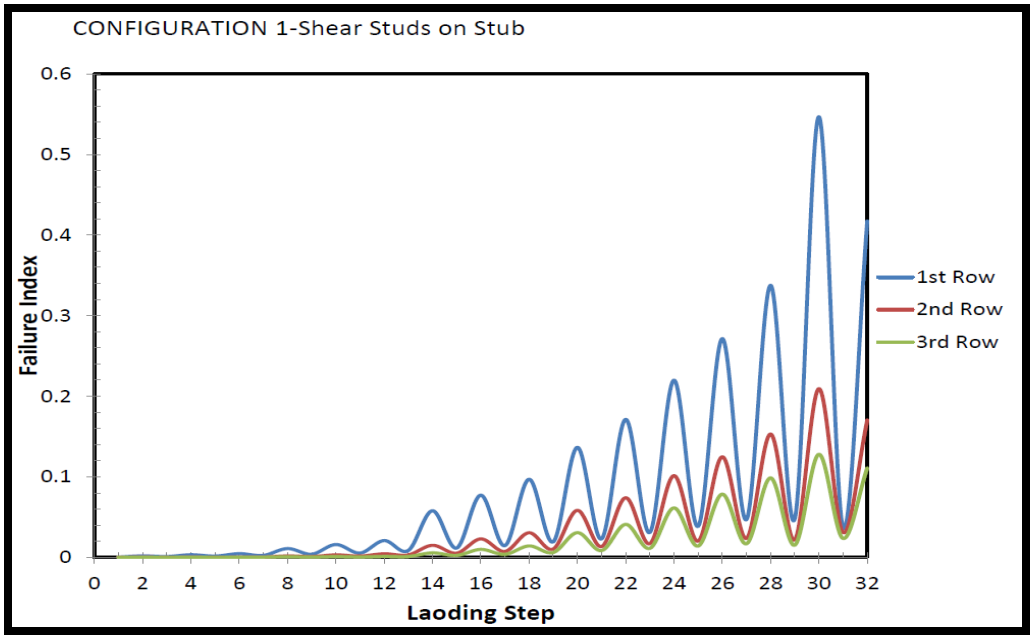

Figure 5-57: Failure Index for Shear Stud Configuration 1 (for Shear Studs, on Stub, near welded region)

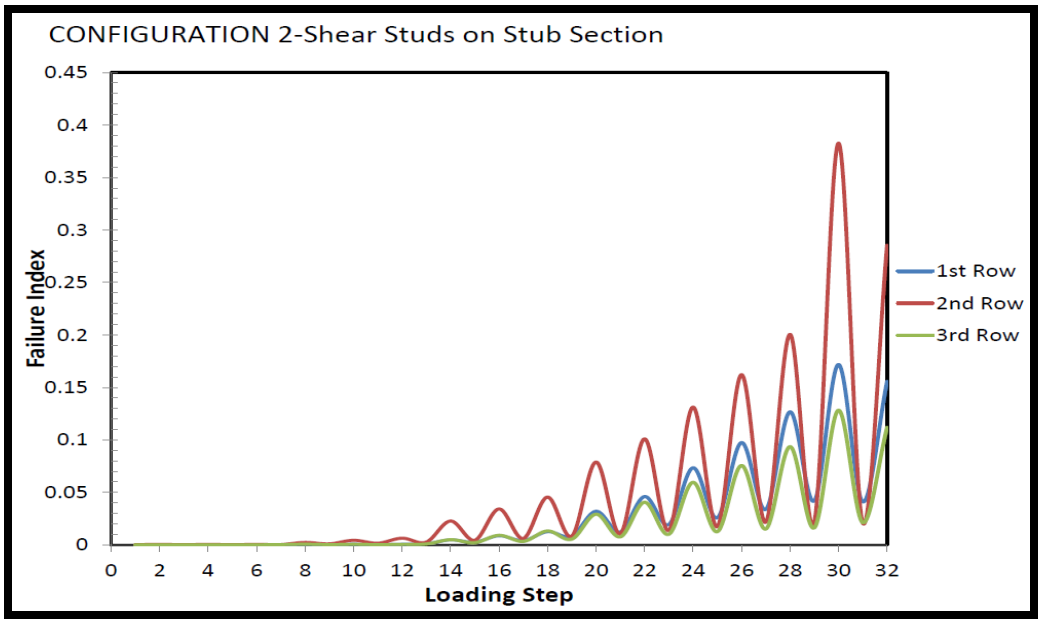

Figure 5-58: Failure Index for Shear Stud Configuration 2 (for Shear Studs, on Stub, near welded region)

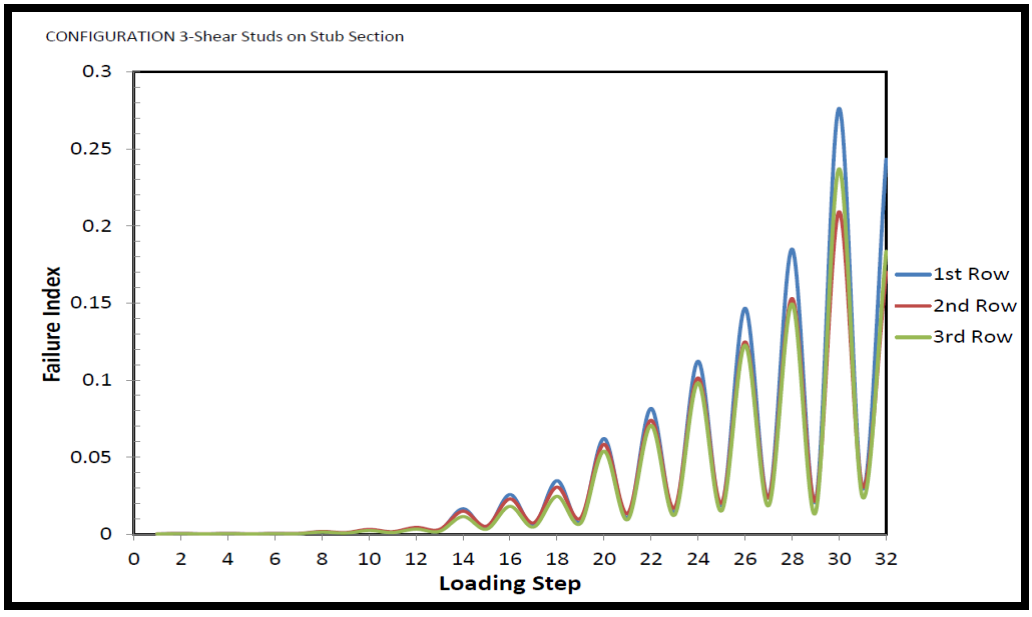

Figure 5-59: Failure Index for Shear Stud Configuration 3 (for Shear Studs, on Stub, near welded region)

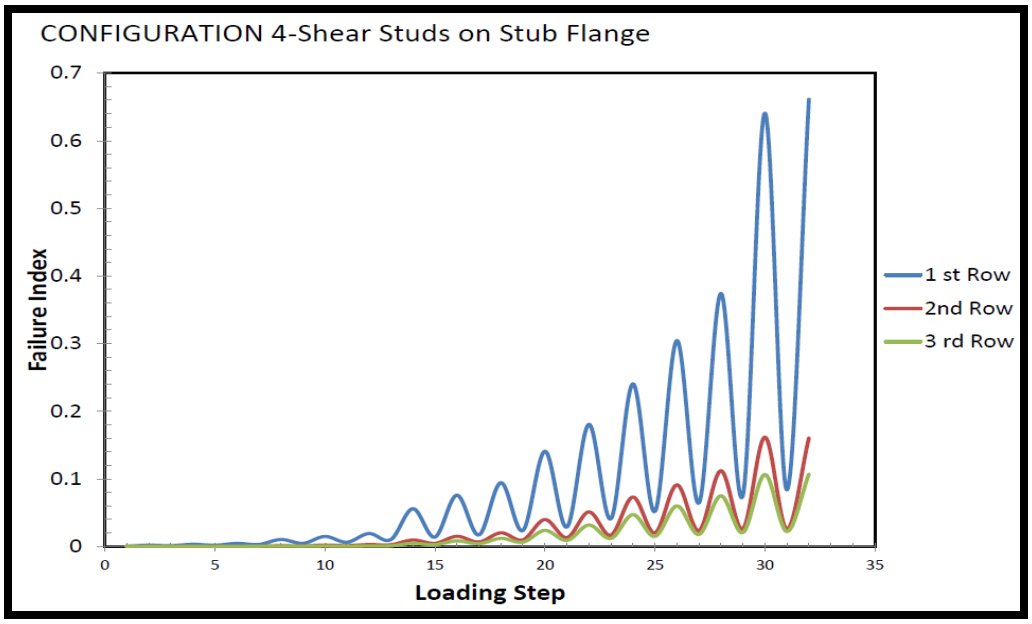

Figure 5-60: Failure Index for Shear Stud Configuration 4 (for Shear Studs, on Stub flange, near welded region)

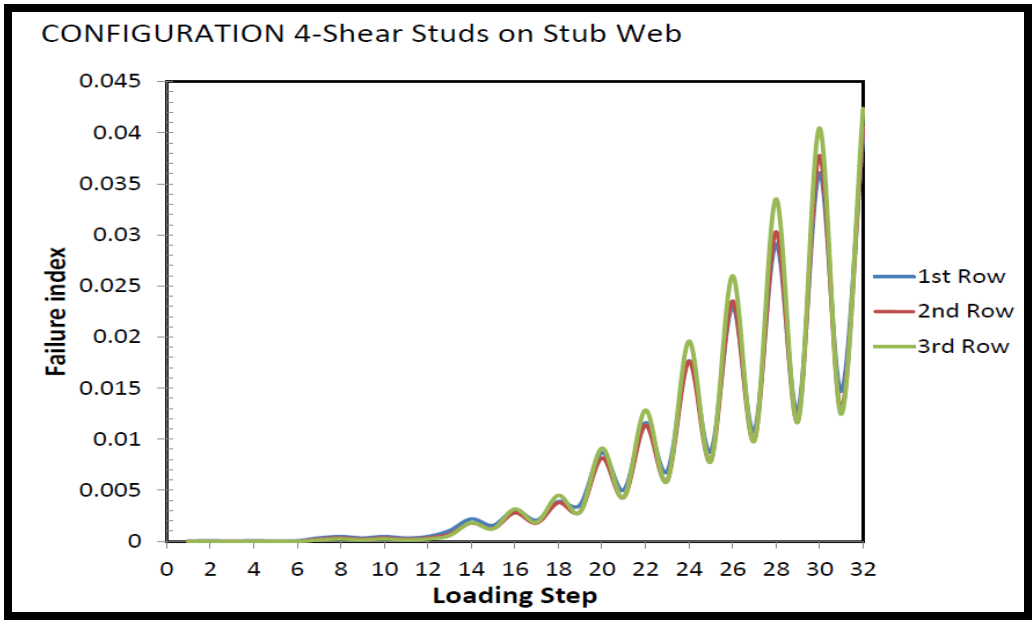

Figure 5-61: Failure Index for Shear Stud Configuration 4 (for Shear Studs, on Stub web, near welded region)

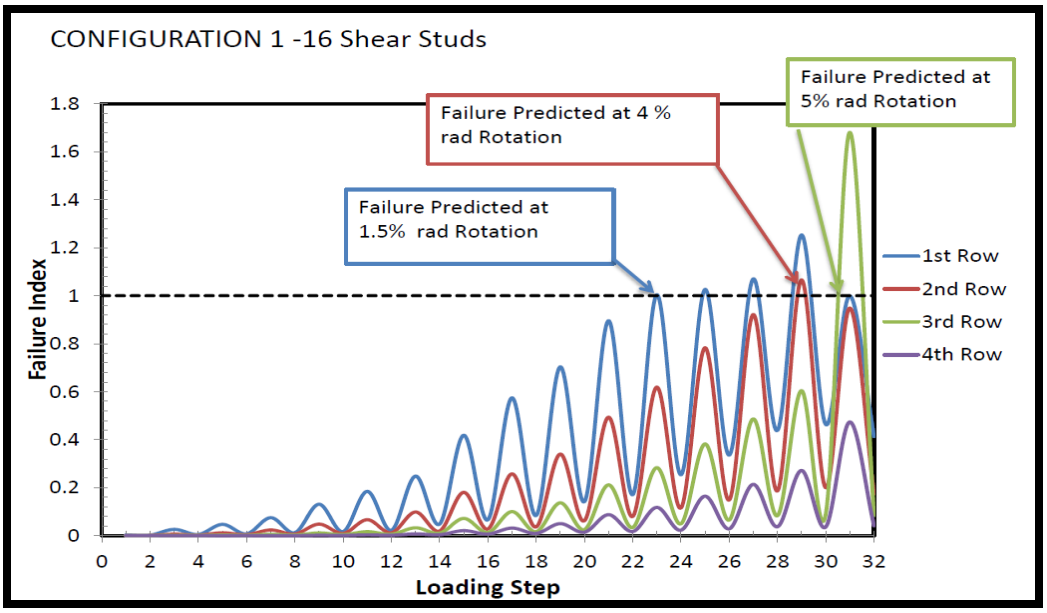

Figure 5-62: Failure Index for Shear Stud Configuration 1 (Shear studs , on Beam, near the plastic hinge region)

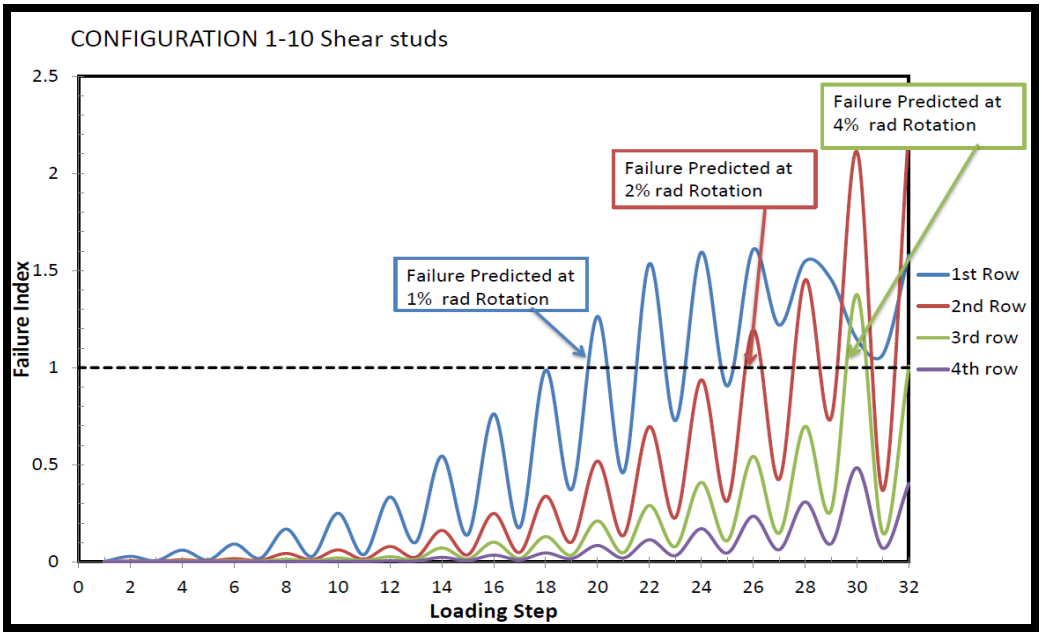

Figure 5-63: Failure Index for Shear Stud Configuration 1 (Shear studs, on Beam, near the plastic hinge region)

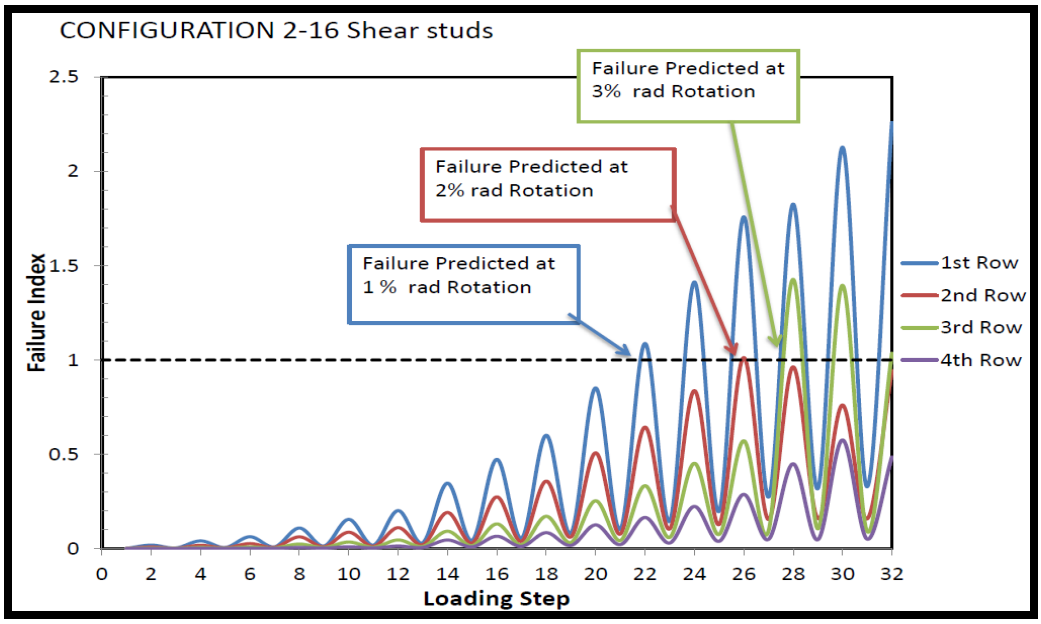

Figure 5-64: Failure Index for Shear Stud Configuration 2 (Shear studs, on Beam, near the plastic hinge region)

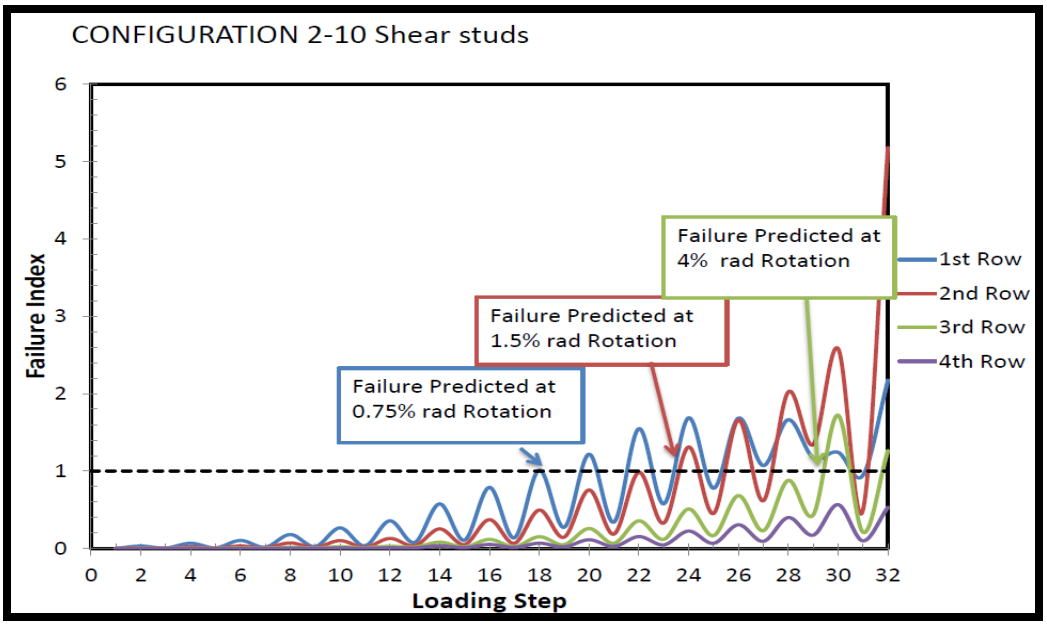

Figure 5-65: Failure Index for Shear Stud Configuration 2 (Shear studs, on Beam, near the plastic hinge region)

5.4.Outcomes of Finite Element Model for Pre-Northridge Connections

Results of the finite element analyses for Pre-Northridge connections are provided in this section.

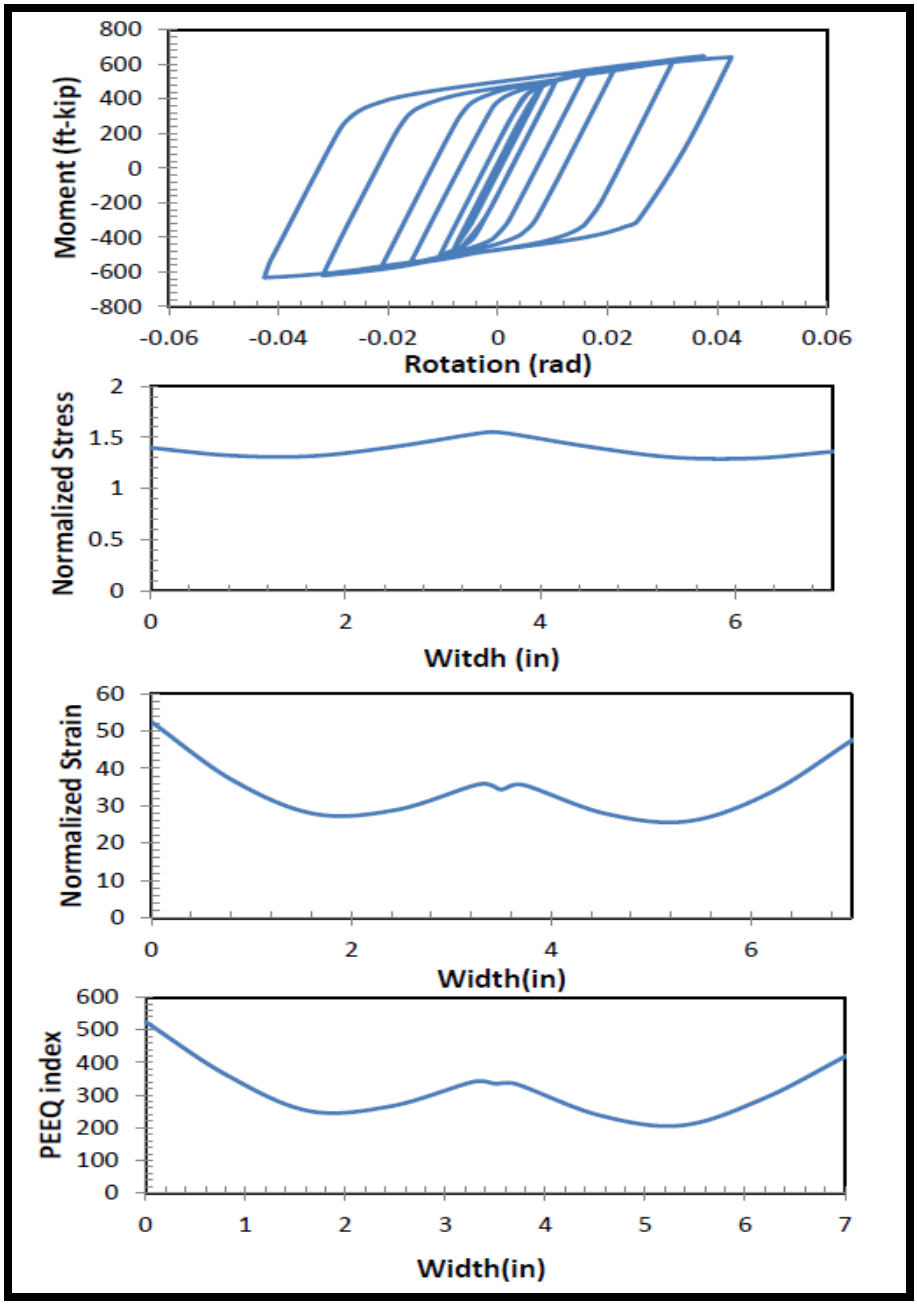

Figure 5-66: Pre-Northridge Connection (Beam W24x62)

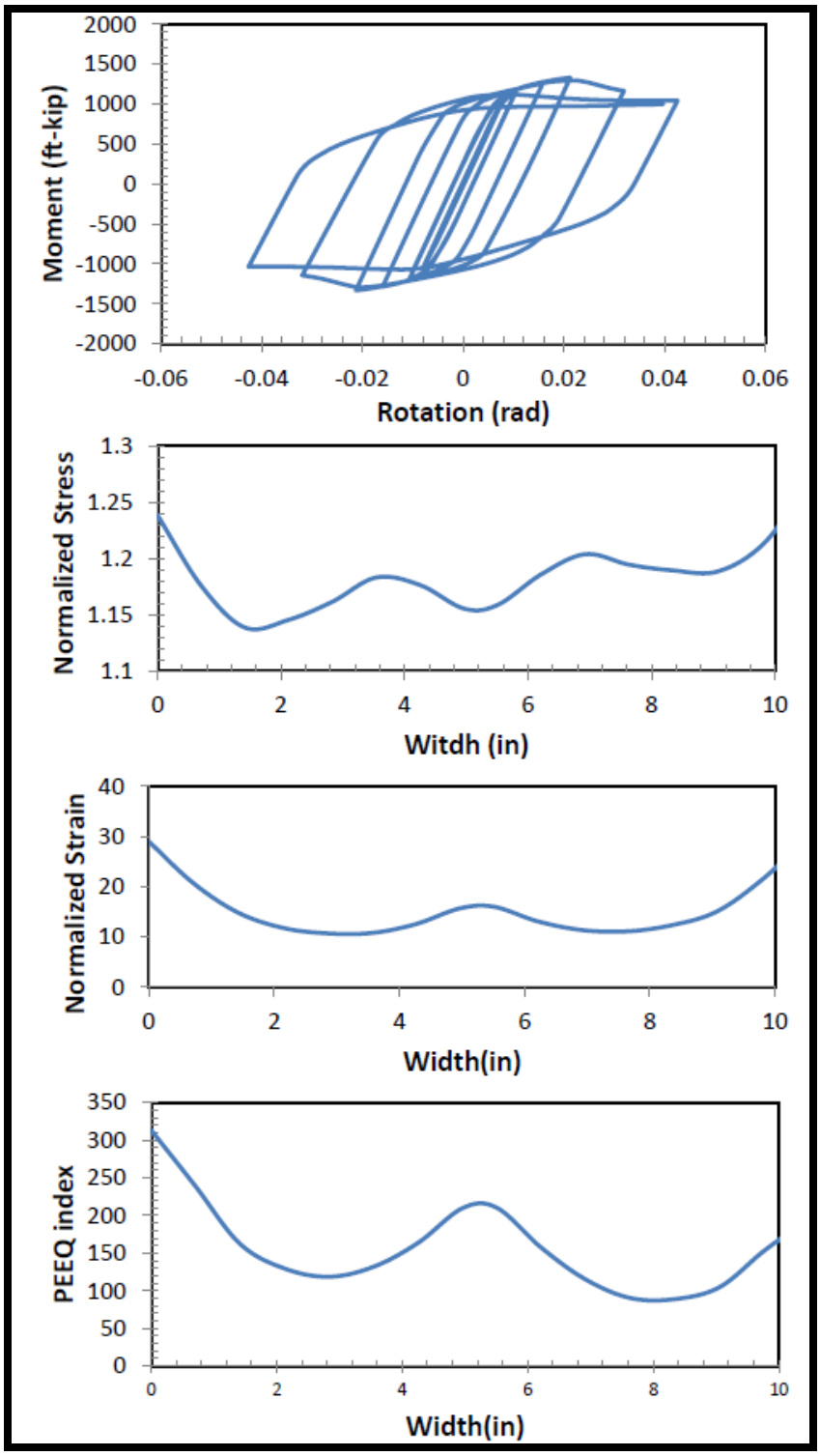

Figure 5-67: Pre-Northridge Connection (Beam W30x108)

CHAPTER 6

6. Discussion of Finite Element Model Analysis Results

6.1.Introduction

The focus of this chapter will be the discussion of the results of the finite element analyses performed with different parameters which were considered to have an impact on the performance of grouted shear stud (GSS) beam to column connections. Based on the results from the numerical analyses given in Chapter 5, the following topics will be addressed:

- Moment-rotation behavior of GSS beam to column connections in section 6.2
- The influence of the stiffener plates in section 6.3
- The effect of stub flange plate thickness in section 6.4
- The effect of stub height in section 6.5
- The effect of different shear stud configurations in section 6.6
- The effect of shear stud configurations on their behavior only for the beam section W24x62 in section 6.7
- Failure predictions on the welded region only for the beam section W24x62 in section 6.8
- Behavior of grout in section 6.9

6.2.Moment-Rotation Behavior of GSS connections

Moment-rotation graphs (at the column flange faces) were plotted in order to investigate the behavior of GSS connections. The graphs include moment-rotation curves for

the W24x62 and W30x108 beam sections with four configurations, which were described in previous chapters.

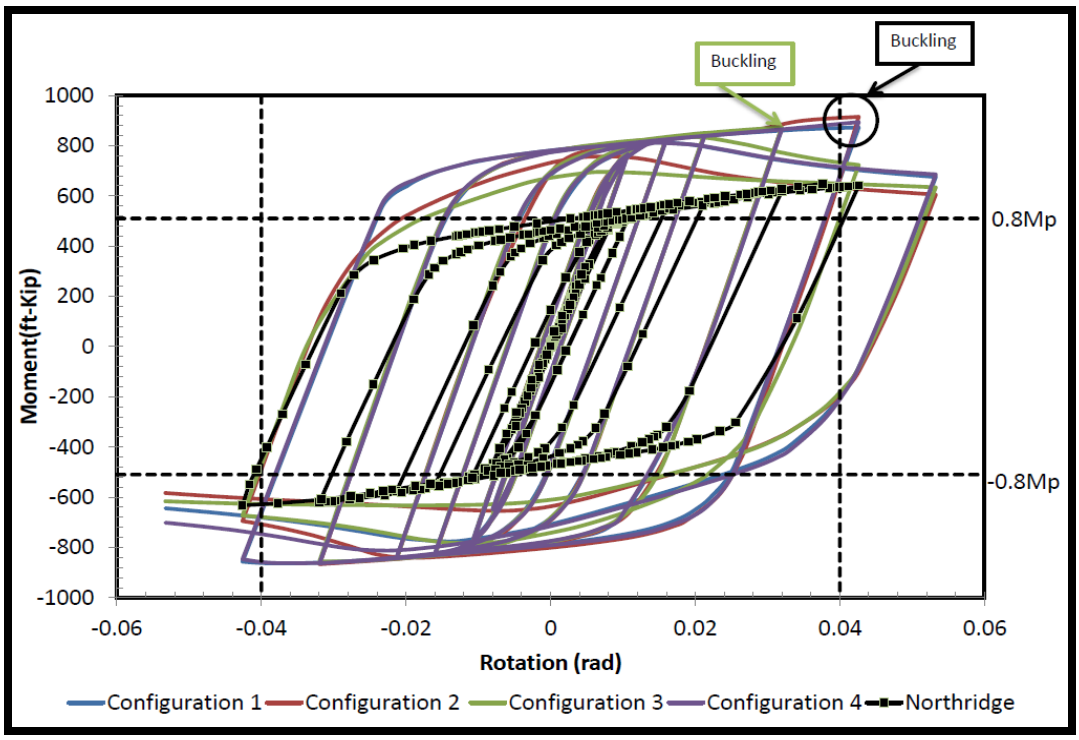

Figure 6-1: Moment-Rotation of GSS Connections for Beam W24x62 (at Column Face)

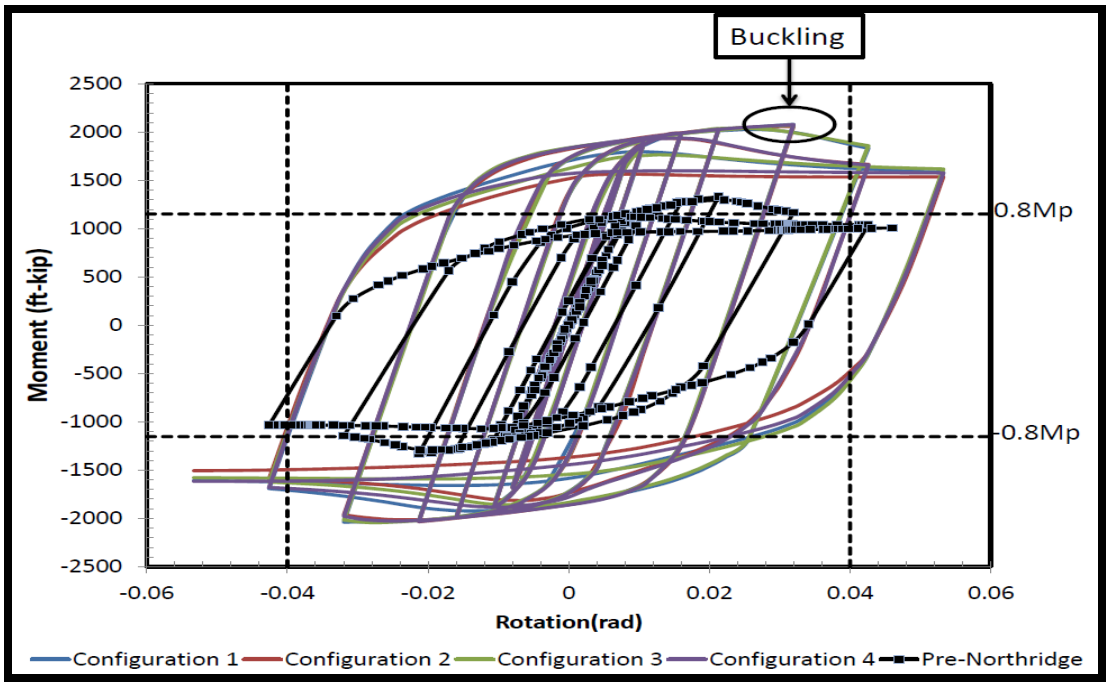

Figure 6-2: Moment-Rotation of GSS Connections for Beam W30x108 (at Column Face)

For discussion purposes, the moment-rotation plots of the parametric study matrix 1(Chapter 5,Figure 5.1) for each beam section are presented in Figure 6.1 and Figure 6.2 along with analysis of pre-Northridge connections with the same beam sections used for modeling the grouted shear stud (GSS) connections. Since fracture behavior was not explicitly included in the finite element models, moment-curvature for Pre-Northridge connections were plotted from -4% to +4% rad beam rotation (Figure 5.66 and Figure 5.67), at which beam rotation level Pre-Northridge connections were assumed to fail. In addition, finite element results confirmed this assumption because higher PEEQ index (see Figure 5.66 and 5.67) values were obtained close to the critical weld regions in both beam sections.

For the W24x62 beam section, local buckling was observed at different beam rotation levels. For configurations 1, 2, and 4, local buckling was first observed at the positive cycle of the 4% rad beam rotation. However, for configuration 3, local buckling first occurred at the positive cycle of the 3% rad beam rotation. The difference in the local buckling behavior is due to the non-symmetrical shear stud configuration (Configuration 3 for the W24x62 beam) which causes stress concentration at different locations of the beam flange; therefore, stress concentration at the shear stud roots caused the beam flange to experience local buckling earlier than other configurations. In addition to the element type that was adopted in the finite element models for defining shear studs, the rigid assumption for the shear stud modeling may be also causing a difference in local buckling behavior. Even though local buckling behavior shows some differences, the moment capacity (at the column face) at the 4% rad beam rotation is more than 80 % of the plastic moment capacity of the beam section. Therefore, the AISC seismic provision (2010) requirement for fixed-end moment connections was satisfied in all configurations. Comparatively, moment-rotation hysteresis curves show that grouted shear stud (GSS) beam to column connections absorbed more energy than the Pre-Northridge connections.

The moment-rotation curves of W24x62 (see Figure 5.2; Figure 5.6; Figure 5.10; Figure 5.14; Figure 5.18; Figure 5.22) for parametric study matrices (see Figure 5.1; Figure 5.5; Figure 5.9; Figure 5.13; Figure 5.15; Figure 5.21) studied in Chapter 5 results in similar behavior where moment capacity of each GSS connection after deterioration is more than plastic moment capacity of beam section.

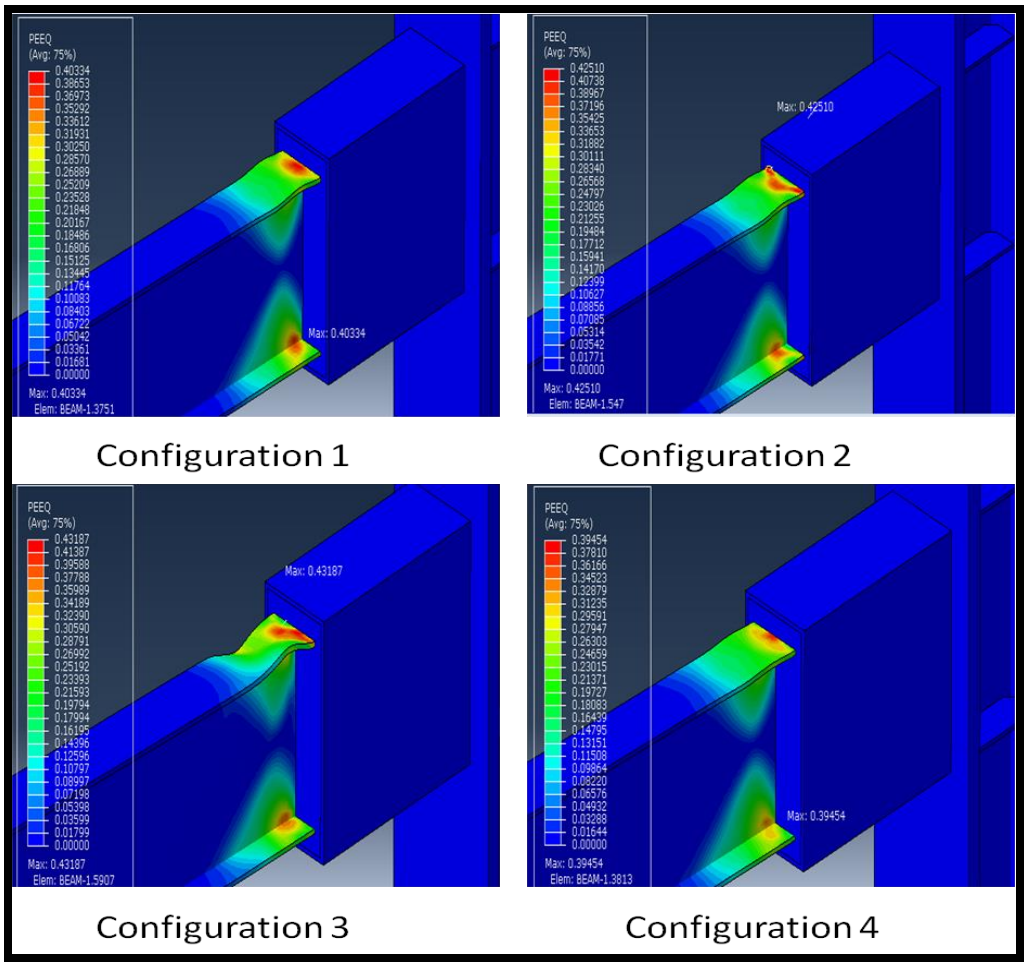

Figure 6-3: Local Buckling at Beam Section (W24x62)

Similar observations can be made for the W30x108 beam section except for local buckling behavior. All connections with studied shear stud configurations produced local buckling at a 3% rad beam rotation. Although the local buckling shapes are different because of the location of the shear studs, strength degradation occurred at the same level of deformation. Unlike the W24x62 beam section, the non-symmetrical configuration of shear studs on the W30x108 beam section (Configuration 2 for beam W30x108) did not cause

early degradation. The reason might be that when the flange of the beam becomes larger, shear studs located on it are far from each other; because of that, stress concentration at the large beam section reduces in comparison to small beam sections. Therefore, the non-symmetrical configuration did not cause early strength degradation. After deterioration in the moment capacity of GSS connection, the moment capacity at the column face is not less than 80% of the plastic moment of the beam; thus, the AISC requirement is also satisfied for the W30x108 beam section.

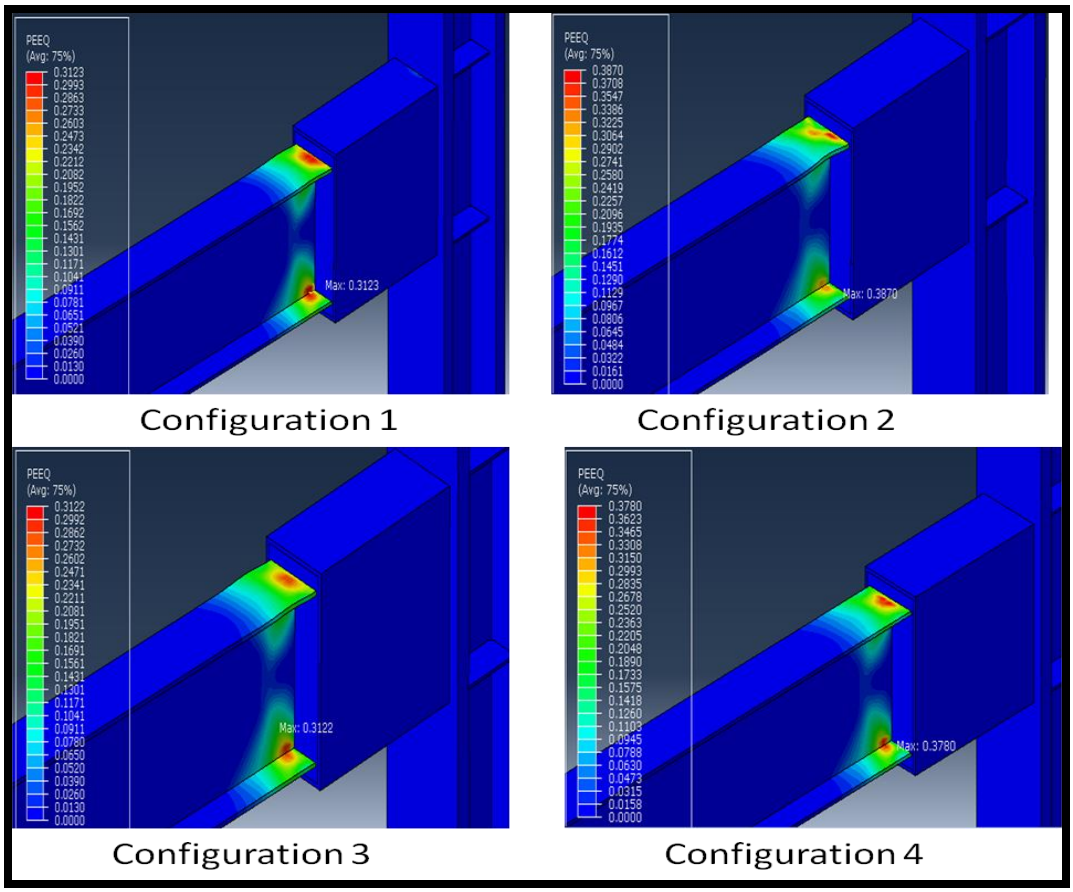

Figure 6-4: Local Buckling at Beam Section (W30x108)

For other studied parametric study matrices (see Figure 5.25; Figure 5.29;Figure 5.33; Figure 5.37; Figure 5.41; Figure 5.45) for W30x108,the moment capacity generated after attenuation of the moment capacity (see Figure 5.26; Figure 5.30; Figure 5.34; Figure 5.38; Figure 5.42; Figure 5.46) of GSS connection is more than nominal moment capacity of beam section.

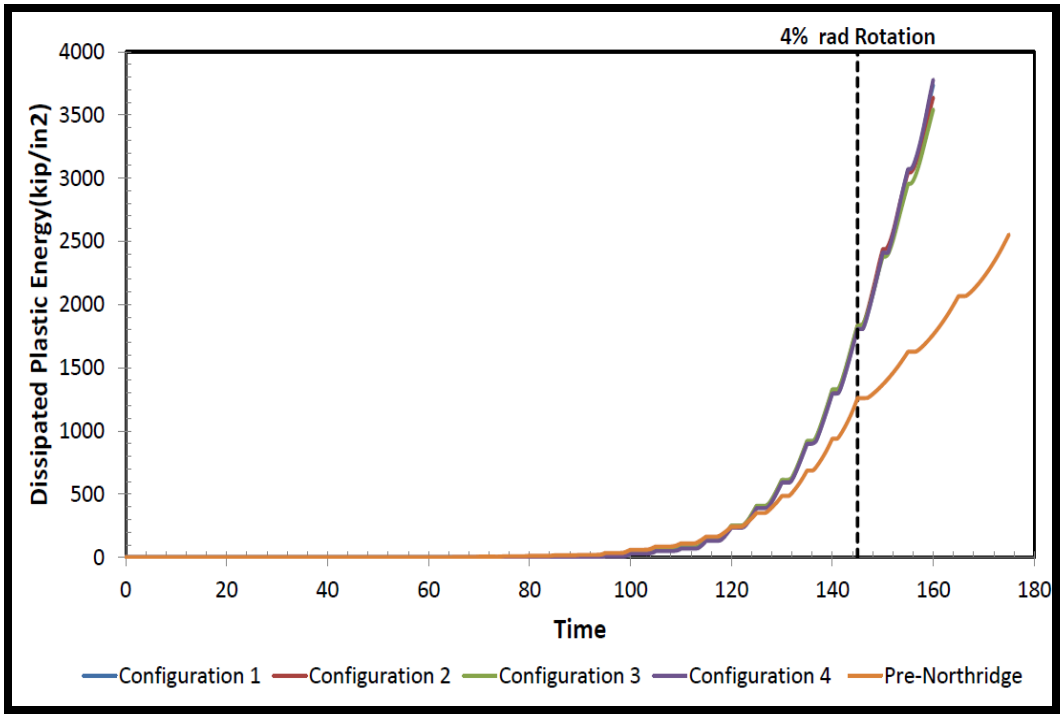

Figure 6-5: Dissipated Plastic Energy Levels for Beam Section W24x62

In order to have a better understanding in terms of the energy absorption level of the connections, dissipated plastic energy levels for each GSS beam to column and Pre-Northridge connection are presented in Figure 6.5 and 6.6. It can be seen that GSS beam to

column connections have the capability of absorbing more energy than Pre-Northridge connections. Based on the assumption that Pre-Northridge connections would fail at a 4% rad beam rotation, energy comparisons are made at to this level of drift. The GSS connection absorbed about 1.5 times more energy than the Pre-Northridge connection for the case of the W24x62 beam section. For the W30x108 beam section, the grouted shear stud (GSS) connection absorbed about 2 times more energy than the Pre-Northridge connection.

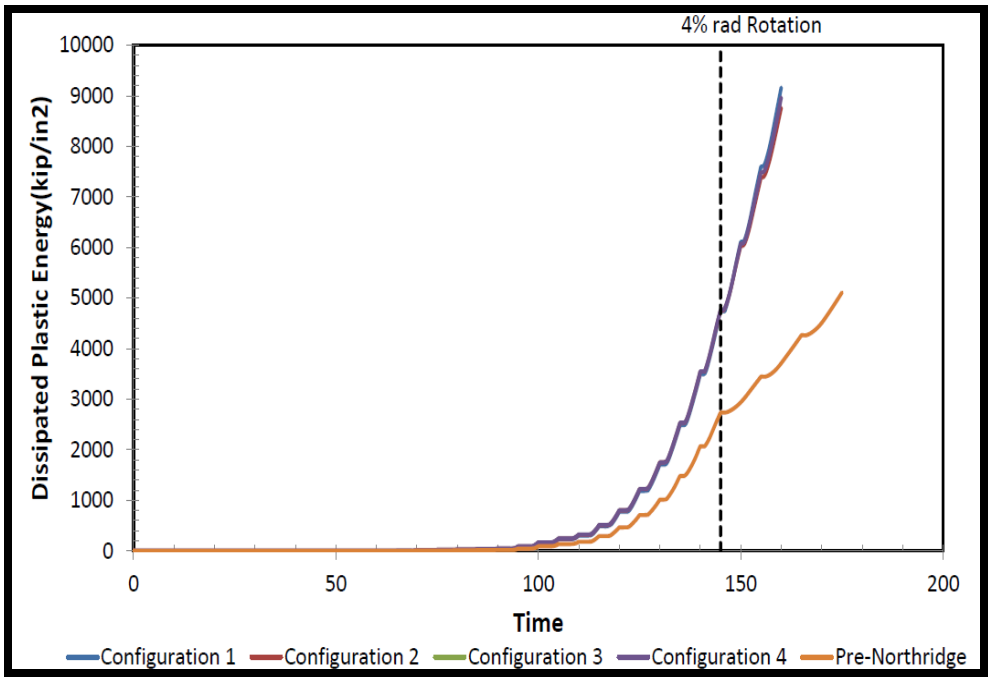

Figure 6-6: Dissipated Plastic Energy Levels for Beam Section W30x108

6.3.The Effect of Stiffener Plates

Although the column size for this connection was selected to avoid the need for stiffener plates, the effect of stiffener plates on the connection performance was examined. Numerical simulations for the W24x62 beam section only were performed using the shear stud configuration 1; it was assumed that different configurations would not lead to behavior changes in terms of stress and strain. Three different models were prepared (see Figure 5.49): a model without a stiffener plate, a model stiffener plate with a thickness of 0.25 inches, and a model stiffener plate with a thickness of 0.5 inches.

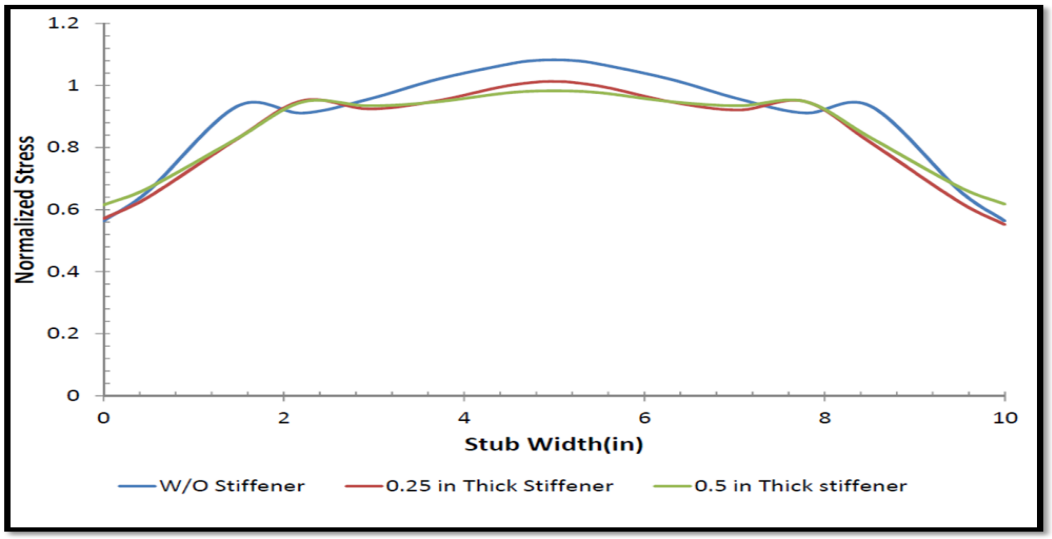

Figure 6-7: Normalized Longitudinal Stress at Interface of Stub Flange Plate and Weld

Analysis results showed that normalized longitudinal stress, which basically ratio of developed stress to yield stress did not substantial change when the thickness of the stub flange plate was reduced from 0.5 inches to 0.25 inches (Figure 6.7, also see Figure 5.50). In

the absence of a stiffener plate, longitudinal stress increased at the location where stub flange plate close to the column web. This is because the column web is the only part of the column that allows for transmitting forces through it. In addition, the presence of stiffener plates prevents the column flanges from being deformed by the beam flanges. Thus, stress concentration, which can be caused by this deformation at the flange plate near the column web centerline, can be prevented by adding stiffener plates (Bruneau et al., 2011).

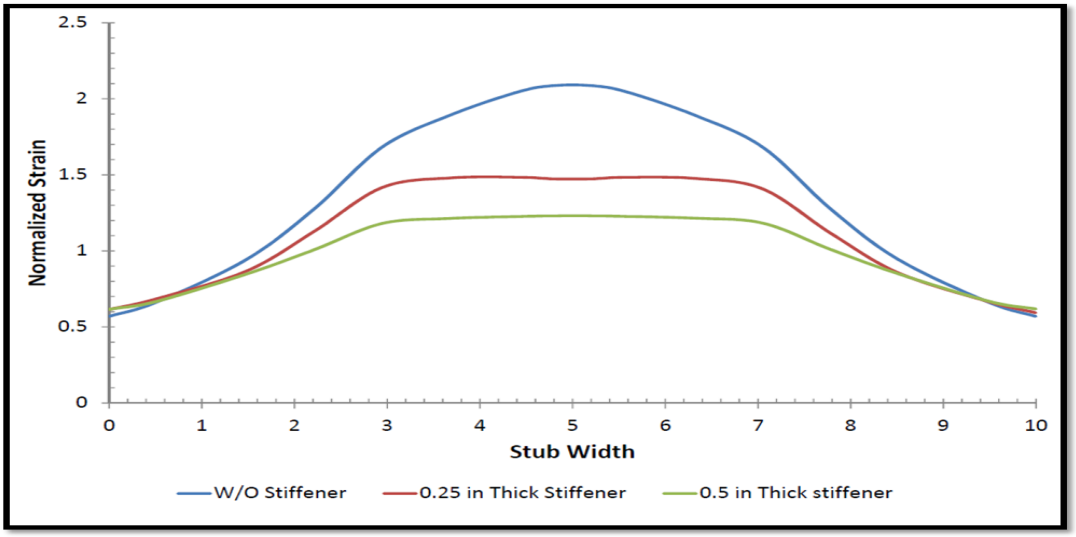

Figure 6-8: Normalized Longitudinal Strain at Interface of Stub Flange Plate and Weld

Similarly, the normalized longitudinal strain, which is calculated by dividing developed strain to yield strain, shown in Figure 6.8 (also see Figure 5.50) became larger when the stiffener plates were not included. The strain values became between 1.2 and 1.5 times larger than the strain values of the connection with stiffener plates.

The PEEQ Index was calculated at the critical weld region (Figure 6.9). It is seen that the model without stiffener plates produces more plastic deformation at the critical weld region in comparison to the other two models with stiffener plates. Models developed with stiffener plate thicknesses of 0.25 inches and 0.5 inches generated similar results in terms of the PEEQ index.

These results show that the connection without a stiffener plate is more prone to ductile fracture initiation. Moreover, El-Tawil et al. (2000) showed in their work that models without stiffener plates experience about 60% higher longitudinal stresses. Therefore, the use of a stiffener plate could prevent stress concentration in the stub section regardless of the thickness provided, as long as the buckling of the stiffener plate itself is not a concern.

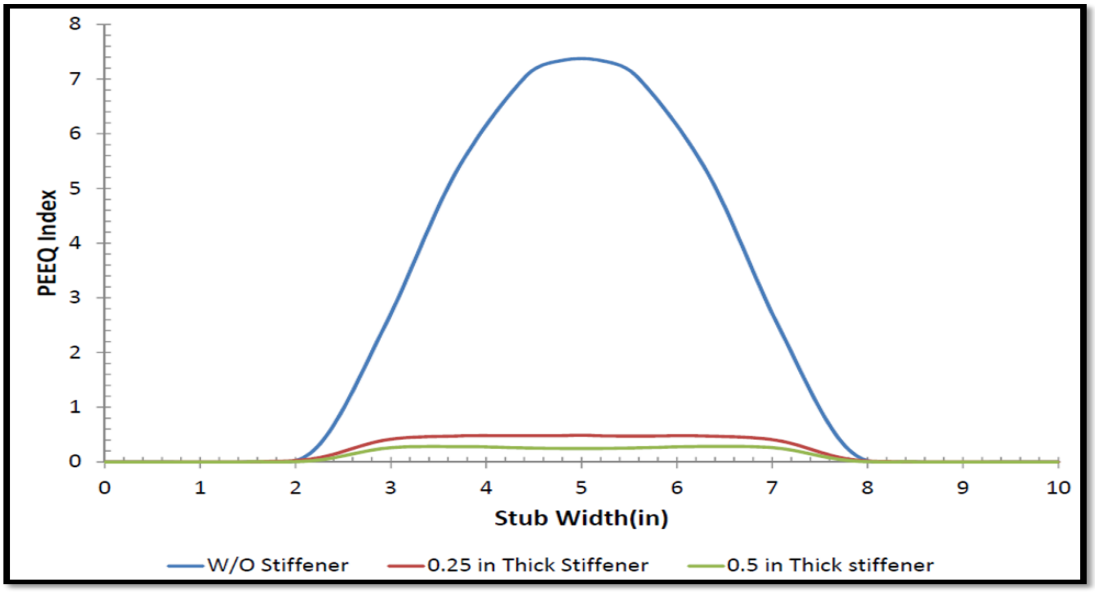

Figure 6-9: PEEQ Index Distribution at the Welded region

6.4.The Effect of Stub Flange Thickness

In order to examine the effect of various stub flange thickness on the connection performance, thicknesses were designed between 1.2 and 2 times of the flange plate thickness of the beam sections. Stub flange thicknesses were adjusted a thickness that can provide various moment capacities more than required.

For the W24x62 beam section, the flange thicknesses of the stub section were 0.6 inches, 0.75 inches and 1inch (see Figure 5.1; Figure 5.5; Figure 5.9). For the W30x108 section, the flange thicknesses of stub section were 0.8 inches, 1 inch and 1.25 inches (see Figure 5.25; Figure 5.29; Figure 5.33). Thickness of the side plates was 0.5 inches for all stub sections.

Normalized longitudinal stress, normalized longitudinal strain, and PEEQ Index at the ultimate load stage of configuration 4 (W24x62) and configuration 3(W30x108), are presented in Figures 6.10 and 6.11. As expected, increasing the flange thickness led to stress, strain, and PEEQ Index reduction in the stub section close to the column flange face as expected.

It can be seen in Figure 6.10 and Figure 6.11 that if the thickness of the stub flange plates is increased, stress and strain distributions tend to become more uniform throughout the stub width. In the case of the thicker plate, the PEEQ index approached zero; as a result, the potential for ductile fracture was reduced.

Normalized longitudinal strain of grouted shear stud (GSS) and Pre-Northridge connections (see Figure 5.66 and Figure 5.67) for the W24x62 and W30x108 beam sections are illustrated in Figure 6.12 for comparison purposes. It can be seen that the grouted shear

stud (GSS) beam to column connection has the ability to reduce the longitudinal strain at the welded region under the same loading condition.

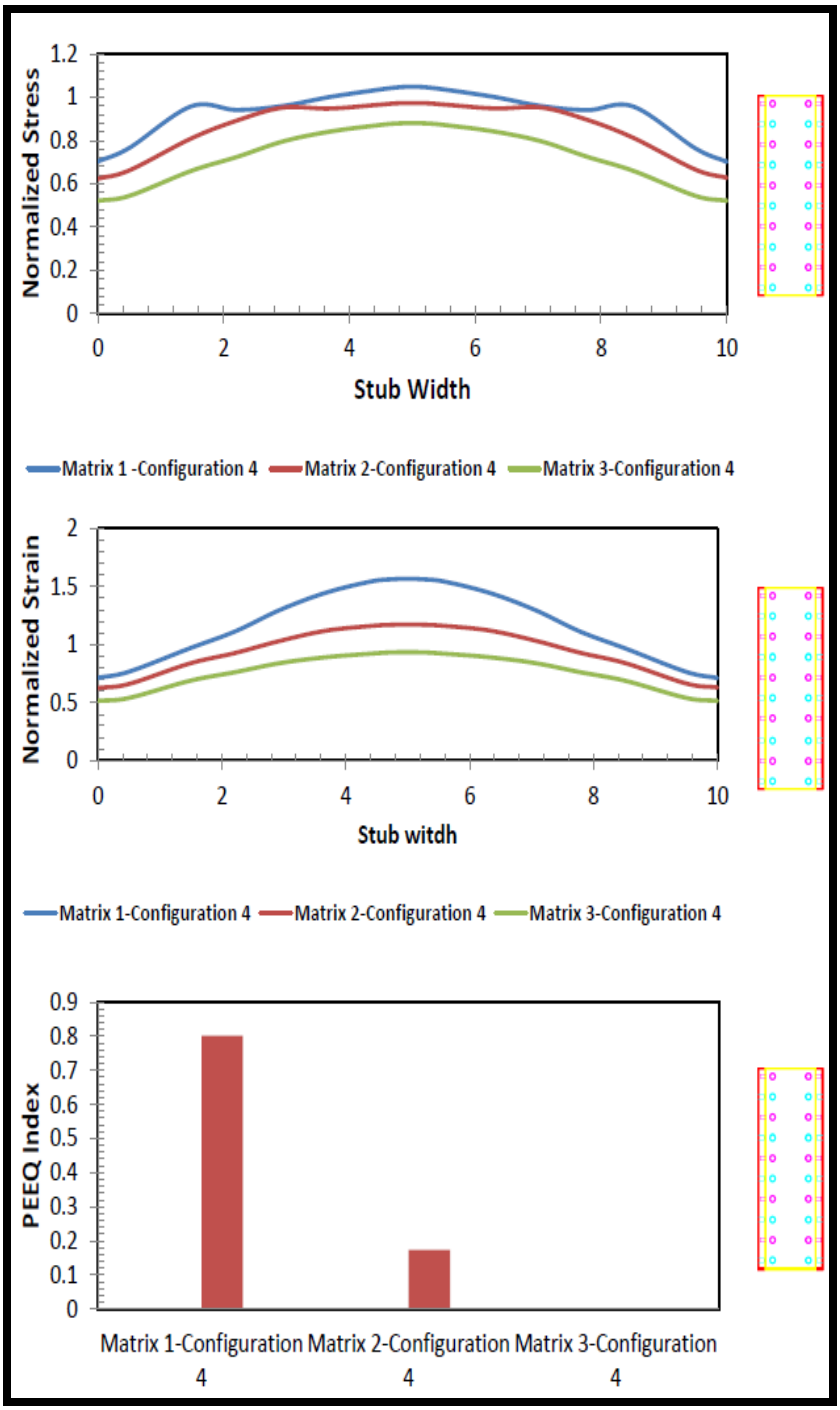

Figure 6-10: Normalized Longitudinal Stress, Normalized Longitudinal Strain, and PEEQ Index for Beam Section W24x62 (Configuration 4)

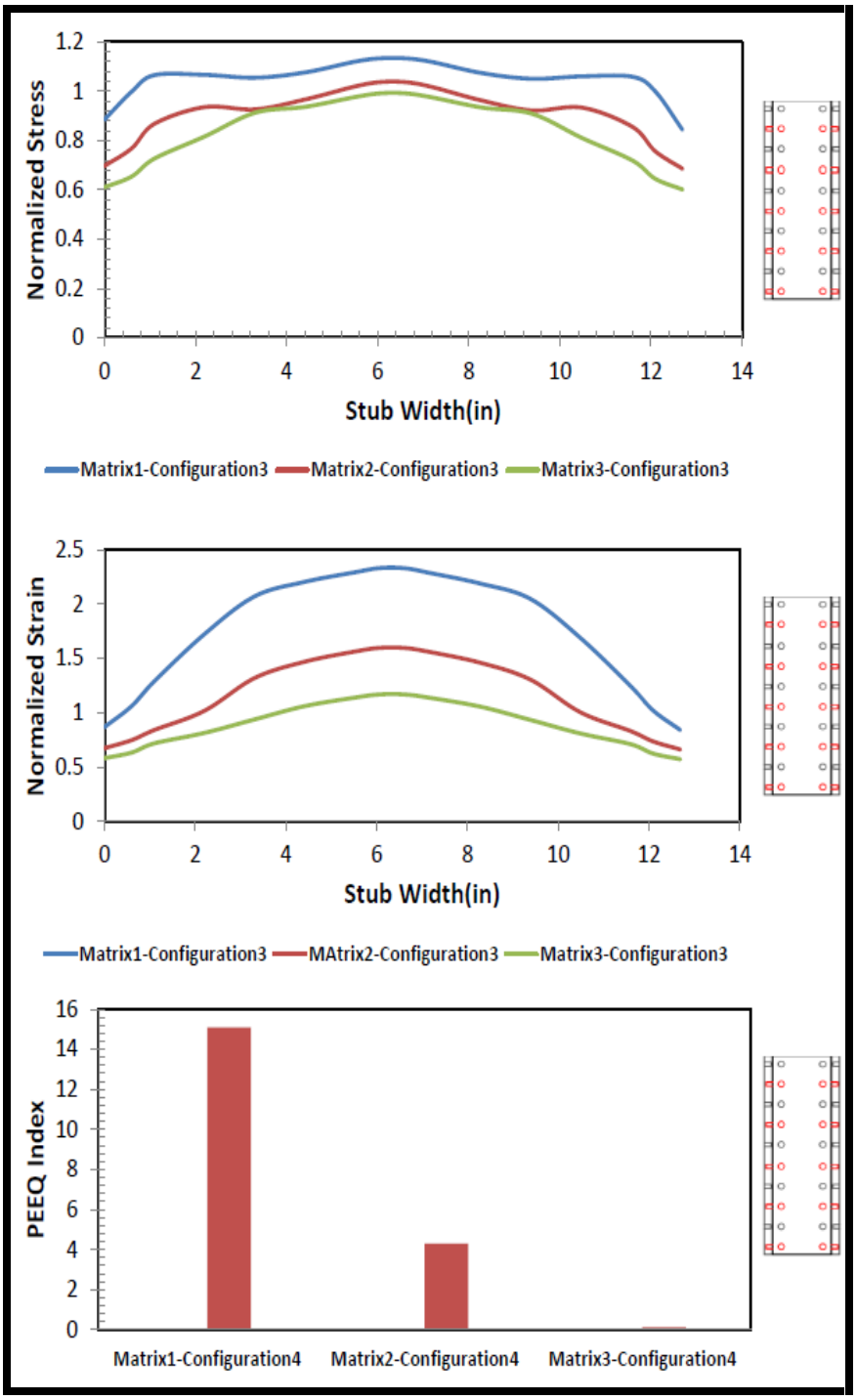

Figure 6-11: Normalized Longitudinal Stress, Normalized Longitudinal Strain, and PEEQ Index for Beam Section W30x108 (Configuration 3)

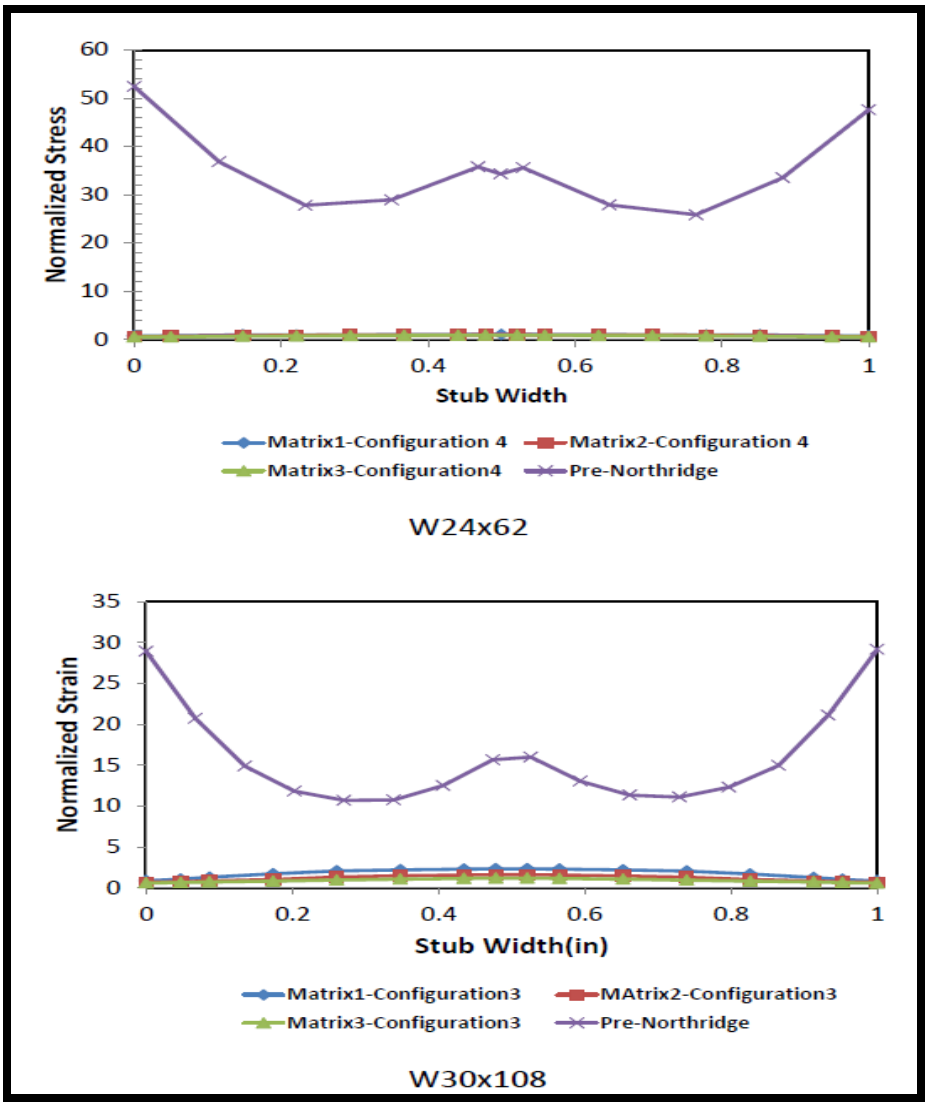

Figure 6-12: Normalized Longitudinal Strain Comparison for Beam Sections W 24x62 and W30x108

6.5.The Effect of Height of the Stub Section

To investigate the effects of stub section height on grouted shear stud (GSS) beam to column connections, the height was increased. For the W24x62 beam section, the inside

height (distance between inside surfaces of the stub flanges) was increased from 28.7 inches (Matrix1-Configuration1) to 32 inches (Matrix 4-Configuration 1). For the W30x108 beam, the inside height of the section was increased from 35 inches to 40 inches. The stub flange thicknesses were 0.6 inches and 0.8 inches for the W24x62 and W30x108 beam sections, respectively. The side plate thickness was 0.5 inches for all stub sections.

Figure 6.13 and Figure 6.14 present normalized longitudinal stress, normalized longitudinal strain and PEEQ Index plots, for the W24x62 and W30x108 beam sections at the ultimate force developed in the models. It can be seen that the increase in the stub height notably reduced the stress and strain magnitude at the critical weld region. Moreover, the potential of ductile fracture reduced when height of the stub section was increased. Unexpected results (Figure 6.15) were obtained for the W24x62 beam section using configuration 4. The increase in height reduced stress and strain magnitudes at the centerline of the stub section flanges, but values increased at the corners.

Such an outcome can be explained as the result of the shear studs, located on the side plates that transmit additional bending forces to the corners of the flanges. The magnitude of the forces delivered by the shear studs was larger than the capacity provided by the increased height of the stub section. Similar results were not observed for the W30x108 beam. It is believed that the capacity provided by the increased height of stub section was less than the demand.

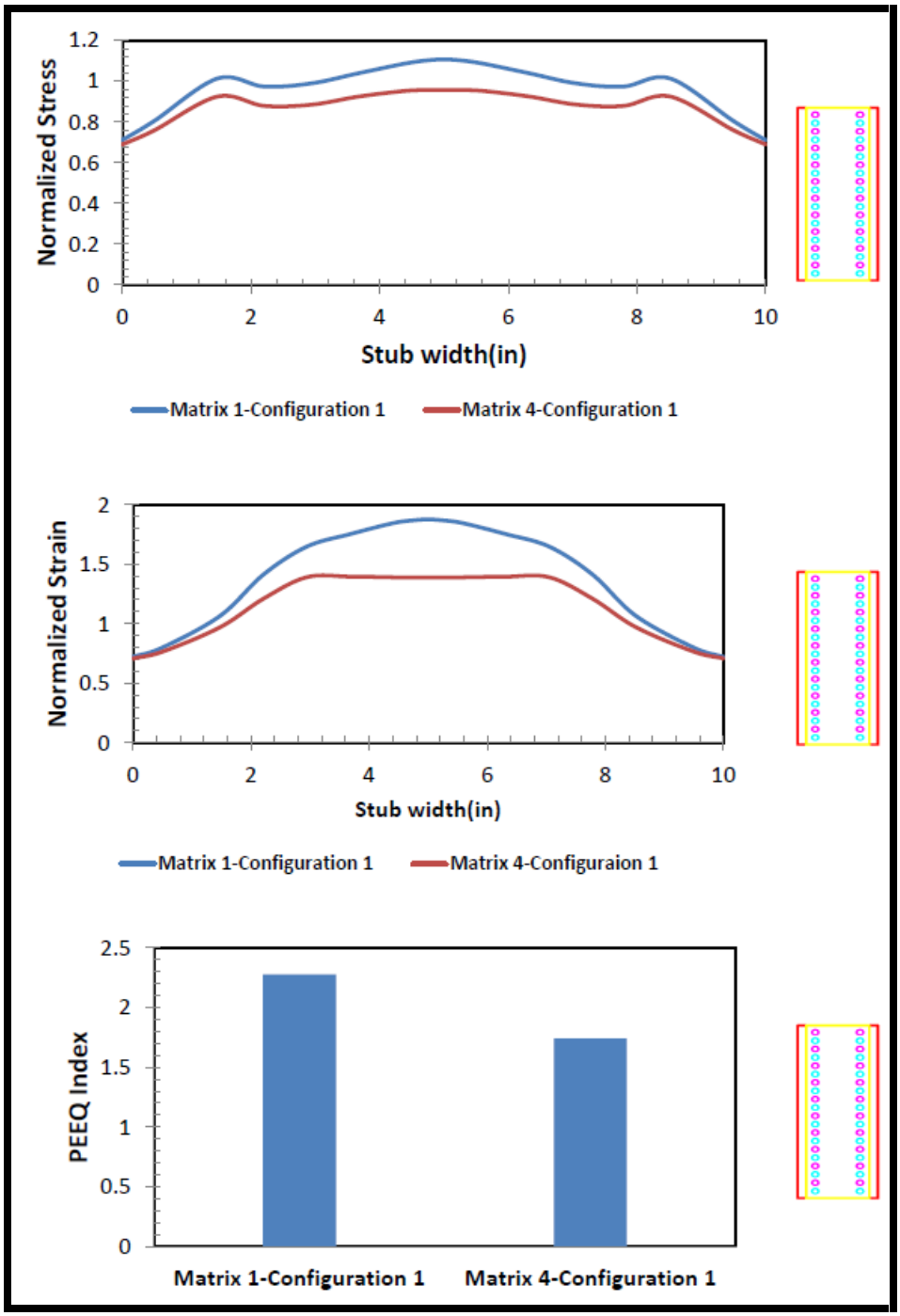

Figure 6-13: Normalized Longitudinal Stress, Normalized Longitudinal Strain and PEEQ Index for Beam Section W24x62 (Increased Height-Configuration1)

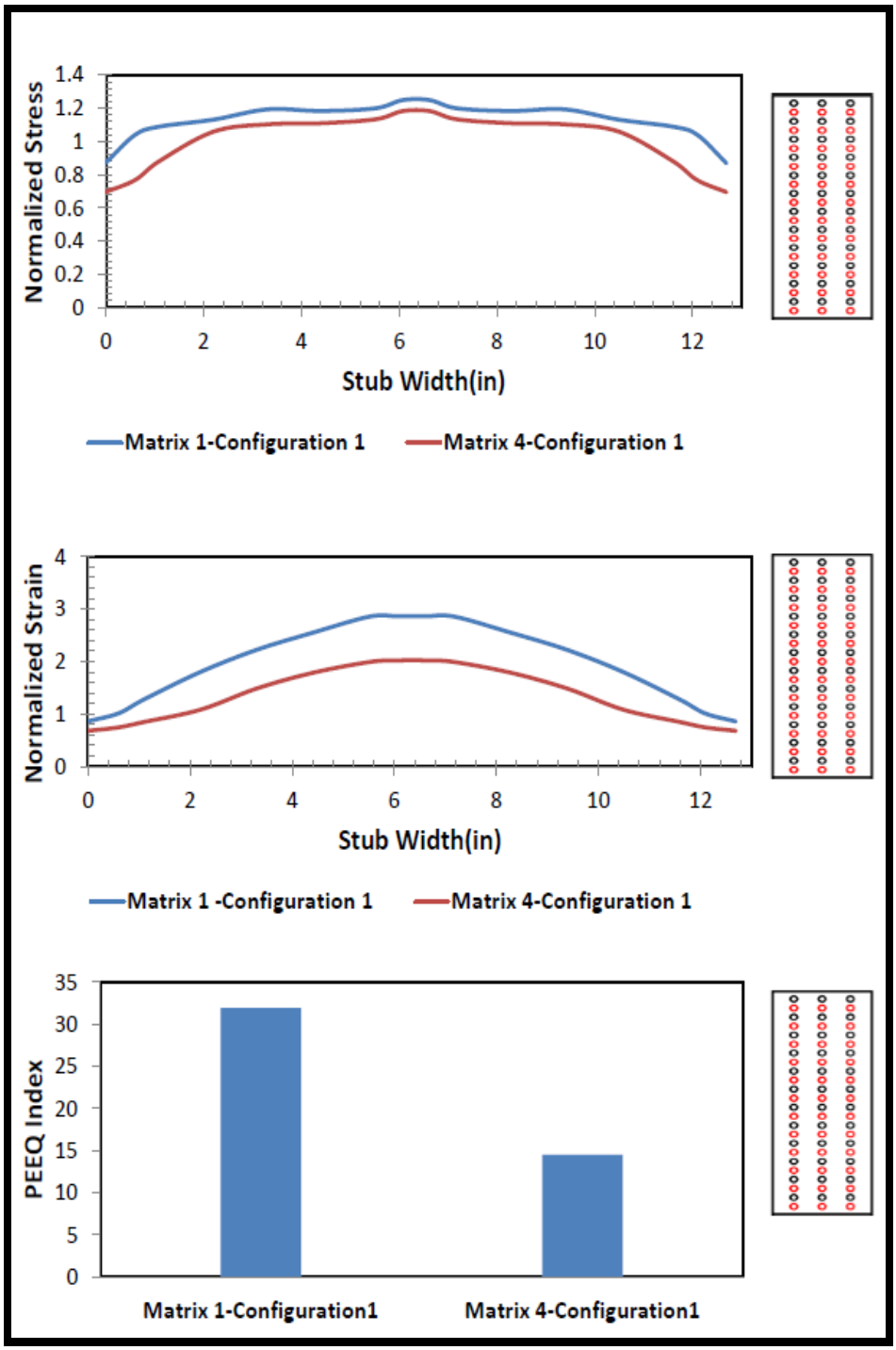

Figure 6-14: Normalized Longitudinal Stress, Normalized Longitudinal Strain and PEEQ Index for Beam Section W30x108 (Increased Height-Comfiguraion1)

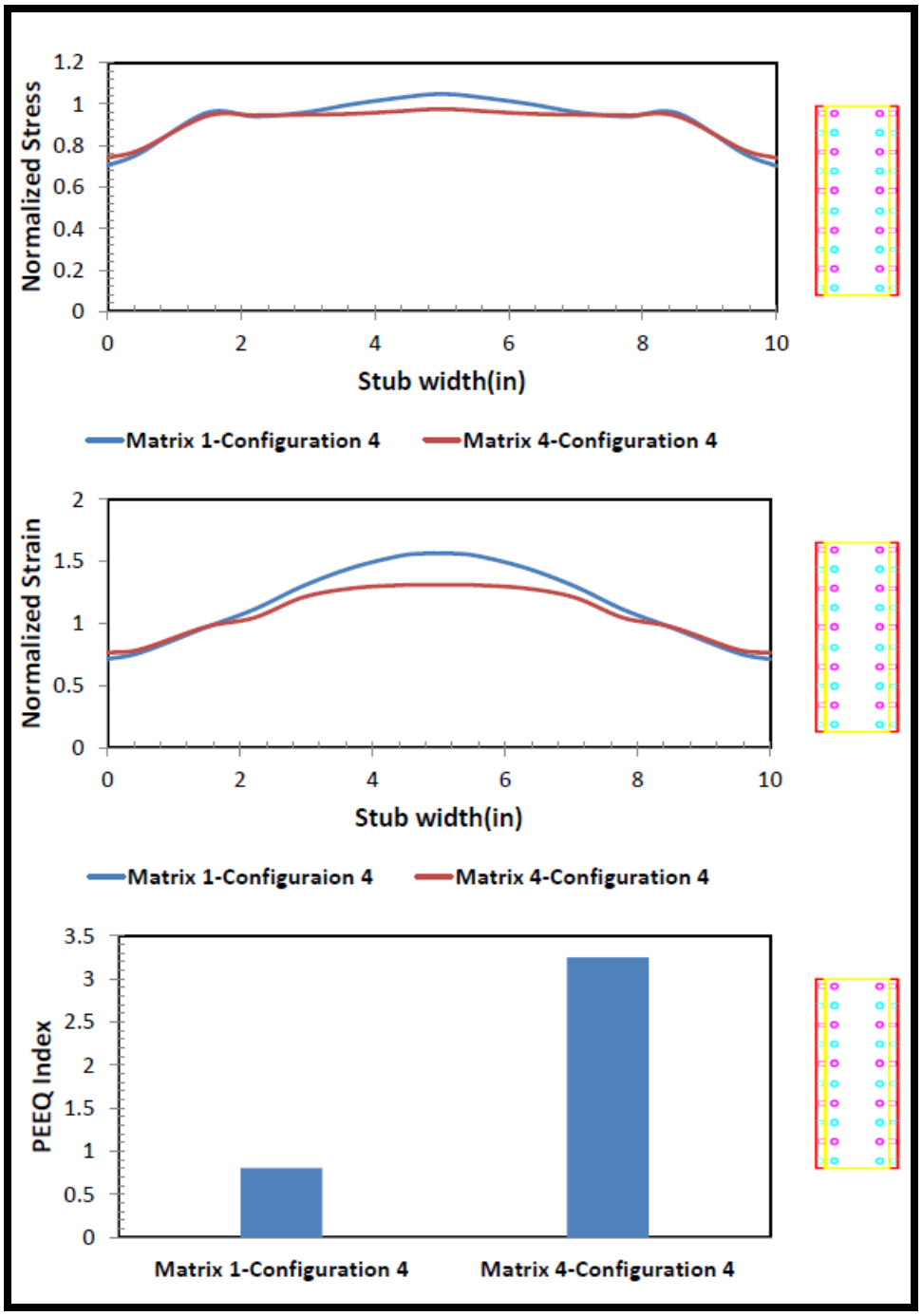

Figure 6-15: Normalized Longitudinal Stress, Normalized Longitudinal Strain and PEEQ Index for Beam Section W24x62 (Increased Height-Configuration 4)

6.6.The Effect of Different Shear Stud Configurations

To examine the effect of the shear stud configurations on beam to column connections for each beam section, four different configurations are discussed. Details of the configurations were provided in Chapter 2. Finite element analyses showed that when the configuration was changed, stress and strain distributions at the stub section also varied. Furthermore, a change in the PEEQ index at the location of the plastic hinge and the critical weld region is also expected. Results of the parametric study matrix 1 are provided for the W24x62 and W30x108 beam sections. Figure 6.16 shows normalized longitudinal stress and strain distributions for the W24x62 beam section that were extracted at the interface of the stub flange plate and column flange weld.

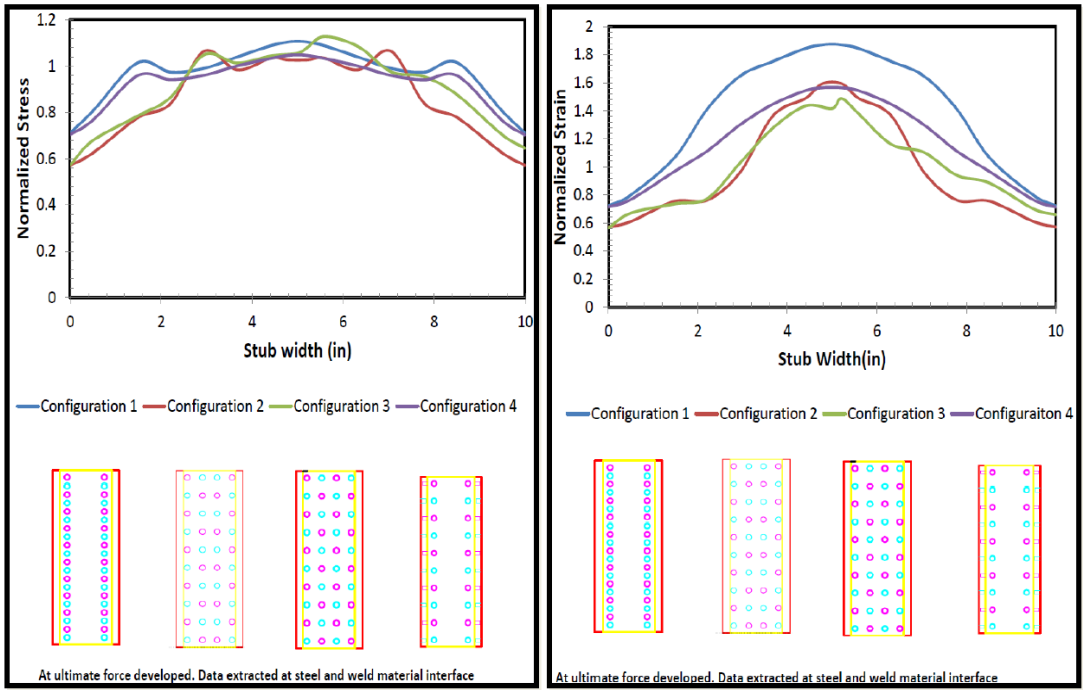

Figure 6-16: Normalized Longitudinal Stress and Strain for Beam Section W24x62

It can be seen that shear stud configuration 3, in which shear studs were non-symmetrically distributed on the beam and stub flanges, produced a non-symmetrical distribution of stress and strain, as expected. It is observed that when the shear studs were located close to the centerline of the beam and stub sections, strain magnitudes decreased. The reason might be that the lever arm between the shear studs and centerline of the stub section increases when the shear studs are located far from the centerline. Therefore, the strains in configurations 1 and 4 are higher than those in configurations 2 and 3. It should be noted that this reasoning is rooted in the belief that the shear studs would generate the same amount of load transferred from the beam section. Similar observations were made for the W30x108 beam section which is shown in Figure 6.17.

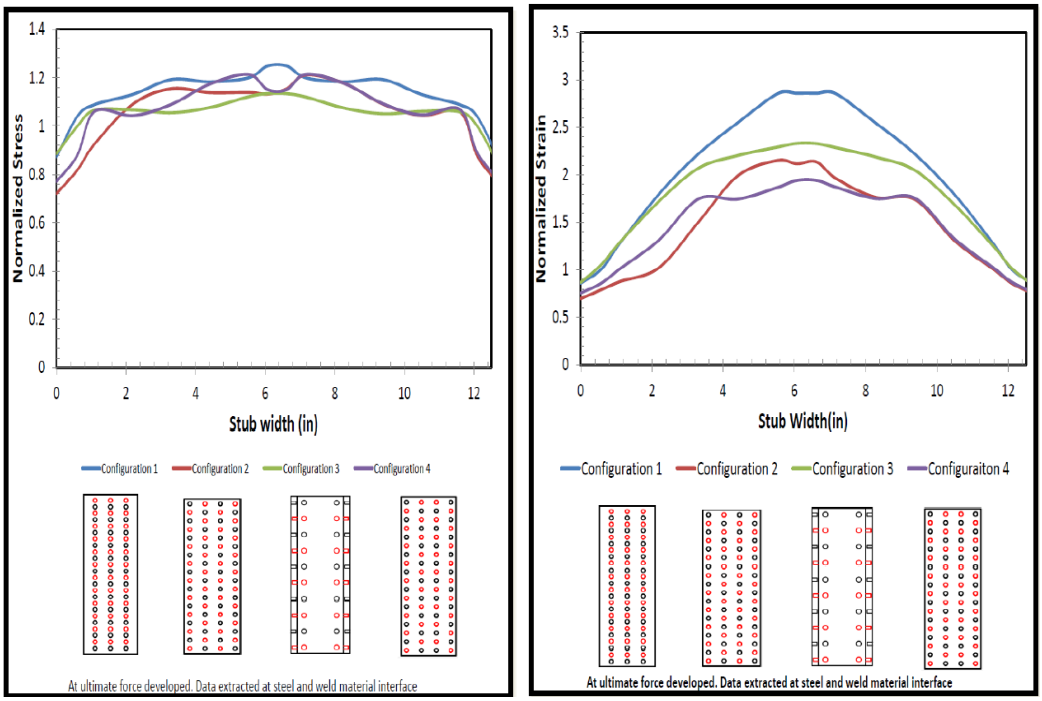

Figure 6-17: Normalized Longitudinal Stress and Strain for Beam Section W30x108

Another effect of the shear stud configuration on the behavior of the connection was discussed in section 6.2. The non-symmetrical configuration led to early strength degradation, as shown in Figure 6.1. There are several possible explanations for this: 1) the increase in the beam flanges may have reduced the stress concentration in the beam flange close to the beam centerline, due to the increase in the distance between non-symmetrically located shear studs; or 2) the increase in the flange thickness dominated the behavior and also reduced the stress concentration.

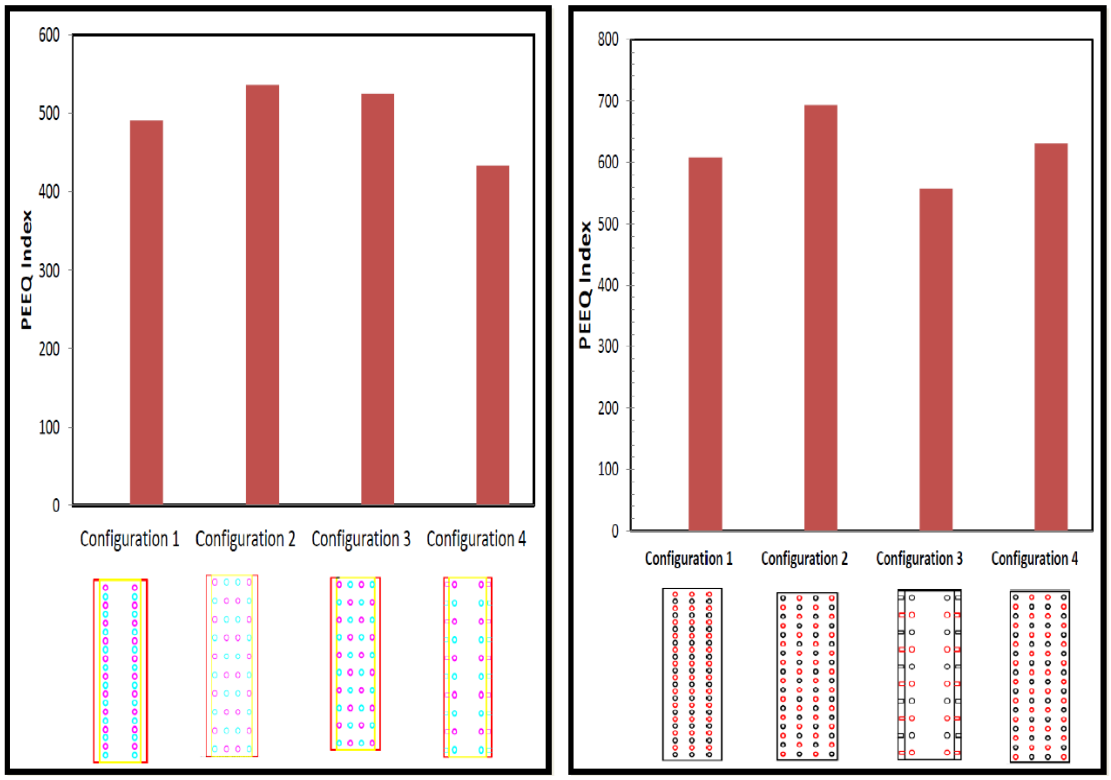

Figure 6-18: PEEQ Index Calculated at Plastic Hinge Regions

In addition, it was also observed that a different configuration of shear studs caused the beam to produce different levels of plastic strain. Figure 6.18 shows the PEEQ Index values which were calculated at hinge locations; these graphs show that the configuration with shear studs located near the beam and stub centerline produced more plastic strain. Although plastic strain levels, which were developed by the connection with different shear stud configurations, were different, the overall energy absorption of all configurations was similar, as shown in Figure 6.19.

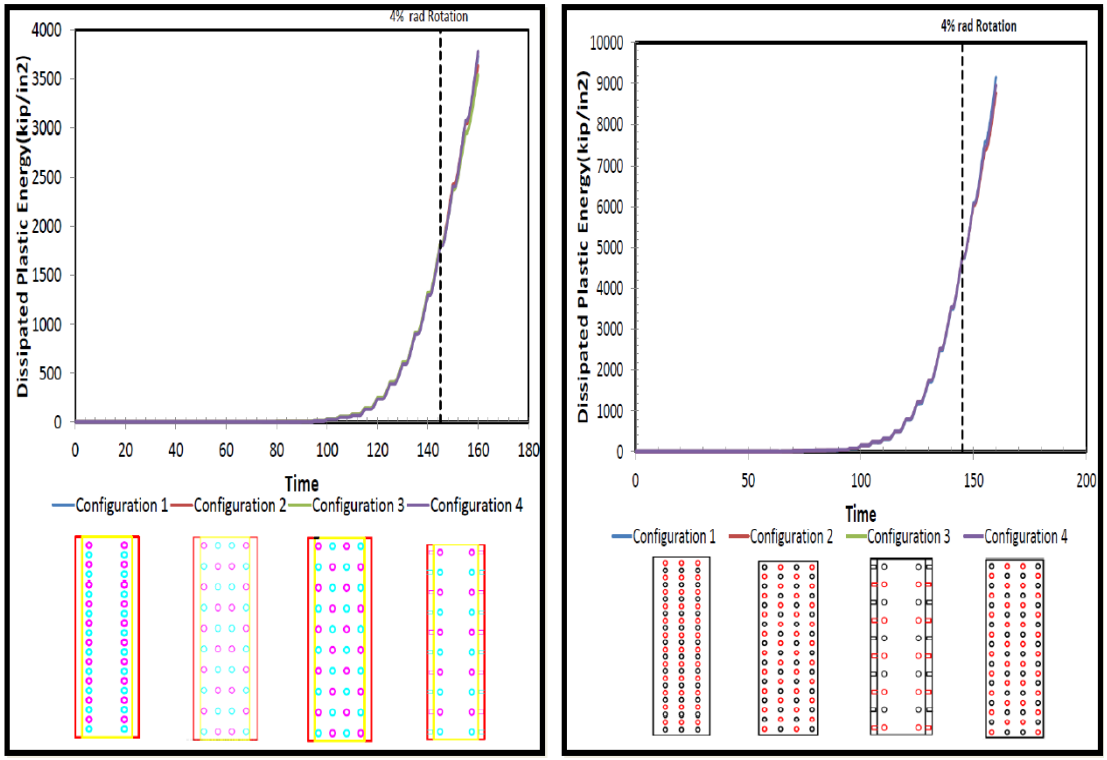

Figure 6-19: Dissipated Plastic Energy Levels

Similar observations can be made for other studied matrices for W24x62 and W30x108 beam sections. The stress and strain distribution for different shear stud configurations of GSS connections with W24x62 (see Figure 5.3; Figure 5.7; Figure 5.11; Figure 5.15; Figure 5.19; Figure 5.23) and W30x108 (see Figure 5.27; Figure 5.31; Figure 5.35; Figure 5.39; Figure 5.43; Figure 5.47) show variation due to the shear stud configuration. In addition, the PEEQ index at plastic hinge location and at the critical weld region for W24x62 (see Figure 5.4; Figure 5.8; Figure 5.12; Figure 5.16; Figure 5.20; Figure 5.24) and W30x108 (see Figure 5.28; Figure 5.32; Figure 5.36; Figure 5.40; Figure 5.44; Figure 5.48; Figure 5.52) beam sections also change when the shear stud configuration is changed.

6.7.The Effect of Shear Stud Configuration on the their Behavior

In order to analyze the behavior of the shear studs used in grouted shear stud (GSS) beam to column connections, four different configurations (discussed in previous chapters) were taken into account for the W24x62 (see Figure 5.51 for studied matrix) section. “Failure index” values of the shear studs were calculated for each configuration to facilitate comparison. As mentioned in Chapter 4, the shear studs were modeled as rectangular elements which can cause stress concentrations at the corners. Because of this stress concentration, the failure index may substantially differ. For comparison purposes, since all configurations were modeled with a similar approach, the “failure index” will be used to discuss behavior of the shear studs. The calculated failure indices for four different configurations are presented in Figure 6.20. As illustrated, shear studs are located on the beam flanges only in configuration 4.

As shown in Figure 6.20 (see Figure 5.52; Figure 5.53; Figure 5.54; Figure 5.5; Figure 5.56 for more larger view), failure index calculations show that the locations of the shear studs may play an important role on their behavior. The first row of all configurations, with the exception of configuration 1, reached failure before a 4% rad beam rotation. Therefore, only configuration 1 can be adopted, because it satisfies the AISC seismic provisions (2010) requirement for qualifying fixed-end moment connections.

Configurations that have shear studs located near the centerline of the beam section experienced failure before other configurations. It is believed that if the shear studs are located near the beam centerline, forces carried by those shear studs are greater than forces carried by shear studs that are located near the beam flange edge due to stiffer beam web. The PEEQ index, which comes into play in calculation of “Failure index”, is shown (Figure 6.21) to have an understanding on force carried by shear studs at different location of beam flange.

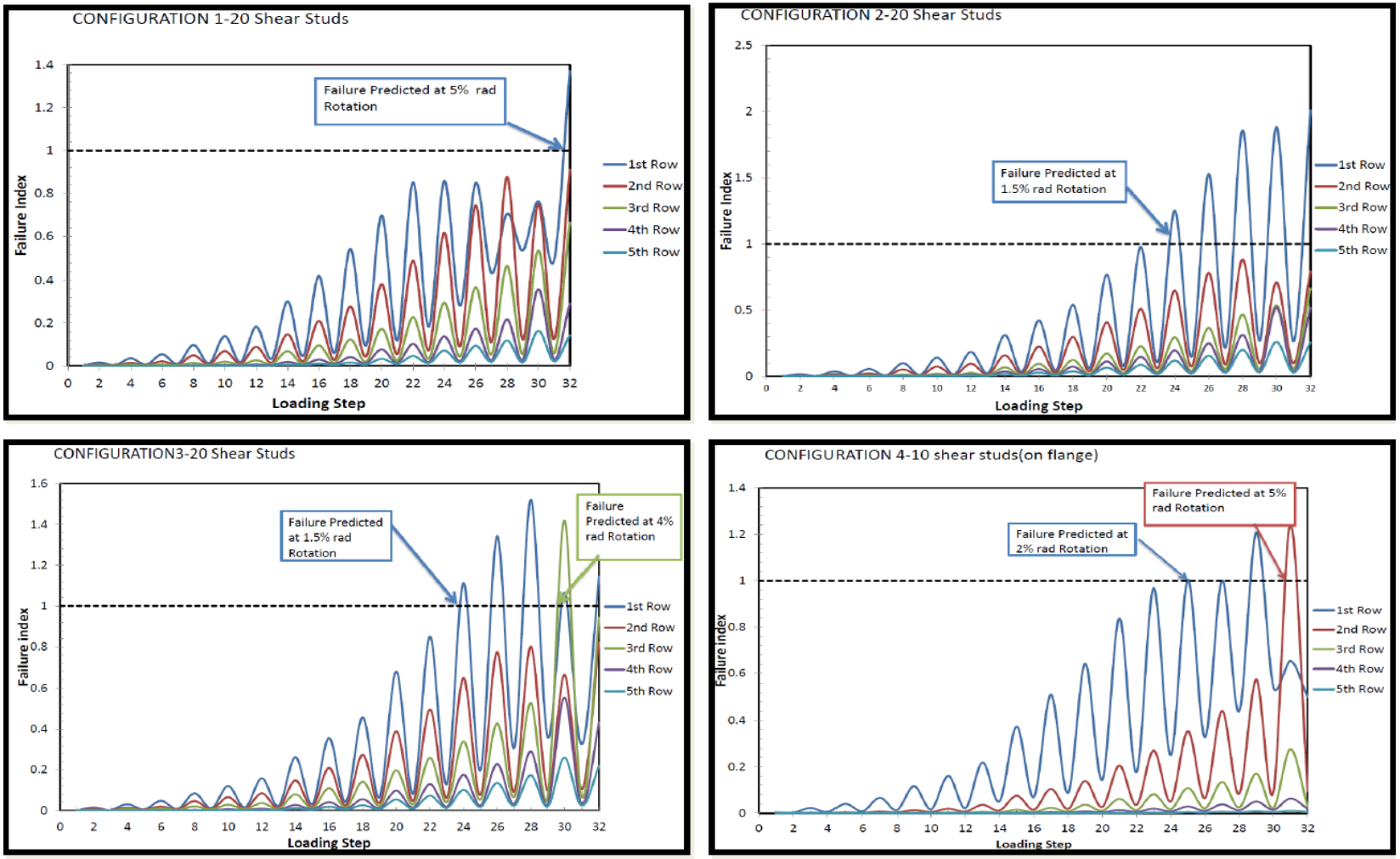

Figure 6-20 : Calculated Failure Index for Four Configurations

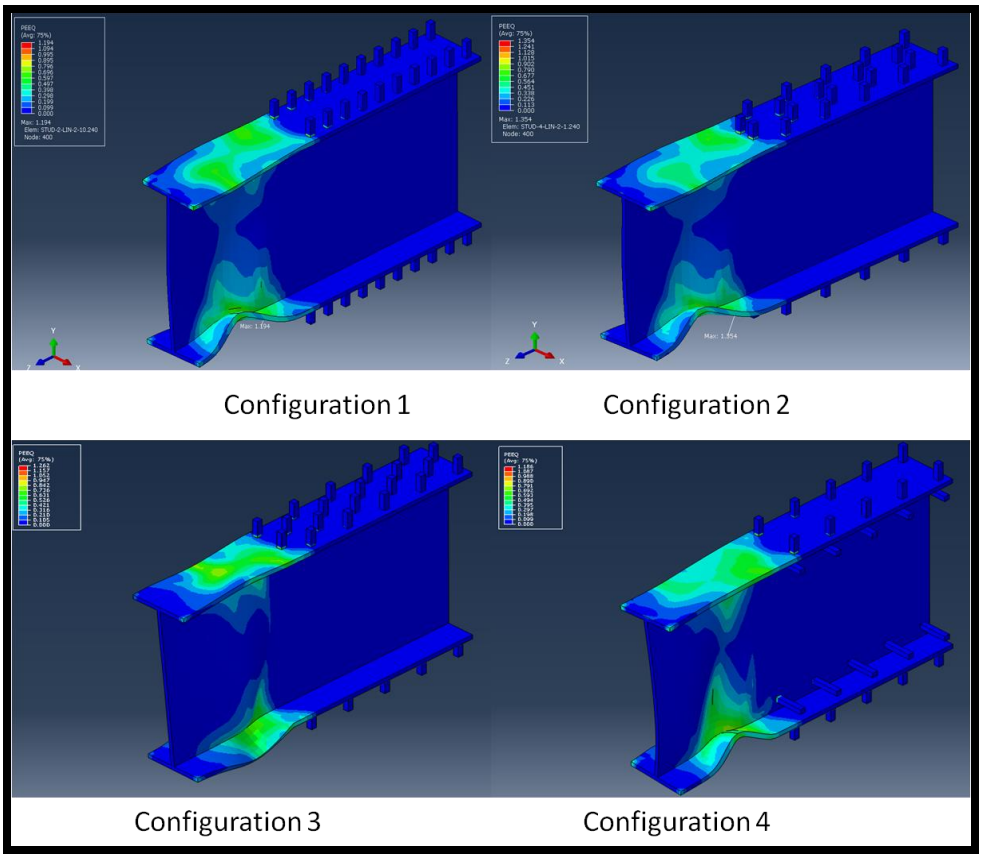

Figure 6-21: PEEQ Distribution in Shear Studs

PEEQ index, which is an indicator of ductile demand, is higher in configurations 2 and 3 in which shear studs are located near the beam flange centerline. The PEEQ index in the first row of configurations 1, 2, 3 and 4 were 1.194, 1.354, 1.262 and 1.186, respectively. From these PEEQ indices, it can be seen that when the shear studs are located near the beam flange centerline, forces transmitted to them increases. This is understood to be the result of the stiffer beam web causing more force to be transferred to those shears studs.

Figure 6.22 shows the failure index values for configuration 4, which were calculated in the shear studs located on the beam web. As it can be seen, the failure index for the first

row reached failure at a 5% rad beam rotation. It can be concluded that when the shear studs are located on the web of the beam, only the shear studs near the plastic hinge region have a higher potential for experiencing ductile failure. This is because the shear studs located on the beam flange transfer more force than those on the beam web.

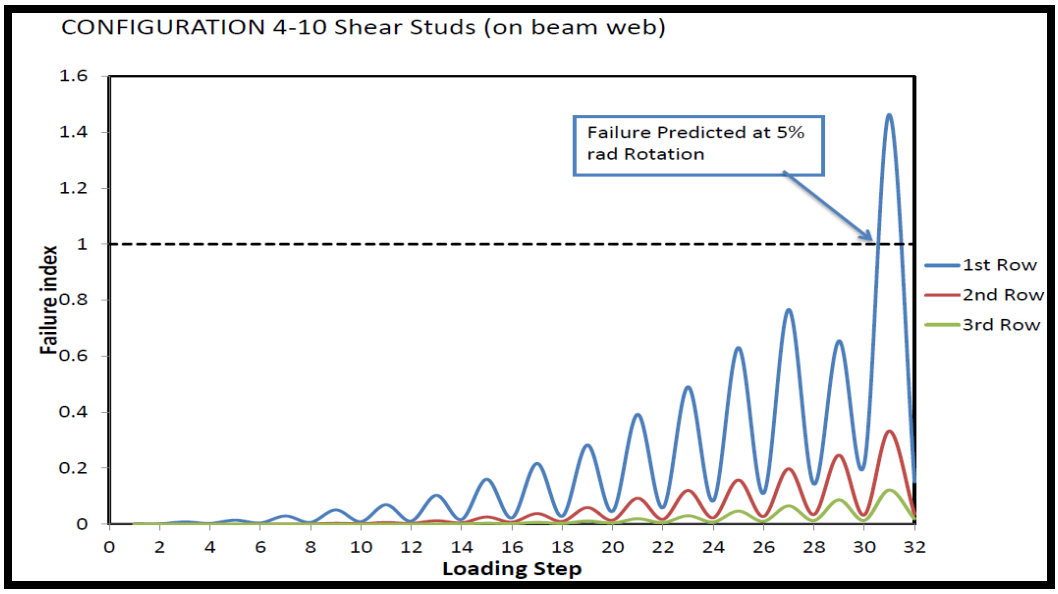

Figure 6-22: Calculated Failure Index for Configuration 4 (on Beam Web)

Shear studs located on the stub sections did not experience failures. Calculated failure index graphs for shear studs on the stub sections are shown in Figure 6.23 (see Figure 5.57; Figure 5.58; Figure 5.59; Figure 5.60; Figure 5.61 for a large view). It can be seen that shear studs on the stub section did not experience failure during loading. These results indicate that the shear stud on the beam section located near the plastic hinge region experience higher stress triaxiality than shear studs located on the stub section. Therefore, failure predicted in

the shear studs near the plastic hinge region is higher due to a decrease in the calculated critical plastic strain. It should be noted that failure index may provide inaccurate results due to cyclic loading (Kavinde and Deierlein , 2004); therefore, the discussion on predictions are somewhat limited.

Unlike column members, beam members are subjected little or no axial force. Considering the amount of axial force carried by beam members, it was thought that the number required of shear studs might be reduced. In order to understand how the number of shear studs affects their performance, the number of shear studs was reduced for configurations 1 and 2. These configurations were modeled with a total of 64 and 40 shear studs in the grouted shear stud (GSS) connection. Figures 6.24(see Figure 5.62 and Figure 5.63) and 6.25 (see Figure 5.64 and 5.65) show failure indices for the cases in which the number of shear studs was reduced. For configuration 1, when the provided shear stud number was 20, failure in the first row occurred at a 5% rad beam rotation. When the number was reduced to 16, failure in the first row took place at a 1.5 % rad beam rotation. When reduced to 10, failure occurred at a 1 % rad beam rotation. These failure index plots show that reduction in the number of shear studs led to early failure of the shear stud, as was expected. Similarly, with 20 shear studs, configuration 2 experienced failures at a 1.5 % rad beam rotation; with 16 shear studs, it had failure at a 1% rad beam rotation. When the number of shear studs was reduced to 10, failure occurred at a 0.75% rad beam rotation. These failure index results indicate that reduction in the number of shear studs is not suitable if a building is located in a region of high seismic activity. However, for regions with low to

moderate seismic risk, the number of shear studs can be reduced for achieving a more economical design.

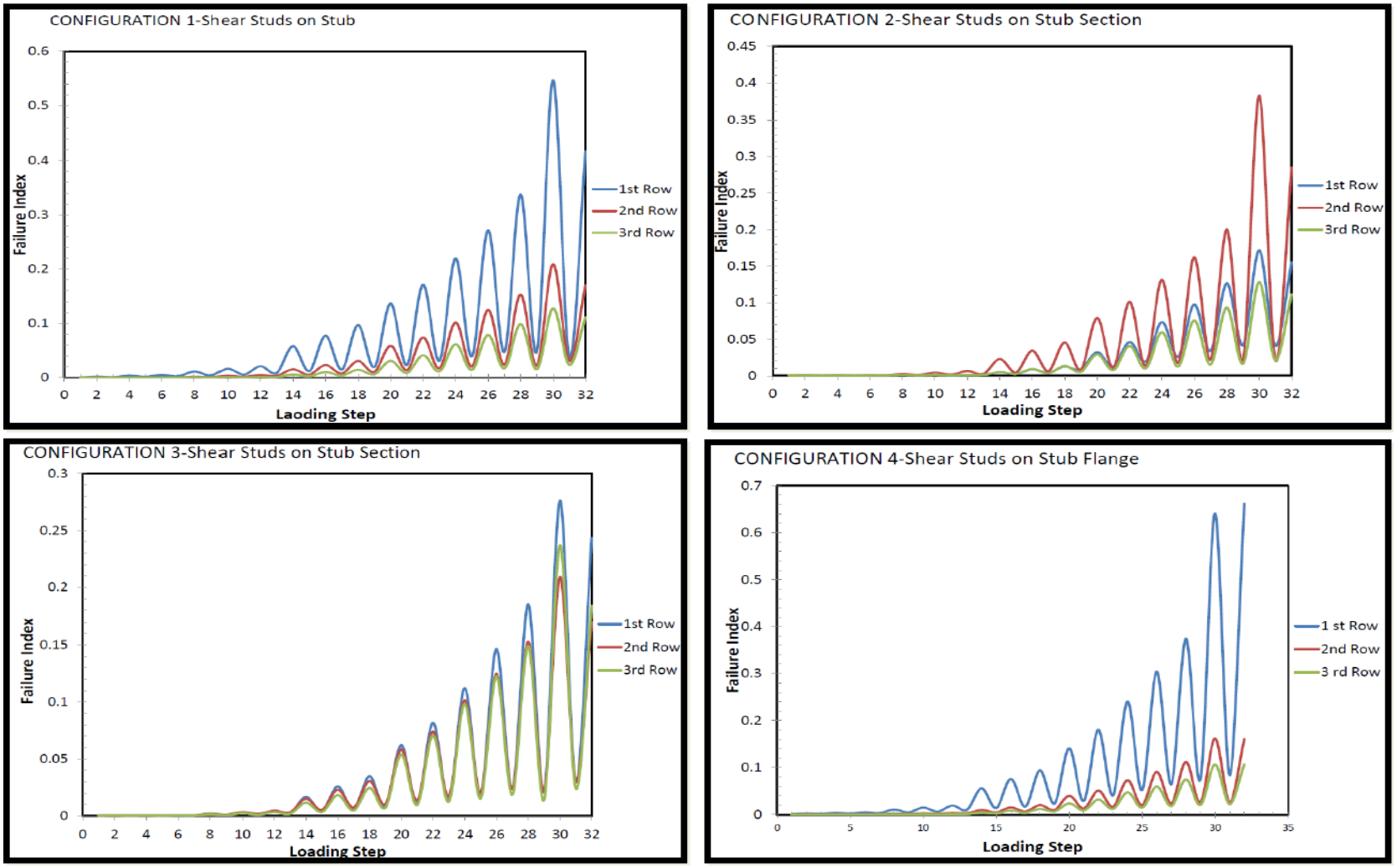

Figure 6-23: Calculated Failure Index for All Configurations (on Stub Section)

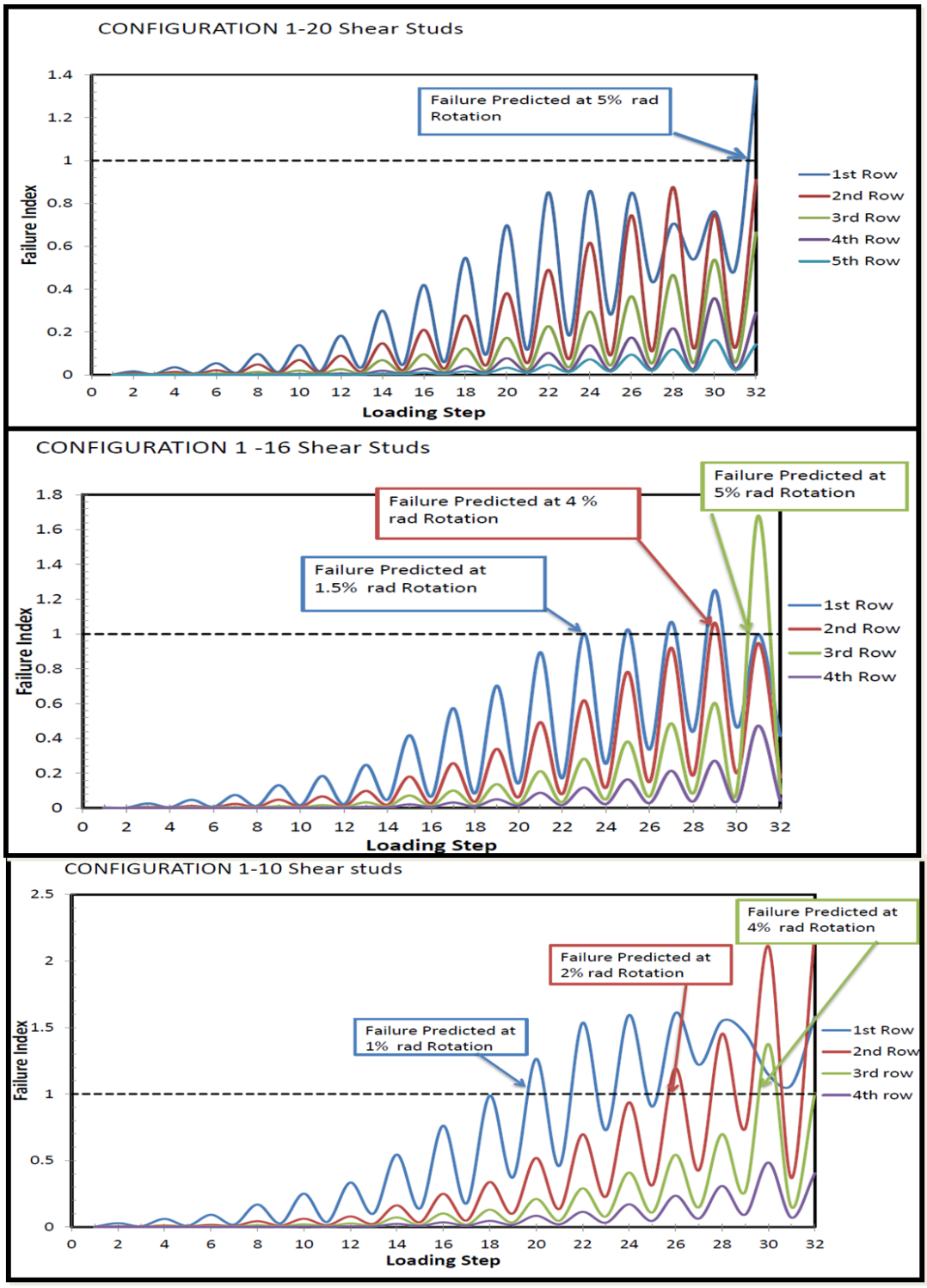

Figure 6-24: Failure Index for Configuration 1 with 80, 64, and 40 Shear Studs

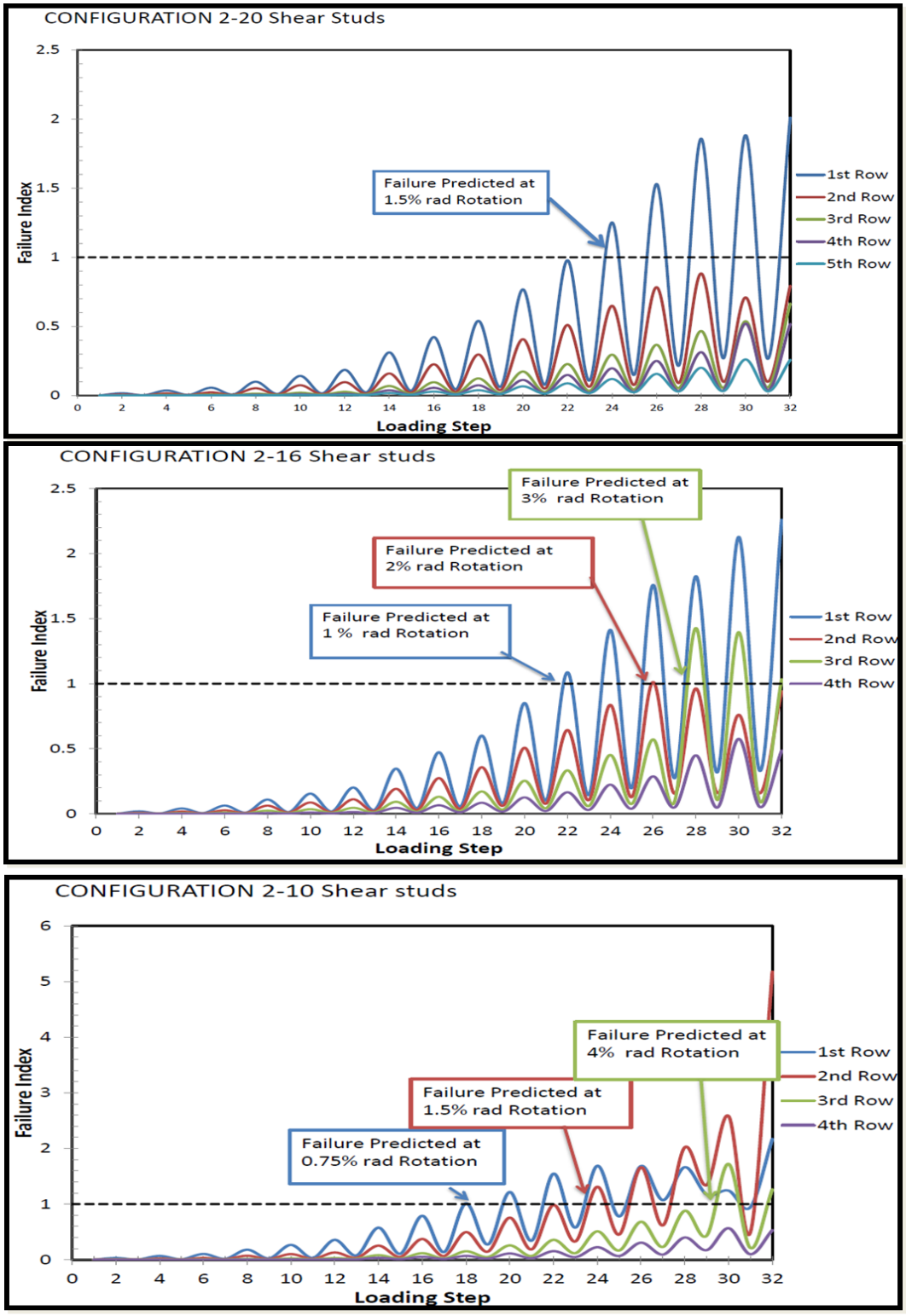

Figure 6-25: Failure Index for Configuration 1 with 80, 64, and 40 Shear Studs

It should be noted that investigation on the shear stud behavior based on the assumption that there is no friction between parts which constitute connection and grout material is elastic. If the grout plasticity is introduced into finite element models, behavior of the shear studs likely change. In the presence of friction, shear forces, which is transmitted to the shear studs, will decrease due to resistance caused by friction between beam, grout and stub section.

Based on the failure index results, it can be concluded that only configuration 1 can be adopted in high seismic regions. Since failure index results are less accurate under reversed cycles (Kavinde and Deierlein, 2004), higher failure index in a member can be suggestive of a high potential for ductile rupture. It is important to acknowledge that these results are limited because of the material model adopted for grout. Because of the absence of experimental data, the assumption made for grout is elastic.

6.8.Failure Prediction in the Critical Weld region

In order to determine failure in the critical weld region for W24x62 beam section, a finite element model was produced. In this model, the stub section was modeled with shell elements instead of solid elements in order to reduce computational effort. Details of modeling are discussed in Chapter 4. Failure predictions for increased thicknesses are shown in Figure 6.26.

Failure index plots were provided for the steel material because the stronger weld material pushed plastic deformation into the steel flanges. It can be seen that even for a thickness of 0.6 inches, the failure index is far from 1. Consequently, if the thickness of the stub flanges is equal to the thickness of the beam flanges, the inside height of the stub section

is 28.7 inches, to achieve the required section modulus. Because the failure index produces less accurate results when cyclic loading is applied (Kavinde and Deierlein, 2004), stub flange plate thickness could be taken as twice that of the beam flanges, to satisfy the required section modulus.

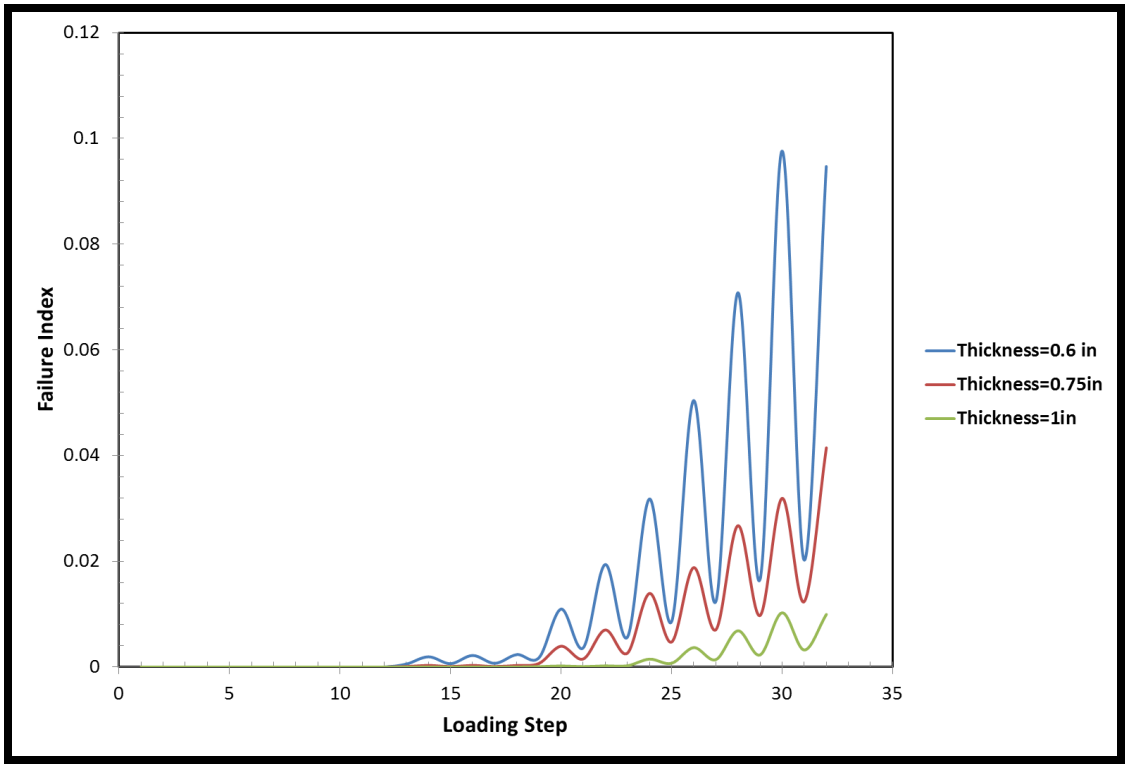

Figure 6-26: Failure Prediction in Welded Region with Increased Flange Thickness

6.9.Discussion of Behavior of Grout

Fulmer et al. (2012) showed that an elastic assumption for the grout material was reasonable because the high-stress region in the simulated grout demonstrated similarity to

experimental outcomes. Therefore, discussions are informed by their observations. Von Mises stress that developed in the grout for the W24x62 and W30x108 beam sections are presented in Figure 6.27 and Figure 6.28 at maximum force developed in the systems.

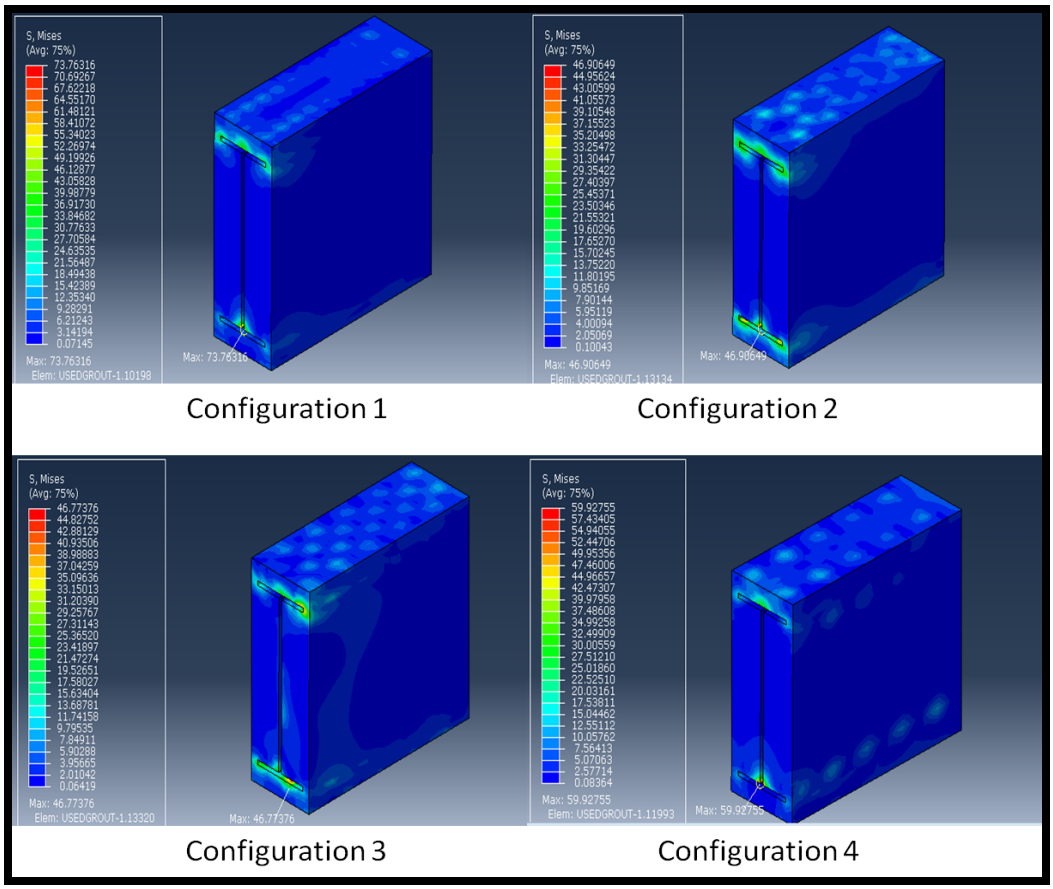

Figure 6-27: Von Mises Stress in Grout for Beam Section W24x62

It can be seen that the grout region is highly stressed where the plastic deformation of the beam penetrates into the grout. The compressive strength of the grout will increase due to confinement provided by stub section. Therefore, cracking of the grout would only be

expected in regions where confinement is comparatively less, that is, the end of the stub section where the plastic hinge penetrates the grout.

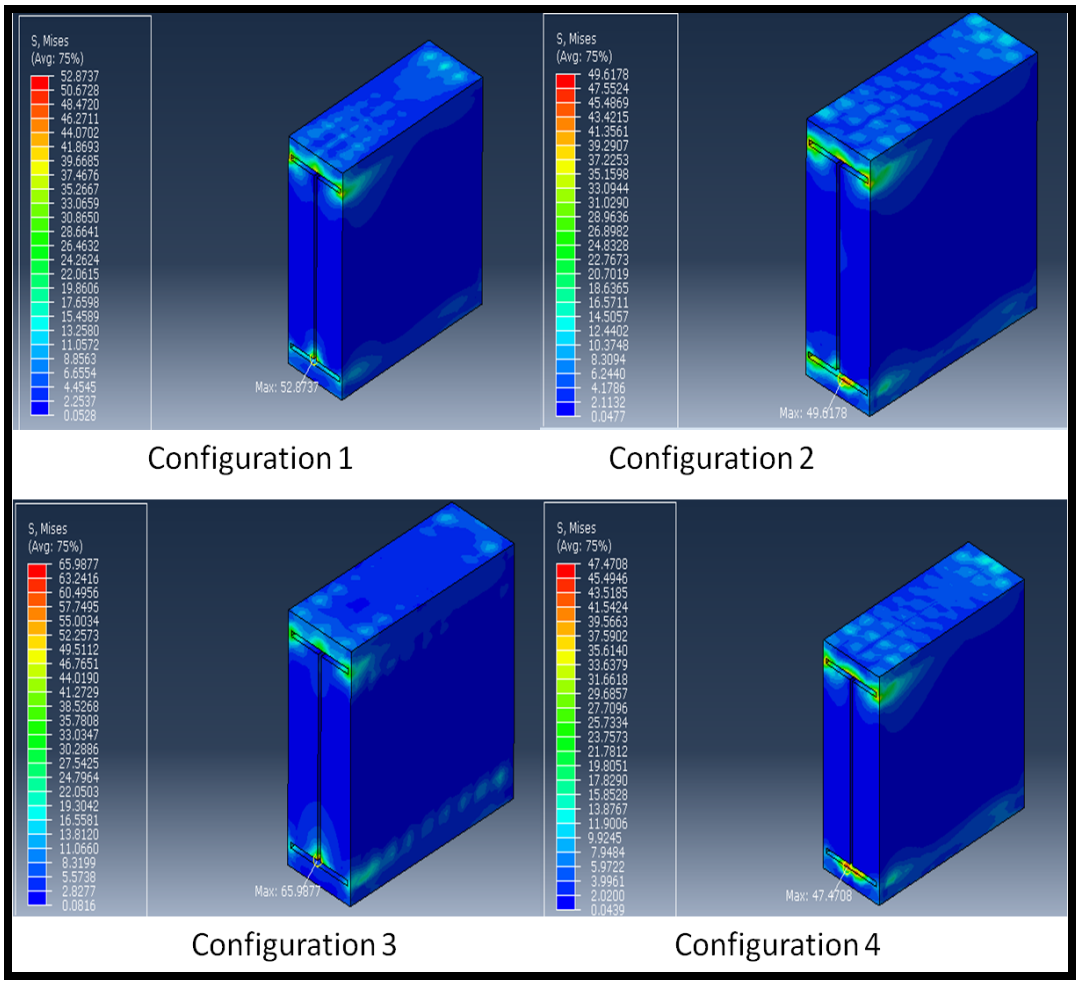

Figure 6-28: Von Mises Stress in Grout for Beam Section W30x108

CHAPTER 7

7. Conclusions, Recommendations and Future Work

7.1. Conclusions and Recommendations

Based on the results from the analyses performed, the following conclusions can be made:

- Increasing the thickness of the stub flange plate reduces the possibility of having fracture at the critical weld region. It is suggested that the stub plate thickness be approximately two times the thickness of the beam flange to satisfy the required elastic section modulus value.
- An increase in the stub section height also reduces the fracture tendency for all configurations that use the W24x62 beam section, except for configuration 4 with a stud flange plate thickness of 0.6 inches. It was observed that when the height of the stub section increased, the plastic deformation concentrated at the welded corner of the stub because the provided capacity of stub section was less than the moment demand at the column face. As a result, in order to provide adequate capacity, designers should consider the forces developed by the shear studs located on the side of the stub section.
- It is noted that when stiffener plates were employed in the design, the fracture tendency of the critical weld region also reduced. If the column size is chosen to avoid the use of stiffener plates, stiffener plates must be at least half of the stub flange plate thickness.
- Moment-rotation curves showed that grouted shear stud (GSS) beam to column connections accommodate more energy absorption than Pre-Northridge connections.

The rational for making the stub length equal to the beam height is reasonable since shorter stub lengths may reduce energy absorption and could cause difficulties for placing the required number of shear studs.

- Levels of dissipated energy showed that connections with different configurations absorb similar amounts of energy; however, the tendency for fracture differed from one to another. Regarding the failure index results for the W24x62 beam section, configurations with symmetrical distributions of shear studs were able to sustain more load than others. In addition, the results also showed that when the shear studs were located near the beam flange centerline, strength degradation occurred in the shear studs at an early step of the applied loading protocol; therefore, it is suggested that shear studs should not be located close to the beam flange centerline. The minimum distance between shear studs and beam centerline was not considered, and is a topic for further study.
- Failure index results also indicated a need for modifying the reasoning behind the process of determining the number of shear studs. Calculation of the required number of shear studs involves a new model capable of accounting for location of shear studs in the GSS connections.
- Failure index results of the critical weld region showed that for the W24x62 beam section, a stub flange thickness equal to that of the beam flange provides a satisfactory level of strength. Since failure index becomes less accurate when cyclic loading is applied (Kavinde and Deierlein, 2004), it is suggested that the stub flange thickness should be approximately twice that of the beam flange, for a safe design.

- It is expected that the grout will be highly stressed at the location of the plastic hinge. Cracking and spalling of a portion of the grout causes increased strain penetration into the grouted region. Although the grout is considered to be elastic, the results appear to be reasonable and consistent with the experimental observations of Fulmer (2012).

7.2.Future Work

Recommendations for further study of GSS beam to column connections are as follows:

- An experimental study should be conducted in order to better understand the behavior of the grout. In addition, a damage model for the grout material should be explored to better predict the behavior of GSS beam to column connections with finite element models.
- Effects of shear stud configurations should be further investigated using finite element models to better capture the geometric details of the studs.
- A model for determining the required shear studs number should be developed to account for location of studs.
- Detailed finite element models including various beam section sizes should be performed.
- In order to determine the stub section capacity, a model to better predict the required stub section should be developed. The model should include geometric limitation caused by construction of other components of steel structure.

- Span to depth ratio for GSS beam to column connections should be determined by detailed finite element analyses.
- Maximum and minimum reasonable lengths for the stub section should be determined as a result of finite element analyses using various beam sections.
- Finite element models for other viable moment resisting frame connections with grouted shear stud (GSS) should be examined.

REFERENCES

American Institute of Steel Construction (AISC). ANSI/AISC 341-10 (2010) *Seismic Provisions for Structural Steel Buildings*. Chicago,IL

American Institute of Steel Construction (AISC).ANSI.AISC 358-10 *Prequalified Connections for Special and Intermediate Steel Moment Frames for Seismic Applications*. Chicago, IL.

American Institute of Steel Construction (AISC). ANSI/AISC 360-10 *Spesifications for Structural Steel Buildings*. Chicago,IL.

American Institute of Steel Construction Manual 14th Edition (2011).Chicago, IL.

Abaqus/CAE User's Manual, (2013). Dassault Systèmes Simulia Corp., Providence, RI

Abaqus Analysis User's Manual (2013). Dassault Systèmes Simulia Corp., Providence, RI.

Bruneau, M., Uang, C.M., and Sabelli,R. (2011) *Ductile Design of Steel Structures*, McGraw Hill, NY.

Chen , S-J.,Yeh,C.H. and Chu,J.M. (1996)"Ductile Steel Beam-to-Column Connections for Seismic Resistance" *Journal of Structural Engineering*, 122(11),1292-1299

Chen,C.C. and Lin, C.C. (2013) " Seismic performance of Steel beam-to-column moment connections with tapered beam flanges*" Engineering Structures*, 48, 588-601

Chi, W.M., Kanvinde, A.M. and Deierlein, G.G. (2006) "Prediction of Ductile Fracture in Steel Connections Using SMCS Criterion" *Journal of Structural Engineering*, 132(2), 171-181

Cook,R.D., Malkus, D.S., Plesha, M.E. and Witt,R.J. (2002) *Concepts and Application of Finite Element Analysis*, John Wiley&Sons,Inc., NJ.

Deylami, A. and Ashraf, R. (2004) "Moment Resisting Connection with Side plate (Geometric Aspetcs)" *Proceedings of the 13th World Conference on Earthquake Engineering*, B.C., Canada ,Paper no. 194

El-Tawil, S., Mikesell,T.D., Vidarsson, E., and Kunnath,S.K. (1998) " Strenght and ductility of FR welded-bolted connections" *Rep. No. SAC/BD/98/01*, Applied Technology Council, Redwood City, California. http://quirver.eerc.berkeley.edu:8080/library/backdoc.

El-Twail, S., Mikesell, T. D. and Kunnath, S.K. (2000) " Effect of Local Details and Yield Ratio on Behavior of FR Steel Connections" *Journal of Structural Engineering*, 126(1),79-87

Engelhardt , M.D. and Sabol,T.A. (1998) " Reinforcing of Steel Moment Connections with Cover Plates: Benefits and Limitations" *Engineering Structures*, 20(4-6), 510-520

Fell, B.V., Myers A.T., Deierlein, G.G. and Kavinde, A. M. (2006) "Testing and Simulation of Ultra-Low Cycle Fatigue and Fracture in Steel Braces" *Proceedings of the 8th Us National Conference on Earthquake Engineering*, Paper no.587

Fulmer, S.J., Kowalsky, M.J., Nau, J.M. and Hassan, T. (2010) "Ductility of Welded Steel Pile to Steel Cap Beam Connections. *ASCE/SEI Structures Congress*, 1, 216-227

Fulmer, S.J., Kowalsky, M.J. and Nau, J.M. (2012) "Seismic Performance of Steel Bridge Piers Containing Composite Connections" *Proceedings of the 15th World Conference on Earthquake Engineering*¸ Lisbon, Portugal

Gholami, M. , Deylami, A. and Tehranizadeh, M. (2013) " Seismic Performance of Flange Plate Connections Between Steel Beams and Box Columns" *Journal of Constructional Steel Research* , 84,36-48

Grauvilardell, J.E., Lee, D., Hajjar , J.F. and Dexter, R.J. (2005) " Synthesis of Design, Testing and Analysis research on Steel Column Base Plate Connections in High-Seismic Zone" *Structural Engineering Report no.ST-04-02.http://www.ce.umn.edu*. Minneapolis, MN.

Hancock, J.W., and Mackenzie, A.C. (1976) "On the Mechanisms of Ductile Failure in High-Strength Steels Subjected to Multi-Axial Stress-Strain" *Journal of Mechanics and Physics of Solids*, 24,147-169

Houghton, D.L. (1998) "The Sideplate Moment Connection: A Design Breakthrough Eliminating Recognized Vulnerabilities in Steel Moment Frame Connections." *Proceedings of the 2nd World Conference on Steel Construction*, San Sebastian, Spain.

Hu, J.W. (2008) "Seismic Performance Evaluations and Analyses for Composite Moment Frames with Smart SMA Pr-CFT Connections" *Phd Dissertation*, Georgia Institute of Technology, Atlanta, Georgia.

Kanvinde, A., and Deierlein, G.G. (2004). "Micromechanical simulation of earthquake induced fractures in steel structures." *Blume Center TR145, http://blume.stanford.edu* Stanford Univ., Stanford, Calif.

Kavinde, A.M., and Deierlein, G.G. (2006) "Void Growth Model and Stress Modified Critical Strain Model to Predict Ductile Fracture in Structural Steels" *Journal of Structural Engineering*, 132(12), 1907-1918

Lindner, J. (2008) " Old and New Solutions for Contact Splices in Columns" *Journal of Constructional Steel Research*, 64, 833-844

Mahin, S.A. (1998) "Lessons from damage to steel buildings during the Northridge earthquake" *Engineering Structures*, 20(4-6), 261-270

Pertold, J., Xiao, R.Y. and Wald F. (200) " Embedded Steel Column Bases 1.Eperiments and Numerical Simulation" *Journal of Constructional Steel Research*,56,253-270.

Prinz, G.S. and Richards, P.W. (2007) "Non-linear Time History Analysis of Refined Mesh Steel Structures" *Proceeding of the 9th Canadian Conference on Earthquake Engineering*, Paper. 1365

Prinz, G.S. and Richards, P.W. (2009) "Eccentrically Braced Frame Links with Reduced Web Sections" *Journal of Constructional Steel Research*, 65, 1971-1978

Ricles, J. M., Mao, C., Lu, L.-W. and Fisher, J. W. (2000). "Development and Evaluation of Improved Details for Ductile Welded Unreinforced Flange Connections," *Report No. SAC/BD-00/24, SAC Joint Venture*, Sacramento, California

Sap2000 V14. Computer and Structures (2014). www.csiberkeley.com/products_SAP.html

Sherbourne, A.N., and Bahaari, M.R. (1994) "3D Simulation of End-Plate- Bolted Connections" *Journal of Structural Engineering*, 120, 3122-3136

Simão, P.D., Coelho, A.M.G.,and Bijlaard, F.S.K. (2012) "Influence of Splices on the Buckling of columns" *International Journal of Non-Linear Mechanics* ,47,806-822

Tao, W., Zhan, W. and Junqi, W. (2013) " Experimental Study and Finite Element Analysis of Hysteretic Behavior of End-plate Connection Semi-Rigid Space Steel Frames" *The Open Civil Engineering Journal*,7,68-76

APPENDICES

Appendix A

Table A-1: Tip Displacement for Beam Section W24x62 and W30x108

Beam W24x62		
Loading Step	Drift Angle(%)	Tip Displacement (in)
1	0.375	0.533
2	0.375	-0.533
3	0.375	0.533
4	0.375	-0.533
5	0.375	0.533
6	0.375	-0.533
7	0.5	0.711
8	0.5	-0.711
9	0.5	0.711
10	0.5	-0.711
11	0.5	0.711
12	0.5	-0.711
13	0.75	1.0665
14	0.75	-1.0665
15	0.75	1.0665
16	0.75	-1.0665
17	0.75	1.0665
18	0.75	-1.0665
19	1	1.422
20	1	-1.422
21	1	1.422
22	1	-1.422
23	1.5	2.133
24	1.5	-2.133
25	2	2.844
26	2	-2.844
27	3	4.266
28	3	-4.266
29	4	5.688
30	4	-5.688
31	5	7.11
32	5	-7.11

Beam W30x108		
Loading Step	Drift Angle(%)	Tip Displacement (in)
1	0.375	0.536
2	0.375	-0.536
3	0.375	0.536
4	0.375	-0.536
5	0.375	0.536
6	0.375	-0.536
7	0.5	0.715
8	0.5	-0.715
9	0.5	0.715
10	0.5	-0.715
11	0.5	0.715
12	0.5	-0.715
13	0.75	1.072
14	0.75	-1.072
15	0.75	1.072
16	0.75	-1.072
17	0.75	1.072
18	0.75	-1.072
19	1	1.430
20	1	-1.430
21	1	1.430
22	1	-1.430
23	1.5	2.144
24	1.5	-2.144
25	2	2.859
26	2	-2.859
27	3	4.289
28	3	-4.289
29	4	5.718
30	4	-5.718
31	5	7.148
32	5	-7.148

Appendix B

B.1 Determination of Stub section and Shear Stud Number for Beam Section W24x62

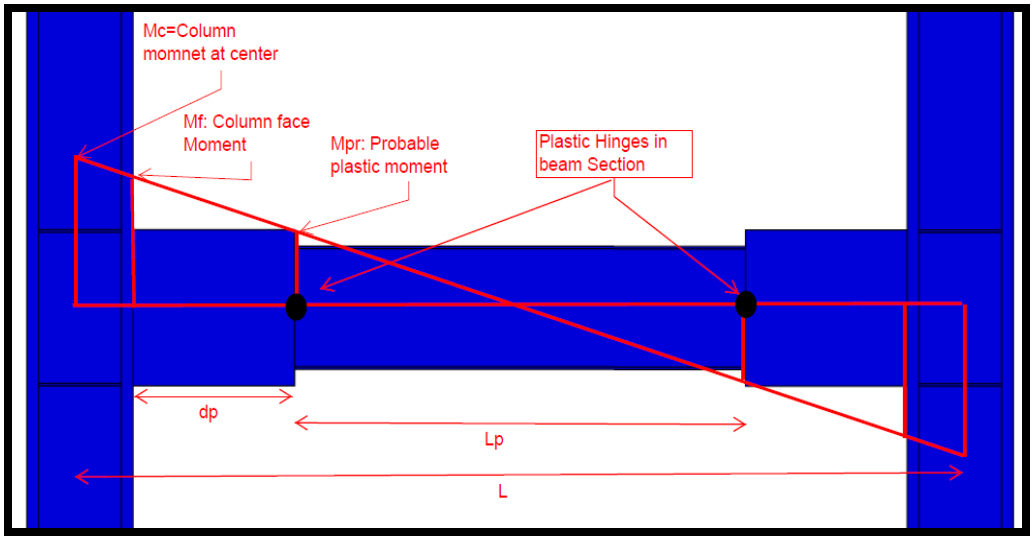

Figure B-1: Moment Demand Distribution Based on Plastic Hinge Formation

Compactness Check:

$$For Beam Web: h/tw < 3.76\sqrt{(E/F_y)} = 50.32 < 90.55, Compact(AISC306-2010)$$

$$For Beam Flange: b_f/(2t_f) < 0.38\sqrt{(E/F_y)} = 5.97 < 14.83, Compact(AISC306-2010)$$

Design Process:

$$Cpr = {Fy+Fu}/{2Fy} = Cpr = {50+65}/{2*50} = 1.15 \le 1.2 \quad , \text{ say } 1.2$$

$$Mpr = CprRyFyZx = 1.2*1.1*50*153 = 10098 \text{ in} - \text{kip} = 841.5 \text{ ft} - \text{kip}$$

$$Mf = Mpr + Vpr.dp = 10098 + 93.33*25 = 12431.36 \text{in} - \text{kip} = 1035.95 \text{ft} - \text{kip}$$

$$Vpr = 2Mpr / Lp = 2*10098 / 218 = 93.33 \text{ kips}$$

$$Sx \geq \frac{Mf}{Fy} = 12431.36 / 50 = 248.63 \text{ in3, required section modulus for stub.}$$

Stub section properties:

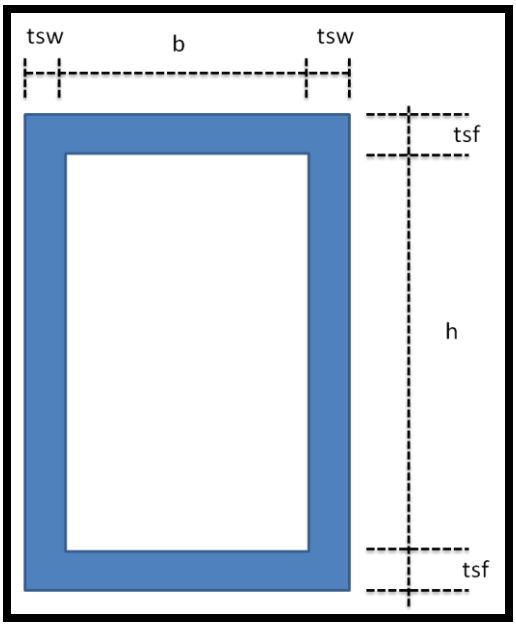

Figure B-2: Stub Section Geometry for Beam Section W24x62

t_{sf}=0.6 in (taken equal to around beam flange thickness)

t_{sw}= 0.5 in (taken equal to around beam web thickness)

b= 9 in (0.5 in distance left between beam flanges and stub side plates)

h=28.7 in (Due to height of shear studs. Shear stud height=2.5 in)

Section Modulus calculated based on given dimension >>> S_x= 304 in3> 248.63 in3, OK.

Required Shear Stud number:

$$Q_n = 0.5 * A_{sc} * \sqrt{f_c^{'} * E_c} \le A_{sc} * F_u = 0.5 * 0.442 * \sqrt{6 * 4276} \le 0.442 * 65$$

=35.38 ksi>28.72 ksi, $Q_n = 28.72\ ksi$

$$N_{sc} = \frac{\left(\frac{Mf}{db - tf}\right)}{Qn} \ge \frac{\left(\frac{Mpr}{db - tf}\right)}{Qn} = \frac{\left(\frac{12431.36}{28.7 - 0.59}\right)}{28.72} = 19 \ge \frac{\left(\frac{10098}{28.7 - 0.59}\right)}{28.72} = 16$$ (Say 20 shear stud on one beam flange face)

Total number of shear studs is 80. 40 shear studs on beam section and 40 shear studs on stub section are located to satisfy equilibrium.

Determination of Column size:

Column size is chosen to eliminate need for stiffener plates. Tension/Compression force generated by plastic moment of beam is 436.95 kips.

Column size: W14x257

Checks AISC (360-2010):

Web Local Yielding:

$$\varnothing R_n = \varnothing F_y t_w \left(5k + b_f\right) = 1 * 50 * 1.18 * \left(5 * 2.49 + 16\right) = 1678\, kips > 436.95\, kips$$, Ok.

Flange Bending:

$$\varnothing R_n = \varnothing 6.25 F_y t_f^2 = 0.9 * 6.25 * 50 * 1.89^2 = 1004\, kips > 436.95 kips$$, Ok

Panel zone Shear: (Pr<0.4Pc):

$$\varnothing R_n = \varnothing 0.6 F_y t_{wc} d_c = 0.9 * 0.6 * 50 * 164 * 1.18 = 522.5 kips > 436.95 kips$$, Ok (No Stiffener Plates Required)

Details for Beam Section W24x62

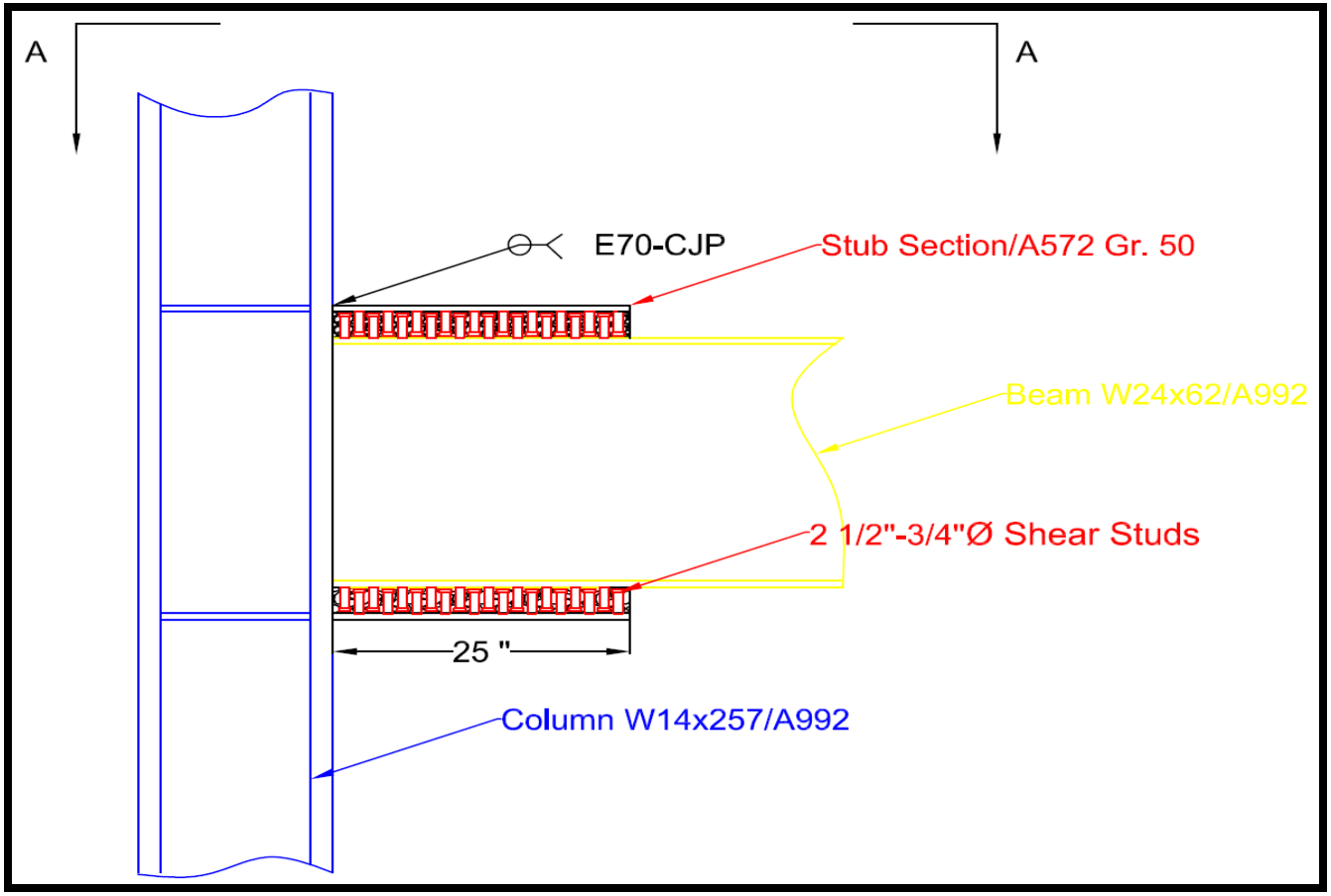

Figure B-3: Details of GSS Connection for Beam Section W24x62

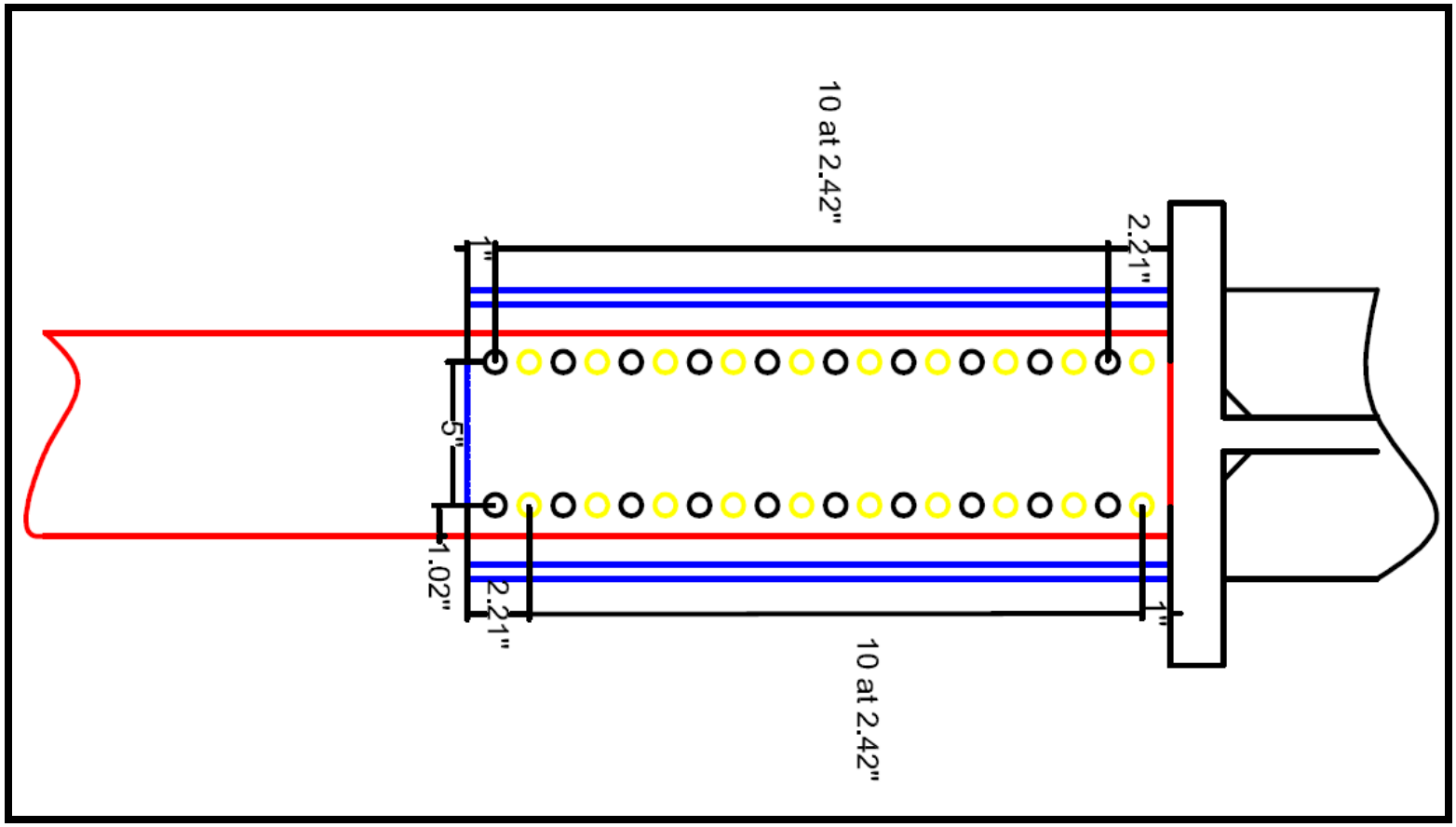

Figure B-4: Details of Configuration 1 for Beam Section W24x62 (A-A Plan view)

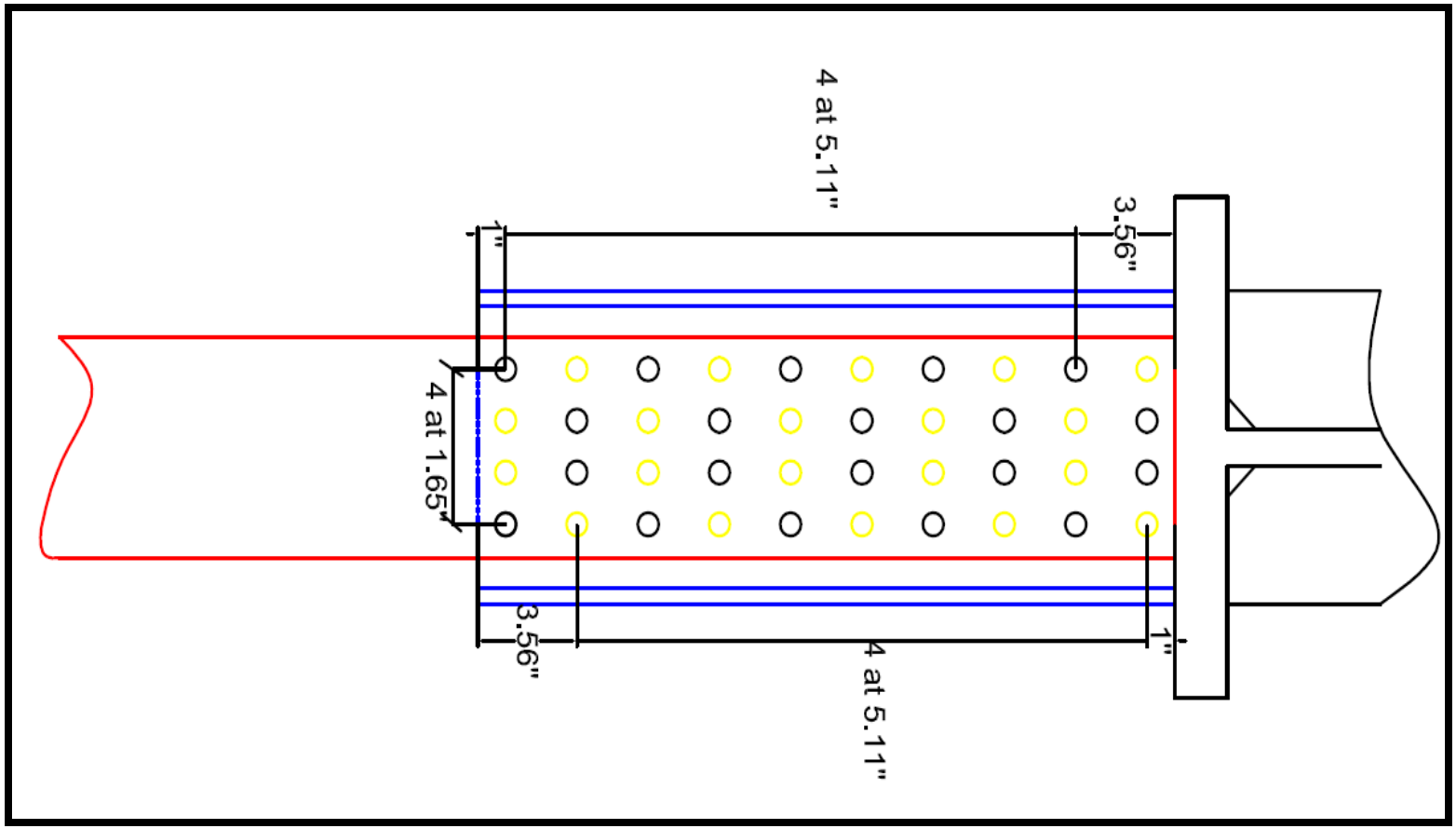

Figure B-5: Details of Configuration 2 for Beam Section W24x62 (A-A Plan view)

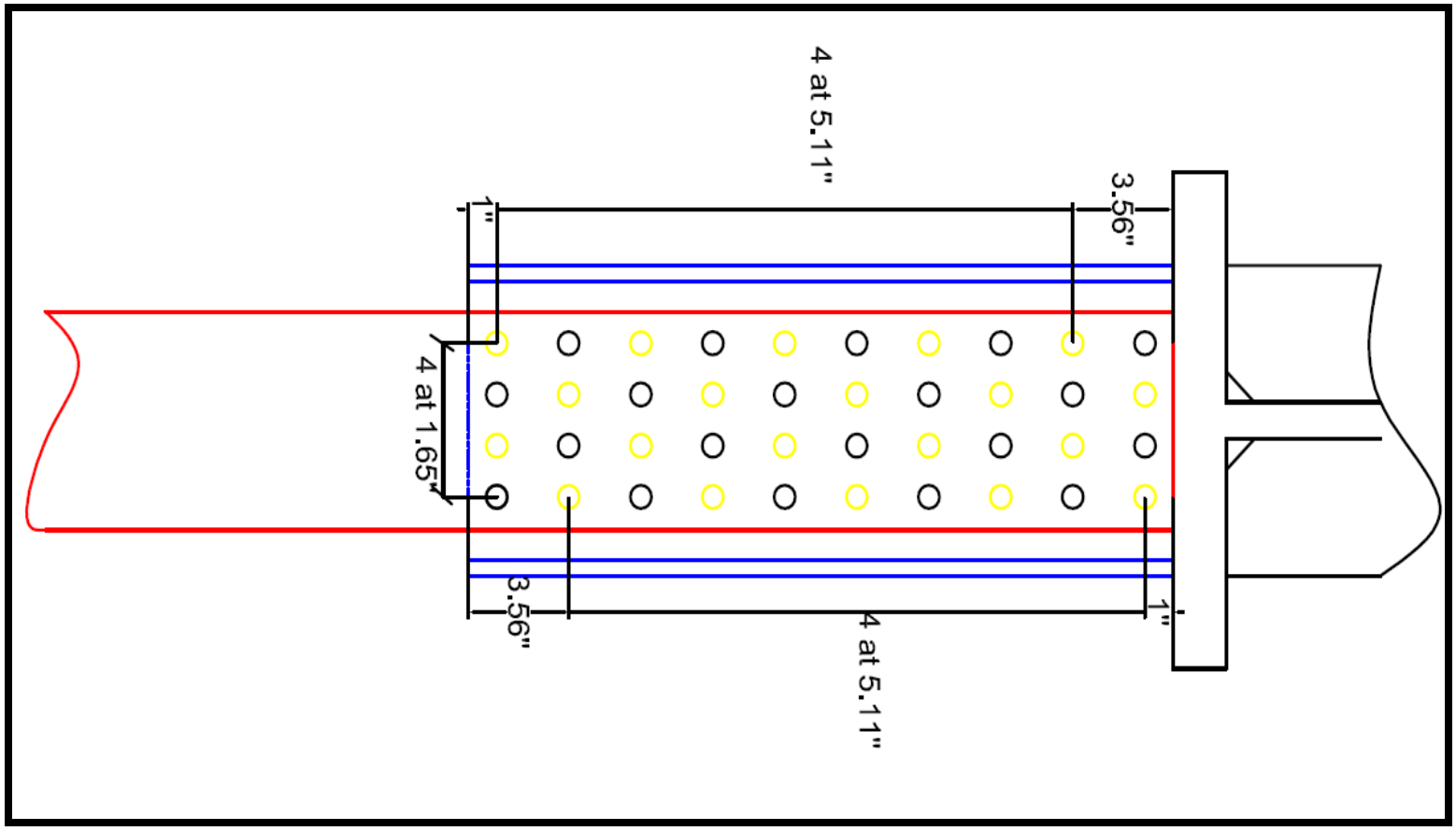

Figure B-6: Details of Configuration 3 for Beam Section W24x62 (A-A Plan view)

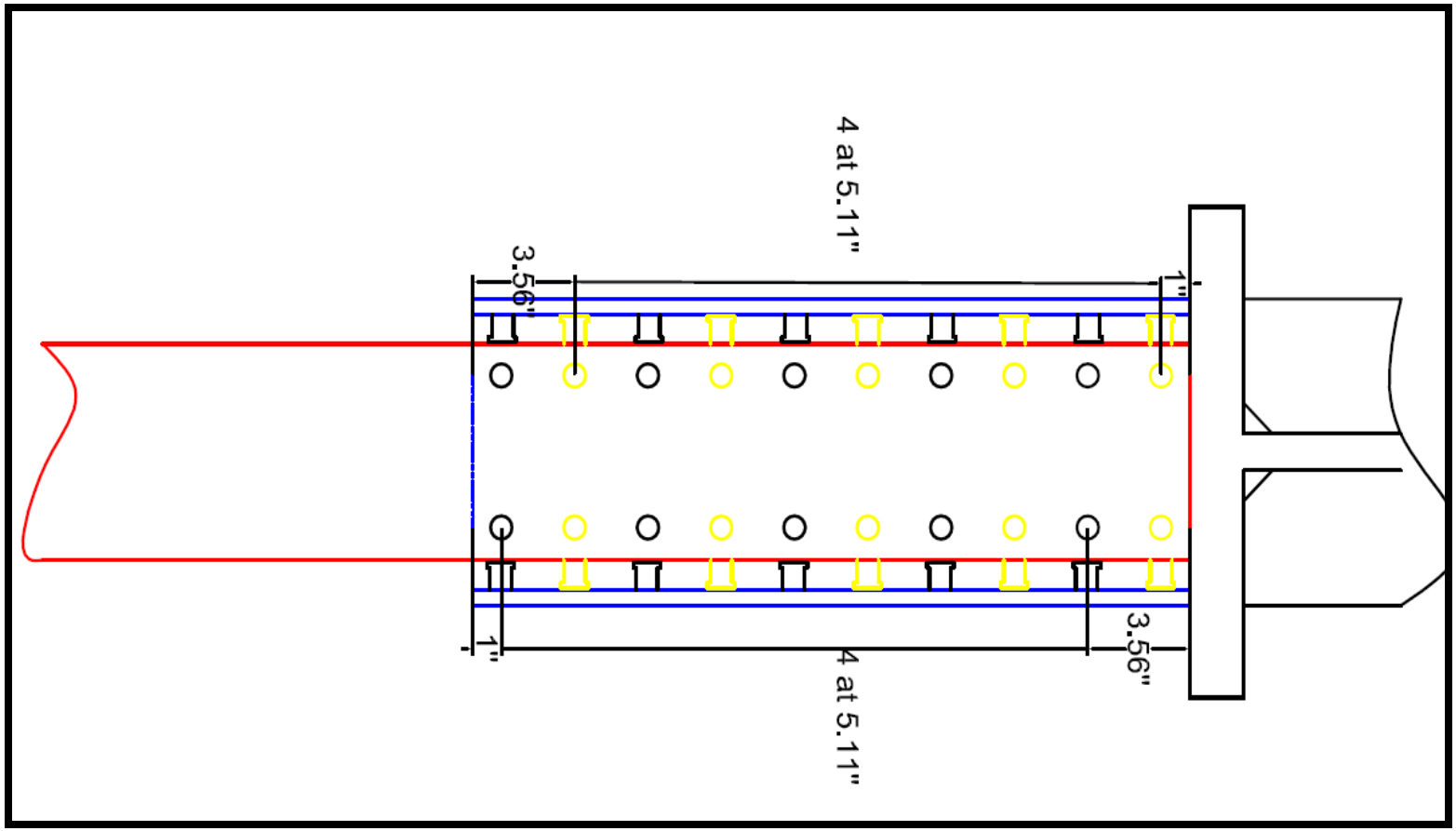

Figure B-7: Details of Configuration 4 for Beam Section W24x62 (A-A Plan view)

B.2 Determination of Stub section and Shear Stud Number for Beam Section W30x108

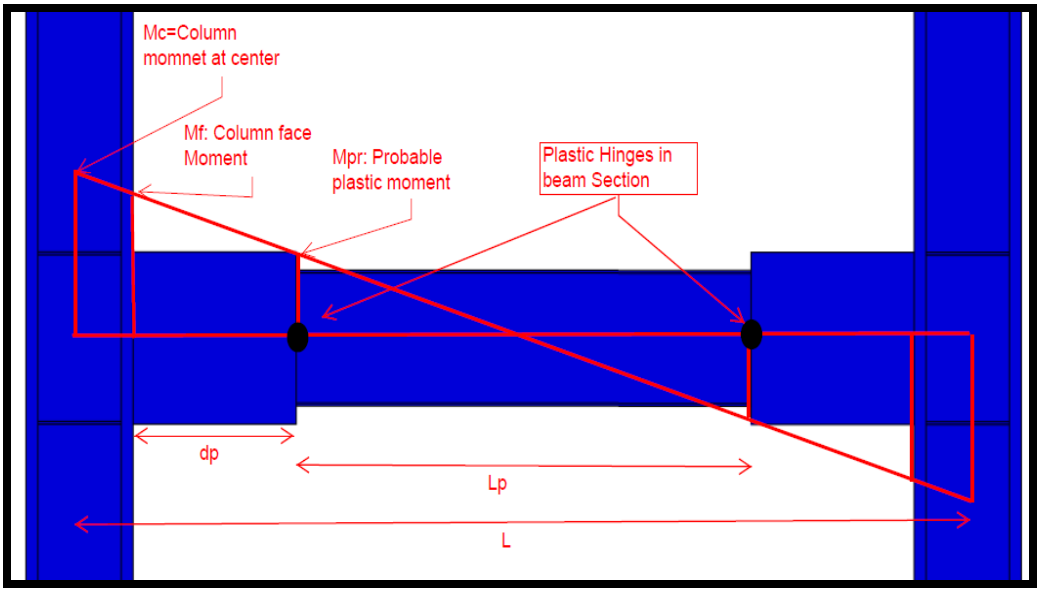

Figure B-8: Moment Demand Distribution Based on Plastic Hinge Formation

Compactness Check:

$$For Beam Flange: b_f/(2t_f) < 0.38\sqrt{(E/F_y)} = 6.91 < 14.83, Compact(AISC360-10)$$

$$For Beam Web: h/tw < 3.76\sqrt{(E/F_y)} = 51.89 < 90.55, Compact(AISC360-10)$$

Design Process:

$$Cpr = {Fy+Fu}/{2Fy} = Cpr = {50+65}/{2*50} = 1.15 \le 1.2 \quad , \text{ say } 1.2$$

$$Mpr = CprRyFyZx = 1.2*1.1*50*346 = 22836 \text{ in} - \text{kip} = 1903 \text{ ft} - \text{kip}$$

$$Mf = Mpr + Vpr.dp = 22836 + 220.78*30 = 29459.49 \text{in} - \text{kip} = 2454.96 \text{ ft} - \text{kip}$$

$Vpr = 2Mpr / Lp = 2*22836/218 = 220.78$ kips

$Sx \geq \frac{Mf}{Fy} =$ 29459.49 / 50 = 589 in3, required section modulus for stub.

Stub section properties:

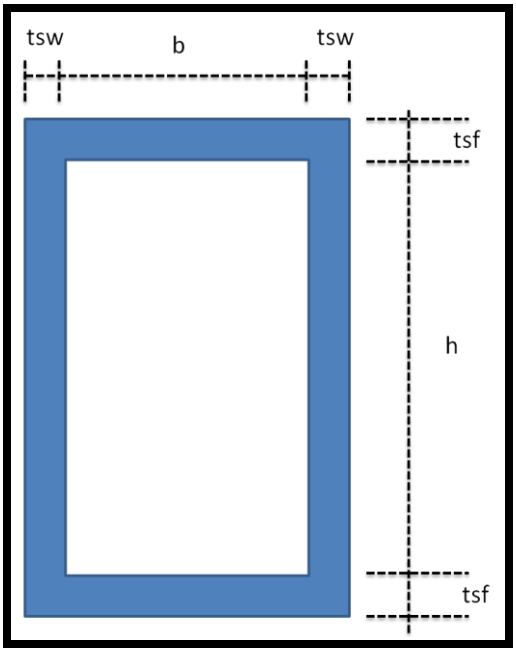

Figure B-9: Stub Section Geometry for Beam Section W30x108

t_{sf}=0.8 in (taken equal to around beam flange thickness)

t_{sw}= 0.8 in (taken equal to around beam web thickness)

b= 12 in (0.5 in distance left between beam flanges and stub side plates)

h=35 in (Due to height of shear studs. Shear stud height=2.5 in)

Section Modulus calculated based on given dimension is >>> S_x= 604 in3> 589 in3, OK.

Required Shear Stud number:

$$Q_n = 0.5 * A_{sc} * \sqrt{f_c^{'} * E_c} \le A_{sc} * F_u = 0.5 * 0.442 * \sqrt{6 * 4276} \le 0.442 * 65$$

=35.38 ksi>28.72 ksi, $Q_n = 28.72\ ksi$

$$N_{sc} = \frac{\left(\frac{Mf}{db-tf}\right)}{Qn} \ge \frac{\left(\frac{Mpr}{db-tf}\right)}{Qn} = \frac{\left(\frac{29459.49}{29.8-0.76}\right)}{28.72} = 36 \ge \frac{\left(\frac{22836}{29.8-0.76}\right)}{28.72} = 28$$ (Say36 shear stud on one beam flange face)

Total number of shear studs is 144.72 shear studs on beam section and 72 shear studs on stub section are located to satisfy equilibrium.

Determination of Column size:

Column size is chosen to eliminate need for stiffener plates. Tension/Compression force generated by plastic moment of beam is 786.36 kips.

Column size: W14x370

Checks AISC (360-2010):

Web Local Yielding:

$$\varnothing R_n = \varnothing F_y t_w \left(5k + b_f\right) = 1 * 50 * 1.66 * \left(5 * 3.26 + 17.9\right) = 2838\,kips > 786.36\,kips$$, Ok.

Flange Bending:

$$\varnothing R_n = \varnothing 6.25 F_y t_f^2 = 0.9 * 6.25 * 50 * 2.66^2 = 1990\,kips > 786.36\,kips$$, Ok

Panel zone Shear: (Pr<0.4Pc):

$$\varnothing R_n = \varnothing 0.6 F_y t_{wc} d_c = 0.9 * 0.6 * 50 * 164 * 1.18 = 522.5 kips > 436.95 kips$$, Ok(No Stiffener Plates Required)

Details for Beam Section W30x108

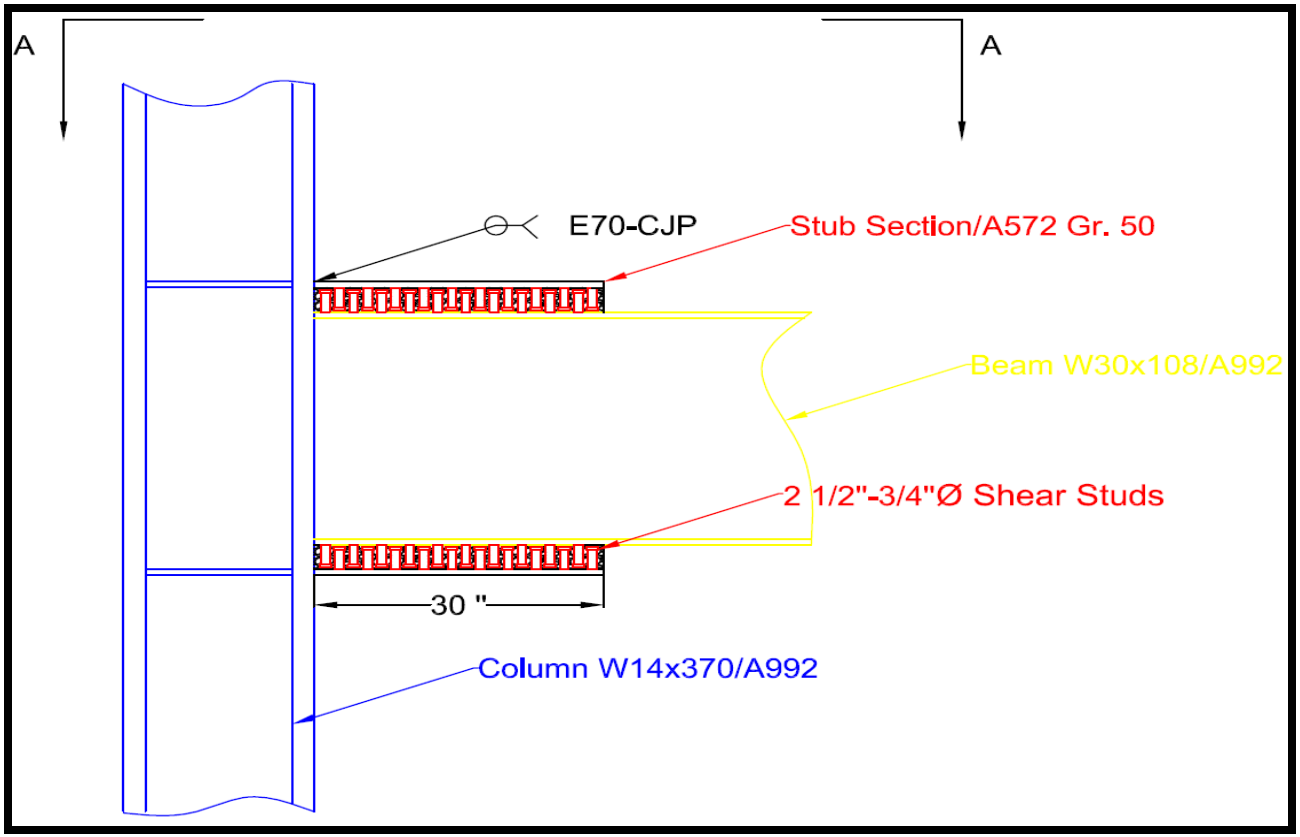

Figure B-10: Details of GSS Connection for Beam Section W30x108

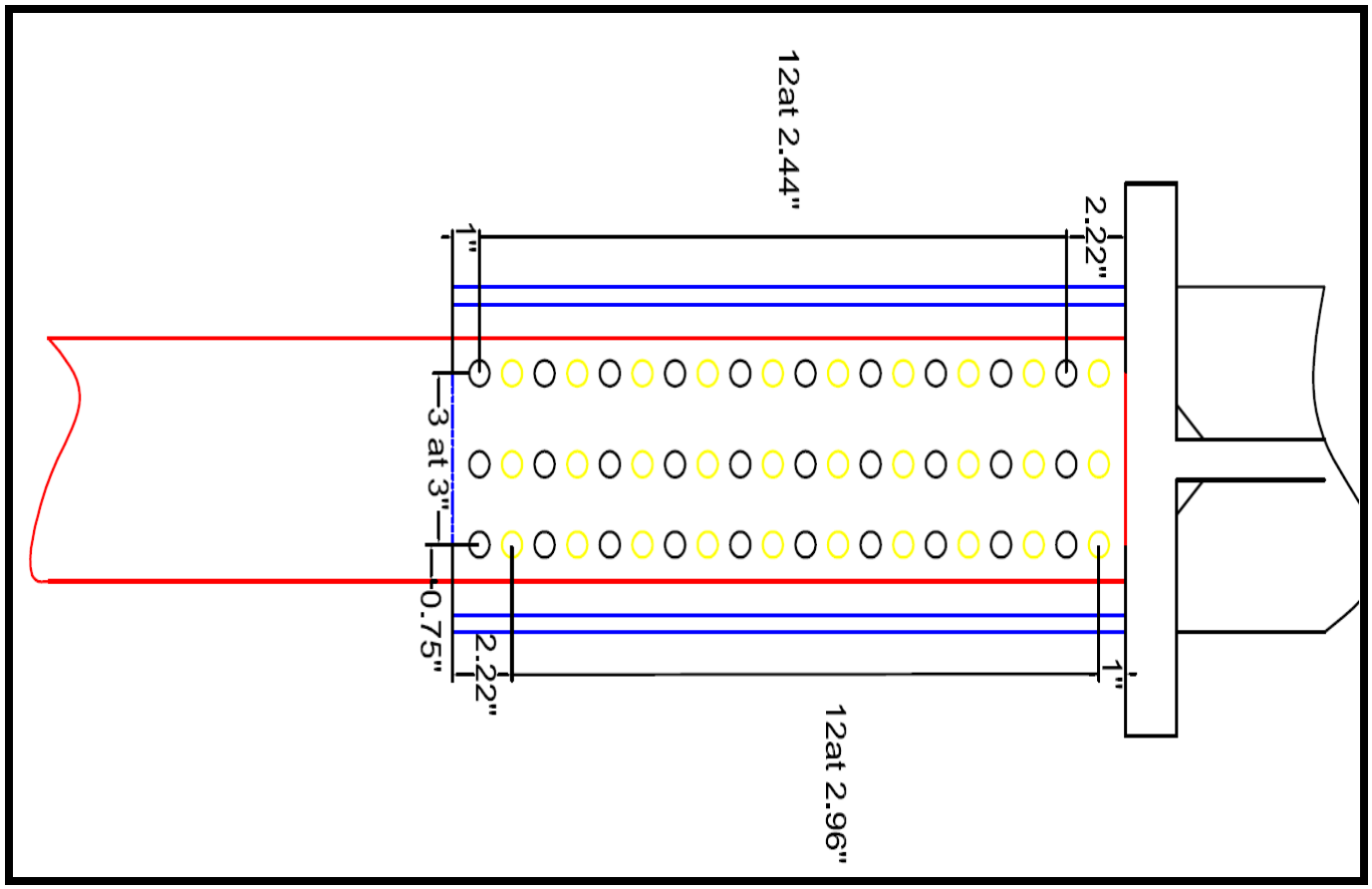

Figure B-11: Details of Configuration 1 for Beam Section W30x108 (A-A Plan view)

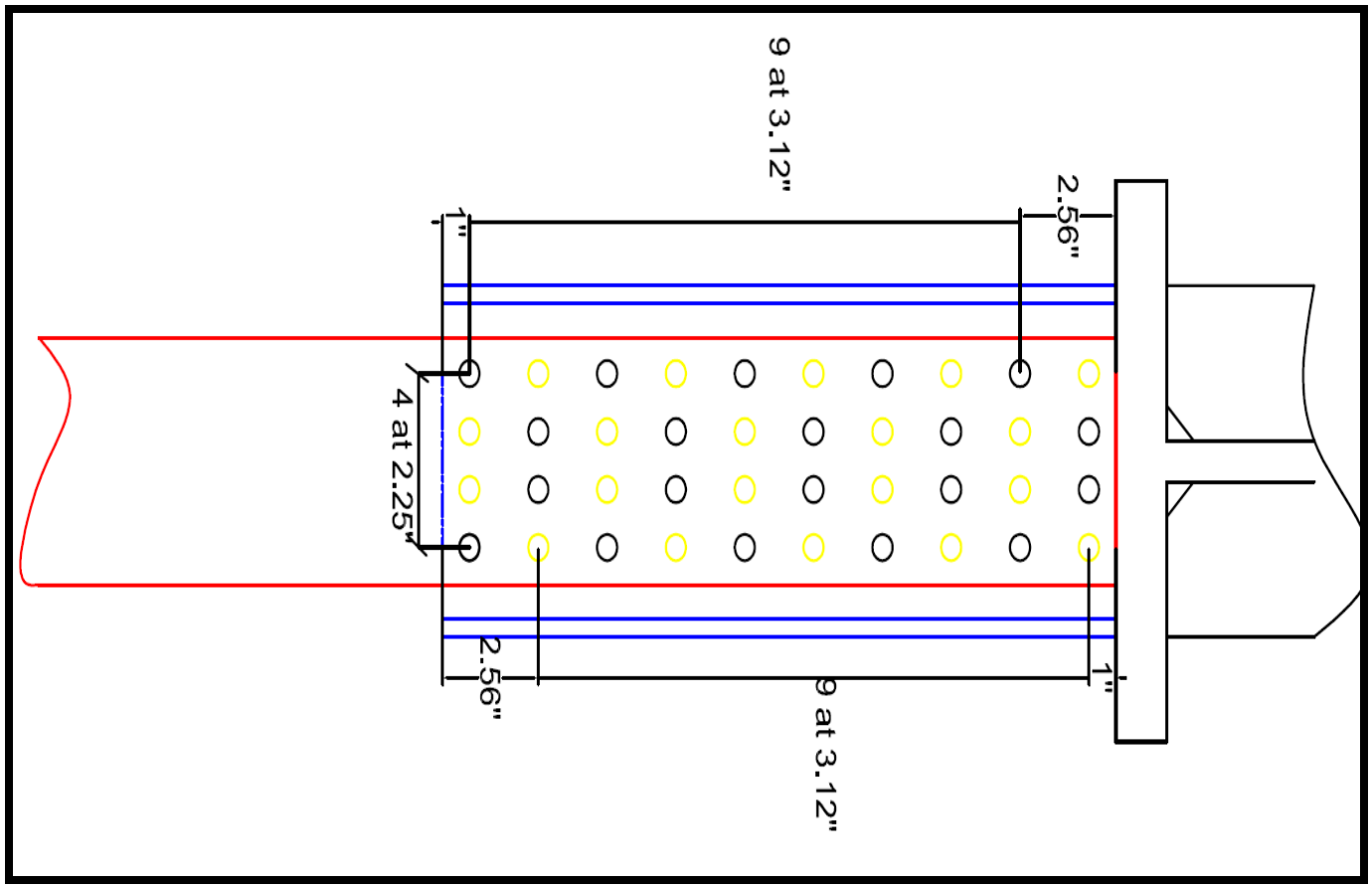

Figure B-12: Details of Configuration 2 for Beam Section W30x108 (A-A Plan view)

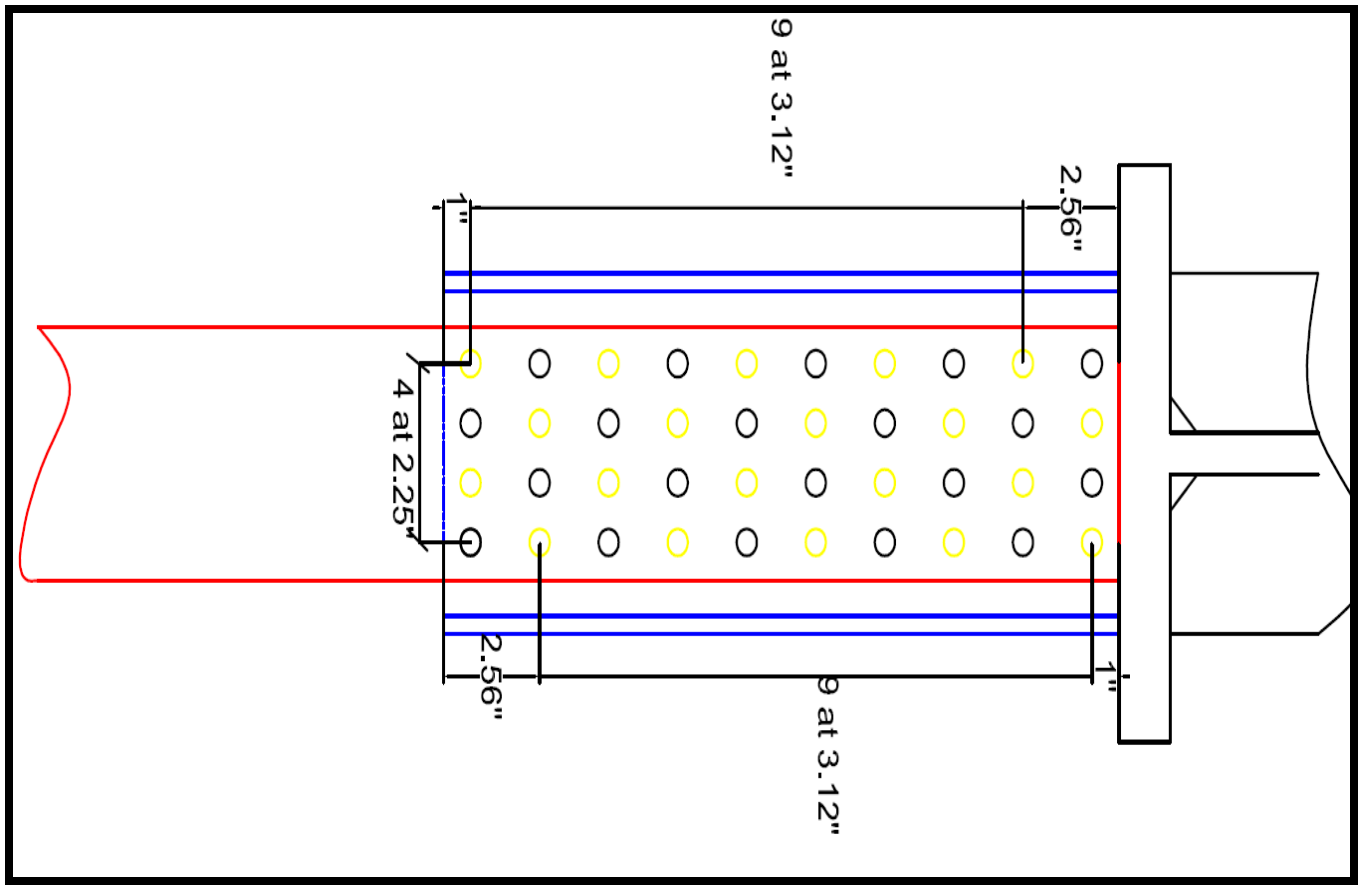

Figure B-13: Details of Configuration 3 for Beam Section W30x108 (A-A Plan view)

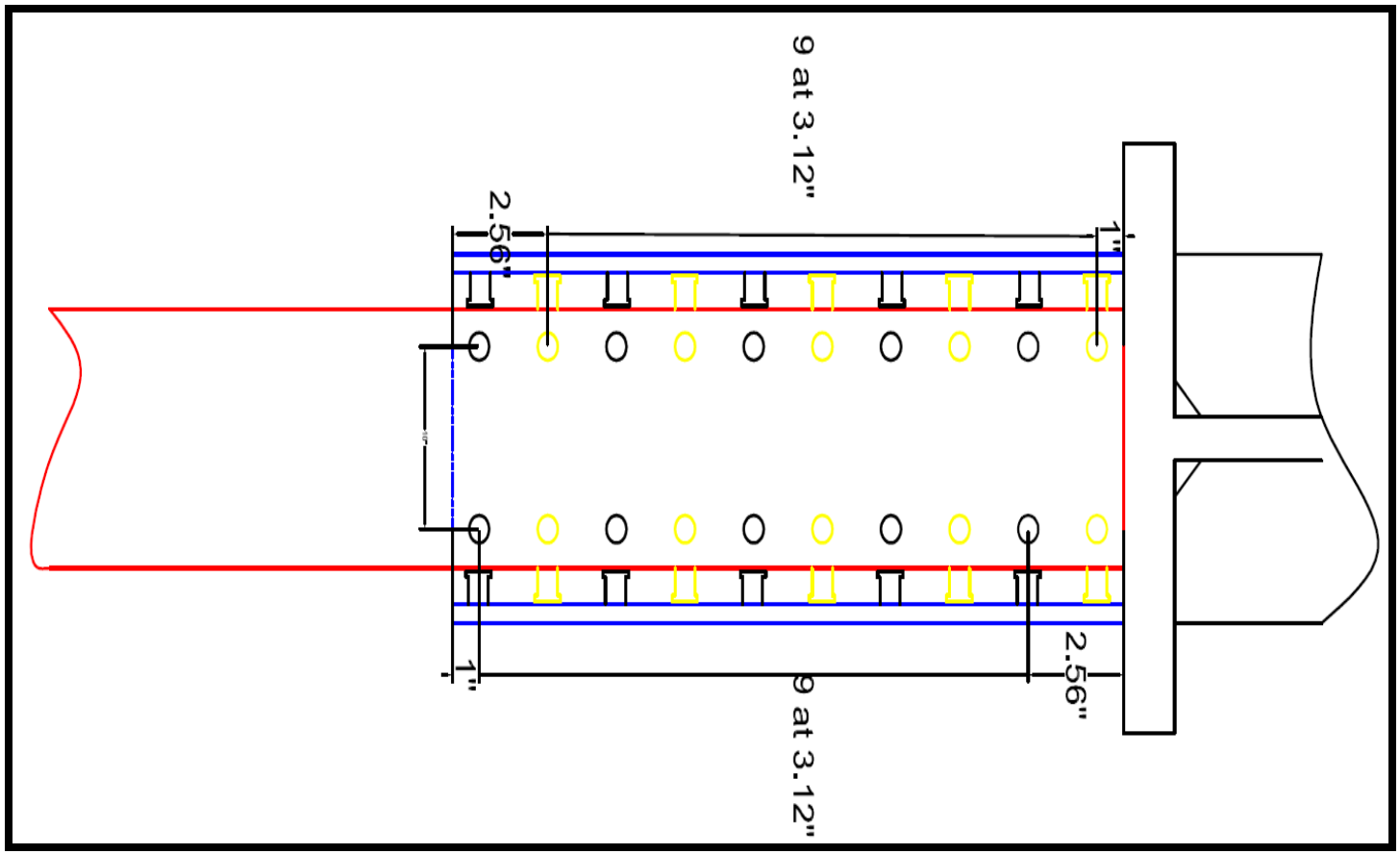

Figure B-14: Details of Configuration 4 for Beam Section W30x108 (A-A Plan view)

B.3 Design of Pre-Northridge Connections

B.3.1 Beam Section W24x62

Similar to grouted shear stud connection plastic hinge are assumed to be occurred distance equal to height of the connection. As a result, resulting shear force from plastic moment of the beam is calculated:

$Vpr = 2Mpr/Lp = 2*10098/218 = 92\ kips$

Required number of bolt:

$\phi Rnv = \phi Ab\ Fnv$

A325-X 1 in. diameter is selected.

$\phi Rnv = 0.75*0.785*68 = 40\ kips,$

$Nb = 92/40 = 2.3$, say 4 bolts.

Shear Tab Check: Dimensions of shear tab are: Thickness=0.5 in, length=5in, height= 16 in selected.

Yielding of Shear Tab: $\phi Rv = \phi 0.6\ Fy\ Agv$ =1*0.6*50*(16*0.5) =240 kips>92, Ok

Rupture of Shear Tab: $\phi Rv = \phi\ 0.6\ Fu\ Anv$ =0.75*0.6*65*(9.5*0.5) =138 kips>92, Ok

Complete penetration weld used for welding of beam flanges and shear tab. As a result, capacity checks were avoided.

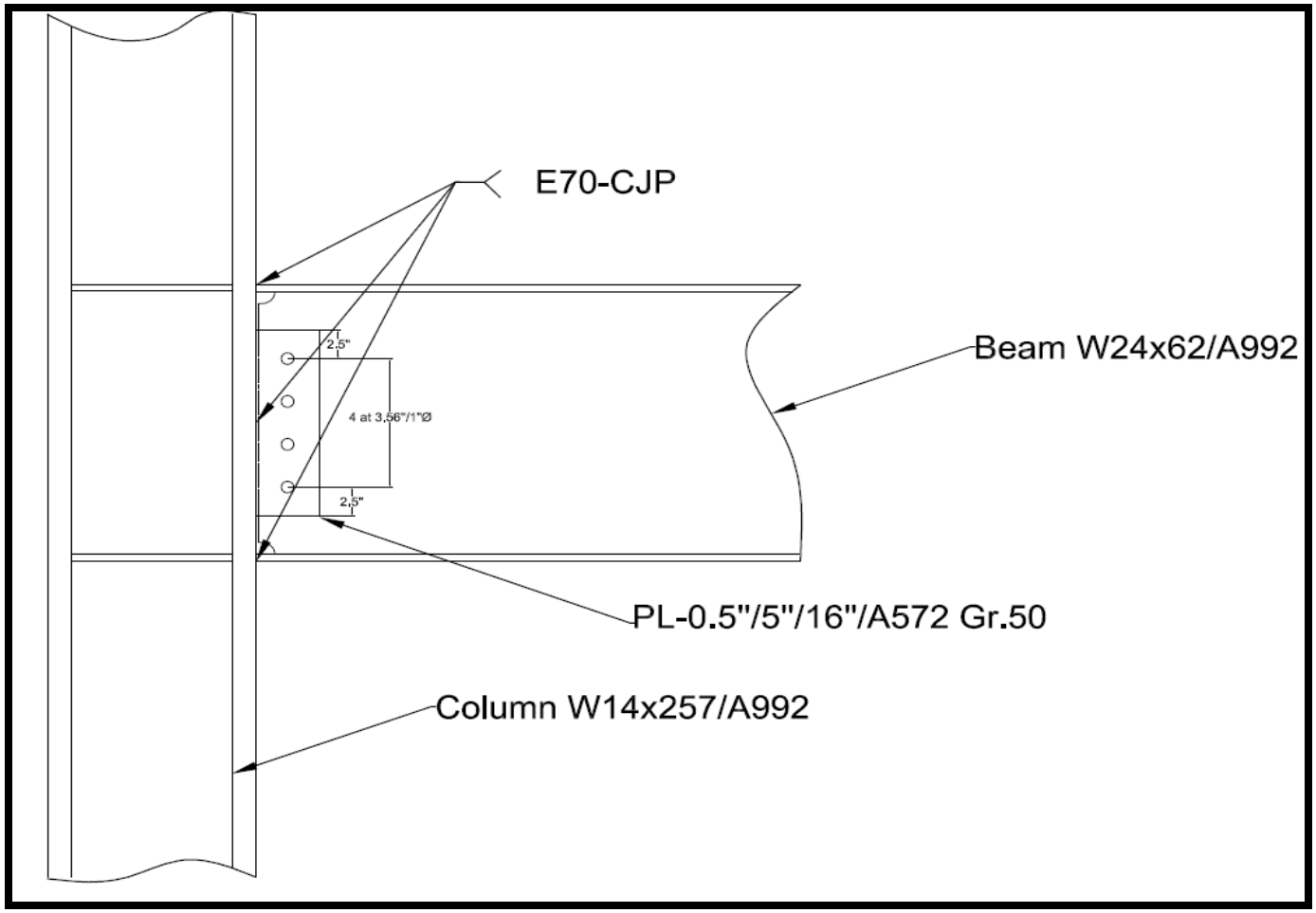

Figure B-15: Pre-Northridge Connection Details for Beam Section W24x62

Beam Section W30x108

Similar to grouted shear stud connection plastic hinge are assumed to be occurred distance equal to height of the connection. As a result, resulting shear force from plastic moment of the beam is calculated:

$$Vpr = 2Mpr/Lp = 2 * 22836/218 = 220.78 \text{ kips}$$

Required number of bolt:

$$\phi Rnv = \phi Ab\, Fnv$$

A325-X 1 in. diameter is selected.

$$\phi Rnv = 0.75 * 0.785 * 68 = 40 \text{ kips},$$

$$Nb = 220/40 = 5.5, \text{ say 7 bolts.}$$

Shear Tab Check: Dimensions of shear tab are: Thickness=0.6 in, length=5in, height= 24 in selected.

Yielding of Shear Tab: $\phi Rv = \phi 0.6\, Fy\, Agv$ =1*0.6*50*(24*0.5) =360 kips>220, Ok

Rupture of Shear Tab: $\phi Rv = \phi\, 0.6\, Fu\, Anv$ =0.75*0.6*65*(15.5*0.5) =226.68 kips>220, Ok

Complete penetration weld used for welding of beam flanges and shear tab. As a result, capacity checks were avoided.

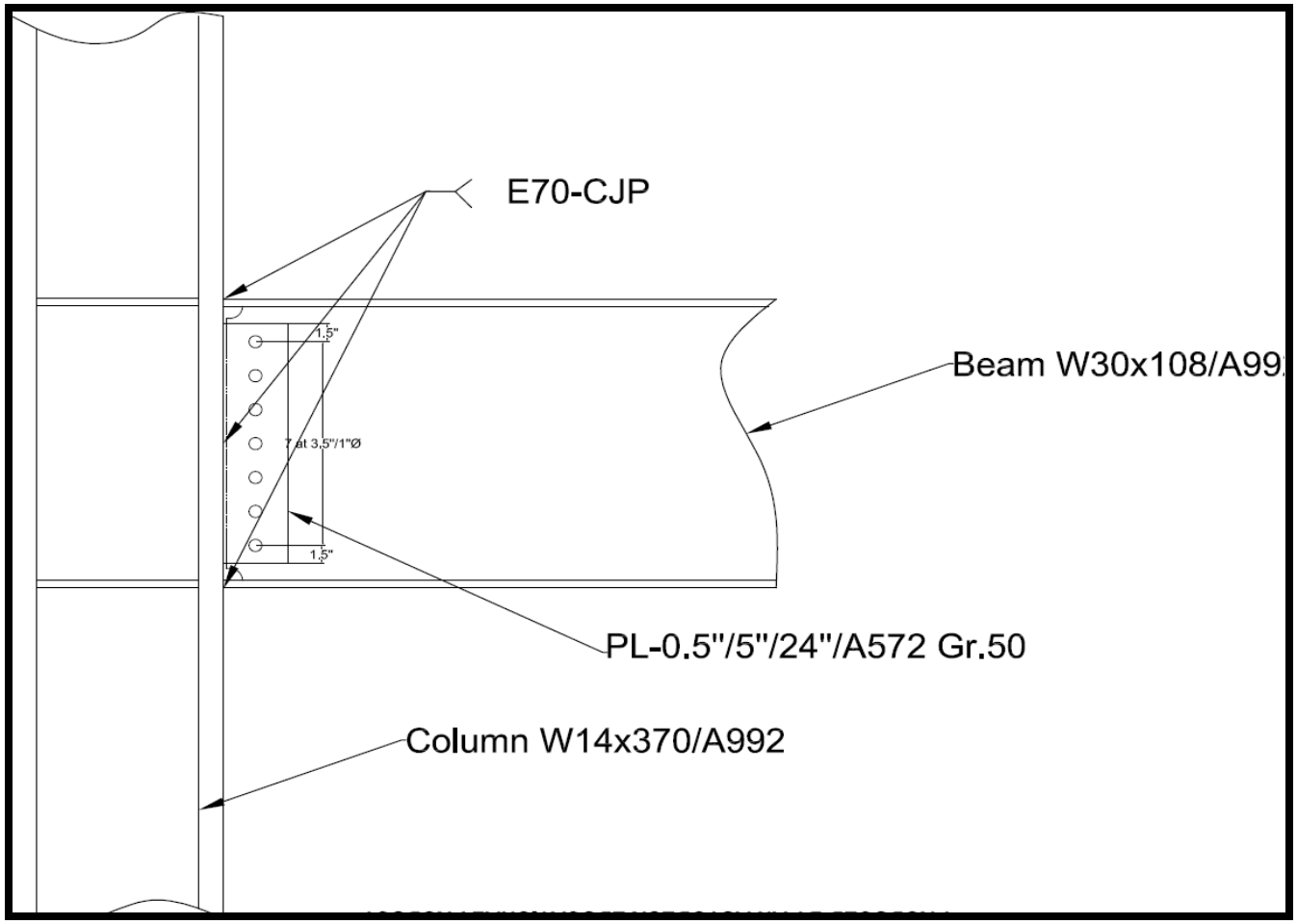

Figure B-16: Pre-Northridge Connection Details for Beam Section W30x108